

Copyright Warning & Restrictions

The copyright law of the United States (Title 17, United States Code) governs the making of photocopies or other reproductions of copyrighted material.

Under certain conditions specified in the law, libraries and archives are authorized to furnish a photocopy or other reproduction. One of these specified conditions is that the photocopy or reproduction is not to be “used for any purpose other than private study, scholarship, or research.” If a user makes a request for, or later uses, a photocopy or reproduction for purposes in excess of “fair use” that user may be liable for copyright infringement,

This institution reserves the right to refuse to accept a copying order if, in its judgment, fulfillment of the order would involve violation of copyright law.

Please Note: The author retains the copyright while the New Jersey Institute of Technology reserves the right to distribute this thesis or dissertation

Printing note: If you do not wish to print this page, then select “Pages from: first page # to: last page #” on the print dialog screen



The Van Houten library has removed some of the personal information and all signatures from the approval page and biographical sketches of theses and dissertations in order to protect the identity of NJIT graduates and faculty.

ABSTRACT

MODELING PROJECTION NEURON AND NEUROMODULATORY EFFECTS ON A RHYTHMIC NEURONAL NETWORK

by
Nickolas Kintos

Projection neurons shape the activity of many neural networks. In particular, neuromodulatory substances, which are often released by projection neurons, alter the cellular and/or synaptic properties within a target network. However, neural networks in turn influence projection neuron input via synaptic feedback. This dissertation uses mathematical and biophysically-realistic modeling to investigate these issues in the gastric mill (chewing) motor network of the crab, *Cancer borealis*. The projection neuron MCN1 elicits a gastric mill rhythm in which the LG neuron and INT1 burst in anti-phase due to their reciprocal inhibition. However, bath application of the neuromodulator PK elicits a similar gastric mill rhythm in the absence of MCN1 participation; yet, the mechanism that underlies the PK-elicited rhythm is unknown. This dissertation develops a 2-dimensional model that is used to propose three potential mechanisms by which PK can elicit a similar gastric mill rhythm. The network dynamics of the MCN1-elicited and PK-elicited rhythms are also compared using geometrical properties in the phase plane. Next, the two gastric mill rhythms are compared using a more biophysically-realistic model. Presynaptic inhibition of MCN1 is necessary for coordinating network activity during the MCN1-elicited rhythm. In contrast, the PK-elicited rhythm is shown to be coordinated by a synapse that is not functional during the MCN1-elicited rhythm.

Next, the gastric mill rhythm that is elicited by two coactive projection neurons (MCN1 and CPN2) is studied. A 2-dimensional model is used to compare the network

dynamics of the MCN1-elicited and MCN1/CPN2-elicited gastric mill rhythms via geometrical properties in the phase plane. While the MCN1-elicited rhythm requires the presence of reciprocal inhibition between INT1 and the LG neuron, the MCN1/CPN2-elicited rhythm persists in the absence of this reciprocal inhibition, due to an inhibitory feedback synapse from INT1 to CPN2 that changes the locus of coordination in the gastric mill rhythm. Next, the effect of a second feedback synapse, from the AB neuron to MCN1, is shown to change the motor pattern of the MCN1- and MCN1/CPN2-elicited rhythms. Finally, a third MCN1/CPN2-elicited rhythm is studied where the AB to MCN1 feedback synapse only affects the LG burst phase of the rhythm.

**MODELING PROJECTION NEURON AND NEUROMODULATORY EFFECTS
ON A RHYTHMIC NEURONAL NETWORK**

**by
Nickolas Kintos**

**A Dissertation
Submitted to the Faculty of
NJIT and Rutgers, The State University of New Jersey - Newark
in Partial Fulfillment of the Requirements for the Degree of
Doctor of Philosophy in Mathematical Sciences**

**Department of Mathematical Sciences, NJIT
Department of Mathematics and Computer Science, Rutgers - Newark**

January 2007

Copyright © 2007 by Nickolas Kintos

ALL RIGHTS RESERVED

APPROVAL PAGE

**MODELING PROJECTION NEURON AND NEUROMODULATORY EFFECTS
ON A RHYTHMIC NEURONAL NETWORK**

Nickolas Kintos

Dr. ~~Farzan~~ Nadim, Dissertation Advisor Date
Director, Division of Biological Sciences, NJIT
Professor, Department of Mathematical Sciences, NJIT and
Department of Biological Sciences, Rutgers University - Newark

Dr. Amitabha K. Bose, Committee Member Date
Professor, Department of Mathematical Sciences, NJIT

~~Dr. Jorge~~ Golowasch, Committee Member Date
Associate Professor, Department of Mathematical Sciences, NJIT and
Department of Biological Sciences, Rutgers University - Newark

Dr. Robert Miura, Committee Member Date
Professor, Department of Mathematical Sciences, NJIT

~~Dr.~~ William C. Hunter, Committee Member Date
Professor and Chair of Biomedical Engineering, NJIT

BIOGRAPHICAL SKETCH

Author: Nickolas Kintos
Degree: Doctor of Philosophy
Date: January 2007

Education:

- Doctor of Philosophy in Mathematical Sciences,
New Jersey Institute of Technology, Newark, NJ, 2007
- Master of Science in Applied Mathematics,
New Jersey Institute of Technology, Newark, NJ, 2005
- Bachelor of Arts in Mathematics, Chemistry
Rutgers University, Newark, NJ, 2000
- Associate in Science
Bergen Community College, Paramus, NJ, 1995

Presentations and Abstracts:

Kintos N., Nadim F., Saideman S.R., Nusbaum M.P.

“Comparing Projection Neuron and Neuromodulatory Effects on Network Activity Using a Biophysically-Realistic Model”, 649.7
Society for Neuroscience 36th Annual Meeting,
Atlanta, Georgia, October 2006.

Nadim F., Bose A., Kintos N., Nusbaum M.P.

“The Role of Feedback to Descending Projection Neurons in Rhythmic Motor Pattern Generation”, MS28
Joint SIAM-SMB Conference on the Life Sciences
Raleigh, NC, July 2006.

Kintos N., Nusbaum M.P., and Nadim, F.

“Investigating Projection Neuron and Neuromodulator Effects on the Operation of a Rhythmic Network: A Modeling Study”
32nd East Coast Nerve Net, Marine Biological Laboratories,
Woods Hole, MA, April 2006.

This dissertation is dedicated to: my wife Sonia for her heartfelt support and warm companionship, the memory of my father Panagiotis for his wisdom and who I wish could see it, my mother Kyriano for her sincere encouragement, and my brothers Konstantine and Tony for their support.

ACKNOWLEDGMENT

First and foremost, I would like to thank my advisor Dr. Farzan Nadim. I have truly appreciated his support, encouragement and guidance. He was always available whenever I had a question, and he has been invaluable for my development as a scientist. I am truly grateful for my experience in his lab. My daily interaction with lab members who performed experiments fostered my appreciation for the beauty of the stomatogastric nervous system and taught me how to present my modeling results to the biologists in our field. I would also like to thank my committee members Dr. Amitabha Bose, Dr. Jorge Golowasch, and Dr. Robert Miura. I have truly appreciated their input and helpful suggestions, and I am grateful for knowing that I could always turn to them whenever I needed something. I am also grateful to Dr. Bose for presenting some of my work at a conference this past summer. I would also like to thank my committee member Dr. William Hunter. He was kind enough to serve on my committee when I needed a replacement. I have truly appreciated his input and encouragement. I would also like to thank my former committee member Dr. Nadine Aubry for her input and helpful suggestions.

Next, I would like to thank all of the graduate students in the Nadim and Golowasch labs. They have all made my experience in graduate school truly rewarding, and I can not imagine working with a nicer group of people. Pascale, Vahid, Shunbing, Lian, Bob, Rodolfo, Yili, Olga, Rosa, and all of the newer lab members, thank you so much for all of your help and support. I especially want to thank Dr. Pascale Rabbah and Vahid Tohidi for their encouragement while I was writing this dissertation. Next, I would like to thank our collaborators from the Nusbaum lab. First, I thank Dr. Michael P. Nusbaum. His insight and helpful suggestions helped me to appreciate many of the

intricacies in the biological system that I would not have noticed on my own. I would also like to thank Dr. Shari Saideman. She was always available whenever I had a question about an experiment, and she gave me many helpful suggestions.

I would also like to thank the Department of Mathematical Sciences at NJIT for their continued support throughout my time as a graduate student. The variety of weekly seminars hosted by the department made it a great place for me to meet people whose research I wanted to learn more about. I also want to thank the Graduate Studies Office for their helpful guidance and support.

Last, but certainly not least, I would like to thank my family. I especially thank my wife Sonia for her warm companionship, which has inspired, helped, and motivated me more than I could have ever asked for. I can not imagine going through graduate school without her. I also thank my father Panagiotis for his guidance in life and my mother Kyriano for her support. Finally, I thank my brothers Konstantine and Tony for their encouragement.

TABLE OF CONTENTS

Chapter	Page
1 INTRODUCTION	1
1.1 Objectives	1
1.2 Significance	2
1.2.1 Difficulties in Studying Mammalian Systems	3
1.2.2 Insights Gained From Invertebrate Systems	4
1.2.3 The Effects of Neuromodulation on Network Activity	5
1.2.4 Projection Neurons Regulate Network Activity	5
1.3 Background	6
1.3.1 The Stomatogastric Nervous System	6
1.3.2 The Pyloric Rhythm	9
1.3.3 The Gastric Mill Rhythm	10
1.3.4 Reciprocal Inhibition	12
1.4 The MCN1-Elicited Gastric Mill Rhythm	13
1.4.1 Insight Gained From a Biophysically-Detailed Model	15
1.4.2 Reduction of the Biophysically-Detailed Model	18
2 COMPARING PROJECTION-NEURON-ELICITED AND NEUROMODULATOR-ELICITED OSCILLATIONS IN A RHYTHMIC NETWORK: A REDUCED MATHEMATICAL MODEL	26
2.1 Introduction	26
2.2 Methods	28
2.2.1 Three-Dimensional Model of the MCN1-Elicited Gastric Mill Rhythm .	28
2.2.2 Reduction to a 2-Dimensional Model of the MCN1-Elicited Gastric Mill Rhythm	32

TABLE OF CONTENTS
(Continued)

Chapter	Page
2.2.3 Building a 2-Dimensional Model of the Pyrokinin-Elicited Gastric Mill Rhythm	38
2.2.4 Generalization to a Single 2-Dimensional Model	53
2.3 Results	57
2.3.1 Investigating the Network Dynamics of the MCN1-Elicited Gastric Mill Rhythm	58
2.3.2 Proposed Mechanisms by Which Pyrokinin (PK) Elicits a Similar Gastric Mill Rhythm	63
2.3.3 Calculation of Bounds on the Gastric Mill Period	75
2.3.4 Summary of Results	82
3 COMPARING PROJECTION NEURON AND NEUROMODULATORY EFFECTS ON NETWORK ACTIVITY USING A BIOPHYSICALLY-REALISTIC MODEL	92
3.1 Introduction	92
3.2 Methods	93
3.2.1 Biophysically-Realistic Model of the MCN1-Elicited Gastric Mill Rhythm	94
3.2.2 Building a Biophysically-Realistic Model of the PK-Elicited Gastric Mill Rhythm	99
3.2.3 Including the Dorsal Gastric Neuron in the Biophysically-Realistic Model	102
3.3 Results	105
3.3.1 The MCN1-Elicited Gastric Mill Rhythm in the Biophysically-Realistic Model	106
3.3.2 The PK-Elicited Gastric Mill Rhythm in the Biophysically-Realistic Model	108

TABLE OF CONTENTS
(Continued)

Chapter	Page
3.3.3 PK Elicits a Similar Gastric Mill Rhythm via the Induction of Plateau Properties in the LG Neuron	113
3.3.4 The MCN1-Elicited and PK-Elicited Gastric Mill Rhythms are Distinguished by a Synaptic Input from AB to INT1	114
3.3.5 Including the Dorsal Gastric (DG) Neuron in the Biophysically-Realistic Model	115
3.3.6 Examining the Effects of Presynaptic Inhibition in the MCN1-Elicited Gastric Mill Rhythm	118
3.3.7 Assessing How Plateau Properties in the LG Neuron Would Affect the MCN1-Elicited Gastric Mill Rhythm	121
3.3.8 Investigating the Properties of the MCN1-Elicited Gastric Mill Rhythm at the Network Level	123
3.3.9 Investigating the Effect of the DG to LG Synapse in the PK-Elicited Gastric Mill Rhythm	124
3.3.10 Investigating the Properties of the PK-Elicited Gastric Mill Rhythm at the Network Level	125
3.3.11 Summary of Results	126
4 INVESTIGATING HOW FEEDBACK TO PROJECTION NEURONS SHAPES ACTIVITY IN A RHYTHMIC NETWORK: A MODELING STUDY	140
4.1 Introduction	140
4.2 Methods	142
4.2.1 Three-Dimensional Model of the MCN1-Elicited Gastric Mill Rhythm ..	142
4.2.2 Reduction to a 2-Dimensional Model of the MCN1-Elicited Gastric Mill Rhythm	145
4.2.3 A 2-Dimensional Model of the MCN1-Elicited Gastric Mill Rhythm that Includes the Effect of Rhythmic Feedback	150

TABLE OF CONTENTS
(Continued)

Chapter	Page
4.2.4 Building a Mathematical Model of the MCN1/CPN2-Elicited Gastric Mill Rhythm	154
4.2.5 Reduction to a 2-Dimensional Model of the MCN1/CPN2-Elicited Gastric Mill Rhythm	157
4.2.6 A 2-Dimensional Model of the MCN1/CPN2-Elicited Gastric Mill Rhythm That Includes the Effect of Rhythmic Feedback to MCN1	160
4.2.7 A 2-Dimensional Model of the VCN-Influenced MCN1/CPN2-Elicited Gastric Mill Rhythm	163
4.3 Results	166
4.3.1 Investigating the Network Dynamics of the MCN1-Elicited Gastric Mill Rhythm	166
4.3.2 Including the Effect of Rhythmic Feedback in the MCN1-Elicited Gastric Mill Rhythm	170
4.3.3 Investigating the Network Dynamics of the MCN1/CPN2-Elicited Gastric Mill Rhythm	178
4.3.4 Investigating How Rhythmic Feedback to MCN1 Affects the Network Dynamics of the MCN1/CPN2-Elicited Gastric Mill Rhythm	186
4.3.5 Investigating the Network Dynamics of the VCN-Influenced MCN1/CPN2-Elicited Gastric Mill Rhythm	191
4.3.6 Summary of Results	199
5 INVESTIGATING HOW COACTIVE PROJECTION NEURONS SHAPE ACTIVITY IN A RHYTHMIC NETWORK USING A BIOPHYSICALLY-REALISTIC MODEL	224
5.1 Introduction	224
5.2 Methods	226
5.3 Results	230
5.3.1 Network Dynamics of the MCN1-Elicited Gastric Mill Rhythm	231

TABLE OF CONTENTS
(Continued)

Chapter	Page
5.3.2 Network Dynamics of the MCN1/CPN2-Elicited Gastric Mill Rhythm in the Biophysically-Realistic Model	232
5.3.3 Effect of the Local AB to INT1 Inhibition	234
5.3.4 Effect of the INT1 to CPN2 Feedback Inhibition	235
5.3.5 Effect of the Local INT1 to LG Inhibition	236
5.3.6 Summary of Results Effect	237
6 CONCLUSION	245
6.1 Summary of Results and Discussion	245
6.1.1 Comparing the MCN1-Elicited and PK-Elicited Gastric Mill Rhythms ..	246
6.1.2 Network Dynamics of the MCN1-Elicited and MCN1/CPN2-Elicited Gastric Mill Rhythms	252
6.2 Applications to More Complex Systems	262
APPENDIX A PARAMETERS FOR THE BIOPHYSICALLY-REALISTIC MODELS OF THE MCN1-ELICITED AND PK-ELICITED GASTRIC MILL RHYTHMS	264
APPENDIX B PARAMETERS FOR THE 2-DIMENSIONAL MODELS OF THE MCN1-ELICITED AND MCN1/CPN2-ELICITED GASTRIC MILL RHYTHMS	269
APPENDIX C PARAMETERS FOR THE BIOPHYSICALLY-REALISTIC MODELS OF THE MCN1-ELICITED AND MCN1/CPN2- ELICITED GASTRIC MILL RHYTHMS	272
REFERENCES	275

LIST OF TABLES

Table	Page
2.1 Parameters Used to Model the MCN1-Elicited Gastric Mill Rhythm.....	52
2.2 Parameters Used for Each of the PK-Elicited Gastric Mill Rhythms.....	52
A.1 Parameters for the Ionic Currents in the MCN1-Elicited Gastric Mill Rhythm	265
A.2 Parameters for the Synaptic Currents in the MCN1-Elicited Rhythm	266
A.3 Parameters for Ionic Currents that are Distinct to the PK-Elicited Gastric Mill Rhythm	267
A.4 Parameters for Synaptic Currents that are Distinct to the PK-Elicited Gastric Mill Rhythm.....	268
B.1 Parameters for the 2-Dimensional Model of the MCN1-Elicited Gastric Mill Rhythm	269
B.2 Parameters that are Distinct for the 2-Dimensional Model of the MCN1/CPN2-Elicited Gastric Mill Rhythm	270
B.3 Parameters which are Distinct for the MCN1-Elicited and MCN1/CPN2-Elicited Gastric Mill Rhythms that Include the Effect of the AB to MCN1 Feedback Inhibition	271
C.1 Parameters for the Ionic Currents in the Biophysically-Realistic Model.....	273
C.2 Parameters for the Synaptic Currents in the Biophysically-Realistic Model ...	274

LIST OF FIGURES

Figure	Page
1.1 Schematic Diagram of the Crab Stomach	20
1.2 The MCN1-Elicited Gastric Mill Rhythm in <i>C. borealis</i>	21
1.3 Biophysically-Detailed Model of the MCN1-Elicited Gastric Mill Rhythm ...	22
1.4 Effect of the Pyloric-Timed Inhibition from the AB Neuron to INT1	23
1.5 Simulation of the MCN1-Elicited Gastric Mill Rhythm	24
1.6 Reduced Model of the MCN1-Elicited Gastric Mill Rhythm where INT1 and LG are Passive Neurons.....	25
2.1 MCN1-Elicited Gastric Mill Rhythm (Reduction to 2 Dimensions).....	84
2.2 The Gastric Mill Rhythm is Not Spontaneously Active Without MCN1 Input.....	85
2.3 Switching From an MCN1-Elicited to a PK-Elicited Gastric Mill Rhythm.....	85
2.4 PK-Elicited Gastric Mill Rhythm (Mechanism 1: PK Induces I_{plat} in the LG Neuron).....	86
2.5 PK-Elicited Gastric Mill Rhythm (Mechanism 2: PK Induces I_h in the LG Neuron).....	87
2.6 PK-Elicited Gastric Mill Rhythm (Mechanism 3: PK Induces I_{proc} and I_K in the LG Neuron).....	87
2.7 Network Oscillations Elicited Through PK Induction of Only I_K	88
2.8 Plateau Potential Generation in the LG Neuron	89
2.9 Generalization of the Individual 2-Dimensional Models	90
2.10 The Pyloric-Timed Input (P) Allows for Cycle-to-Cycle Variability in the Period of the Gastric Mill Rhythm	91
3.1 Bath Application of the Neuropeptide Pyrokinin (PK) Elicits a Gastric Mill Rhythm that is Similar to the MCN1-Elicited Rhythm	128

LIST OF FIGURES
(Continued)

Figure	Page
3.2 Biophysically-Realistic Model Used to Assess the Proposed PK Mechanisms	129
3.3 Investigating the Role of I_{Proc} in the Last PK Mechanism	130
3.4 PK Elicits a Gastric Mill Rhythm via the Activation of Plateau Properties in the LG Neuron.....	131
3.5 The MCN1-Elicited and PK-Elicited Gastric Mill Rhythm are Distinguished by the Effect of the AB to INT1 Inhibition.....	132
3.6 The Model DG Neuron Reproduces the Observed Behavior in the Biological System.....	133
3.7 The Model DG Neuron is Included in the MCN1-Elicited and PK-Elicited Gastric Mill Rhythms	134
3.8 Effect of Presynaptic Inhibition in the MCN1-Elicited Gastric Mill Rhythm .	135
3.9 Assessing the Role of Presynaptic Inhibition if Plateau Properties are Included in the LG Neuron.....	136
3.10 Network-Level Properties of the MCN1-Elicited Gastric Mill Rhythm	137
3.11 Investigating the Role of the PK-Strengthened DG to LG Synapse During the PK-Elicited Gastric Mill Rhythm	138
3.12 Network-Level Properties of the PK-Elicited Gastric Mill Rhythm	139
4.1 Reduced (3-Dimensional) Model of the MCN1-Elicited Gastric Mill Rhythm	202
4.2 Reduction to a 2-Dimensional Model of the MCN1-Elicited Gastric Mill Rhythm	203
4.3 Network Dynamics of the MCN1-Elicited Gastric Mill Rhythm.....	204
4.4 Adding the Effect of the AB to MCN1 Feedback Inhibition to the 2-Dimensional Model.....	205

LIST OF FIGURES
(Continued)

Figure	Page
4.5 Biological Recording of the MCN1-Elicited Gastric Mill Rhythm When the AB to MCN1 Feedback Inhibition is Intact	206
4.6 Investigating How the AB to MCN1 Feedback Inhibition Changes the Network Dynamics of the MCN1-Elicited Rhythm	207
4.7 The Local AB to INT1 Inhibition Prolongs the Duration of the LG Burst Phase and Slows the Frequency of Network Oscillations in this MCN1-Elicited Gastric Mill Rhythm	208
4.8 Building a 2-Dimensional Model of the MCN1/CPN2-Elicited Gastric Mill Rhythm	209
4.9 Investigating How CPN2 Affects the Network Dynamics of the Gastric Mill Rhythm	210
4.10 The Local AB to INT1 Inhibition Triggers the Onset of the LG Burst Phase During the MCN1/CPN2-Elicited Gastric Mill Rhythm (When MCN1 is Tonically Active).....	211
4.11 The Frequency of Network Oscillations is Slower When the AB to INT1 Inhibition is Removed	212
4.12 The Duration of the LG Interburst Phase is Shorter Without the INT1 to CPN2 Feedback Inhibition	213
4.13 Network Oscillations Persist After the INT1 to LG Inhibitory Synapse is Removed.....	214
4.14 The Effect of the AB to MCN1 Feedback Inhibition is Added to the 2-Dimensional Model of the MCN1/CPN2-Elicited Gastric Mill Rhythm.....	215
4.15 Investigating How the AB to MCN1 Feedback Inhibition Affects the MCN1/CPN2-Elicited Gastric Mill Rhythm	216
4.16 The Local AB to INT1 Inhibition Prolongs the Duration of the LG Burst Phase and Slows the Frequency of Network Oscillations in this MCN1/CPN2-Elicited Gastric Mill Rhythm	217
4.17 The Ventral Cardiac Neurons (VCN) Elicit a Gastric Mill Rhythm in the Biological System via Co-activation of the MCN1 and CPN2	218

LIST OF FIGURES
(Continued)

Figure	Page
4.18 The Gastric Mill Rhythm Elicited by MCN1 and CPN2 in their VCN-Influenced Activity Patterns	219
4.19 The AB to INT1 Inhibition has no Influence on the Frequency of Network Oscillations When its Effect is Transmitted Simultaneously Through the INT1 to LG Synapse and the INT1 to CPN2 Feedback Pathway	220
4.20 In the Biological System, the Pyloric-Timed Activity in CPN2 During the LG Interburst Phase Occurs Approximately in Anti-Phase with the Pyloric-Timed Interruptions in MCN1 and Hyperpolarizations in the LG Neuron	221
4.21 Pyloric-Timed Activity Through the INT1 to CPN2 Feedback Pathway Influences the Network Dynamics of this Gastric Mill Rhythm	222
4.22 The AB to INT1 Inhibition Increases the Frequency of Network Oscillations When Its Forcing Effect is Delayed Through the INT1 to CPN2 Feedback Pathway	223
5.1 The MCN1/CPN2-Elicited Gastric Mill Rhythm.....	239
5.2 The Biophysically-Realistic Model of the MCN1/CPN2-Elicited Gastric Mill Rhythm	240
5.3 Comparing the MCN1-Elicited and MCN1/CPN2-Elicited Gastric Mill Rhythms.....	241
5.4 Effect of the Local AB to INT1 Inhibition.....	242
5.5 Effect of the INT1 to CPN2 Feedback Inhibition.....	243
5.6 Effect of the Local INT1 to LG Inhibitory Synapse.....	244
A.1 Simplified Circuit Diagram of the Model MCN1-Elicited Gastric Mill Rhythm	264
A.2 Simplified Circuit Diagram of the Model PK-Elicited Gastric Mill Rhythm ..	267
C.1 Simplified Circuit Diagram of the Model MCN1/CPN2-Elicited Gastric Mill Rhythm	272

LIST OF ABBREVIATIONS

MCN1	Modulatory Commissural Neuron 1
PK	Pyrokinin
CPN2	Commissural Projection Neuron 2
CPG	Central Pattern Generator
INT1	Interneuron 1
LG	Lateral Gastric Neuron
DG	Dorsal Gastric Neuron
AB	Anterior Burster Neuron
PD	Pyloric Dilator Neuron
VCN	Ventral Cardiac Neurons
STNS	Stomatogastric Nervous System
CoG	Commissural Ganglion
OG	Oesophageal Ganglion
STG	Stomatogastric Ganglion
<i>ion</i>	Inferior Oesophageal Nerve
<i>son</i>	Superior Oesophageal Nerve
<i>stn</i>	Stomatogastric Nerve

CHAPTER 1

INTRODUCTION

1.1 Objectives

The objectives of this dissertation are to 1 propose potential mechanisms by which a neuromodulator can elicit a gastric mill rhythm in the crab, *Cancer borealis* 2 investigate how descending inputs from two coactive projection neurons shape the gastric mill rhythm.

In the first objective, a reduced two-dimensional mathematical model of the gastric mill rhythm is developed. Then, potential ionic currents are proposed, by way of a phase-plane analysis, which allow the neuromodulator pyrokinin to elicit a gastric mill rhythm. In particular, this dissertation investigates how pyrokinin elicits a gastric mill rhythm that is similar to the gastric mill rhythm elicited by the projection neuron MCN1, as reported in recent experiments (Hertzberg and Nusbaum, 2005). Then, the predictions of the reduced model are examined in the context of a more biophysically-realistic model of the gastric mill rhythm. The biophysical model is also used to compare how activity is coordinated in the MCN1-elicited and pyrokinin-elicited gastric mill rhythms.

In the second objective, the reduced model is used to investigate how the coactivity of two projection neurons, MCN1 and CPN2, shapes the gastric mill rhythm. A phase-plane analysis is used to study how descending inputs from the coactive projection neurons shape the motor pattern of the gastric mill rhythm. In addition, the role of ascending feedback to the projection neurons is also examined. Then, the effects of MCN1 and CPN2 are investigated in the context of a biophysically-detailed model.

1.2 Significance

Oscillatory activity is pervasive within the nervous system of an animal. For example, oscillations in the mammalian nervous system are involved in sensory processing (Gray, 1994), sleep and arousal (McCormick and Bal, 1997), and learning (Lisman, 1997). However, synchronous oscillatory activity in the brain can also be pathological (McCormick and Bal, 1997). For example, mechanisms that give rise to focal epilepsy involve the synchronization of rhythmic oscillations among cortical pyramidal neurons (Wong et al., 1986). Thus, due to the widespread significance of oscillatory activity within our brain and nervous system, it is important to understand the mechanisms that generate these oscillations.

In their interaction with the surrounding environment, animals perform a vast range of behaviors that involve a repeating set of movements such as walking, flying, or swimming. Such behaviors are generated in different parts of the nervous system by networks of neurons that produce a sequence of electrical signals called motor output, which in turn instructs muscles to perform the appropriate movements. However, instead of generating one specific type of output, neural networks are involved in the generation of many different types of motor output (Marder and Thirumalai, 2002). For example, leg muscles are involved in walking, jumping, and running. A great deal of what is known about the neural basis of behavior comes from the study of central pattern generators (CPGs), which are neural networks that generate self-sustained rhythmic activity patterns in the absence of sensory input. Rhythmic behaviors include all motor acts that involve a repeating set of movements such as locomotion, respiration, and

mastication. In addition, the stereotyped activity patterns generated by CPGs make them easier to study.

1.2.1 Difficulties in Studying Mammalian Systems

In the effort to understand how the nervous system generates movement in animals, neuroscientists would ideally like to answer this question in mammals. However, mammalian nervous systems contain a huge number of neurons with complex synaptic connections; therefore, an understanding of how movement is generated by neural networks in mammals has been limited (Marder and Calabrese, 1996; Marder, 2002). In fact, one of the most difficult tasks facing neuroscientists is identifying neurons that participate in rhythmic pattern-generating networks. The majority of such neurons are situated within ganglia, nuclei, and brains, which contain many other types of neurons that perform different functions, and all of this neural circuitry is housed within a complex nervous system. In addition, the fact that neural network activity can be modulated (Katz and Frost, 1996; Marder and Thirumalai, 2002) has further complicated the task of identifying neurons that participate in rhythmic pattern generation. Consequently, a single recording is not sufficient to identify a neuron since it can display multiple activity patterns due to the effects of neuromodulation (Marder and Calabrese, 1996). Thus, it has been extremely difficult to gain insights into the workings of pattern-generating networks within the mammalian nervous system using today's experimental techniques.

1.2.2 Insights Gained From Invertebrate Systems

Many neuroscientists have turned to investigating how neural networks generate rhythmic motor behaviors in invertebrates. One advantage of studying invertebrates is that they have more simplified nervous systems, and, as a result, they often exhibit less complicated forms of behavior. In addition, many of the general principles that form the basis for our understanding of neurons and neural circuits were established in previous studies with invertebrate preparations. For example, the squid giant axon was used to understand the mechanisms that generate the action potential (Hodgkin and Huxley, 1952), presynaptic inhibition was first demonstrated at the crustacean neuromuscular junction (Dudel and Kuffler, 1961), and electrical coupling between neurons was first studied in the crayfish (Furshpan and Potter, 1959). Today, researchers continue to use invertebrate preparations to study a variety of different rhythmic motor behaviors such as: heartbeat in leeches, feeding in crustaceans, and locomotion in insects (Marder and Calabrese, 1996; Nusbaum and Beenhakker, 2002). In addition, more recent work has established that CPG circuits operate under the same general principles in both vertebrate and invertebrate nervous systems (Stein, 1997; Marder and Bucher, 2001; Marder et al., 2005). Thus, invertebrate preparations have been invaluable for understanding the general principles that govern motor pattern generation. However, many important questions still remain such as: the roles of neuromodulators in modifying circuit output, the roles of descending inputs from projection neurons in regulating rhythmic circuits, and applications to higher animals such as humans.

1.2.3 The Effects of Neuromodulation on Network Activity

Neuromodulation alters neural network activity in both vertebrate and invertebrate systems. For example, in lamprey, neuromodulation of the pattern-generating networks that control locomotion leads to modified swimming patterns and body orientations (Grillner et al., 1995). Similarly, neuromodulation controls the vigor of escape swim in the mollusk, *Tritonia* (Katz and Frost, 1995a, 1995b). Furthermore, neuromodulation adjusts the oscillatory patterns in the mammalian brain during the sleep/wake cycle (Steriade et al., 1993; McCormick and Bal, 1994). Neuromodulators are typically released as naturally occurring peptides, hormones, or gases, which alter network activity by modifying the intrinsic properties of individual neurons within a network or the strength of synaptic connections between network neurons (Pearson, 1993; Katz, 1995a; Marder and Thirumalai, 2002; Nusbaum and Beenhakker, 2002). Moreover, network activity is conditional upon the presence of neuromodulators in many systems (Marder and Thirumalai, 2002). One of the objectives of this dissertation is to elucidate potential mechanisms by which a neuromodulator can generate oscillations in a rhythmic motor network.

1.2.4 Projection Neurons Regulate Network Activity

Descending inputs from projection neurons generally initiate, terminate, or modify activity in pattern-generating networks (Kasicki and Grillner, 1986; Deliagina et al., 2002; Blitz et al., 2004; Rossignol et al., 2006). In mammals, descending projection neuron pathways from the cerebellum and brainstem influence locomotor activity generated by rhythmic motor circuits in the spinal cord (Matsuyama et al., 2004; Sommer

and Wurtz, 2004a, b). In lower vertebrates such as the lamprey, bulbospinal neurons from the reticular nuclei shape the activity of rhythmic motor circuits that generate swimming patterns in the spinal cord (Swain et al., 1993; Bussieres et al., 1999). In invertebrates such as crustaceans, descending input from projection neurons in the stomatogastric nervous system activates the gastric mill and pyloric CPG circuits, which generate food chewing and food filtering motor patterns, respectively (Nusbaum et al., 2001; Nusbaum and Beenhakker, 2002). Generally, projection neurons in turn receive rhythmic feedback from their target circuits (Perreault et al., 1993; Norris et al., 1996; Wood et al., 2004; Zelenin, 2005). However, the role of such feedback to projection neurons is not well understood. One of the objectives of this dissertation is to determine how descending input from two coactive projection neurons and ascending rhythmic feedback to these projection neurons shapes the activity of a rhythmic motor network.

1.3 Background

1.3.1 The Stomatogastric Nervous System

This dissertation investigates how 1 bath application of a neuromodulator and 2 descending inputs from two coactive projection neurons shape the activity of a rhythmic motor network in the stomatogastric nervous system (STNS) of the crab, *Cancer borealis*. The STNS, which is an extension of the central nervous system in *C. borealis*, generates the rhythmic motor patterns that control the digestion of food in the crab stomach. The stomach of *C. borealis* (Figure 1.1) is composed of four compartments

(oesophagus, cardiac sac, gastric mill, and pylorus) where the swallowing, storage, chewing, and filtering of food take place, respectively (Nusbaum and Beenhakker, 2002). The STNS sits on the dorsal side of the stomach (Figure 1.1), and it is composed of four ganglia along with their connecting and peripheral nerves (Figure 1.2.A). The four ganglia of the STNS include the paired commissural ganglia (CoGs), the oesophageal ganglion (OG), and the stomatogastric ganglion (STG). The number of neurons in each ganglion has been determined to be: roughly 500 neurons in each CoG, 14 neurons in the OG (Beenhakker et al., 2004), and 26 neurons in the STG (Kilman and Marder, 1996). Within the STNS, a set of distinct, but interacting, CPG circuits generate the rhythmic motor patterns that control different aspects of the digestion process (Nusbaum and Beenhakker, 2002). However, the CPG circuits that have been studied most extensively are the gastric mill and pyloric circuits, which are distinct but coactive rhythmic circuits located within the STG that generate the gastric mill rhythm and pyloric rhythm, respectively (Harris-Warrick et al., 1992; Marder and Calabrese, 1996; Nusbaum and Beenhakker, 2002). The gastric mill rhythm (frequency ~ 0.1 Hz) contracts the striated muscles that control the movements of three teeth responsible for food chewing in the gastric mill compartment of the crab stomach. The pyloric rhythm (frequency ~ 1 Hz) contracts the pylorus, which filters the chewed food from the gastric mill compartment. Both the small number of neurons within the gastric mill and pyloric circuits and the fact that both circuits remain functional in the isolated STNS has facilitated their analysis. In particular, when the STNS is removed from the animal and placed in a saline solution whose salt concentrations mimic those in the blood of the crab, the gastric mill and pyloric circuits in this isolated, *in vitro*, preparation still generate rhythmic motor patterns

that are essentially identical to those of the *in vivo* motor patterns of the intact animal (Heinzel et al., 1993). Moreover, both the gastric mill and pyloric circuits have been extensively studied with the aid of modern experimental techniques, and investigators have identified all of the neurons and anatomical connections within both circuits (Marder and Calabrese, 1996; Nusbaum and Beenhakker, 2002).

However, the STG, which contains the gastric mill and pyloric circuits, receives synaptic input from roughly 20 pairs of projection neurons whose cell bodies lie in the CoGs and OG (Figure 1.2.A). Of these ~20 pairs of projection neurons, 6 have been identified (Nusbaum and Beenhakker, 2002), but the axons of all ~20 pairs of projection neurons that innervate the STG do so via the stomatogastric nerve (*stn*) (Figure 1.2.A). Two of the identified projection neurons are the modulatory commissural neuron 1 (MCN1) and the commissural projection neuron 2 (CPN2), and their coactivity elicits a gastric mill rhythm in the STG (Beenhakker and Nusbaum, 2004). One of the objectives of this dissertation is to investigate how the coactive synaptic inputs from MCN1 and CPN2 shape the gastric mill rhythm.

In addition, the gastric mill and pyloric rhythms are affected by neuromodulatory substances that are released from the axon terminals of the projection neurons that innervate the STG. Both the gastric mill and pyloric rhythms are dependent upon the release of these neuromodulators, and both rhythms are disrupted when action potential propagation is blocked through the *stn* (Figure 1.2.A), which disrupts the release of neuromodulators into the STG (Nusbaum et al., 2001; Nusbaum and Beenhakker, 2002). More than 20 different neuromodulators have been identified within the STG axonal arbors of the projection neurons (Marder and Rehm, 2005). The effects of these

neuromodulators on the cellular and synaptic properties of the gastric mill and pyloric rhythms have been extensively studied (Nusbaum et al., 2001; Marder and Thirumalai, 2002). In some cases, bath application of a neuromodulator produces the same effect on a network as the projection neuron from which the neuromodulator is released (Nusbaum and Marder, 1989; Harris-Warrick et al., 1992). However, this is not true in general since a projection neuron often exhibits complex synaptic interactions with its target network (Perrins and Weiss, 1996; Nusbaum and Beenhakker, 2002). Recently, bath application of the neuromodulator pyrokinin (PK) to the isolated STG was shown to elicit a gastric mill rhythm that is surprisingly similar to that elicited by the projection neuron MCN1, which does not release PK (Hertzberg et al., 2003). Another objective of this dissertation is to determine potential mechanisms by which PK can elicit such a gastric mill rhythm.

1.3.2 The Pyloric Rhythm

The pyloric rhythm drives the rhythmic muscle contractions in the pylorus during the digestion process in the crab (Harris-Warrick et al., 1992; Marder and Calabrese, 1996). The activity of the pyloric rhythm is generated by the anterior burster (AB) neuron, which is a robust oscillatory pacemaker that typically oscillates with a frequency of ~1 Hz (Marder and Calabrese, 1996). In particular, the AB neuron is an endogenous oscillator that continues to generate regular bursts of action potentials even when it is isolated from all other neurons in the pyloric circuit. Moreover, the AB neuron maintains its relatively fixed pattern of activity unless it is perturbed by the obstruction of neuromodulator release from the *stn* (Figure 1.2.A) or by the synaptic influence of another neuron (Marder and Calabrese, 1996). In addition, the AB neuron is strongly

electrically coupled to the pyloric dilator (PD) neurons (Harris-Warrick et al., 1992). This strong electrical coupling allows for the bilateral transmission of electrical signals between the AB and PD neurons, and, as a result, these neurons exhibit synchronous activity, in which the PD neurons fire action potentials in time with the AB neuron (Marder and Calabrese, 1996). The resulting AB/PD ensemble is often referred to as the pyloric pacemaker group, which makes inhibitory synaptic connections with all other neurons in the pyloric circuit. Moreover, the inhibitory synapses emanating from the pyloric pacemaker produce the inactive phase of the postsynaptic pyloric neurons and therefore set the timing of activity in the rest of the pyloric circuit.

1.3.3 The Gastric Mill Rhythm

The gastric mill rhythm drives the rhythmic movements of three teeth responsible for food chewing in the gastric mill compartment of the crab stomach (Harris-Warrick et al., 1992; Marder and Calabrese, 1996). Unlike the pyloric rhythm which is driven by a pacemaker, the gastric mill rhythm is instead driven by the reciprocal inhibition between two of its member neurons. In particular, interneuron 1 (INT1) and the lateral gastric (LG) neuron reciprocally inhibit each other and oscillate in anti-phase, where the active phase of each neuron in this pair occurs in alternation. Moreover, the anti-phase INT1-LG oscillation occurs with a frequency of ~ 0.1 Hz, and the INT1-LG pair, via its inhibitory synaptic connections within the STG, sets the timing of activity in the rest of the gastric mill circuit (Nusbaum and Beenhakker, 2002). In addition, LG neuron activity underlies the protraction phase of the lateral gastric teeth, while INT1 activity coincides with the retraction phase (Heinzel et al., 1993). The dorsal gastric (DG) neuron is

another member of the gastric mill circuit whose activity coincides with that of INT1, where DG neuron activity underlies the retraction phase of the medial gastric tooth (Heinzel et al., 1993). However, the DG neuron, due to its lack of synaptic connections onto the other gastric mill neurons, does not generally contribute to the timing of activity in the gastric mill rhythm (Nusbaum and Beenhakker, 2002).

The gastric mill rhythm, which is generally not spontaneously active (Nusbaum and Beenhakker, 2002), is elicited by stimulation of projection neurons *in vitro* or bath application of neuromodulators (Nusbaum et al., 2001; Marder and Rehm, 2005). Previous work has shown that tonic stimulation of the projection neuron MCN1 readily elicits a gastric mill rhythm (Coleman et al., 1995). The cell body of MCN1 occurs as a single copy in each CoG (Figure 1.2.A), and each MCN1 elicits a gastric mill rhythm independently (Coleman and Nusbaum, 1994). Moreover, this gastric mill rhythm is activated by excitatory synaptic input from MCN1 axon terminals within the STG (Coleman et al., 1995). CPN2 is another projection neuron whose cell body is located in the CoG (Norris et al., 1994). CPN2 axon terminals innervate the STG and excite the LG neuron, while the CPN2 cell body in the CoG is strongly inhibited by INT1 (Norris et al., 1994). Although stimulation of CPN2 alone does not faithfully elicit a gastric mill rhythm (Norris et al., 1994), co-stimulation of MCN1 and CPN2 elicits a gastric mill rhythm that has a distinct motor pattern from that elicited by MCN1 stimulation alone (Blitz and Nusbaum, 1997; Beenhakker and Nusbaum, 2004). This dissertation investigates how identified synaptic connections shape the MCN1/CPN2-elicited gastric mill rhythm.

The gastric mill rhythm is also influenced by neuromodulators, which are released from the axon terminals of the projection neurons that innervate the STG (Nusbaum and Beenhakker, 2002). Previously, the gastric mill rhythm was thought to be elicited only by stimulation of projection neurons (Marder and Calabrese, 1996). However, recent experiments showed that, in the absence of projection neuron input, bath application of the neuropeptide pyrokinin (PK) to the isolated STG also elicits a gastric mill rhythm (Hertzberg et al., 2003). Hence, PK is the first known neuromodulator that faithfully elicits a gastric mill rhythm when it is bath applied to the STG. In addition, although PK elicits a gastric mill rhythm in the absence of MCN1 participation, the PK-elicited gastric mill rhythm is surprisingly similar to the MCN1-elicited rhythm, even though MCN1 does not release PK (Hertzberg et al., 2003). Thus, PK relies on a distinct functional mechanism to elicit a similar gastric mill rhythm to that elicited by MCN1 (Hertzberg and Nusbaum, 2005). This dissertation also proposes potential mechanisms by which PK can elicit such a gastric mill rhythm.

1.3.4 Reciprocal Inhibition

Reciprocal inhibition, which is at the heart of the gastric mill rhythm, is one of the most basic circuit mechanisms by which neural networks can produce rhythmic motor output (Brown, 1914; Friesen, 1994; Marder and Bucher, 2001; Marder et al., 2005). In some cases the two neurons involved in the reciprocal inhibition are identical. For example, an identical pair of reciprocally inhibitory neurons lies at the core of the rhythmic circuit that controls heartbeat in the medicinal leech (Calabrese, 1995). There have been numerous theoretical studies that have explored the properties of symmetrical reciprocally

inhibitory oscillators composed of identical pairs of neurons (Perkel and Mulloney, 1974; Wang and Rinzel, 1992; Skinner et al., 1993; Skinner et al., 1994; Van Vreeswijk et al., 1994; Nadim et al., 1995; Olsen et al., 1995; Gerstner et al., 1996; Sharp et al., 1996; White et al., 1998). However, in many other cases, the reciprocal inhibition is asymmetrical and involves a pair of neurons that is not identical. For example, a pair of non-identical neurons makes up the half-center oscillator that controls the flexor and extensor muscles in the wings of the locust (Ramirez and Pearson, 1990). In addition, the reciprocally inhibitory INT1-LG pair that lies at the heart of the gastric mill circuit is asymmetric as well (Manor et al., 1999). However, less theoretical work has been done on such asymmetrical half-center oscillators. In addition, the detailed cellular mechanisms by which projection neurons activate or modulate activity in reciprocally inhibitory circuits are generally not well understood (Zelenin, 2005). This dissertation proposes potential cellular mechanisms by which the neuromodulator PK can elicit network oscillations in the asymmetrical, reciprocally inhibitory INT1-LG pair of the gastric mill circuit.

1.4 The MCN1-Elicited Gastric Mill Rhythm

Tonic stimulation of the projection neuron MCN1 elicits a gastric mill rhythm *in vitro* (Coleman et al., 1995). In particular, excitatory synaptic input from MCN1 axon terminals in the STG activates the half-center oscillation between INT1 and the LG neuron, which are a reciprocally inhibitory pair of neurons (Figure 1.2.B) that burst in alternation (Figure 1.2.C). In addition, the LG neuron, during its burst phase,

presynaptically inhibits MCN1 axon terminals in the STG (Figure 1.2.B), which blocks the local chemical excitation from MCN1 within the STG but does not affect the MCN1 soma in the CoG (Coleman et al., 1995). Also, the LG neuron is electrically coupled locally to the MCN1 axon terminals in the STG (Figure 1.2.B). This electrical coupling is not affected by the LG presynaptic inhibition of MCN1, but the role of the electrical coupling during the gastric mill rhythm is not well understood (Coleman et al., 1995). Another member of the gastric mill circuit, the DG neuron, also receives chemical excitation from MCN1 axon terminals in the STG, and bursting in the DG neuron occurs in alternation with LG neuron bursts (Figure 1.2.C). In addition, the DG neuron is an effective reporter of MCN1 activity within the STG (Coleman et al., 1995). In particular, the DG neuron bursts in response to MCN1 excitation within the STG, but DG becomes inactive when MCN1 chemical excitation is blocked by LG neuron presynaptic inhibition of MCN1 (Figure 1.2.B). Furthermore, due to its lack of functional synaptic connections onto other STG neurons, DG is a follower neuron in the MCN1-elicited gastric mill rhythm (Coleman et al., 1995).

Subsequently, a “word model” was developed to describe how MCN1 elicits a gastric mill rhythm (Coleman et al., 1995). First, MCN1 axon terminals within the STG provide fast chemical excitation to INT1 and slow chemical excitation to the LG and DG neurons (Figure 1.2.B). MCN1 excitation allows INT1 and the DG neuron to burst, while the LG neuron remains in its interburst phase when it is inhibited by INT1 (Figure 1.2.B). Therefore, MCN1 chemical excitation slowly builds up in the LG neuron as it is inhibited by INT1. Then, when enough MCN1 excitation builds up in the LG neuron, it escapes from INT1 inhibition and begins to burst (Figure 1.2.B). During the LG burst phase, the

LG neuron inhibits INT1, which terminates the INT1 burst, and presynaptically inhibits MCN1 axon terminals. This presynaptic inhibition blocks MCN1 chemical excitation within the STG, which terminates the DG burst. The LG neuron continues in its burst phase though, since MCN1 excitation decays slowly in LG (Coleman et al., 1995). Also, the local electrical coupling between MCN1 axon terminals and the LG neuron, which is not affected by presynaptic inhibition, is believed to prolong the LG burst phase (Coleman et al., 1995). Thus, the LG neuron continues in its burst phase with the slow decay of MCN1 excitation. Then, when enough MCN1 excitation decays in the LG neuron, it falls back into its interburst phase (Figure 1.2.B) where it is inhibited by INT1. Moreover, the removal of LG presynaptic inhibition of MCN1 allows the DG neuron burst again. Subsequently, the cycle begins again as MCN1 excitation slowly builds up in the LG neuron. Thus, the slow buildup and decay of MCN1 excitation in the LG neuron determines the frequency of the MCN1-elicited gastric mill rhythm (Coleman et al., 1995).

1.4.1 Insight Gained From a Biophysically-Detailed Model

Using a biophysically-detailed model, it was then shown that the frequency of the MCN1-elicited gastric mill rhythm is very sensitive to a local synaptic input from the faster pyloric rhythm (Nadim et al., 1998). In particular, an inhibitory synapse from the pacemaker of the pyloric circuit (the AB neuron) to INT1 was shown to both increase the frequency of the MCN1-elicited gastric mill rhythm and to determine the onset of the LG burst phase (Nadim et al., 1998). The effect of the AB to INT1 inhibition is seen by the subthreshold depolarizations in the LG neuron during its interburst phase (Figure 1.3). In

particular, AB inhibition of INT1 in turn removes INT1 inhibition of the LG neuron (Figure 1.3), which effectively disinhibits the LG neuron from INT1. Moreover, this pyloric-timed interruption of the INT1 to LG inhibitory synapse shortens the duration of the LG interburst phase which increases the frequency of the MCN1-elicited gastric mill rhythm (Figure 1.4.A). Furthermore, the AB to INT1 inhibition time-locks the onset of the LG burst phase to a burst in the AB neuron (Figure 1.4.B), thus coordinating the timing of activity in the gastric mill and pyloric rhythms (Nadim et al., 1998). In particular, each burst in the LG neuron is initiated by an AB burst, and a fixed latency occurs between the onset of the LG burst and the preceding burst in AB (Nadim et al., 1998). Moreover, the period of the gastric mill rhythm is an integer multiple of the pyloric period in that an integer number of AB bursts occur in the time between the onset of two consecutive LG neuron bursts (Nadim et al., 1998).

Thus, the frequency of the MCN1-elicited gastric mill rhythm is dependent upon both the slow modulatory excitation from MCN1 and the fast pyloric-timed inhibition from AB to INT1 (Nadim et al., 1998). In addition, the biophysically-detailed model demonstrated a novel mechanism by which the frequency of a slow network oscillator is controlled by a much faster oscillatory network. For example, strengthening the AB to INT1 inhibition further shortens the duration of the LG interburst phase, which in turn further increases the frequency of the MCN1-elicited gastric mill rhythm. Moreover, the pyloric-timed AB to INT1 inhibition can adjust the gastric mill period over a range that is many times larger than the pyloric period itself (Nadim et al., 1998). Thus, the frequency of the MCN1-elicited gastric mill rhythm can be adjusted both by a direct mechanism, via

modulation of the MCN1 to LG excitatory synapse, or by an indirect mechanism, via modulation of the AB to INT1 inhibitory synapse.

Then, the predictions of the biophysically-detailed model were confirmed by experiments in the biological system (Bartos et al., 1999). In particular, it was shown that the AB to INT1 synapse in the biological system is crucial for maintaining the frequency of the natural gastric mill rhythm (Bartos et al., 1999). Moreover, the frequency of the gastric mill rhythm becomes significantly slower when the AB to INT1 synapse is removed (Bartos et al., 1999). A computational simulation based on the biological recordings of (Bartos et al., 1999) is shown in Figure 1.5.

To investigate the influence of the pyloric rhythm on the frequency of the MCN1-elicited gastric mill rhythm in the biological system, the natural pyloric rhythm was first turned off by injecting hyperpolarizing current into the AB neuron, thus disrupting its activity. Then, with the pyloric rhythm disrupted in the biological system, the dynamic clamp technique (Sharp et al., 1993a, b; Manor and Nadim, 1997) was used to create an artificial AB-to-INT1-like synaptic current. The advantage of using this artificial current is that its strength and timing could be readily manipulated by the investigator, which is something that can not be done with the endogenous currents of the biological system. Subsequently, the artificial AB-to-INT1-like synaptic current induced pyloric-timed disinhibitions in the LG neuron, similar to those which occur with the natural AB to INT1 synapse. Moreover, a significantly slower gastric mill rhythm occurred in the absence of the artificial pyloric-timed synapse, and, even though more vigorous stimulation of MCN1 elicits a faster gastric mill rhythm, the speed of the gastric mill rhythm was always slower in the absence of the pyloric-timed synapse (Bartos et al., 1999). On the

other hand, increasing the strength or frequency of the artificial synaptic input increased the frequency of the gastric mill rhythm (Bartos et al., 1999). In addition, as seen in the biophysically-detailed model, the onset of the LG burst phase remained time-locked to the artificial pyloric-timed input, even for an increased frequency in gastric mill rhythm (Bartos et al., 1999). Furthermore, as in the biophysically-detailed model, the artificial pyloric-timed input adjusted the period of the gastric mill rhythm over a range many times larger than the artificial pyloric period itself (Bartos et al., 1999). Hence, the experimental study confirmed the predictions of the biophysically-detailed model.

1.4.2 Reduction of the Biophysically-Detailed Model

The biophysically-detailed model of (Nadim et al., 1998) was then reduced to a 3-dimensional mathematical model, which was used to examine the synaptic mechanisms that give rise to the MCN1-elicited gastric mill rhythm via a mathematical analysis (Manor et al., 1999). INT1 and the LG neuron were treated as passive neurons in this reduced model; therefore, action potential generation was ignored. As a result, only the slow envelope of network oscillations was considered in the reduced model in order to simplify the network interactions and perform a mathematical analysis (Manor et al., 1999). Moreover, only graded synaptic transmission was considered in the reduced model (Manor et al., 1999). Voltage traces of INT1 and the LG neuron for the 3-dimensional model are shown in Figure 1.6.

In the absence of the AB to INT1 inhibition (Figure 1.6.A), the frequency of the MCN1-elicited gastric mill rhythm in the 3-dimensional model is dependent upon the strength and time course of the slow excitatory input from MCN1 to the LG neuron

(Manor et al., 1999), as also shown in the biophysically-detailed model (Nadim et al., 1998). However, since INT1 and LG are passive neurons in this reduced model, the transitions between their active or inactive states occur when their membrane potentials cross a synaptic threshold, not an intrinsic threshold. For example, when the LG neuron enters its active state, it presynaptically inhibits MCN1 because the LG membrane potential crosses the synaptic threshold that activates the presynaptic inhibition. Then, in the presence of the AB to INT1 inhibition, the frequency of the MCN1-elicited gastric mill rhythm is increased in the 3-dimensional model (Figure 1.6.B), as also shown in the biological system (Bartos et al., 1999). In particular, the AB to INT1 inhibition shortens the duration of the LG interburst phase which increases the frequency of the MCN1-elicited gastric mill rhythm in the reduced model (Manor et al., 1999).

Subsequently, the reduced model showed that network oscillations could be elicited in two entirely passive neurons that are connected by a graded reciprocal inhibition and receive a periodic input (Manor et al., 1999). In particular, the periodic inputs in the reduced model include a fast inhibitory synaptic input from the pyloric rhythm and a slow excitatory synaptic input from MCN1, which is converted to a periodic input by the presynaptic inhibition.

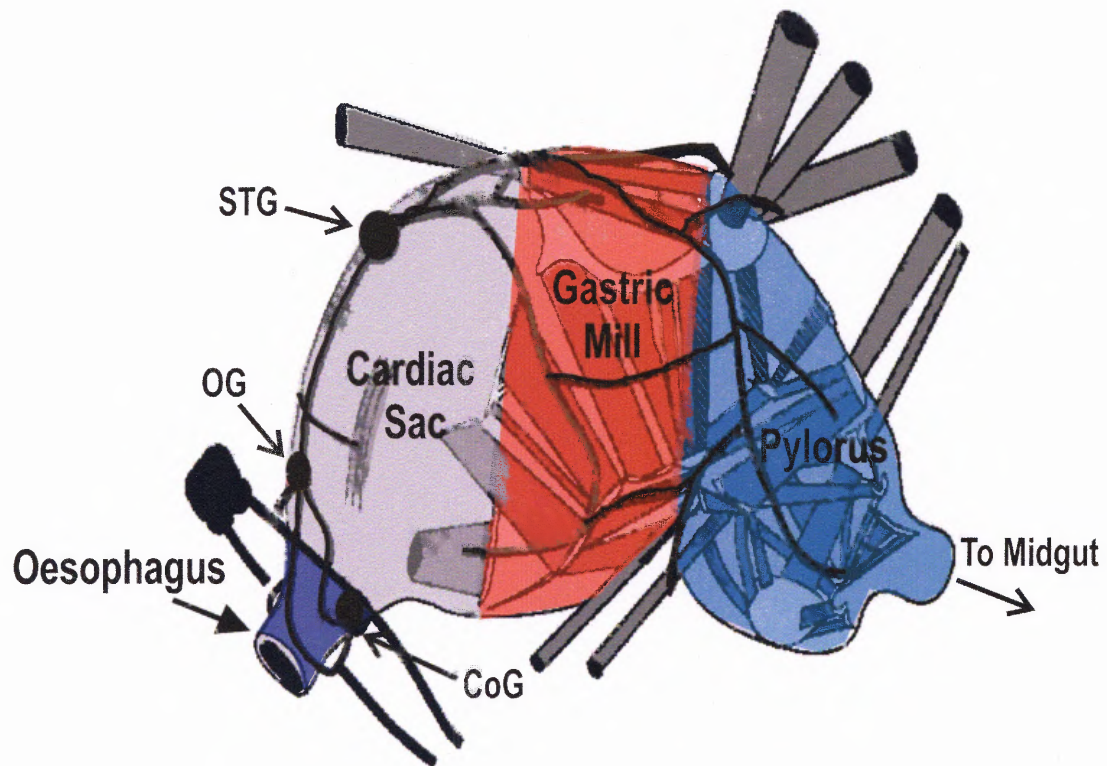


Figure 1.1 Schematic Diagram of the Crab Stomach. The four compartments of the stomach are shown. Food enters through the Oesophagus and is stored in the Cardiac Sac. Food chewing and the filtering of chewed food occur in the Gastric Mill and Pylorus, respectively. The stomatogastric nervous system (STNS) controls digestion through the stomach. The CoG, OG, and STG are ganglia within the STNS, while the dvn, lvn, and mvn are major nerves that contract the musculature of the of the Gastric Mill and Pylorus. Abbreviations: Ganglia - CoG, Commissural ganglion; OG, Oesophageal ganglion; STG, stomatogastric ganglion. Nerves - dvn, dorsal ventricular nerve; lvn, lateral ventricular nerve; mvn, medial ventricular nerve.

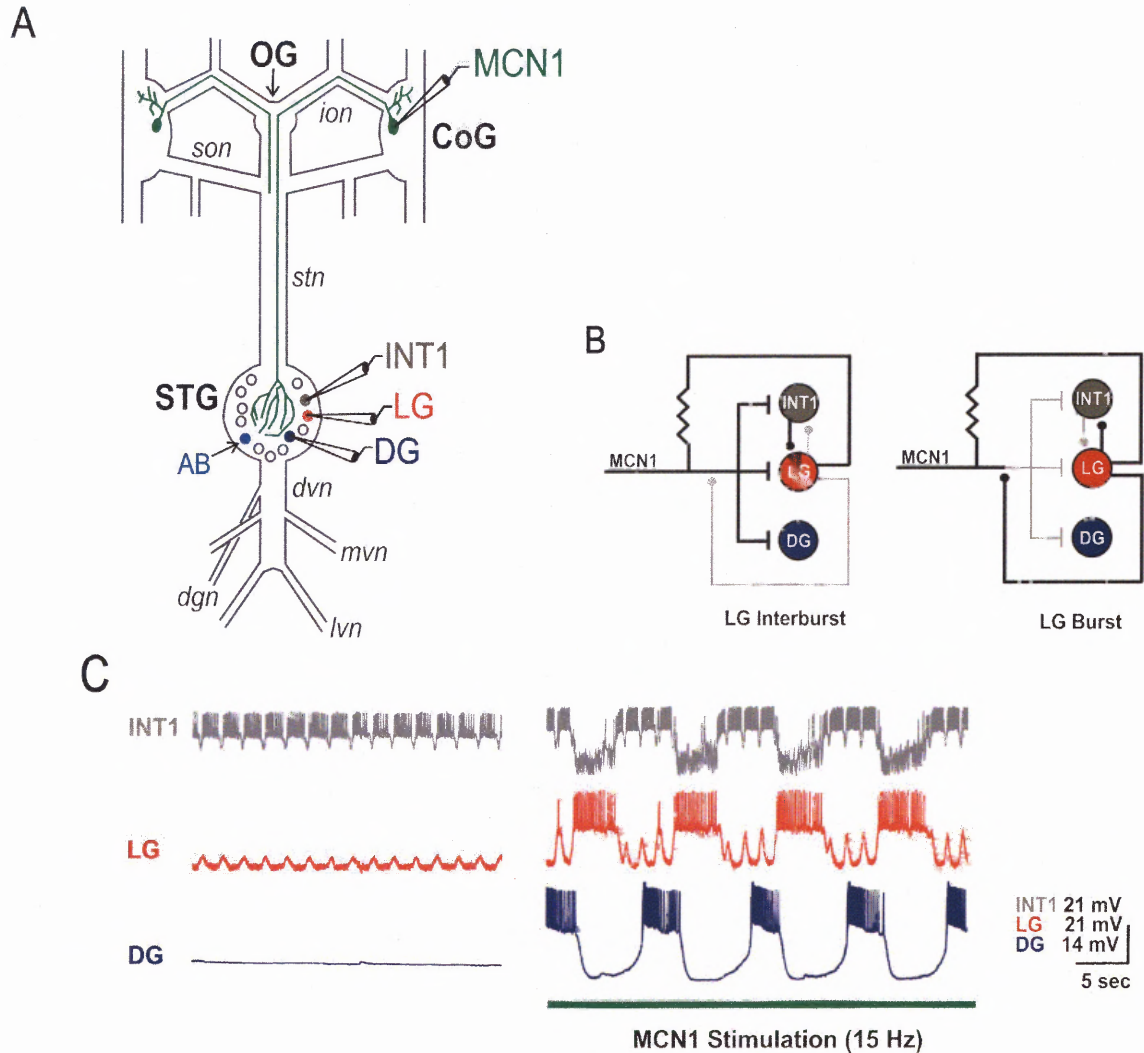


Figure 1.2 The MCN1-Elicited Gastric Mill Rhythm in *C. borealis*. *A*, Simplified diagram of the stomatogastric nervous system. The cell body of the projection neuron MCN1 occurs as a single copy in each CoG, and each MCN1 influences the gastric mill circuit independently. MCN1 projects through the *ion* and *stn* nerves into the STG, where its axon terminals influence the gastric mill neurons INT1, LG and DG. Abbreviations: Nerves – *ion*, inferior oesophageal nerve; *son*, superior oesophageal nerve; *stn*, stomatogastric nerve. Neurons – INT1, interneuron 1; LG, lateral gastric neuron; DG, dorsal gastric neuron. *B*, MCN1 axon terminals provide chemical excitation (t-bars) to the gastric mill neurons. The LG neuron presynaptically inhibits (filled circle) MCN1 within the STG and is also electrically coupled to MCN1 terminals (resistor symbol). INT1 and LG reciprocally inhibit each other. *C*, Tonic stimulation of MCN1 elicits a gastric mill rhythm where the LG neuron bursts in anti-phase with INT1 and DG (Adapted by permission from Macmillan Publishers Ltd: Nature (Coleman et al., 378:502-505, 1995), copyright (1995)). INT1 and the LG neuron burst in anti-phase due to their reciprocal inhibition. The LG and DG neurons burst in anti-phase due to LG presynaptic inhibition of MCN1. Most hyperpolarized membrane potentials: INT1 -46 mV; LG -58 mV; DG -64 mV.

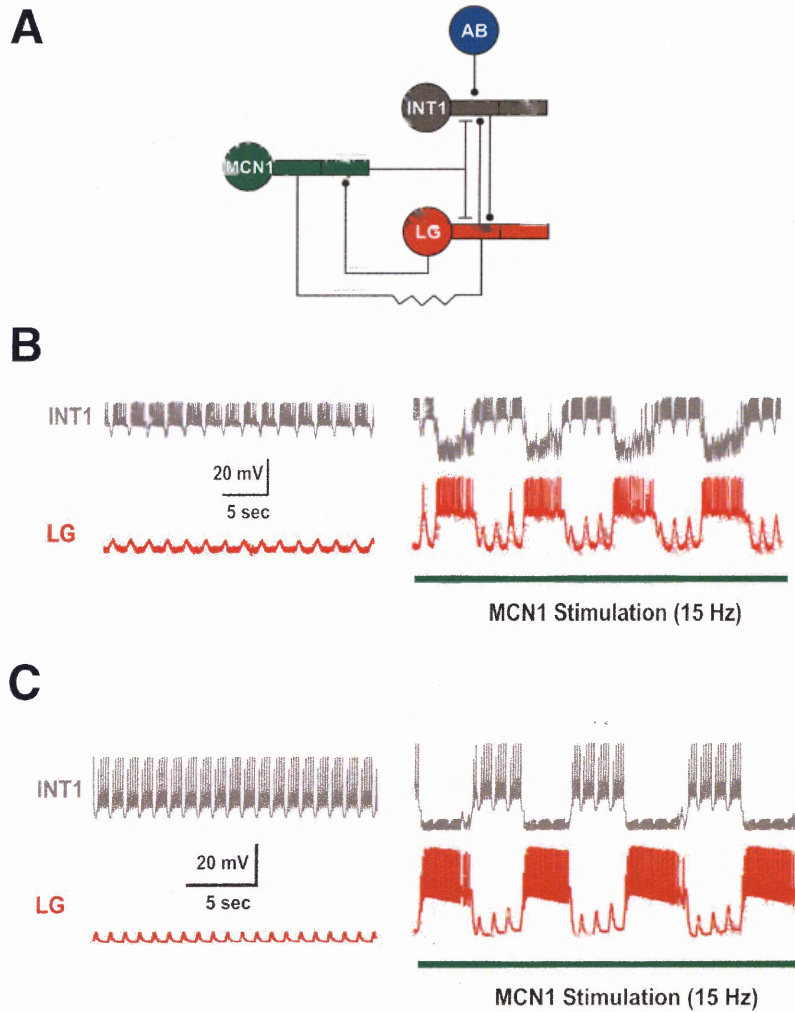


Figure 1.3 Biophysically-Detailed Model of the MCN1-Elicited Gastric Mill Rhythm. *A*, Schematic representation of the model neurons. *B*, Intracellular recordings of INT1 and the LG neuron in the biological system (Adapted by permission from Macmillan Publishers Ltd: Nature (Coleman et al., 378:502-505, 1995), copyright (1995)). Most hyperpolarized membrane potentials: INT1 -46 mV; LG -58 mV. *C*, Voltage traces of INT1 and the LG neuron in a simulation of the biophysically-realistic model. Most hyperpolarized membrane potentials: INT1 -71 mV; LG -56 mV.

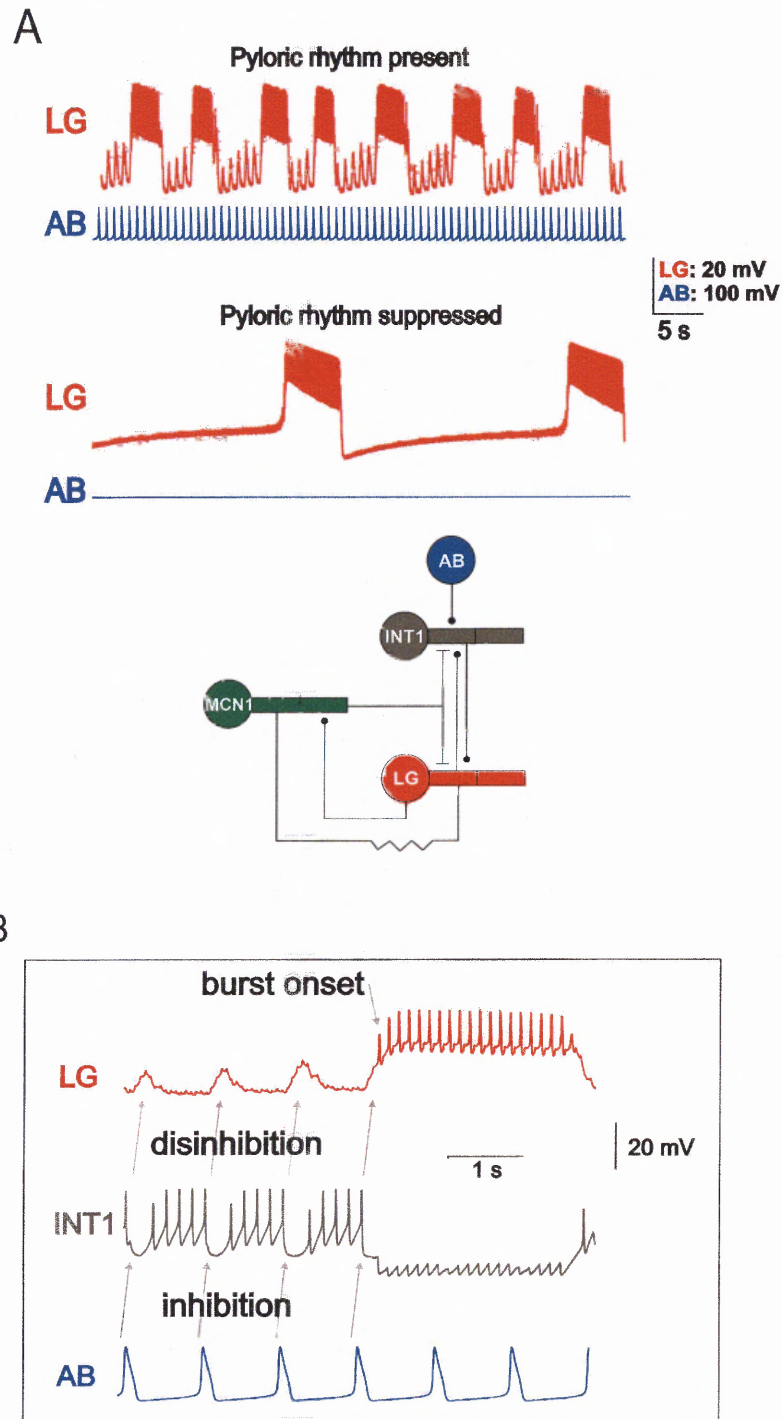


Figure 1.4 Effect of the Pyloric-Timed Inhibition from the AB Neuron to INT1. A, AB neuron inhibition of INT1 increases the frequency of the MCN1-elicited gastric mill rhythm. **B,** AB inhibition of INT1 in turn disrupts INT1 inhibition of the LG neuron which disinhibits the LG neuron from INT1, as seen by the subthreshold depolarizations in the LG membrane potential. Moreover, AB inhibition of INT1 triggers the onset of the LG burst phase.

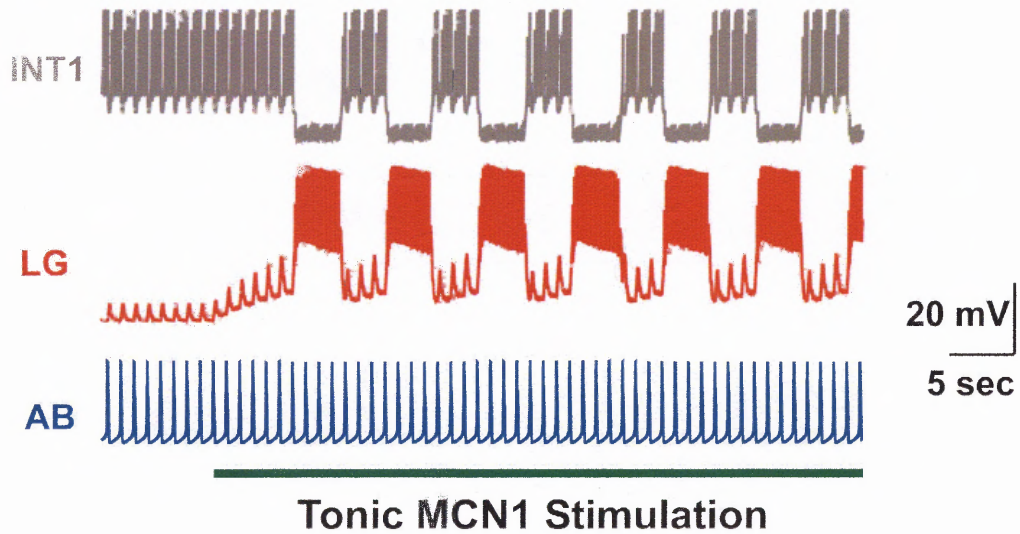


Figure 1.5 Simulation of the MCN1-Elicited Gastric Mill Rhythm. This simulation is based upon the intracellular biological recordings of Bartos et al., 1999. Voltage traces for INT1, the LG neuron and the AB neuron are shown, and the gastric mill rhythm is not spontaneously active in the absence of MCN1 stimulation. Most hyperpolarized membrane potentials: INT1 -61 mV, LG -60 mV, AB -64 mV.

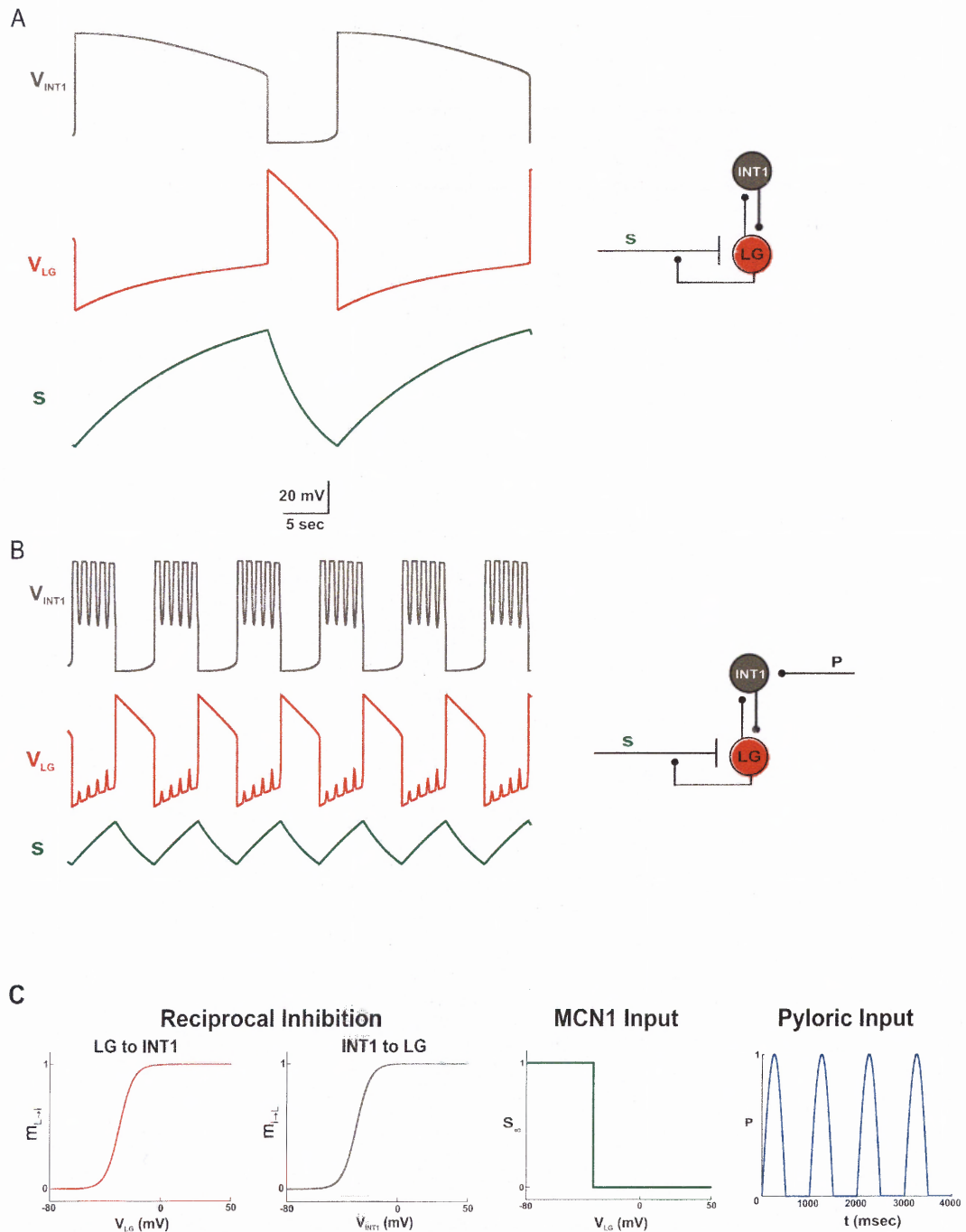


Figure 1.6 Three-Dimensional Model of the MCN1-Elicited Gastric Mill Rhythm where INT1 and LG are Passive Neurons. *A*, MCN1 input (s) drives the gastric mill rhythm, where s builds up in the LG neuron during its inactive state but decays during the active state of LG due to the presynaptic inhibition of MCN1. *B*, The inhibitory synaptic input from AB to INT1 increases the frequency of network oscillations. *C*, Synaptic transfer functions in the three-dimensional model.

CHAPTER 2

COMPARING PROJECTION-NEURON-ELICITED AND NEUROMODULATOR-ELICITED OSCILLATIONS IN A RHYTHMIC NETWORK: A REDUCED MATHEMATICAL MODEL

2.1 Introduction

Network activity is often conditional upon the presence of neuromodulators, which are typically released as hormones or neurotransmitters of projection neurons (Marder and Thirumalai, 2002). In some cases, bath application of a neuromodulator produces the same result as the projection neuron from which it is released (Nusbaum et al., 2001). However, this is generally not the case since bath application of a neuromodulator does not account for the often complex synaptic interactions between a projection neuron and its target network (Nusbaum and Beenhakker, 2002).

This dissertation uses the gastric mill rhythm of the crab, *Cancer borealis*, to investigate these issues. The gastric mill rhythm is generally not spontaneously active, but tonic stimulation of the projection neuron MCN1 elicits a gastric mill rhythm *in vitro* (Coleman et al., 1995). Both excitatory synaptic input from MCN1 axon terminals within the STG plus presynaptic inhibition of these terminals by the LG neuron are believed to be necessary for generating a gastric mill rhythm (Coleman et al., 1995). However, recent experiments showed that bath application of the neuromodulator pyrokinin (PK) to the isolated STG elicits a similar gastric mill rhythm in the absence of MCN1 participation (Hertzberg and Nusbaum, 2004). Thus, PK relies on distinct network components to elicit a gastric mill rhythm (Hertzberg and Nusbaum, 2005). In addition, MCN1 does not release PK, and no combination of MCN1 co-transmitters elicits a gastric mill rhythm upon bath application to the STG (Wood et al., 2000). Moreover, PK is the

first known neuromodulator to elicit a gastric mill rhythm when bath applied to the STG. Yet, the mechanism by which PK elicits a gastric mill rhythm is unknown.

This dissertation uses mathematical modeling to propose three potential mechanisms by which PK can elicit a gastric mill rhythm that is similar to the MCN1-elicited rhythm. First, a reduced 2-dimensional model of the MCN1-elicited gastric mill rhythm is developed which is based upon the 3-dimensional model of Manor et al., (1999). The 3-dimensional model is a reduction of a more biophysically-detailed model (Nadim et al., 1998), and it was used to investigate, via a mathematical analysis, the synaptic mechanisms that underlie the MCN1-elicited gastric mill rhythm. A later study proved the existence and stability of periodic oscillations in the mathematical model and computed their frequency (Ambrosio-Mouser et al., 2006). Now, this dissertation reduces the 3-dimensional model of (Manor et al., 1999) down to 2 dimensions, where both state variables are directly involved in generating network oscillations. As a result, the network dynamics of the 2-dimensional model are readily examined via a phase-plane analysis. Next, three types of ionic currents, which may be potentially activated by PK in the gastric mill neurons, are proposed which allow for PK to elicit a gastric mill rhythm that is similar to the MCN1-elicited rhythm. Then, after generalizing the MCN1- and PK-elicited rhythms into a single 2-dimensional model, geometrical properties are used to compute bounds on the gastric mill period to account for the cycle-to-cycle variability induced by a synaptic input from the pyloric circuit.

2.2 Methods

2.2.1 Three-Dimensional Model of the MCN1-Elicited Gastric Mill Rhythm

First, the 3-dimensional model of (Manor et al., 1999), that was introduced in the previous chapter, is described in more detail. The MCN1-elicited gastric mill rhythm is shaped by the reciprocal inhibition between INT1 and the LG neuron. As most synapses in the STG have a large graded component (Graubard et al., 1980), INT1 and the LG neuron operate with graded synaptic transmission in the 3-dimensional model of the MCN1-elicited gastric mill rhythm (Manor et al., 1999). Moreover, INT1 and LG are treated as passive neurons in the 3-dimensional model. In particular, they do not include voltage-gated ionic currents so that action potential generation in them can be ignored. As a result, only the slow envelope of network oscillations was considered by (Manor et al., 1999) in order to simplify the network interactions and perform a mathematical analysis.

The state variables of the 3-dimensional model are designated by V_I (V_H in (Manor et al., 1999)), V_L and s which represent, respectively, the membrane potential of INT1, the membrane potential of the LG neuron, and the slow, excitatory synaptic input from MCN1 to the LG neuron. This model is governed by the set of coupled ordinary differential equations given by

$$C_I \frac{dV_I}{dt} = - \underbrace{g_{Leak,I} (V_I - E_{Leak,I})}_{I_{Leak,I}} - \underbrace{\bar{g}_{L \rightarrow I} m_{L \rightarrow I} (V_L) (V_I - E_{L \rightarrow I})}_{I_{L \rightarrow I}} - \underbrace{\bar{g}_P P(t) (V_I - E_P)}_{I_P} \quad (2.1)$$

$$C_L \frac{dV_L}{dt} = - \underbrace{g_{Leak,L} (V_L - E_{Leak,L})}_{\mathbf{I}_{Leak,L}} - \underbrace{\bar{g}_{I \rightarrow L} m_{I \rightarrow L} (V_I) (V_L - E_{I \rightarrow L})}_{\mathbf{I}_{I \rightarrow L}} - \underbrace{\bar{g}_s s (V_L - E_s)}_{\mathbf{I}_s} \quad (2.2)$$

$$\frac{ds}{dt} = \begin{cases} \frac{1-s}{\tau_{LO_{mcn1}}}, & V_L \leq v_{pre} \\ \frac{-s}{\tau_{HI_{mcn1}}}, & V_L > v_{pre} \end{cases}, \quad (2.3)$$

whose derivation is explained in detail in (Manor et al., 1999). The parameters C_I and C_L represent the membrane capacitance of INT1 and of the LG neuron, respectively, and are set to 1 for simplicity. The terms $\mathbf{I}_{Leak,I}$ and $\mathbf{I}_{Leak,L}$ in Equations (2.1) and (2.2), respectively, model the leak current in each neuron. In particular, the parameters $g_{Leak,I}$ and $E_{Leak,I}$ represent the conductance and reversal potential, respectively, of the leak current in INT1, while $g_{Leak,L}$ and $E_{Leak,L}$ represent the same quantities for the leak current in the LG neuron. In the absence of projection neuron input in the biological system, INT1 remains active and exhibits a high membrane potential while the LG neuron remains inactive and exhibits a low membrane potential (Bartos et al., 1999). This asymmetry between INT1 and the LG neuron is modeled by assigning a high value to $E_{Leak,I}$ and a low value to $E_{Leak,L}$ (see **Table 2.1**).

The terms $\mathbf{I}_{L \rightarrow I}$ and $\mathbf{I}_{I \rightarrow L}$ in Equations (2.1) and (2.2), respectively, model the reciprocally inhibitory synapses between INT1 and the LG neuron (inset of Figure 2.1). In particular, the parameters $\bar{g}_{L \rightarrow I}$ and $E_{L \rightarrow I}$ in Equation (2.1) represent the maximal conductance and reversal potential, respectively, of the inhibitory synapse from the LG neuron to INT1, while $\bar{g}_{I \rightarrow L}$ and $E_{I \rightarrow L}$ in Equation (2.2) represent the same quantities for

the INT1 to LG synapse. Moreover, these reciprocally inhibitory synapses are controlled by the synaptic gating functions $m_{L \rightarrow I}(V_L)$ and $m_{I \rightarrow L}(V_I)$, which depend only on the membrane potential of the presynaptic neuron and are modeled by the sigmoidal functions

$$m_{L \rightarrow I}(V_L) = \frac{1}{1 + \exp((v_{L \rightarrow I} - V_L)/k_{L \rightarrow I})} \quad (2.4)$$

$$m_{I \rightarrow L}(V_I) = \frac{1}{1 + \exp((v_{I \rightarrow L} - V_I)/k_{I \rightarrow L})}. \quad (2.5)$$

The parameters $v_{L \rightarrow I}$ and $k_{L \rightarrow I}$ in Equation (2.4) specify the synaptic inflection point voltage and steepness, respectively, of the sigmoid that gates the LG to INT1 synapse. Similarly, $v_{I \rightarrow L}$ and $k_{I \rightarrow L}$ of Equation (2.5) specify the same quantities for the sigmoid that gates the INT1 to LG synapse. It is noted that Equations (2.4) and (2.5) are obtained from

$$\tau_{m_{pre \rightarrow post}}(V_{pre}) \frac{dm_{pre \rightarrow post}}{dt} = m_{\infty_{pre \rightarrow post}}(V_{pre}) - m_{pre \rightarrow post}, \quad (2.6)$$

where *pre* and *post* designate the pre- and postsynaptic neuron, by setting the time constant $\tau_{m_{pre \rightarrow post}}(V_{pre}) = 0$, so that the sigmoids which gate the reciprocally inhibitory synapses act instantaneously and depend only on the presynaptic membrane potential.

The term \mathbf{I}_P in Equation (2.1) is modeled as a synaptic input that represents the local inhibitory synapse from the pacemaker of the pyloric circuit (the AB neuron) to INT1. The parameters \bar{g}_p and E_p represent its maximal conductance and reversal potential, respectively. In the biological system, the frequency of the pyloric rhythm ($\sim 1\text{Hz}$) is much faster than that of the gastric mill rhythm ($\sim 10\text{ Hz}$) (Bartos et al., 1999). Therefore, in the 3-dimensional model of (Manor et al., 1999), $P(t)$, within the \mathbf{I}_P term of Equation (2.1), is modeled a fast, periodic forcing function that oscillates in $[0,1]$. In particular, $P(t)$ is modeled by the half-sine function

$$P(t) = \sin\left(\frac{\pi \text{mod}(t, per)}{dur}\right) H(dur - \text{mod}(t, per)), \quad (2.7)$$

where the parameters per and dur represent its period and duty cycle, while $\text{mod}()$ and $H()$ designate modulo and Heaviside functions, respectively.

The term \mathbf{I}_s in Equation (2.2) models the slow, excitatory synaptic input from the axon of MCN1 to the LG neuron. The parameters \bar{g}_s and E_s represent its maximal conductance and reversal potential, respectively. This slow synaptic input is gated by the membrane potential of the LG neuron (V_L) via presynaptic inhibition of MCN1 (Manor et al., 1999), and the dynamics of this input are modeled by Equation (2.3). In particular, MCN1 excitation (s) builds up in the LG neuron with time constant $\tau_{LO_{mcn1}}$ when V_L is below the synaptic threshold voltage v_{pre} for presynaptic inhibition of MCN1. As a result, the buildup of s in the LG neuron causes V_L to slowly rise (see Figure 1.6 of the previous chapter). When V_L exceeds v_{pre} , s decays in the LG neuron with time constant

$\tau_{HI_{mcn1}}$, due to presynaptic inhibition of MCN1, which causes V_L to slowly fall (see Figure 1.6). It is noted that $\tau_{LO_{mcn1}}$, $\tau_{HI_{mcn1}}$, and v_{pre} are designated by τ_r , τ_f , and v_T in (Manor et al., 1999).

In the biological system, the frequency of the MCN1-elicited gastric mill rhythm is controlled by the excitatory synapse from MCN1 to the LG neuron which acts on a slower time scale than that of all other synapses in the network (Coleman et al., 1995). As a result, the time constants $\tau_{LO_{mcn1}}$ and $\tau_{HI_{mcn1}}$ in Equation (2.3) are assigned with large values to model the slow synaptic time scale of the MCN1 to LG synapse. This slow time scale is revealed by rewriting Equation (2.3) in the form

$$\frac{ds}{dt} = \frac{H(v_{pre} - V_L) - s}{\tau_{HI_{mcn1}} + (\tau_{LO_{mcn1}} - \tau_{HI_{mcn1}}) H(v_{pre} - V_L)} = \varepsilon \left(\frac{H(v_{pre} - V_L) - s}{1 + (\tilde{\tau} - 1) H(v_{pre} - V_L)} \right), \quad (2.8)$$

where $0 < \varepsilon = \frac{1}{\tau_{HI_{mcn1}}} \ll 1$ and $\tilde{\tau} = \frac{\tau_{LO_{mcn1}}}{\tau_{HI_{mcn1}}}$. As a result, since ε is small, the state variable s in Equation (2.3) evolves much more slowly than the other state variables and controls the frequency of network oscillations (see Figure 1.6).

2.2.2 Reduction to a 2-Dimensional Model of the MCN1-Elicited Gastric Mill Rhythm

While INT1 is only influenced by synaptic inputs that occur on a fast time scale, the LG neuron, on the other hand, is influenced by the slow excitatory synapse from MCN1 (see Figure 1.6). This difference in synaptic time scales can be exploited to reduce the 3-

dimensional model of (Manor et al., 1999) down to 2 dimensions involving the state variables V_L and s . In particular, the membrane potential of INT1 (V_I) can be assumed to adjust instantaneously to its steady for each value of V_L and s , since INT1 is only influenced by fast synaptic inputs. Thus, dividing through Equation (2.1) by the leak conductance $g_{Leak,I}$ gives

$$\tau_I \frac{dV_I}{dt} = -(V_I - E_{Leak,I}) - \frac{\bar{g}_{L \rightarrow I}}{g_{Leak,I}} m_{L \rightarrow I}(V_L)(V_I - E_{L \rightarrow I}) - \frac{\bar{g}_P}{g_{Leak,I}} P(t)(V_I - E_P), \quad (2.9)$$

where $\tau_I = \frac{C_I}{g_{Leak,I}}$ is the membrane time constant of INT1. Then, setting $\tau_I = 0$ sets the

left hand side of Equation (2.9) to zero and allows for an explicit solution of the INT1 membrane potential given by

$$V_I = u(V_L; P(t)) = \frac{g_{Leak,I} E_{Leak,I} + \bar{g}_{L \rightarrow I} m_{L \rightarrow I}(V_L) E_{L \rightarrow I} + \bar{g}_P P(t) E_P}{g_{Leak,I} + \bar{g}_{L \rightarrow I} m_{L \rightarrow I}(V_L) + \bar{g}_P P(t)}. \quad (2.10)$$

As a result, V_I is now expressed in terms of the state variable V_L and the periodic forcing function $P(t)$, which models the fast inhibition of INT1 by the pyloric circuit (inset of Figure 2.1). However, in the biological system, this pyloric inhibition of INT1 does not affect the gastric mill rhythm during the active state of the LG neuron (Bartos et al., 1999). This biological fact is incorporated into the model by making the pyloric forcing function dependent upon the membrane potential of LG as well

$$P(t, V_L) = P(t)q(V_L). \quad (2.11)$$

In particular, $P(t)$ is the same periodic forcing function of Equation (2.7) while $q(V_L)$ is a decreasing sigmoid of V_L given by

$$q(V_L) = \frac{1}{1 + \exp\left(\frac{V_L - v_q}{k_q}\right)}, \quad (2.12)$$

where the parameters v_q and k_q represent its inflection point voltage and steepness, respectively. Thus, the pyloric inhibition term of Equation (2.11) now only affects the gastric mill rhythm during the inactive state of the LG neuron (see Results).

Subsequently, after replacing $P(t)$ with the $P(t, V_L)$ term of Equation (2.11), the expression for the membrane potential of INT1 in Equation (2.10) becomes $V_I = u(V_L; P(t, V_L))$. Then, substitution of this V_I expression into the $m_{I \rightarrow L}(V_I)$ term of Equation (2.2) gives a 2-dimensional model of the MCN1-elicited gastric mill rhythm

$$\frac{dV_L}{dt} = - \underbrace{g_{Leak,L}(V_L - E_{Leak,L})}_{I_{Leak,L}} - \underbrace{\bar{g}_{I \rightarrow L} m_{I \rightarrow L}(u(V_L; P(t, V_L))) (V_L - E_{I \rightarrow L})}_{I_{I \rightarrow L}} - \underbrace{\bar{g}_s s(V_L - E_s)}_{I_s} \quad (2.13)$$

$$\frac{ds}{dt} = \begin{cases} \frac{1-s}{\tau_{LO_{mcn1}}}, & V_L \leq v_{pre} \\ -s, & V_L > v_{pre} \\ \frac{-s}{\tau_{HI_{mcn1}}}, & \end{cases} \quad (2.14)$$

Thus, the dynamics of INT1 have been absorbed into the dynamics of the state variable V_L (Figure 2.1). As a result, the effects of the fast inhibitory synapses that influence INT1 are absorbed into the INT1 to LG synapse, as indicated by the $m_{I \rightarrow L}(u(V_L; P))$ term of Equation (2.13) (see also Figure 2.1). It is also noted that the membrane capacitance $C_L = 1$ in Equation (2.13). Thus, the 3-dimensional model of (Manor et al., 1999) has been reduced to 2 dimensions where both state variables are directly involved in generating network oscillations. This allows for a complete examination of the network dynamics of the MCN1-elicited gastric mill rhythm via a phase-plane analysis in the V_L - s plane.

Next, the phase-plane geometry of the 2-dimensional model is examined. First, the V_L - and s -nullclines are computed, which designate the curves in the V_L - s phase plane where $dV_L/dt = 0$ and $ds/dt = 0$, respectively. Physiologically, the V_L -nullcline specifies the value to which V_L would settle for a given value of s , the excitation from MCN1. Similarly, the s -nullcline specifies the steady-state value of s for a given value of V_L . The V_L -nullcline is computed by setting $dV_L/dt = 0$ in Equation (2.13) and solving for s . However, it is noted that the 2-dimensional model is non-autonomous due to the pyloric forcing term $P(t, V_L)$ of Equation (2.13). This allows a family of V_L -nullclines to exist in the phase plane. In particular, a one-parameter family of V_L -nullclines indexed by the values p in $[0,1]$ of $P(t, V_L)$ exists in the V_L - s phase plane as given by

$$s(V_L; p) = - \frac{g_{Leak,L}(V_L - E_{Leak,L}) + \bar{g}_{I \rightarrow L} m_{I \rightarrow L}(u(V_L; p))(V_L - E_{I \rightarrow L})}{\bar{g}_s (V_L - E_s)}. \quad (2.15)$$

Equation (2.15) describes a cubic V_L -nullcline for a given value of p , where the extreme values $p = 0$ ($p = 1$) correspond to the unforced (maximally forced) system. The s -nullcline, on the other hand, is computed by setting $ds/dt = 0$ in Equation (2.14) and solving for s to obtain the step function

$$s = \begin{cases} 0, & V_L \leq v_{pre} \\ 1, & V_L > v_{pre} \end{cases}. \quad (2.16)$$

In the unforced system, where $p = 0$ in Equation (2.15), a single cubic V_L -nullcline exists in the phase plane, given by $s(V_L; 0)$. Equivalently, this corresponds to when $P(t, V_L) = 0$ in Equation (2.13), so that the 2-dimensional system becomes autonomous and only one V_L -nullcline exists in the phase plane. Within the V_L - s phase plane, $dV_L/dt > 0$ (< 0) above (below) the V_L -nullcline while $ds/dt > 0$ (< 0) below (above) the s -nullcline. Therefore, the outer branches of the cubic V_L -nullcline are stable (attracting) while its middle branch is unstable (repelling). In addition, the V_L - and s -nullclines intersect along the unstable middle branch of the cubic, which allows the system to exhibit oscillations (Rinzel and Ermentrout, 1998). Furthermore, the time constants of MCN1 excitation ($\tau_{LO_{mcn1}}$, $\tau_{HI_{mcn1}}$) are chosen to be large in order to put the system in a relaxation regime. As a result, the periodic orbit in the V_L - s phase plane consists of two fast and two slow portions (Figure 2.1.C.1), in which the slow portions track the outer branches of the cubic to which they are strongly attracted by the fast horizontal flow. Furthermore, the periodic orbit in the V_L - s phase plane describes the

oscillation in the LG membrane potential (Figure 2.1.C.2) during the gastric mill rhythm (see Results).

In the forced system, where $0 \leq p \leq 1$ in Equation (2.15), a family of cubic V_L -nullclines exists in the phase plane. Two members of this family are shown in Figure 2.1.D.1. In particular, the higher cubic occurs when $p = 0$ and corresponds to the unforced system of Figure 2.1.C.1, while the lower cubic occurs when $p = 1$ and corresponds to the maximally forced system at the peak of the pyloric forcing. Thus, the pyloric forcing term shifts the V_L -nullcline as p varies in $[0,1]$, which causes the trajectory to shift back and forth between the higher and lower cubics (Figure 2.1.D.1). The transitions between cubics are impulsive since the pyloric peak is small compared to the pyloric period. Thus, when $p = 0$ in Equation (2.15), the trajectory in the V_L - s phase plane tracks the higher (unforced) cubic (Figure 2.1.D.1), then shifts through a family of lower cubics for nonzero values of p and touches the lowest (maximally forced) cubic at $p = 1$ (Figure 2.1.D.1). Physiologically, the pyloric forcing term models the effect of the inhibitory synapse from the pyloric circuit to INT1 (inset of Figure 2.1) on the network dynamics of the gastric mill rhythm. In particular, the pyloric inhibition of INT1 in turn weakens the INT1 to LG inhibition (inset of Figure 2.1), which effectively “disinhibits” the LG neuron from INT1, as illustrated by the periodic subthreshold depolarizations in the membrane potential of LG (Figure 2.1.D.2) (see Results). Moreover, as modeled by Equation (2.11), the pyloric forcing only affects the inactive state of the LG neuron and therefore only shifts the left branch of the V_L -nullcline. The right branch of the V_L -nullcline, which corresponds to the active state of the LG neuron, remains stationary

since the effect of the pyloric forcing is not effectively transmitted through the INT1 to LG synapse during the active state of the LG neuron (see Results).

The simulations in Figure 2.1 were performed with the parameter values given in **Table 2.1**. The unforced system (Figures 2.1.A, 2.1.C.1, 2.1.C.2) was simulated by setting the maximal conductance $\bar{g}_p = 0$. The software XPPAUT (Ermentrout, 2002) was used to perform the numerical simulations in this chapter.

2.2.3 Building a 2-Dimensional Model of the Pyrokinin-Elicited Gastric Mill Rhythm

The 2-dimensional model of the MCN1-elicited rhythm given by Equations (2.13) and (2.14) is now used to investigate how the neuropeptide pyrokinin (PK) can elicit a similar gastric mill rhythm in the absence of MCN1 participation. First, the slow, excitatory input from MCN1 is removed from the model by setting its conductance $\bar{g}_s = 0$ on the right hand side of Equation (2.13) to get

$$\frac{dV_L}{dt} = - \underbrace{g_{Leak,L} (V_L - E_{Leak,L})}_{I_{Leak,L}} - \underbrace{\bar{g}_{I \rightarrow L} m_{I \rightarrow L} (u(V_L; P(t, V_L))) (V_L - E_{I \rightarrow L})}_{I_{I \rightarrow L}}. \quad (2.17)$$

In the absence of MCN1 input in the biological system, the LG neuron remains inactive as it is strongly inhibited by INT1 (Bartos et al., 1999). Therefore, the reciprocal inhibition between INT1 and the LG neuron is asymmetric, and the model gastric mill rhythm is not spontaneously active in the absence of MCN1 input (see Figure 2.2), as also occurs in the biological system (Bartos et al., 1999). Recent experiments showed

that bath application of PK to the isolated STG elicits a gastric mill rhythm that is very similar to the MCN1-elicited rhythm (Hertzberg and Nusbaum, 2004, 2005). However, the mechanism by which PK elicits a gastric mill rhythm is unknown. This dissertation proposes three potential mechanisms by which PK can elicit a gastric mill rhythm. The hypothesis of this work is that PK elicits a gastric mill rhythm via activation of voltage-gated ion channels in the LG neuron to balance the asymmetry in the INT1-LG reciprocal inhibition. Three different types of ionic currents are proposed that, when potentially activated by PK in the LG neuron, will elicit a gastric mill rhythm that is similar to the MCN1-elicited rhythm.

2.2.3.1 *Introducing I_{plat} in the LG neuron.* As a first proposed mechanism by which PK elicits a similar gastric mill rhythm, a slowly-inactivating inward current is introduced into the LG neuron given by

$$I_{plat} = \bar{g}_{plat} a_{\infty}(V_L) n(V_L - E_{plat}). \quad (2.18)$$

The parameters \bar{g}_{plat} and E_{plat} designate its maximal conductance and equilibrium potential, respectively. In addition, E_{plat} is set above the resting potential of the LG neuron (given by $E_{Leak,L}$ in Equation (2.13)) to model I_{plat} as an inward current. The kinetics of activation for I_{plat}

$$\tau_a(V_L) \frac{da}{dt} = a_{\infty}(V_L) - a \quad (2.19)$$

are ignored by setting the time constant $\tau_a(V_L) = 0$. Therefore, activation of I_{Plat} is approximated by an instantaneous sigmoidal function of the LG membrane potential given by

$$a_\infty(V_L) = \frac{1}{1 + \exp((v_a - V_L)/k_a)}, \quad (2.20)$$

where the parameters v_a and k_a specify the inflection point voltage and steepness of the sigmoid, respectively. On the other hand, inactivation of I_{Plat} given by

$$\tau_n(V_L) \frac{dn}{dt} = H(v_{inact} - V_L) - n \quad (2.21)$$

is slow and follows the time constant

$$\tau_n(V_L) = \begin{cases} \tau_{LO_{inact}}, & V_L \leq v_{inact} \\ \tau_{HI_{inact}}, & V_L > v_{inact} \end{cases}. \quad (2.22)$$

Thus, the dynamics for inactivation of I_{Plat} are modeled by

$$\frac{dn}{dt} = \begin{cases} \frac{1-n}{\tau_{LO_{inact}}}, & V_L \leq v_{inact} \\ \frac{-n}{\tau_{HI_{inact}}}, & V_L > v_{inact} \end{cases}. \quad (2.23)$$

In particular, I_{Plat} slowly de-inactivates with time constant $\tau_{LO_{inact}}$ when V_L is below the voltage threshold v_{inact} for inactivation (Figure 2.3). This allows I_{Plat} to flow into and depolarize the LG neuron so that V_L slowly rises (see Results, Figure 2.4). When V_L exceeds v_{inact} , I_{Plat} inactivates with time constant $\tau_{HI_{inact}}$. This restricts the flow of I_{Plat} into the LG neuron so that V_L slowly falls (see Results, Figure 2.4). It is noted that I_{Plat} in this work is similar to the low-threshold, slowly-inactivating, Ca^{2+} -dependent current (I_{CaS}) found in the medicinal leech which promotes rhythmic bursting in the reciprocally inhibitory circuit that controls heartbeat (Angstadt and Calabrese, 1991; De Schutter et al., 1993).

To build a 2-dimensional model of the PK-elicited gastric mill rhythm, Equation (2.18) is subtracted from the right hand side of Equation (2.17), and the inactivation of I_{Plat} forms the second state variable. Therefore, a 2-dimensional model of the PK-elicited gastric mill rhythm in which PK activates I_{Plat} in the LG neuron is given by

$$\begin{aligned} \frac{dV_L}{dt} = & -g_{Leak,L} (V_L - E_{Leak,L}) - \bar{g}_{I \rightarrow L} m_{I \rightarrow L} (u(V_L; P(t, V_L))) (V_L - E_{I \rightarrow L}) \\ & - \underbrace{\bar{g}_{plat} a_\infty(V_L) n(V_L - E_{plat})}_{I_{Plat}} \end{aligned} \quad (2.24)$$

$$\frac{dn}{dt} = \begin{cases} \frac{1-n}{\tau_{LO_{inact}}}, & V_L \leq v_{inact} \\ \frac{-n}{\tau_{HI_{inact}}}, & V_L > v_{inact} \end{cases} \quad (2.25)$$

Next, the phase-plane geometry of this 2-dimensional model is examined. As in the case of the MCN1-elicited rhythm, the periodic, pyloric-timed forcing term modeled by $P(t, V_L)$ makes the system in Equations (2.24) and (2.25) non-autonomous so that a family of cubic V_L -nullclines, indexed by the forcing parameter values $p \in [0, 1]$, exists in the phase plane. This family of cubics is computed by setting $dV_L/dt = 0$ in Equation (2.24) and solving for n to get

$$n(V_L; p) = -\frac{g_{Leak,L}(V_L - E_{Leak,L}) + \bar{g}_{I \rightarrow L} m_{I \rightarrow L}(u(V_L; p))(V_L - E_{I \rightarrow L})}{\bar{g}_{plat} a_\infty(V_L)(V_L - E_{plat})}. \quad (2.26)$$

As in the case of the MCN1-elicited rhythm, $p=0$ ($p=1$) in the above equation corresponds to the unforced (maximally forced) system, where the pyloric-timed forcing indexed by $p \in [0, 1]$ disinhibits the LG neuron from INT1. The n -nullcline is computed by setting $dn/dt = 0$ in Equation (2.25) to get the step function

$$n = \begin{cases} 1, & V_L \leq v_{inact} \\ 0, & V_L > v_{inact} \end{cases}. \quad (2.27)$$

Simulations of the PK-elicited gastric mill rhythm in which I_{Plat} is activated in the LG neuron are shown in Figure 2.4 (see Results). The simulations in Figure 2.4 were performed by replacing the MCN1 parameters (see Table 2.1) with the I_{Plat} parameters (see Table 2.2). All other parameters from Table 2.1 were left unchanged for the simulations in Figure 2.4.

2.2.3.2 *Introducing I_h in the LG neuron.* A second proposed mechanism by which PK could elicit a gastric mill rhythm that is similar to the MCN1-elicited rhythm is through a slow, hyperpolarization-activated, inward current (I_h) in the LG neuron

$$I_h = \bar{g}_h h (V_L - E_h). \quad (2.28)$$

The parameters \bar{g}_h and E_h designate its maximal conductance and reversal potential, respectively. Moreover, E_h is set above the resting potential of the LG neuron to model I_h as an inward current. However, unlike I_{plat} from the previous mechanism, I_h is a non-inactivating current; thus, the conductance of I_h operates only with activation. Moreover, the activation of I_h is triggered by a hyperpolarization in the LG neuron (inset of Figure 2.5) and it follows a time constant. The dynamics of I_h activation are modeled by

$$\frac{dh}{dt} = \begin{cases} \frac{1-h}{\tau_{LO_{hyp}}}, & V_L \leq v_{hyp} \\ \frac{-h}{\tau_{HI_{hyp}}}, & V_L > v_{hyp} \end{cases}. \quad (2.29)$$

Thus, I_h activates with time constant $\tau_{LO_{hyp}}$ when V_L is below the voltage threshold v_{hyp} (inset of Figure 2.5). This allows I_h to flow into and depolarize the LG neuron so that V_L slowly rises (see Results, Figure 2.5). When V_L exceeds v_{hyp} , I_h de-activates with time constant $\tau_{HI_{hyp}}$ which restricts the flow of I_h into the LG neuron so that V_L to slowly falls

(see Results Figure 2.5). In the biological system, I_h has been characterized as a mixed cation current that is carried by Na^+ and K^+ ions (Angstadt and Calabrese, 1989).

To build a 2-dimensional model of the PK-elicited gastric mill rhythm in which PK induces I_h in the LG neuron, Equation (2.28) is subtracted from the right hand side of Equation (2.17) and the slow activation of I_h forms the second state variable. Thus, a 2-dimensional model of this PK-elicited gastric mill rhythm is given by

$$\frac{dV_L}{dt} = -g_{Leak,L}(V_L - E_{Leak,L}) - \bar{g}_{l \rightarrow L} m_{l \rightarrow L}(u(V_L; P(t, V_L)))(V_L - E_{l \rightarrow L}) - \underbrace{\bar{g}_h h(V_L - E_h)}_{I_h} \quad (2.30)$$

$$\frac{dh}{dt} = \begin{cases} \frac{1-h}{\tau_{LO_{hyp}}}, & V_L \leq v_{hyp} \\ \frac{-h}{\tau_{HI_{hyp}}}, & V_L > v_{hyp} \end{cases} \quad (2.31)$$

Next, the phase-plane geometry of this 2-dimensional system is described. The periodic forcing function $P(t, V_L)$ in Equation (2.30) allows a family of cubic V_L -nullclines to exist in the V_L - h phase plane. This family of cubics is computed by setting $dV_L/dt = 0$ in Equation (2.30) and solving for h to get

$$h(V_L; p) = -\frac{g_{Leak,L}(V_L - E_{Leak,L}) + \bar{g}_{l \rightarrow L} m_{l \rightarrow L}(u(V_L; p))(V_L - E_{l \rightarrow L})}{\bar{g}_h(V_L - E_h)}. \quad (2.32)$$

As in the previous systems, the forcing parameter p varies in $[0,1]$ where $p=0$ ($p=1$) again corresponds to the unforced (maximally forced) system. The h -nullcline is computed by setting $dh/dt = 0$ in Equation (2.31) to get the step function

$$h = \begin{cases} 1, & V_L \leq v_{hyp} \\ 0, & V_L > v_{hyp} \end{cases}. \quad (2.33)$$

Simulations for this PK-elicited gastric mill rhythm, where I_h is induced in the LG neuron, are shown in Figure 2.5 (see Results). Moreover, as the MCN1- and PK-elicited models are interchangeable, the simulations in Figure 2.5 are performed by replacing the MCN1 column of Table 2.1 with the I_h column of Table 2.2.

2.2.3.3 Introducing $I_{Proc} + I_K$ in the LG neuron. A third proposed mechanism by which PK could elicit a similar gastric mill rhythm is by inducing two non-inactivating currents in the LG neuron. The two currents play complementary roles in eliciting the gastric mill rhythm. In particular, an inward current (I_{Proc}) depolarizes the LG neuron and facilitates the transition to its active state, while an outward current (I_K) repolarizes the LG neuron and facilitates the transition back to its inactive state (see Results).

The inward current (I_{Proc}), which is known as the proctolin current, was first shown to be activated in STG neurons by the neuropeptide proctolin (Golowasch and Marder, 1992). Many different neuropeptides have since been shown to activate a similar proctolin-like current in STG neurons (Swensen and Marder, 2000, 2001). Accordingly,

this work assumes that PK, being a neuropeptide, activates a proctolin-like current in the LG neuron modeled by

$$I_{proc} = \bar{g}_{proc} b_{\infty}(V_L)(V_L - E_{proc}). \quad (2.34)$$

The parameters \bar{g}_{proc} and E_{proc} designate its maximal conductance and reversal potential, respectively, and E_{proc} is set above the resting potential of the LG neuron to model I_{proc} as an inward current. However, unlike I_h which has slow kinetics and is activated by a hyperpolarization in the LG neuron, I_{proc} has fast kinetics and is activated by a depolarization in LG (Golowasch and Marder, 1992). The activation of I_{proc} is approximated by an instantaneous sigmoidal function of the LG membrane potential given by

$$b_{\infty}(V) = \frac{1}{1 + \exp((v_b - V)/k_b)}, \quad (2.35)$$

where the parameters v_b and k_b designate the inflection point voltage and steepness of the sigmoid, respectively. Physiologically, I_{proc} is carried primarily by Na^+ ions (Golowasch and Marder, 1992).

The second current induced by PK in the LG neuron is a slow, non-inactivating, outward K^+ current

$$I_K = \bar{g}_K w(V_L - E_K). \quad (2.36)$$

The parameters \bar{g}_K and E_K designate its maximal conductance and reversal potential, respectively. In addition, E_K is set below the resting potential of the LG neuron to model I_K as an outward current. The slow activation of I_K is modeled by

$$\frac{dw}{dt} = \begin{cases} \frac{-w}{\tau_{LO_K}}, & V_L \leq v_K \\ \frac{1-w}{\tau_{HI_K}}, & V_L > v_K \end{cases}. \quad (2.37)$$

Thus, when V_L is below the voltage threshold v_K , I_K de-activates with time constant τ_{LO_K} . This restricts the flow of I_K out of the LG neuron, which allows V_L to slowly depolarize as I_{Proc} flows into LG. In particular, activation of I_{Proc} occurs in the same voltage range as de-activation of I_K (inset of Figure 2.6). Then, when V_L rises above v_K , I_K activates with time constant τ_{HI_K} . This allows I_K to flow out of the LG neuron, which causes V_L to slowly fall. Physiologically, I_K in this model is similar to the slow, non-inactivating K^+ current (I_{K2}) found in the medicinal leech which facilitates bursting in the reciprocally inhibitory CPG circuit that controls heartbeat (Calabrese et al., 1995).

To build a 2-dimensional model of the PK-elicited gastric mill rhythm in which PK induces both I_{Proc} and I_K in the LG neuron, Equations (2.34) and (2.36) are subtracted from Equation (2.17) and the slow activation of I_K forms the second state variable. Thus, a 2-dimensional model of this PK-elicited gastric mill rhythm is given by

$$\begin{aligned} \frac{dV_L}{dt} = & -g_{Leak,L}(V_L - E_{Leak,L}) - \bar{g}_{I \rightarrow L} m_{I \rightarrow L}(u(V_L; P(t, V_L)))(V_L - E_{I \rightarrow L}) \\ & - \underbrace{\bar{g}_{proc} b_\infty(V_L)(V_L - E_{proc})}_{I_{Proc}} - \underbrace{\bar{g}_K w(V_L - E_K)}_{I_K} \end{aligned} \quad (2.38)$$

$$\frac{dw}{dt} = \begin{cases} \frac{-w}{\tau_{LO_K}}, & V_L \leq v_K \\ \frac{1-w}{\tau_{HI_K}}, & V_L > v_K \end{cases}. \quad (2.39)$$

Next, in describing the phase-plane geometry of this system, the periodic forcing function $P(t, V_L)$ in Equation (2.38) allows a family of cubic V_L -nullclines to exist in the V_L - w phase plane. This family of cubics is computed by setting $dV_L/dt = 0$ in Equation (2.38) and solving for w to get

$$w(V_L; p) = - \frac{\left[g_{Leak,L}(V_L - E_{Leak,L}) + \bar{g}_{I \rightarrow L} m_{I \rightarrow L}(u(V_L; p))(V_L - E_{I \rightarrow L}) + \bar{g}_{Proc} b_\infty(V_L)(V_L - E_{Proc}) \right]}{\bar{g}_K (V_L - E_K)}. \quad (2.40)$$

As in the previous systems, the forcing parameter p varies in $[0,1]$ where $p=0$ ($p=1$) again corresponds to the unforced (maximally forced) system. However, instead of the N-shaped cubic V_L -nullclines of the previous systems, Equation (2.40) describes an inverted N-shaped cubic for a given value of p . This is due to the fact that the slow variable w grows during repolarization of the LG neuron (along the right branch of the V_L -nullcline) and decays during LG depolarization (along the left branch), which is the

opposite behavior from that of the slow variable in the previous systems (see Results, Figure 2.6). The w -nullcline is computed by setting $dw/dt = 0$ in Equation (2.39) to get the step function

$$w = \begin{cases} 0, & V_L \leq v_K \\ 1, & V_L > v_K \end{cases}. \quad (2.41)$$

Simulations for the PK-elicited gastric mill rhythm in which both I_{Proc} and I_K are induced in the LG neuron are shown in Figure 2.6 (see Results). Moreover, as the MCN1- and PK-elicited models are interchangeable, the simulations in Figure 2.6 are performed by replacing the MCN1 column of Table 2.1 with the I_{Proc} and I_K columns of Table 2.2.

Consequences of the ($I_{Proc} + I_K$) Mechanism in the LG neuron. This work also suggests that PK is capable of eliciting a gastric mill rhythm via activation of an outward current (I_K) in the LG neuron. In particular, while PK activation of the inward current (I_{Proc}) in LG is necessary for eliciting a gastric mill that is similar to the MCN1-elicited rhythm, I_{Proc} is not necessary for eliciting network oscillations (see Results). This result is used to suggest that network oscillations can be elicited in an asymmetric reciprocally inhibitory circuit via activation of an outward current (see Results). In addition, since there are no known pharmacological blockers for I_{Proc} in the biological system, this result provides a

way to check if the PK-elicited gastric mill rhythm requires the induction of I_{Proc} in the LG neuron (see Results).

In order to elicit network oscillations in the absence of PK-induced I_{Proc} in the LG neuron, the I_{Proc} term is removed from Equation (2.38) and a nonzero value for externally applied current to the LG neuron is included.

$$\frac{dV_L}{dt} = I_{Ext} - g_{Leak,L}(V_L - E_{Leak,L}) - \bar{g}_{l \rightarrow L} m_{l \rightarrow L}(u(V_L; P(t, V_L)))(V_L - E_{l \rightarrow L}) - \underbrace{\bar{g}_K w(V_L - E_K)}_{I_K} \quad (2.42)$$

$$\frac{dw}{dt} = \begin{cases} \frac{-w}{\tau_{LO_K}}, & V_L \leq v_K \\ \frac{1-w}{\tau_{HI_K}}, & V_L > v_K \end{cases} \quad (2.43)$$

The I_{Ext} term of the LG neuron was set to zero in the previous systems, but I_{Ext} is given a nonzero value in this system to facilitate network oscillations. Moreover, Equation (2.43) is equivalent to Equation (2.39).

In the V_L - w phase plane of the above system, the forcing function $P(t, V_L)$ again allows for a family of cubic V_L -nullclines indexed by the forcing parameter values p in $[0, 1]$ to exist in the phase plane

$$w(V_L; p) = - \frac{[-I_{Ext} + g_{Leak,L}(V_L - E_{Leak,L}) + \bar{g}_{l \rightarrow L} m_{l \rightarrow L}(u(V_L; p))(V_L - E_{l \rightarrow L})]}{\bar{g}_K (V_L - E_K)} \quad (2.44)$$

The w -nullcline is given by the same step function in Equation (2.41).

When $I_{Ext} = 0$ in Equation (2.44), the V_L - and w -nullclines intersect at a stable fixed point so that network oscillations do not occur (see Results, Figure 2.7). Yet, the V_L -nullcline is still cubic in shape due to the reciprocal inhibition between INT1 and the LG neuron (see Results, Figure 2.7), so the system still has the capability to exhibit network oscillations. When external current is applied to the LG neuron, the V_L - and w -nullclines intersect along the unstable middle branch of the cubic; as a result, the system exhibits network oscillations, where $I_{Ext} = 150 \mu S/cm^2$ in Figure 2.7.B (see Results). The resulting network oscillations are controlled by the slow dynamics (w) of the outward current (I_K) which is induced by PK in the LG neuron (see Results, Figure 2.7). Moreover, since the gastric mill rhythm which is elicited in the absence of I_{Proc} is different from the MCN1-elicited rhythm, Figure 2.7 suggests that induction of both I_{Proc} and I_K in the LG neuron is necessary for PK to elicit a gastric mill rhythm that is similar to the MCN1-elicited rhythm (see Results).

Table 2.1 Parameters Used to Model the MCN1-Elicited Gastric Mill Rhythm.

INT1	Pyloric	LG	MCN1
$g_{Leak,I} = 0.75 \text{ mS/cm}^2$	$\bar{g}_p = 0.85 \text{ mS/cm}^2$	$g_{Leak,L} = 1 \text{ mS/cm}^2$	$\bar{g}_s = 3 \text{ mS/cm}^2$
$E_{Leak,I} = 10 \text{ mV}$	$E_p = -60 \text{ mV}$	$E_{Leak,L} = -60 \text{ mV}$	$E_s = 50 \text{ mV}$
$\bar{g}_{L \rightarrow I} = 2 \text{ mS/cm}^2$	$per = 1 \text{ sec}$	$\bar{g}_{I \rightarrow L} = 5 \text{ mS/cm}^2$	$v_{pre} = -33 \text{ mV}$
$E_{L \rightarrow I} = -80 \text{ mV}$	$dur = 0.5$	$E_{I \rightarrow L} = -80 \text{ mV}$	$\tau_{LO_{mcn1}} = 14 \text{ sec}$
$v_{L \rightarrow I} = -30 \text{ mV}$	$v_q = -35 \text{ mV}$	$v_{I \rightarrow L} = -30 \text{ mV}$	$\tau_{HI_{mcn1}} = 5 \text{ sec}$
$k_{L \rightarrow I} = 5 \text{ mV}$	$k_q = 3 \text{ sec}$	$k_{I \rightarrow L} = 5 \text{ mV}$	

Table 2.2 Parameters Used For Each of the PK-Elicited Gastric Mill Rhythms

I _{plat}	I _h	I _{proc}	I _K
$\bar{g}_{plat} = 6 \text{ mS/cm}^2$	$\bar{g}_h = 3 \text{ mS/cm}^2$	$\bar{g}_{proc} = 12 \text{ mS/cm}^2$	$\bar{g}_K = 4 \text{ mS/cm}^2$
$E_{plat} = 20 \text{ mV}$	$E_h = 30 \text{ mV}$	$E_{proc} = 12 \text{ mV}$	$E_K = -80 \text{ mV}$
$v_a = -40 \text{ mV}$	$v_{hyp} = -33 \text{ mV}$	$v_b = -20 \text{ mV}$	$v_K = -33 \text{ mV}$
$k_a = 17 \text{ mV}$	$\tau_{LO_{hyp}} = 10.5 \text{ sec}$	$k_b = 19 \text{ mV}$	$\tau_{LO_K} = 3.5 \text{ sec}$
$v_{inact} = -33 \text{ mV}$	$\tau_{HI_{hyp}} = 6 \text{ sec}$		$\tau_{HI_K} = 5.5 \text{ sec}$
$\tau_{LO_{inact}} = 5 \text{ sec}$			
$\tau_{HI_{inact}} = 4 \text{ sec}$			

Each PK-elicited gastric mill rhythm is run by replacing the MCN1 parameters (see Table 2.1) with the appropriate PK-induced current(s) (see Table 2.2).

2.2.4 Generalization to a Single 2-Dimensional Model

Next, the individual 2-dimensional models that govern the MCN1-elicited and PK-elicited gastric mill rhythms are generalized into a single 2-dimensional model. In particular, instead of relying on the specific properties induced by MCN1 or PK, the generalized model is described by the common geometrical properties shared within the phase planes of the individual 2-dimensional models. The generalized model is given by

$$\frac{dV_L}{dt} = f(V_L, y; P) \quad (2.45)$$

$$\frac{dy}{dt} = \frac{H(v_{thresh} - V_L) - y}{\tau_{HI} + (\tau_{LO} - \tau_{HI})H(v_{thresh} - V_L)} = \begin{cases} \frac{1-y}{\tau_{LO}}, & V_L \leq v_{thresh} \\ \frac{-y}{\tau_{HI}}, & V_L > v_{thresh} \end{cases} \quad (2.46)$$

where the state variable y designates the slow variable of the individual MCN1, I_{plat} , I_h , or $I_{Proc} + I_K$ systems. In particular, the slow variable of the general model is such that $y = s$, n , h , or $1-w$ of Equations (2.14), (2.25), (2.31), or (2.39), respectively (see also Results, Figure 2.9). Moreover, the right hand side of Equation (2.45) is such that

$$f(V_L, y; P) = \underbrace{-\bar{g}_{Leak,L}(V_L - E_{Leak,L})}_{I_{Leak,L}} - \underbrace{\bar{g}_{I \rightarrow L} m_{I \rightarrow L}(u(V_L; P))(V_L - E_{I \rightarrow L})}_{I_{I \rightarrow L}} - I_{Osc} \quad (2.47)$$

where $P = P(t, V_L)$ and

$$I_{Osc} = \underbrace{\bar{g}_s s(V_L - E_s)}_{I_s} + \underbrace{\bar{g}_{Plat} a_\infty(V_L)(V_L - E_{Plat})}_{I_{Plat}} + \underbrace{\bar{g}_h h(V_L - E_h)}_{I_h} + \underbrace{\bar{g}_{Proc} b_\infty(V_L)(V_L - E_{Proc})}_{I_{Proc}} + \underbrace{\bar{g}_K w(V_L - E_K)}_{I_K} \quad (2.48)$$

of the individual MCN1, I_{Plat} , I_h , or $I_{Proc} + I_K$ systems, respectively.

The behavior of the generalized model in Equations (2.45) and (2.46) can be largely determined by its geometrical properties in the phase plane. These geometrical properties are shared with a broader class of equations that describe 2-dimensional relaxation oscillators with fast periodic inputs. Moreover, with the 2-dimensional model described in this broader context, geometrical singular perturbation theory (Mishchenko and Rozov, 1980) can be used to track the trajectory of the generalized system in the V_L - y phase plane. This trajectory in the V_L - y phase plane involves distinct time scales. In particular, the dynamics of the slow variable (y) are dominant along the stable outer branches of the cubic V_L -nullcline; therefore, the trajectory evolves slowly along the outer

branches of the cubic. In contrast, the dynamics of the fast variable are dominant during the transitions between the outer branches of the V_L -nullcline so that the trajectory is much faster during these transitions (see also Figure 2.9). The difference in time scales is revealed in the model by factoring out the common time constant τ_{HI} in Equation (2.46) to give what is called the fast system

$$\frac{dV_L}{dt} = f(V_L, y; P) \quad (2.49)$$

$$\frac{dy}{dt} = \frac{1}{\tau_{HI}} \left(\frac{H(v_{thresh} - V_L) - y}{1 + \left(\frac{\tau_{LO}}{\tau_{HI}} - 1 \right) H(v_{thresh} - V_L)} \right) = \varepsilon \begin{cases} \frac{1-y}{\tilde{\tau}}, & V_L \leq v_{thresh} \\ -y, & V_L > v_{thresh} \end{cases} \quad (2.50)$$

where $\varepsilon = \frac{1}{\tau_{HI}} \ll 1$ is a small positive parameter and $\tilde{\tau} = \frac{\tau_{LO}}{\tau_{HI}}$ is the ratio of time constants. Rescaling time in the fast system by $\xi = \varepsilon t$ gives what is called the slow system

$$\varepsilon \frac{dV_L}{d\xi} = f(V_L, y; P) \quad (2.51)$$

$$\frac{dy}{d\xi} = \begin{cases} \frac{1-y}{\tilde{\tau}}, & V_L \leq v_{thresh} \\ -y, & V_L > v_{thresh} \end{cases} \quad (2.52)$$

Both systems are equivalent in describing the dynamics of network oscillations as long as the parameter $\varepsilon \neq 0$. However, as $\varepsilon \rightarrow 0$, each system approaches a distinct singular limit that controls a different part of the trajectory. In particular, setting $\varepsilon = 0$ in Equation (2.50) gives the singular fast system

$$\frac{dV_L}{dt} = f(V_L, y; P) \quad (2.53)$$

$$\frac{dy}{dt} = 0, \quad (2.54)$$

which governs the fast transitions between the stable outer branches of the cubic V_L -nullcline. These transitions occur instantaneously with respect to the slow time scale ξ , and each is a solution of Equation (2.53) where y and P act as parameters. In contrast, setting $\varepsilon = 0$ in Equation (2.51) gives the singular slow system

$$0 = f(V_L, y; P) \quad (2.55)$$

$$\frac{dy}{d\xi} = \begin{cases} \frac{1-y}{\tilde{\tau}}, & V_L \leq v_{thresh} \\ -y, & V_L > v_{thresh} \end{cases} \quad (2.56)$$

where Equation (2.55) restricts the trajectory to lie strictly on the cubic V_L -nullcline and Equation (2.56) governs the slow evolution of the trajectory on the cubic. Moreover,

although the pyloric-timed forcing (P) causes the left branch of the cubic to move, Equation (2.55) still requires the trajectory to remain on the moving cubic.

A singular orbit is constructed by pasting together the individual solutions of the singular fast system and singular slow system. When $\varepsilon > 0$ is small, the non-singular trajectory described by Equations (2.51) and (2.52) becomes $O(\varepsilon)$ close (as $\varepsilon \rightarrow 0$) to the singular orbit (Mishchenko and Rozov, 1980). Therefore, the simplified properties of the singular orbit can be utilized for tracking the trajectory of the generalized 2-dimensional system in Equations (2.51) and (2.52) and for calculating bounds on gastric mill period (see Results).

2.3 Results

The 2-dimensional models that were developed in Methods are used to investigate how the neuromodulator PK can elicit a gastric mill rhythm that is similar to the MCN1-elicited rhythm. The state variables of each 2-dimensional model are directly involved in generating network oscillations, so the dynamics of each network model are fully described via a phase-plane analysis. First, the network dynamics of the MCN1-elicited gastric mill rhythm are described. Next, three different mechanisms are proposed by which the neuromodulator PK can elicit a gastric mill rhythm that is similar to the MCN1-elicited rhythm. Each mechanism involves PK-activation of voltage-gated ionic currents in the LG neuron. Then, the individual models of the MCN1-elicited and PK-elicited gastric mill rhythms are generalized into a single 2-dimensional model that is used to compute bounds on the gastric mill period. These bounds account for the

variability in the gastric mill period of the biological system due to a local synaptic input from the pyloric circuit.

2.3.1 Investigating the Network Dynamics of the MCN1-Elicited Gastric Mill Rhythm

The MCN1-elicited gastric mill rhythm is described by the 2-dimensional model in Equations (2.13) and (2.14) (see Methods). The state variable s describes the slow, presynaptically-gated excitation from MCN1 to the LG neuron, and s drives the network oscillations in this system (Figure 2.1). Moreover, the time constants of s in Equation (2.14) are chosen to be large so that the system operates in a relaxation regime (see Methods). In the V_L - s phase plane, the left branch of the V_L -nullcline corresponds to the inactive state of the LG neuron, while the right branch corresponds to the active state of LG. Physiologically, during its inactive state the LG neuron is inhibited by INT1 and it receives a slow modulatory excitation (s) from MCN1. On the other hand, when the LG neuron is active, it inhibits INT1 and presynaptically inhibits MCN1.

The forcing function $P(t, V_L)$ in Equation (2.13) makes the 2-dimensional system non-autonomous so that a family of cubic V_L -nullclines exists in the phase plane. This family of cubics is modeled by Equation (2.15), while the s -nullcline is modeled by Equation (2.16) (see Methods). Physiologically, the $P(t, V_L)$ forcing function describes the local AB to INT1 inhibition of the biological system, where the AB neuron is the pacemaker of the pyloric circuit (see Methods).

First, the unforced MCN1-elicited gastric mill rhythm is examined, which corresponds to when the forcing function $P(t, V_L) = 0$ in Equation (2.13). The 2-

dimensional model is autonomous in the absence of this forcing function so that a single cubic V_L -nullcline, given by $s(V_L; 0)$ in Equation (2.15), exists in the phase plane (see Methods). The network dynamics of the unforced MCN1-elicited gastric mill rhythm are described using the geometrical properties in the V_L - s phase plane (Figure 2.1.C.1). In particular, during the inactive state of the LG neuron, where it is inhibited by INT1, the slow modulatory excitation from MCN1 (s), slowly builds up in the LG neuron. As a result, a phase point slowly climbs up the left branch of the cubic V_L -nullcline from point 1 to point 2 as s builds up in LG (Figure 2.1.C.1). Moreover, this slow buildup of s excitation causes the LG membrane potential, modeled by the state variable V_L , to slowly rise (Figure 2.1.C.2). When the phase point reaches the left knee of the cubic at the point 2 (Figure 2.1.C.1), it becomes unstable and undergoes a saddle-node bifurcation. As a result, the phase point jumps to the stable right branch of the cubic at the point 3 (Figure 2.1.C.1), since $dV_L/dt > 0$ above the V_L -nullcline (see Methods). Physiologically, this jump corresponds to when enough MCN1 excitation builds up in the LG neuron to allow it to overcome its inhibition by INT1. As a result, the LG neuron jumps into its active state on the right branch of the cubic, where it inhibits INT1 and presynaptically inhibits MCN1. The presynaptic inhibition of MCN1 causes s to slowly decay in the LG neuron so that the phase point slowly falls down the right branch of the cubic, which causes V_L to slowly fall toward its resting potential (Figure 2.1.C.2). When the phase point reaches the right knee of the cubic at the point 4 (Figure 2.1.C.1), it becomes unstable and undergoes another saddle-node bifurcation. As a result, the phase point jumps back to the stable left branch of the cubic at the point 1 (Figure 2.1.C.1), since $dV_L/dt < 0$ below the V_L -nullcline (see Methods). Physiologically, this jump corresponds to when V_L falls

enough to allow the graded inhibition from INT1 to push the LG neuron back down into its inactive state, which in turn removes the LG presynaptic inhibition of MCN1. Then, the cycle begins again as the phase point slowly climbs up the left branch of the cubic and s slowly builds up in the LG neuron. Thus, the periodic orbit in the V_L - s phase plane, which consists of two fast and two slow portions, describes the network dynamics that underlie oscillations in the LG neuron during the gastric mill rhythm in the absence of the pyloric input (Figure 2.1.C).

Next, the forced MCN1-elicited gastric mill rhythm is examined in which $0 \leq P(t, V_L) \leq 1$ in Equation (2.13). This forcing function allows a family of cubic V_L -nullclines to exist in the phase plane (see Methods). Two members of this family which correspond to the extreme values of $p = 0$ and $p = 1$ in Equation (2.15) are shown in Figure 2.1.D.1. In particular, the higher (unforced) cubic occurs when $p = 0$ and corresponds to the unforced system of Figure 2.1.C.1, while the lower (maximally forced) cubic occurs when $p = 1$ and corresponds to the maximally forced system at the peak of the pyloric-timed synaptic input (see Methods). Thus, during the inactive state of the LG neuron where s slowly builds up in LG, the phase point slowly climbs up the left branch of the V_L -nullcline as it is bounced back and forth between the unforced and maximally forced cubics (Figure 2.1.D.1). In particular, each pyloric peak (shown in Figure 2.1.D.2) shifts the unforced cubic down to the maximally forced cubic. In addition, the fast, pyloric-timed transitions between left branches of the V_L -nullcline correspond to the small-amplitude depolarizations in V_L during the inactive state of the LG neuron (Figure 2.1.D.2). In particular, the pyloric-timed AB to INT1 inhibition interrupts the INT1 to LG inhibition in turn (inset of Figure 2.1), which effectively disinhibits the LG neuron

from INT1 and causes the small pyloric-timed depolarizations in V_L . When the phase point reaches the level of the lower left knee, the next forcing peak shifts the cubic below the phase point and initiates the jump to the stable right branch at the point 2 (Figure 2.1.D.1), since $dV_L/dt > 0$ above the V_L -nullcline (see Methods). Thus, in the presence of the pyloric-timed forcing, the jump to the right branch occurs below the higher left knee of the unforced cubic, so less MCN1 excitation is required to build up in the LG neuron before it jumps into its active state.

During the active state of the LG neuron, the phase point slowly falls down the right branch of the cubic as s slowly decays in LG due to its presynaptic inhibition of MCN1; as a result, V_L slowly falls toward its resting potential (Figure 2.1.D.2). There is only one right branch of the V_L -nullcline since the pyloric forcing term $P(t, V_L)$ described by Equation (2.11) does not affect the active state of the LG neuron (see Methods). In particular, when the active LG neuron inhibits INT1, the reverse INT1 to LG inhibition becomes very weak (inset of Figure 2.1); therefore, the forcing effect of the AB to INT1 inhibition is not effectively transmitted through the weakened synapse and does not affect the active state of the LG neuron, as described in the biological system (Bartos et al., 1999). When the phase point reaches the right knee of the cubic at the point 4, it becomes unstable and undergoes a saddle-node bifurcation, where it jumps back to the point 1 on the stable left branch (Figure 2.1.D.1). This jump corresponds to when the LG neuron falls back into its inactive state, which removes the presynaptic inhibition of MCN1. Then, the cycle begins again as the phase point slowly climbs up the left branch.

Hence, in the forced system, the jump to the right branch of the V_L -nullcline is initiated by a pyloric forcing peak. Physiologically, this means that the onset of the LG

burst phase is triggered by the AB to INT1 inhibition (Figure 2.1.D.2). In addition, the effect of the pyloric forcing shortens the duration on the left branch on the V_L -nullcline as the jump occurs below the higher left knee of the unforced cubic. This in turn shortens the duration on the right branch since the jump from the point 2 to the point 3 occurs at a lower value of s than in the unforced system (Figure 2.1.D). Therefore, the AB to INT1 inhibition also increases the frequency of network oscillations in the gastric mill rhythm (Figure 2.1.D).

In the absence of MCN1 input, the LG neuron remains in its inactive state so that the gastric mill rhythm is not spontaneously active (Figure 2.2). In particular, setting the conductance of the MCN1 input $\bar{g}_s = 0$ in Equation (2.15) makes the cubic V_L -nullcline a straight line (Figure 2.2.A). Specifically, the s -value of the cubic V_L -nullcline blows up when $\bar{g}_s \rightarrow 0$ in Equation (2.15). The resulting V_L -nullcline in Figure 2.2.A is attracting so that $dV_L/dt > 0$ (< 0) to the left (right) of the V_L -nullcline (see Methods). In particular, the V_L -nullcline in Figure 2.2.A corresponds to the stable left branch of the cubic in Figure 2.1 after the s -value of the cubic blows up when $\bar{g}_s \rightarrow 0$ in Equation (2.15). Thus, in the absence of MCN1 input, the V_L - and s -nullclines intersect at a stable fixed point to which the trajectory settles. Two V_L -nullclines are shown in Figure 2.A to illustrate the unforced ($p = 0$) and maximally forced ($p = 1$) systems due to the pyloric-timed forcing, which still underlies the subthreshold depolarizations in the LG neuron (Figure 2.2.B). Physiologically, Figure 2.2 illustrates that the gastric mill rhythm is not spontaneously active without synaptic input from the projection neuron MCN1 (s) to balance the asymmetry in the INT1-LG reciprocal inhibition. In particular, the LG neuron remains in its inactive state, where it is inhibited by INT1, in the absence of

MCN1 input. This corresponds to the biological system, where the gastric mill rhythm is not spontaneously active before MCN1 stimulation (Bartos et al., 1999) (see also Figure 1.5).

2.3.2 Proposed Mechanisms by Which Pyrokinin (PK) Elicits a Similar Gastric Mill Rhythm

Next, the gastric mill rhythm elicited by the neuropeptide pyrokinin (PK) is investigated. Recent experiments showed that bath application of PK to the isolated STG elicits a similar gastric mill rhythm in the absence of MCN1 participation (Hertzberg and Nusbaum, 2004, 2005). This result is surprising because PK is not released by MCN1, which releases only GABA, proctolin, and CabTRP Ia as its co-transmitters (Blitz et al., 1999). Moreover, no combination of the MCN1 co-transmitters elicits a gastric mill rhythm when bath applied to the isolated STG (Wood et al., 2000). Thus, PK relies on distinct network properties to elicit a similar gastric mill rhythm (Hertzberg and Nusbaum, 2005). However, although PK boosts the activity of gastric mill neurons *in vitro*, the mechanism by which it elicits a gastric mill rhythm is unknown.

This work develops a 2-dimensional model to investigate how PK can elicit a gastric mill rhythm that is similar to the MCN1-elicited rhythm (see Methods). Three different mechanisms are proposed by which PK can elicit a similar gastric mill rhythm via activation of voltage-gated ionic currents in the LG neuron to balance the asymmetry in the INT1-LG reciprocal inhibition. The proposed PK-induced currents in the LG neuron include: **1** a slowly inactivating inward current (I_{Plat}), **2** a slow, hyperpolarization-activated inward current (I_{h}), **3** a fast, non-inactivating inward current (I_{Proc}) plus a slow

non-inactivating outward current (I_K). When induced by PK in the LG neuron, each of the above mechanisms is shown to elicit a gastric mill rhythm that is similar to the MCN1-elicited rhythm.

2.3.2.1 PK Induction of I_{Plat} in the LG Neuron Elicits a Similar Gastric Mill Rhythm.

First, PK induction of I_{Plat} (a slowly-inactivating inward current) in the LG neuron is shown to elicit a gastric mill rhythm that is similar to the MCN1-elicited rhythm. I_{Plat} has both a fast activation plus a slow inactivation (see Methods, Equation (2.18)); thus, I_{Plat} is a current with regenerative properties that elicits network oscillations when induced in the LG neuron. However, unlike the MCN1-elicited gastric mill rhythm which is driven by the slow excitation from MCN1 to LG plus the presynaptic inhibition from LG back to MCN1, the gastric mill rhythm elicited by PK-induction of I_{Plat} is instead controlled by the activation and inactivation of I_{Plat} in the LG neuron (Figure 2.3).

The gastric mill rhythm elicited by PK-induction of I_{Plat} in the LG neuron is governed by the 2-dimensional model in Equations (2.24) and (2.25) (see Methods). The dynamics of this gastric mill rhythm are driven by the slow inactivation (n) of I_{Plat} , and the geometrical properties in the V_L - n phase plane are used to describe the network oscillations (Figure 2.4). As in the MCN1-elicited rhythm, a family of N-shaped cubic V_L -nullclines exists in the V_L - n phase plane due to the pyloric-timed input, and this family of cubics is expressed by Equation (2.26) (see Methods). Moreover, as in the MCN1-elicited rhythm, $dV_L/dt > 0$ (< 0) above (below) the V_L -nullcline while $dn/dt > 0$ (< 0) below (above) the n -nullcline. Therefore, the outer branches of the cubic are again stable while the middle branch is unstable.

First, the dynamics of the unforced system are examined, where the forcing function $P(t, V_L) = 0$ in Equation (2.24) (see Methods). The 2-dimensional system in Equations (2.24) and (2.25) becomes autonomous in the absence of this pyloric-timed input so that a single cubic V_L -nullcline exists in the V_L - n phase plane (Figure 2.4.A.1). However, unlike the MCN1-elicited rhythm where the nullclines intersect along the unstable middle branch of the cubic to allow oscillations (Figure 2.1.C.1), the nullclines of the PK-induced I_{plat} system (Figure 2.4.A.1) intersect along the stable left branch, so the trajectory settles to a stable fixed point and there are no oscillations in the absence of the pyloric-timed input (Figure 2.4.A.2). As a result, PK-induction of I_{plat} does not elicit a gastric mill rhythm in the absence of the pyloric-timed inhibition of INT1. This result agrees with experiments. In particular, in the absence of the AB to INT1 inhibition, MCN1 still elicits a gastric mill rhythm, albeit slower (Bartos et al., 1999), but PK does not elicit a gastric mill rhythm in the absence of the AB to INT1 inhibition (Hertzberg and Nusbaum, 2004). Thus, one difference between the MCN1- and PK-elicited gastric mill rhythms is that PK fails to elicit a gastric mill rhythm in the absence of the AB to INT1 inhibition.

Next, the forced system is examined, where $0 \leq P(t, V_L) \leq 1$ in Equation (2.24). This pyloric-timed forcing function makes the 2-dimensional system in Equations (2.24) and (2.25) non-autonomous so that a family of cubics exists in the V_L - n phase plane (see Methods). The higher cubic (Figure 2.4.B.1) occurs when $p = 0$ in Equation (2.26) and is equivalent to the unforced cubic in Figure 2.4.A.1. The lower cubic (Figure 2.4.B.1) occurs when $p = 1$ in Equation (2.26) and corresponds to the maximally forced system. In the presence of the pyloric-timed forcing input, the trajectory in the V_L - n phase plane is

very similar to that of the MCN1-elicited rhythm (compare Figures 2.4.B.1 and 2.1.D.1). Thus, PK elicits a similar gastric mill rhythm via the induction of I_{Plat} in the LG neuron. However, the PK-elicited gastric mill rhythm is controlled by different network components. In particular, during the inactive state of the LG neuron, I_{Plat} slowly de-inactivates (increase in n) which allows for activation to occur (see Figure 2.3) so that I_{Plat} flows into and depolarizes the LG neuron. As a result, a phase point slowly climbs up the left branch of the V_L -nullcline from the point 1 to the point 2 as it is bounced back and forth between cubics by the pyloric-timed forcing (Figure 2.4.B.1). When the phase point reaches the level of the lower left knee, the next forcing peak shifts the cubic below the phase point and initiates the jump to the stable right branch at the point 2 (Figure 2.4.B.1), since $dV_L/dt > 0$ above the V_L -nullcline. Physiologically, this jump corresponds to when the LG neuron transitions into its active state, where it inhibits INT1 and where inactivation of I_{Plat} occurs (slow decrease in n) to restrict the flow of I_{Plat} into the LG neuron. As a result, the phase point slowly falls down the right branch of the cubic as I_{Plat} slowly inactivates in the LG neuron (decrease in n). When the phase point reaches the right knee of the cubic at the point 4 (Figure 2.4.B.1), it becomes unstable and undergoes a saddle-node bifurcation, where it jumps back to the point 1 on the stable left branch since $dV_L/dt < 0$ below the V_L -nullcline. Physiologically, the jump back to the left branch corresponds to when the LG neuron falls back down into its inactive state. Then, the cycle begins again as I_{Plat} slowly de-inactivates (increase in n) in the LG neuron. Thus, in the presence of the AB to INT1 inhibition, PK-induction of I_{Plat} in the LG neuron elicits a gastric mill rhythm that is similar to the MCN1-elicited rhythm (compare Figures 2.4.B.2 and 2.1.D.2).

2.3.2.2 PK-Induction of I_h in the LG neuron Elicits a Similar Gastric Mill Rhythm.

Alternatively, PK-induction of I_h (a slow, hyperpolarization-activated, inward current) in the LG neuron can elicit a similar gastric mill rhythm. I_h is modeled by Equation (2.28) (see Methods), but, unlike I_{plat} which has both activation and inactivation, I_h is a non-inactivating current. In particular, as shown in the inset of Figure 2.5, I_h activates when the LG neuron is hyperpolarized and de-activates when the LG neuron is depolarized. This behavior is equivalent to the inactivation of I_{plat} in the previous mechanism (Figure 2.3). Therefore, since PK-induction of I_h alone in the LG neuron can elicit a similar gastric mill rhythm, this work predicts that an inactivating current (such as I_{plat}) is not necessary for PK to elicit a gastric mill rhythm.

The gastric mill rhythm elicited by PK-induction of I_h in the LG neuron is governed by the 2-dimensional model in Equations (2.30) and (2.31). The dynamics of the network oscillations are driven by the slow activation (h) of I_h , and the geometrical properties in the V_L - h phase plane are used to describe these network oscillations (Figure 2.5). A family of N-shaped, cubic V_L -nullclines exists in the V_L - h phase plane due to the pyloric-timed forcing, and this family of cubics is described by Equation (2.32) (see Methods). The dynamics within the V_L - h phase plane are similar to that of previous systems, where $dV_L/dt > 0$ (< 0) above (below) the cubic V_L -nullcline while $dh/dt > 0$ (< 0) below (above) the h -nullcline. Therefore, the outer branches of the cubic V_L -nullcline are again stable while its middle branch is unstable.

In the case of the unforced system where the pyloric-timed input is absent, the 2-dimensional model in Equations (2.30) and (2.31) becomes autonomous so that only a

single V_L -nullcline, corresponding to the higher (unforced) cubic in Figure 2.5.A, will exist in the V_L - h phase plane. Moreover, similar to that which occurs in the PK-induced I_{Plat} system of Figure 2.4.A, the h -nullcline intersects the unforced (higher) V_L -nullcline along the stable left branch (Figure 2.5.A); therefore, no network oscillations will result in the unforced system since the trajectory would settle to the stable fixed point at the intersection of the unforced (higher) V_L -nullcline and h -nullcline (arrow in Figure 2.5.A).

In the forced system where the pyloric-timed input is present, the 2-dimensional model in Equations (2.30) and (2.31) becomes non-autonomous so that a family of cubic V_L -nullclines exists in the V_L - h phase. The higher cubic again corresponds to the unforced system and occurs when $p = 0$ in Equation (2.32), while the lower cubic again corresponds to the maximally forced system and occurs when $p = 1$ in Equation (2.32) (see Methods). The network oscillations in this system are driven by the slow activation (h) dynamics of I_h (Figure 2.5.B). In particular, during the inactive state of the LG neuron, activation of I_h (slow increase in h) allows the current to flow into and depolarize the LG neuron. Therefore, a phase point slowly climbs up the left branch of the V_L -nullcline as it is bounced back and forth between cubics by the pyloric-timed forcing. When the phase point reaches the level of the lower left knee, the next peak of $P(t, V_L)$ initiates the jump to the right branch at the point 2 (Figure 2.5.A), since $dV_L/dt > 0$ above the V_L -nullcline. As a result, the LG neuron jumps into its active state, where it inhibits INT1 and where de-activation of I_h (slow decrease in h) occurs to restrict the flow of I_h into the LG neuron. As a result, the phase point slowly falls down the right branch of the cubic as I_h de-activates in LG. When the phase point reaches the right knee of the cubic at the point 4 (Figure 2.5.A), it becomes unstable and undergoes a saddle-

node bifurcation, where it jumps back to the point 1 on the stable left branch. As a result, the LG neuron falls back down into its inactive state where it is inhibited by INT1. Then, the cycle begins again as I_h is activated in the LG neuron (slow increase in h). Thus, PK-induction of I_h in the LG neuron is sufficient to elicit a similar gastric mill rhythm.

2.3.2.3 PK-Induction of $I_{Proc} + I_K$ in the LG Neuron Elicits a Similar Gastric Mill Rhythm. In the final mechanism, PK induces two non-inactivating currents in the LG neuron (inset of Figure 2.6). In particular, PK-induction of a fast inward current (I_{Proc}) plus a slow outward current (I_K) in the LG neuron elicits a similar gastric mill rhythm. In the biological system, several different neuropeptides have been shown to induce I_{Proc} in STG neurons (Swensen and Marder, 2000, 2001). Accordingly, in this work PK, being a neuropeptide, is assumed to induce I_{Proc} in the LG neuron, as modeled by Equation (2.34) (see Methods). In addition, the PK-induced slow outward current (I_K) is modeled by Equation (2.36). I_{Proc} and I_K perform different roles for eliciting network oscillations. In particular, I_{Proc} depolarizes the LG neuron and facilitates the jump to its active state, while I_K repolarizes the LG neuron and facilitates the jump back down into its inactive state. In the previous two PK-induced mechanisms, both depolarization and repolarization of LG were performed by a single current. Thus, this final mechanism addresses the case in which PK induces more than one current in the LG neuron to elicit a gastric mill rhythm.

The gastric mill rhythm elicited by PK-induction of $I_{Proc}+I_K$ in the LG neuron is governed by the 2-dimensional model in Equations (2.38) and (2.39). The network oscillations are controlled by the slow dynamics (w) of I_K (Figure 2.6.B), so the

geometrical properties in the V_L - w phase plane are used to describe the network dynamics of the system. However, since I_K is an outward current, the V_L -nullcline is an inverted N-shaped cubic in the V_L - w phase plane (Figure 2.6.A), where $dV_L/dt > 0$ (< 0) below (above) the V_L -nullcline while $dw/dt > 0$ (< 0) below (above) the w -nullcline (see Methods). Therefore, the outer branches of the cubic V_L -nullcline are again stable while the middle branch is unstable. Moreover, a family of cubic V_L -nullclines exists in the V_L - w phase plane due to the pyloric-timed forcing, as described by Equation (2.40) (see Methods).

In the unforced system where the pyloric-timed input is absent, the 2-dimensional model in Equations (2.38) and (2.39) becomes autonomous so that only a single cubic V_L -nullcline, corresponding to the lower (unforced) cubic in Figure 2.6.A, will exist in the V_L - w phase plane. As in the previous PK-induced mechanisms, no network oscillations will occur in the unforced system since the w -nullcline intersects the unforced (lower) V_L -nullcline along its stable (attracting) left branch (arrow in Figure 2.6.A), so the trajectory would settle to a stable fixed point.

In the forced system where the pyloric-timed input is present, the 2-dimensional model is non-autonomous so that a family of cubic V_L -nullclines exists in the V_L - w phase plane. In this model, the lower cubic (Figure 2.6.A) corresponds to the unforced system which occurs when $p = 0$ in Equation (2.40), while the higher cubic corresponds to the maximally forced system which occurs when $p = 1$ in Equation (2.40) (see Methods). The network oscillations in this model are driven by the slow activation (w) dynamics of the outward current (I_K) (Figure 2.6.B). In particular, during the inactive state of the LG neuron, de-activation of I_K (slow decrease in w) allows for activation of the fast inward

current (I_{Proc}), which facilitates depolarization of the LG neuron (inset of Figure 2.6). As a result, a phase point slowly falls down the left branch of the V_L -nullcline from the point 1 to the point 2 as it is bounced back and forth between cubics by the pyloric-timed forcing (Figure 2.6.A). When the phase point reaches the level of the higher left knee, the next peak of $P(t, V_L)$ raises the unforced cubic above the phase point and initiates the jump to the stable right branch at the point 2 (Figure 2.6.A), since $dV_L/dt > 0$ below the V_L -nullcline. As a result, the LG neuron jumps into its active state where it inhibits INT1 and where activation of the outward current I_K occurs (slow increase in w), where I_K flows out of and repolarizes the LG neuron. Consequently, the phase point slowly climbs up the right branch of the V_L -nullcline (Figure 2.6.A) as I_K repolarizes the LG neuron and causes V_L to fall toward its resting potential (Figure 2.6.B). When the phase point reaches the right knee of the cubic at the point 4 (Figure 2.6.A), it becomes unstable and undergoes a saddle-node bifurcation, where it jumps back to the point 1 on the stable left branch since $dV_L/dt < 0$ above the V_L -nullcline. As a result, the LG neuron falls back down into its inactive state where it is inhibited by INT1 and where de-activation of I_K occurs (slow decrease in w). This restricts the flow of I_K out of the LG neuron, and the cycle begins again as I_K slowly de-activates in the LG neuron which allows for I_{Proc} to be activated in LG. Thus, PK-induction of $I_{Proc} + I_K$ in the LG neuron also elicits a similar gastric mill rhythm.

Oscillations Elicited Through PK-Induction of I_K in the LG neuron. This work also shows that network oscillations are capable of being elicited via PK-induction of only the outward current (I_K) in the LG neuron (Figure 2.7). Furthermore, Figure 2.7 also shows

that although PK-induction of the inward current (I_{Proc}) is not necessary for eliciting network oscillations, I_{Proc} is necessary for eliciting a gastric mill rhythm that is similar to the MCN1-elicited rhythm (Figure 2.1).

In particular, removal of I_{Proc} from the 2-dimensional model in Equations (2.38) and (2.39) (see Methods) leaves only the PK-induced outward current (I_K) for repolarization of the LG neuron, as described by the 2-dimensional model in Equations (2.42) and (2.43) (see Methods). Subsequently, with no inward current (I_{Proc}) for depolarization, the LG neuron remains in its inactive state as the V_L - and w -nullclines intersect along the stable left branch of the cubic, and the trajectory settles to a stable fixed point so that network oscillations do not occur (Figure 2.7.A.1). The subthreshold oscillations in the LG neuron (Figure 2.7.A.2) are due to the effect of the pyloric-timed forcing input, which again allows a family of cubics to exist in the V_L - w phase plane. The unforced (lower) cubic and maximally forced (higher) cubic are shown in Figure 2.7.A.1.

However, the V_L -nullcline in Figure 2.7.A.1 is still cubic in shape due to the reciprocal inhibition between INT1 and the LG neuron, so the system still has the capability for exhibiting network oscillations. In particular, externally applied current in the LG neuron (I_{Ext}) allows the V_L - and w -nullclines to intersect along the unstable middle branch of the cubic (Figure 2.7.B) so that a gastric mill rhythm can result. However, the network oscillations are controlled by the slow dynamics (w) of the PK-induced outward current (I_K) in the LG neuron, similar to that which occurs when PK induces both I_{Proc} and I_K in the LG neuron (Figure 2.6).

Thus, Figure 2.7 first illustrates that network oscillations are still capable of being elicited in this asymmetrical reciprocally inhibitory circuit via the induction of a slow, non-inactivating outward current (I_K) in the LG neuron. However, Figure 2.7 also illustrates that the gastric mill rhythm elicited without I_{Proc} in the LG neuron is different from the gastric mill rhythm that involves PK-induction of I_{Proc} (Compare Figure 2.7.B and Figure 2.6). Thus, Figure 2.7 suggests that PK-induction of I_{Proc} in the LG neuron is necessary for eliciting a gastric mill rhythm that is similar to the MCN1-elicited rhythm. In the biological system, there are no known pharmacological agents that effectively block I_{Proc} in STG neurons (M.P. Nusbaum, personal communication), so current blockers can not be effectively used to check if I_{Proc} is involved in the PK-elicited gastric mill rhythm of the biological system. However, Figure 2.7 suggests that both I_{Proc} and I_K are required for PK to elicit a gastric mill rhythm that is similar to the MCN1-elicited rhythm.

2.3.2.4 PK Allows for Plateau Potential Generation in the LG neuron. Bath application of PK allows for plateau potential generation in the LG neuron of the biological system (Hertzberg and Nusbaum, 2004). In particular, a brief depolarizing current pulse in the LG neuron elicits a prolonged depolarization in LG that outlasts the brief pulse (Figure 2.8.A). This indicates that PK activates a slow mechanism in the LG neuron that supports the prolonged depolarization (Figure 2.8.A). Otherwise, the depolarized state in LG would terminate with the brief pulse. Also, since PK does not elicit a gastric mill rhythm when the pyloric-timed AB to INT1 inhibition is absent, the plateau potential in

Figure 2.8.A was generated in the absence of the pyloric-timed input to keep the LG neuron inactive before the brief current pulse.

For all three mechanisms proposed in this work, PK elicits a gastric mill rhythm via the induction of a slow current in the LG neuron. For example, in the first mechanism, PK induces a slowly-inactivating inward current in the LG neuron (I_{Plat}), where the slow inactivation of $I_{Plat}(n)$ drives the gastric mill rhythm (see Figure 2.4). As a result, the slow dynamics I_{Plat} inactivation allows for the generation of plateau properties in the LG neuron. In particular, after a brief depolarizing current pulse in the model LG neuron, the slow dynamics of I_{Plat} inactivation (n) sustain the prolonged active state in LG for a duration that outlasts the brief pulse (Figure 2.8.B). Specifically, a phase point can only jump back to the left branch after falling all the way down to the right knee of the V_L -nullcline (Figure 2.8.B). Thus, PK-induction of I_{Plat} in the model LG neuron allows for the generation of a plateau potential, similar to that which occurs in the biological system. The remaining two PK mechanisms proposed in this work also involve activation of a slow current in the LG neuron that drives the gastric mill rhythm. In particular, the slow dynamics (h) of I_h drive the gastric mill rhythm in Figure 2.5, while the slow dynamics (w) of I_K drive the gastric mill rhythm in Figure 2.6. As a result, all three proposed mechanisms can elicit plateau properties in the LG neuron since a phase point can only jump back to the left branch after reaching the right knee of the V_L -nullcline.

2.3.3 Calculation of Bounds on the Gastric Mill Period

This work has proposed three potential mechanisms by which PK can elicit a gastric mill rhythm that is similar to the MCN1-elicited rhythm. Now, the individual MCN1-elicited and PK-elicited gastric mill rhythms are generalized into a single 2-dimensional model given by Equations (2.45) and (2.46) (see Methods). This model is used to describe the general properties of the gastric mill rhythm instead of the specific properties induced by MCN1 or the individual PK mechanisms (Figure 2.9). The phase-plane trajectory of the general model can be tracked with singular (lower dimensional) sets of equations that govern different parts of the trajectory along its orbit (see Methods), and the simplified properties of the singular orbit can be used to compute bounds on the gastric mill period. In particular, the gastric mill period is bounded by upper and lower limits due to the pyloric-timed forcing, and these bounds model the variability in the gastric mill period that is observed in the biological system (Bartos et al., 1999).

The gastric mill rhythm of the generalized 2-dimensional model involves distinct time scales. In particular, the evolution of the phase-plane trajectory along the stable outer branches of the cubic V_L -nullcline is much slower than the jumps between these outer branches and the pyloric-timed transitions between left branches (Figure 2.9). Moreover, as the peaks of the pyloric forcing function $P(t, V_L)$ are small compared to the pyloric period, the time spent transitioning between left branches of the V_L -nullcline is negligible compared to the slow evolution up the left branch, so the pyloric-timed transitions between left branches can be ignored for computing the gastric mill period. Subsequently, the gastric mill rhythm can be described by the 2-dimensional model in Equations (2.51) and (2.52) (see Methods). In the singular limit where $\varepsilon \rightarrow 0$ in Equation

(2.51), the jumps between the stable branches of the cubic occur instantaneously with respect to the slow time scale ξ (see Methods). Using the results of (Mishchenko and Rozov, 1980), it can be shown that the non-singular orbit (where $\varepsilon \neq 0$ in Equation (2.51)) becomes $O(\varepsilon)$ close (as $\varepsilon \rightarrow 0$) to the singular orbit composed of the solutions to the singular Equations (2.53)-(2.54) and (2.55)-(2.56) (see Methods). As a result, the simplified properties of the singular orbit (where the phase-plane trajectory tracks the stable outer branches of the cubic and the jumps between stable branches are instantaneous) can be used to compute bounds on the gastric mill period.

Thus, beginning at the jump to the stable left branch where $y = y_{RK}$ in Figure 2.10 and utilizing the simplified properties of the singular orbit, a phase point climbs up the left branch according to $\frac{dy}{d\xi} = \frac{1-y}{\tilde{\tau}}$ of Equation (2.52) as y grows linearly toward 1. The shortest possible duration on the left branch occurs when the y -coordinate of the phase point reaches y_{LO} (Figure 2.10) at exactly the same time a pyloric forcing peak occurs. In this case, the forcing peak initiates the jump to the right branch of the V_L -nullcline at $y = y_{LO}$. In particular, the time of the jump corresponds to the time of the forcing peak since the forcing is impulsive (width of the pyloric forcing peak is small compared to pyloric period); therefore, the jump is not affected by amplitude-dependent forcing variations. Thus, the duration from y_{RK} to y_{LO} on the left branch of the V_L -nullcline is called the “minimum interburst duration” since it represents the shortest possible inactive phase of the LG neuron. To compute the minimum interburst duration, integration of $\frac{dy}{d\xi} = \frac{1-y}{\tilde{\tau}}$ gives

$$y(\xi) = 1 - (1 - y_{RK}) \exp\left(-\frac{\xi}{\tilde{\tau}}\right) \quad (2.57)$$

where $y(0) = y_{RK}$ initially on the left branch (Figure 2.10). Then, the smallest possible duration on the left branch of the V_L -nullcline is the time ξ_L required for y to increase from y_{RK} to y_{LO} (Figure 2.10). Solving Equation (2.57) for ξ_L with $y(\xi_L) = y_{LO}$ gives the minimum interburst duration

$$\xi_L = \tilde{\tau} \log\left(\frac{1 - y_{RK}}{1 - y_{LO}}\right). \quad (2.58)$$

Similarly, the shortest possible duration on the right branch is given by the time ξ_R required for the phase point to fall from $y = y_{LO}$ to $y = y_{RK}$ (Figure 2.10). This duration is called the “minimum burst duration” since it represents the shortest possible active phase of the LG neuron. To compute the minimum burst duration, integration of $\frac{dy}{d\xi} = -y$ in Equation (2.52) gives

$$y(\xi) = y_{LO} \exp(-[\xi - \xi_L]) \quad (2.59)$$

where $y(\xi_L) = y_{LO}$ at the point of the jump to the right branch. Moreover, by denoting the time at which the trajectory reaches $y = y_{RK}$ on the right branch by $\xi = T_{min}$, the minimum burst duration (ξ_R) in Figure 2.10 is expressed by $\xi_R = T_{min} - \xi_L$, where T_{min} is the period

of this gastric mill oscillation. Then, solving Equation (2.59) for ξ_R with $y(T_{min}) = y_{RK}$ gives the minimum burst duration

$$\xi_R = \log\left(\frac{y_{LO}}{y_{RK}}\right). \quad (2.60)$$

Thus, since the jumps between the stable branches of the cubic V_L -nullcline occur instantaneously with respect to the slow time scale ξ , the shortest possible gastric mill period is the sum of the minimum interburst and burst durations:

$$T_{min} = \xi_L + \xi_R. \quad (2.61)$$

However, T_{min} expresses the gastric mill period only for when a forcing peak initiates the jump to the right branch at precisely $y = y_{LO}$. Otherwise, the phase point continues to climb up the left branch above y_{LO} until the next forcing peak initiates the jump at $y = y_j$ (Figure 2.10). The jump at y_j occurs at most one pyloric period (T_P) after the phase point climbs above y_{LO} , since the jump to the right branch of the V_L -nullcline is initiated by a forcing peak. Thus, an upper bound for the duration on the left branch is given by

$$\bar{\xi}_L = \xi_L + T_P, \quad (2.62)$$

which is called the “maximum interburst duration”. Then, the duration on the right branch is given by the time required for the phase point to fall from y_j to y_{LO} plus the minimum burst duration (fall from y_{LO} to y_{RK}). If the time constants are assumed to be equal on both branches so that $\tilde{\tau} = \frac{\tau_{LO}}{\tau_{HI}} = 1$ in Equation (2.52) (see Methods), then the rate of evolution for the phase-plane trajectory will be the same on both branches. Therefore, the time required for the phase point to fall down the right branch from y_j to y_{LO} (Figure 2.10) is at most one pyloric period (T_P) more than the minimum burst duration. Thus, the “maximum burst duration” is given by

$$\bar{\xi}_R = \xi_R + T_P. \quad (2.63)$$

Consequently, an upper limit for the gastric mill period is given by the sum of Equations (2.62) and (2.63) to get

$$T_{\max} = \underbrace{\xi_L + \xi_R}_{T_{\min}} + 2T_P. \quad (2.64)$$

Although the jump to the right branch is initiated by a pyloric forcing peak, the jump back to the left branch does not necessarily coincide with a forcing peak since the pyloric forcing function does not affect the active state of the LG neuron (see Methods). Similarly, in the biological system the onset of the LG burst phase (modeled by the jump to the right branch) is always initiated by a pyloric peak, but the LG burst termination

(modeled by the jump back to the left branch) does not necessarily coincide with a pyloric peak (Bartos et al., 1999).

Consequently, since the jump to the right branch is always initiated by a pyloric forcing peak, an integer number of forcing peaks occur in the time between two consecutive jumps to the right branch during the gastric mill oscillation. Therefore, the gastric mill period (T) is an integer multiple of the pyloric period (T_p) so that $T = kT_p$, where k is an integer. From Equations (2.61) and (2.64), the gastric mill period is bounded by

$$T_{min} \leq T = kT_p < T_{min} + 2T_p. \quad (2.65)$$

Solving for the integer k gives

$$\frac{T_{min}}{T_p} \leq k < \frac{T_{min}}{T_p} + 2, \quad (2.66)$$

which indicates an upper and lower bound for the number of pyloric periods that occur during a gastric mill period.

In particular, when $T = T_{min}$ so that jumps to the right branch occur at $y = y_{LO}$ (**Figure 2.10**), T_{min}/T_p is an integer that gives the number of pyloric periods that occur during the gastric mill period. However, if $T > T_{min}$, then jumps to the right branch do not occur at precisely y_{LO} and are instead initiated by the next forcing peak at y_j (**Figure 2.10**), where $y_{LO} < y_j \leq y_{LO} + T_p$. Therefore, $T_{min}/T_p + 2$ is an upper bound in Equation

(2.66) for the number of pyloric periods that occur during the gastric mill period, but this upper bound is not an integer when $T(= kT_p) \neq T_{min}$. However, since k is an integer in Equation (2.66), the upper bound can be tightened to the integer

$$\frac{T_{min}}{T_p} \leq k \leq \left\lfloor \frac{T_{min}}{T_p} \right\rfloor + 2, \quad (2.67)$$

where $\lfloor \bullet \rfloor$ is the greatest integer function.

Subsequently, an expression for the lower bound of the gastric mill period (T_{min}) is derived from Equations (2.58), (2.60), and (2.61) to get

$$T_{min} = \tilde{\tau} \log \left(\frac{1 - y_{RK}}{1 - y_{LO}} \right) + \log \left(\frac{y_{LO}}{y_{RK}} \right). \quad (2.68)$$

Therefore, Equation (2.67) can be rewritten as

$$\frac{\tilde{\tau} \log \left(\frac{1 - y_{RK}}{1 - y_{LO}} \right) + \log \left(\frac{y_{LO}}{y_{RK}} \right)}{T_p} \leq k \leq \left\lfloor \frac{\tilde{\tau} \log \left(\frac{1 - y_{RK}}{1 - y_{LO}} \right) + \log \left(\frac{y_{LO}}{y_{RK}} \right)}{T_p} \right\rfloor + 2. \quad (2.69)$$

As a result, the bounds on the gastric mill period in Equation (2.65) are rewritten as

$$\tilde{\tau} \log\left(\frac{1-y_{RK}}{1-y_{LO}}\right) + \log\left(\frac{y_{LO}}{y_{RK}}\right) \leq T = kT_p \leq \left(\left[\frac{\tilde{\tau} \log\left(\frac{1-y_{RK}}{1-y_{LO}}\right) + \log\left(\frac{y_{LO}}{y_{RK}}\right)}{T_p} \right] + 2 \right) T_p. \quad (2.70)$$

Hence, an analytical formula has been derived that gives upper and lower limits for the gastric mill period. These limits are due to the effect of the pyloric-timed forcing in the model. Physiologically, the pyloric-timed forcing is used to describe the effect of the local inhibitory synaptic input from the AB neuron to INT1 in the biological system. Previous modeling (Nadim et al., 1998) and experiments (Bartos et al., 1999) showed that this synaptic input regulates the frequency of the MCN1-elicited gastric mill rhythm and time-locks the onset of the LG burst phase with a burst in the AB neuron of the pyloric circuit. In this work, the formula in Equation (2.70) describes the cycle-to-cycle variability that is observed in the gastric mill period of the biological system due to the effect of the pyloric-timed AB to INT1 synaptic input.

2.3.4 Summary of Results

In this chapter, a 2-dimensional model was derived to examine the network dynamics of the MCN1-elicited gastric mill rhythm and to propose three potential mechanisms by which PK can elicit a similar gastric mill rhythm in the absence of MCN1 participation. The following voltage-gated currents were shown to elicit a similar gastric mill rhythm when induced (potentially) by PK in the LG neuron

- I_{plat} (low-threshold, slowly inactivating plateau current)

- I_h (slow, hyperpolarization-activated inward current)
- $I_{Proc}+I_K$ (fast inward current + slow outward current, both non-inactivating)

In addition, each proposed PK-induced current

- Generates a plateau potential in the LG neuron, as occurs in the biological system
- Does not elicit a gastric mill rhythm in the absence of the AB to INT1 inhibition, as occurs in the biological system.

The proposed PK-induced currents can be checked in the biological system via the use of current blockers.

Finally, the individual MCN1-elicited and PK-elicited gastric mill rhythms were generalized into a single 2-dimensional model. This generalized model was used to compute bounds on the period of the gastric mill rhythm by determining the maximum and minimum values attained by the slow variable in the phase plane.

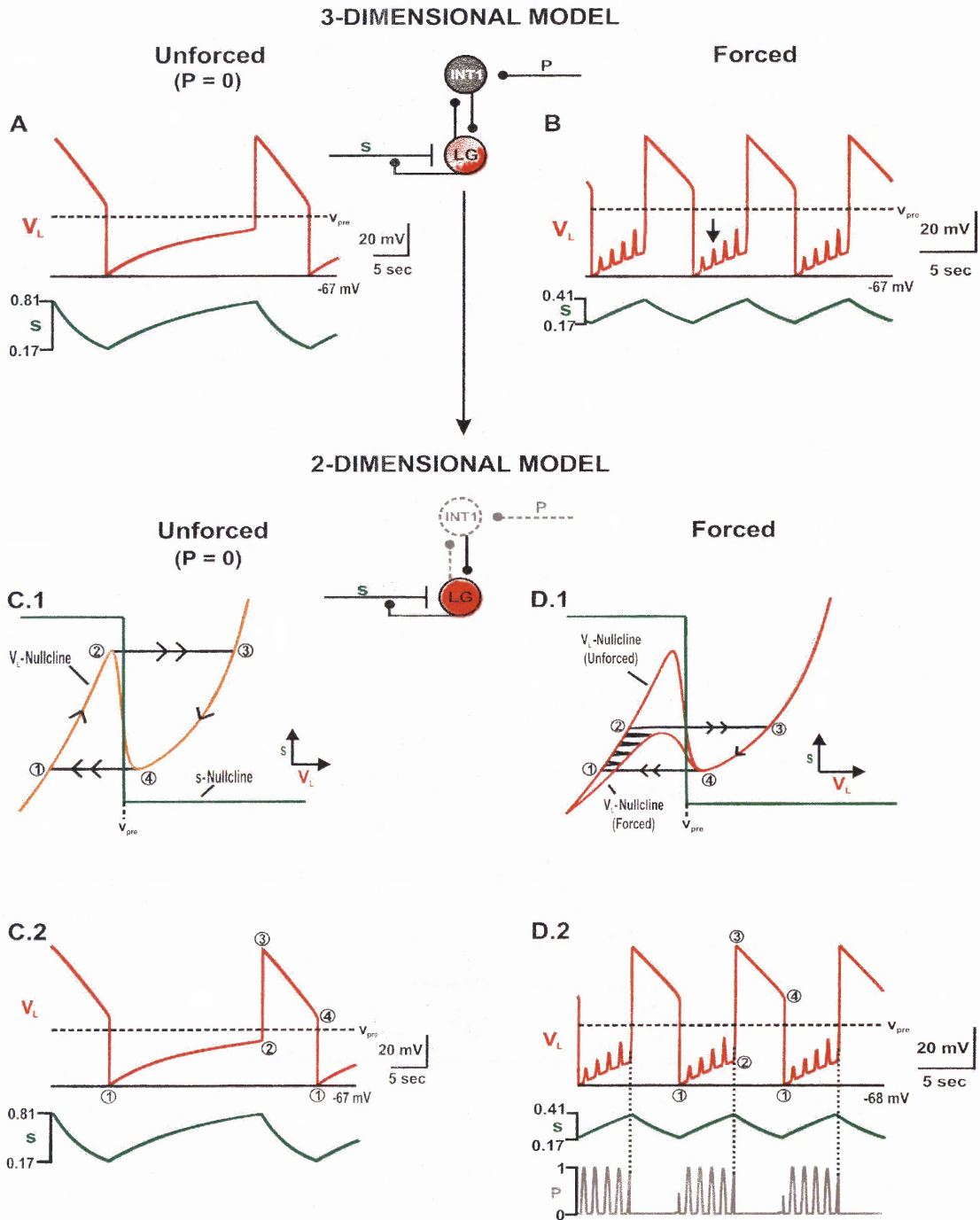


Figure 2.1 MCN1-Elicited Gastric Mill Rhythm (Reduction to 2 Dimensions). *A-B*, Network oscillations are driven by the slow variable s , which builds up in LG when $V_L \leq v_{pre}$ and decays when $V_L > v_{pre}$ due to LG presynaptic inhibition of MCN1. The pyloric inhibition of INT1 (P) disrupts INT1 inhibition of LG (arrow). *C.1-C.2*, Reduction to 2 dimensions (synapses onto INT1 absorbed into INT1 \rightarrow LG synapse). A phase point (V_L - s plane) climbs up the left branch of the V_L -nullcline as s builds up in LG and falls down the right branch when s decays in LG. *D.1-D.2*, The unforced (forced) cubics occur when $P=0$ ($P=1$) in *D.2*. The trajectory shifts between left branches due to P input, which increases the frequency of network oscillations and triggers the LG burst phase onset.

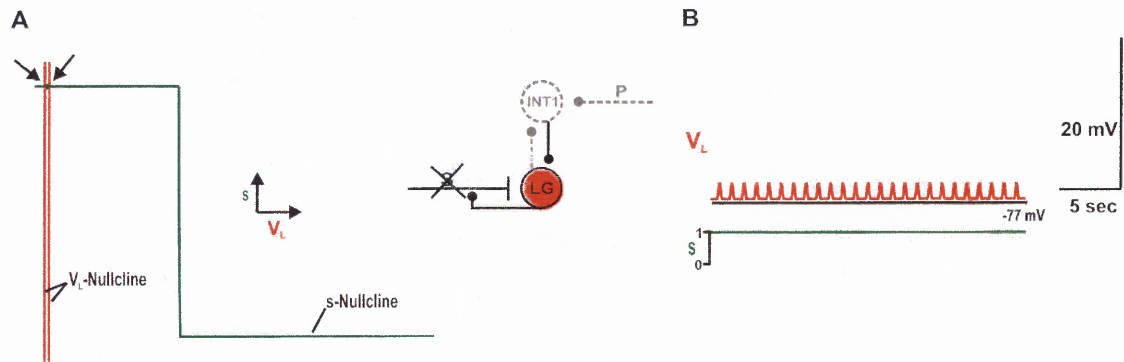


Figure 2.2 The Gastric Mill Rhythm is Not Spontaneously Active Without MCN1 Input. **A**, The V_L - and s -nullclines intersect at a stable fixed point to which the trajectory settles (arrows). Due to the effect of the pyloric-timed input P , multiple V_L -nullclines exist in the phase plane. The left V_L -nullcline corresponds to the unforced (higher) cubic of Figure 2.1.D.1 while the right V_L -nullcline corresponds to the forced (lower) cubic of the same figure. **B**, In the absence of MCN1 input, the LG neuron remains in its inactive state. The small depolarizations in V_L are due to the effect of P . Thus, the gastric mill rhythm is not spontaneously active in the absence of MCN1 input since the LG neuron never reaches its active state. This also occurs in the biological system (see Figure 1.5 – before MCN1 stimulation).

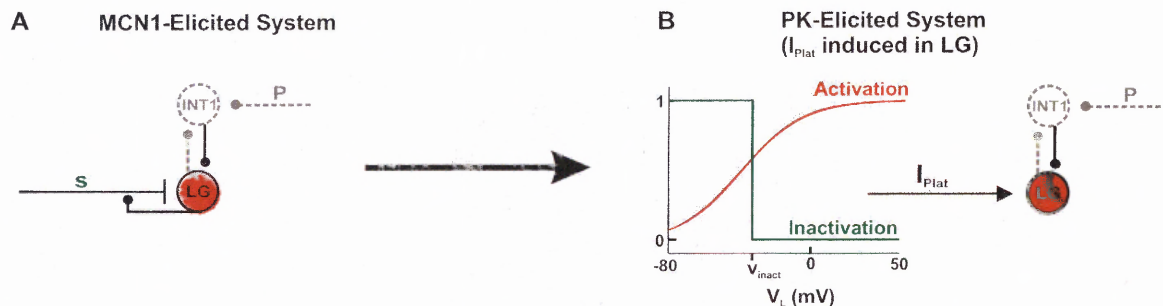


Figure 2.3 Switching From an MCN1-Elicited to a PK-Elicited Gastric Mill Rhythm. **A**, The MCN1-elicited gastric mill rhythm is driven by the slow excitation from MCN1 to LG (buildup in s) plus the presynaptic inhibition from LG back to MCN1 (decay in s), see also Figure 2.1. **B**, The PK-elicited gastric mill rhythm (where PK induces I_{Plat} in the LG neuron) is driven by the activation and inactivation of I_{Plat} in LG. Inactivation of I_{Plat} is much slower than activation of I_{Plat} . When switching between MCN1 and I_{Plat} for eliciting a gastric mill rhythm, all other model parameters remain the same (see also Tables 2.1 and 2.2).

PK-ELICITED GASTRIC MILL RHYTHM
(PK Induces I_{Plat} in LG)

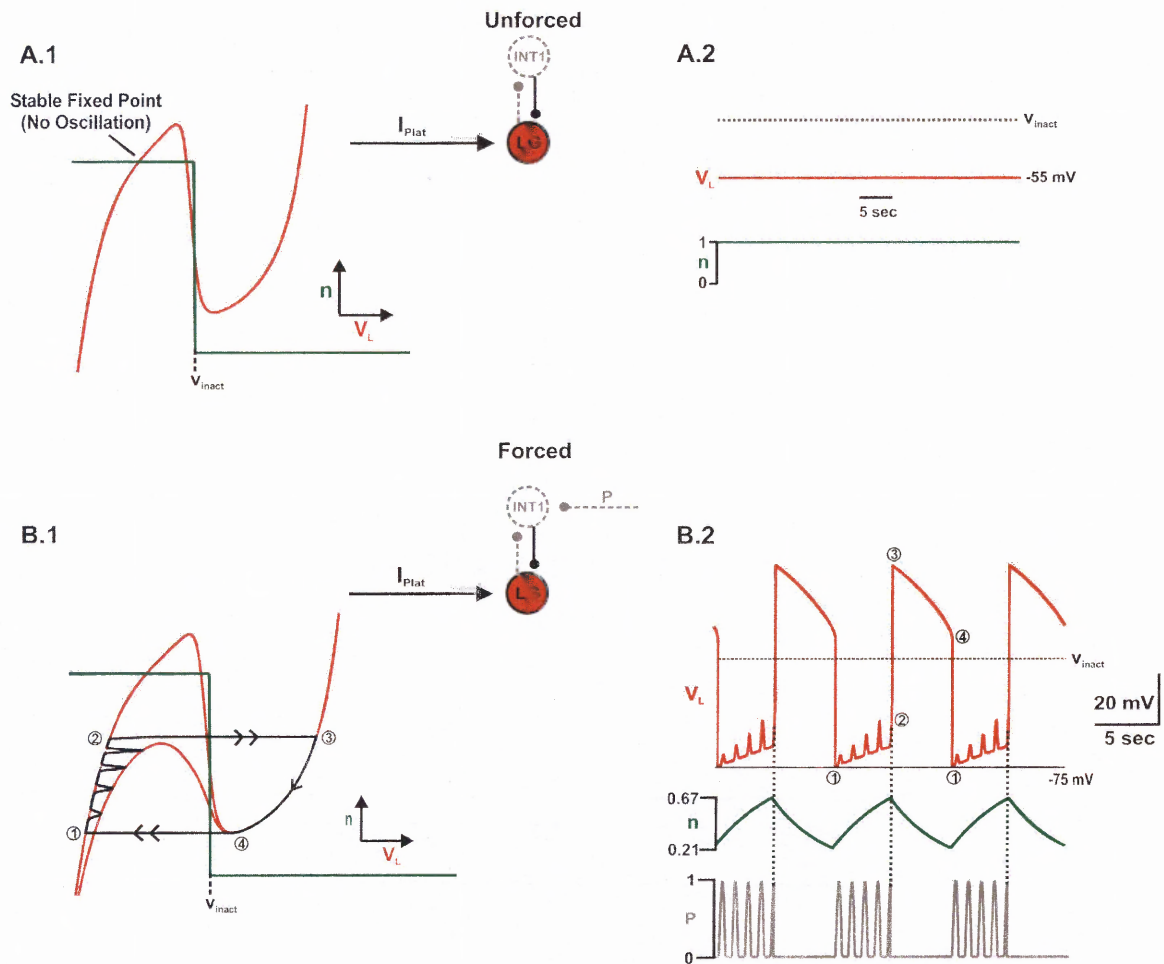


Figure 2.4 PK-Elicited Gastric Mill Rhythm (Mechanism 1: PK Induces I_{Plat} in the LG Neuron). *A.1-A.2*, In the unforced system (no P input), the trajectory in the V_L - s phase plane settles to the stable fixed point at the intersection of the V_L - and n -nullclines. As a result, PK does not elicit a gastric mill rhythm without the pyloric-timed inhibition of INT1 (P). This also occurs in the biological system (Hertzberg and Nusbaum, 2004). *B.1-B.2*, In the presence of P input, PK elicits a gastric mill rhythm that is similar to the MCN1-elicited rhythm (of Figure 2.1.D) via the induction of I_{Plat} in the LG neuron. A phase point climbs up the left branch of the cubic V_L -nullcline as I_{Plat} slowly de-inactivates (increase of n) in the LG neuron, and the phase point shifts between cubics due to the effect of P in *B.2*. The phase point then falls down the right branch of the V_L -nullcline as I_{Plat} slowly inactivates (decrease of n) in the LG neuron.

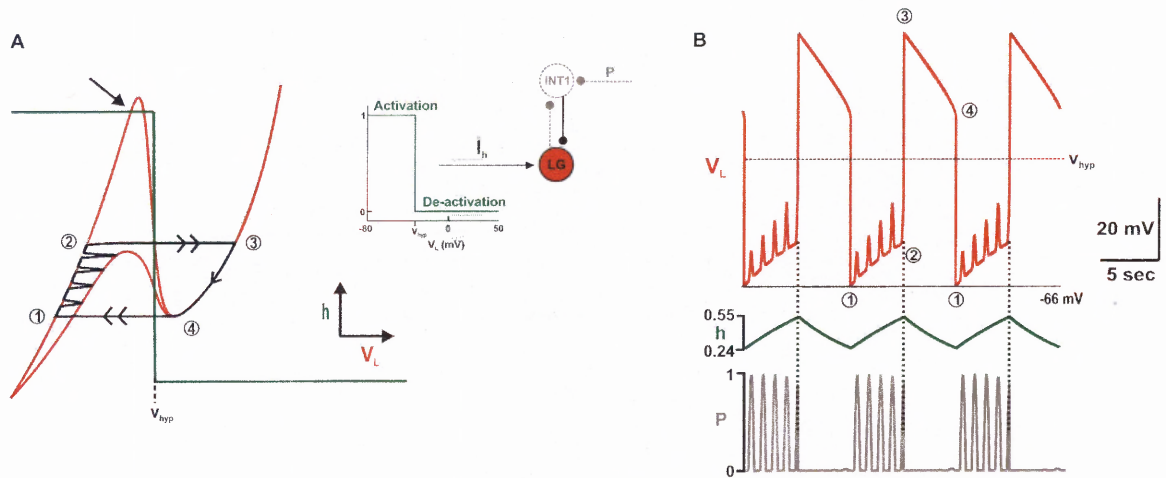


Figure 2.5 PK-Elicited Gastric Mill Rhythm (Mechanism 2: PK Induces I_h in the LG Neuron). *A*, Without P input, the h -nullcline intersects the stable left branch of the unforced (higher) V_L -nullcline. Thus, the trajectory would settle to a stable fixed point (arrow) and no network oscillations would occur without P input. *A-B*, In the presence of P input, PK elicits a similar gastric mill rhythm via the induction of I_h in LG. Activation of I_h (slow increase of h) in LG allows for a phase point to climb up the left branch of the V_L -nullcline as it is shifted between cubics, while de-activation of I_h (slow decrease of h) in LG causes the phase point to fall down the right branch of the V_L -nullcline.

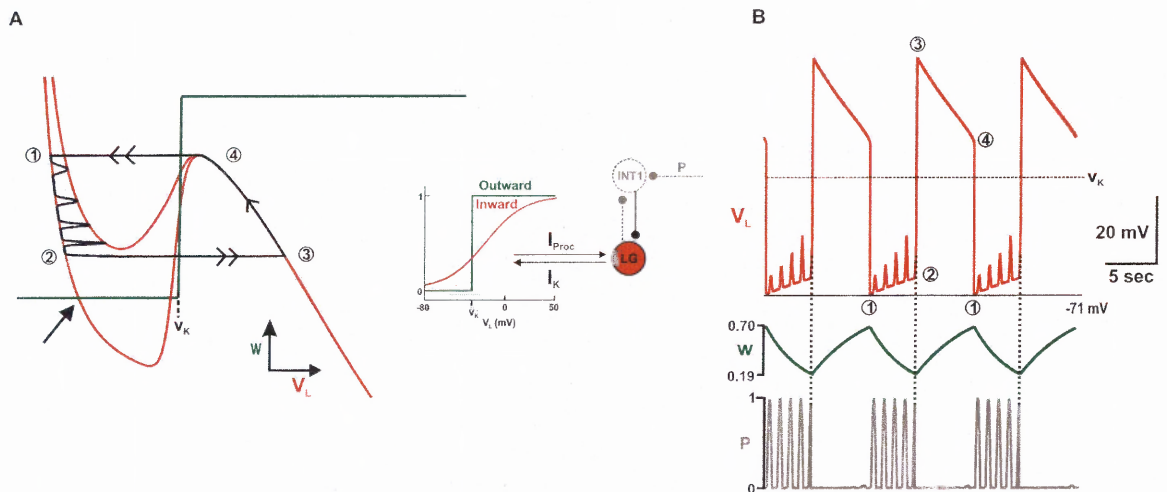


Figure 2.6 PK-Elicited Gastric Mill Rhythm (Mechanism 3: PK Induces I_{Proc} and I_K in the LG Neuron). I_{Proc} is a fast inward current while I_K is a slow outward current. The slow dynamics (w) of I_K control the network oscillations, where the lower (higher) V_L -nullcline occurs when $P=0$ ($P=I$) in *B*. *A*, Network oscillations do not occur without P input since the w -nullcline intersects the stable left branch of the unforced cubic (arrow). *A-B*, In the presence of P input, PK elicits a similar gastric mill rhythm. De-activation of I_K (decrease of w) allows for depolarization of LG as a phase point falls down the left branch of the V_L -nullcline and is shifted between cubics. Activation of I_K (increase of w) repolarizes LG as a phase point climbs up the right branch of the V_L -nullcline.

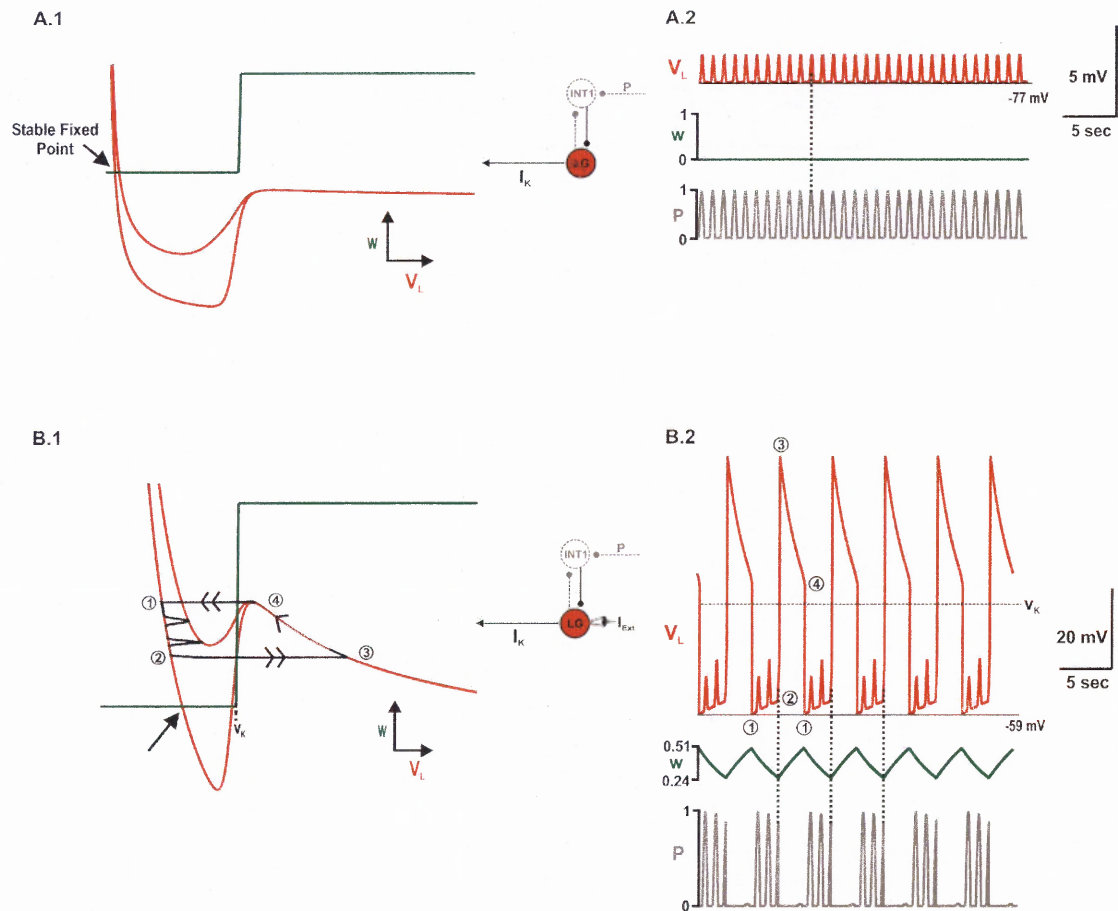


Figure 2.7 Network Oscillations Elicited Through PK Induction of Only I_K . **A.1-A.2,** When only the slow outward current (I_K) is induced by PK in the LG neuron, the V_L - and w -nullclines intersect at a stable fixed point (arrow). Therefore, without I_{Proc} to depolarize it, the LG neuron remains in its inactive state. The small depolarizations in V_L are due to the effect of P , where the lower (higher) V_L -nullclines correspond to when $P=0$ ($P=1$). However, the V_L -nullcline is still cubic in shape, so the PK-induced outward current (I_K) still has the capability of producing network oscillations. **B.1-B.2,** The intersection of the V_L - and w -nullclines can be moved to the unstable middle branch of the cubic by injecting external current (I_{Ext}) in LG. As a result, network oscillations are controlled by the slow dynamics (w) of I_K . Therefore, PK induction of the inward current (I_{Proc}) in LG is not necessary for eliciting network oscillations, but I_{Proc} is necessary for PK to elicit a gastric mill rhythm that is similar to the MCN1-elicited rhythm (compare B.2 above with Figure 2.1.D.2).

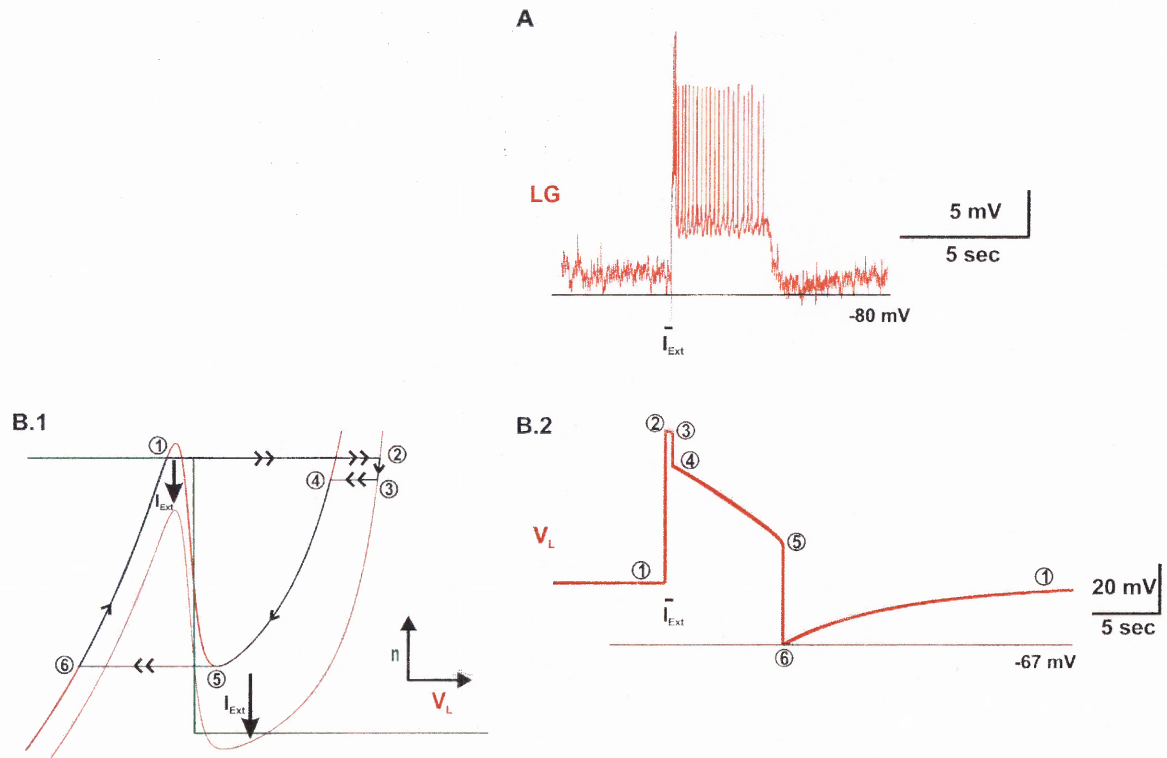


Figure 2.8 Plateau Potential Generation in the LG Neuron. **A**, In the biological system, PK elicits plateau properties in the LG neuron. In particular, a brief depolarizing current pulse elicits a prolonged depolarization in LG that outlasts the brief pulse. This indicates that PK induces a current with sufficiently slow dynamics in the LG neuron to support this prolonged depolarization. Also, the plateau potential is generated in the absence of the pyloric-timed inhibition of INT1 (P - see Figure 2.4.A) to keep the LG neuron inactive before the brief current pulse. **B.1-B.2**, PK-induced I_{Plat} in the LG neuron elicits plateau properties. In particular, the slow dynamics of I_{Plat} inactivation (n) support a prolonged depolarization in LG after a brief current pulse, since a phase point can only jump back to the left branch of the V_L -nullcline after falling all the way down to the right knee at the point 5. Similarly, the slow dynamics of both I_h and I_K in the other two PK mechanisms can also elicit plateau properties in LG due to the fact that a phase point only jumps back to the left branch of the V_L -nullcline after reaching the right knee.

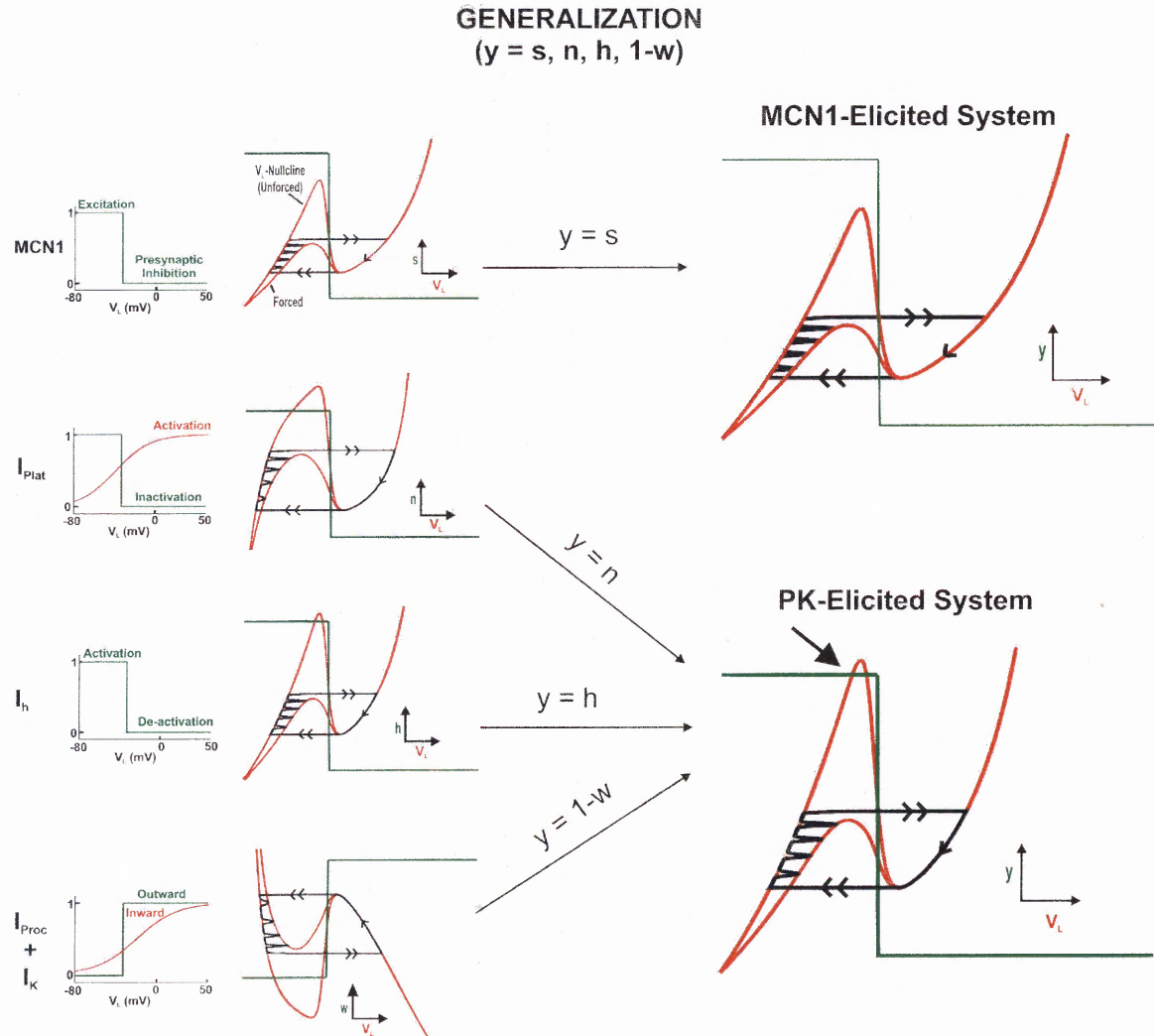


Figure 2.9 Generalization of the Individual 2-Dimensional Models. The gastric mill rhythms that are elicited by MCN1 and by each of the individual PK mechanisms (left) can be analyzed in a more general context. In particular, the slow variable that drives oscillations for each individual mechanism can be represented by the same variable (y). In this general context, PK still does not elicit a gastric mill rhythm in the absence of the pyloric-timed synaptic input P (bold arrow in PK-elicited system), but the MCN1-elicited and PK-elicited gastric mill rhythms are the same in the generalized context when the P input is present. As a result, the common geometrical properties of the phase-plane trajectory in the V_L - y phase plane (in the presence of P input) can be used to compute bounds on the gastric mill period.

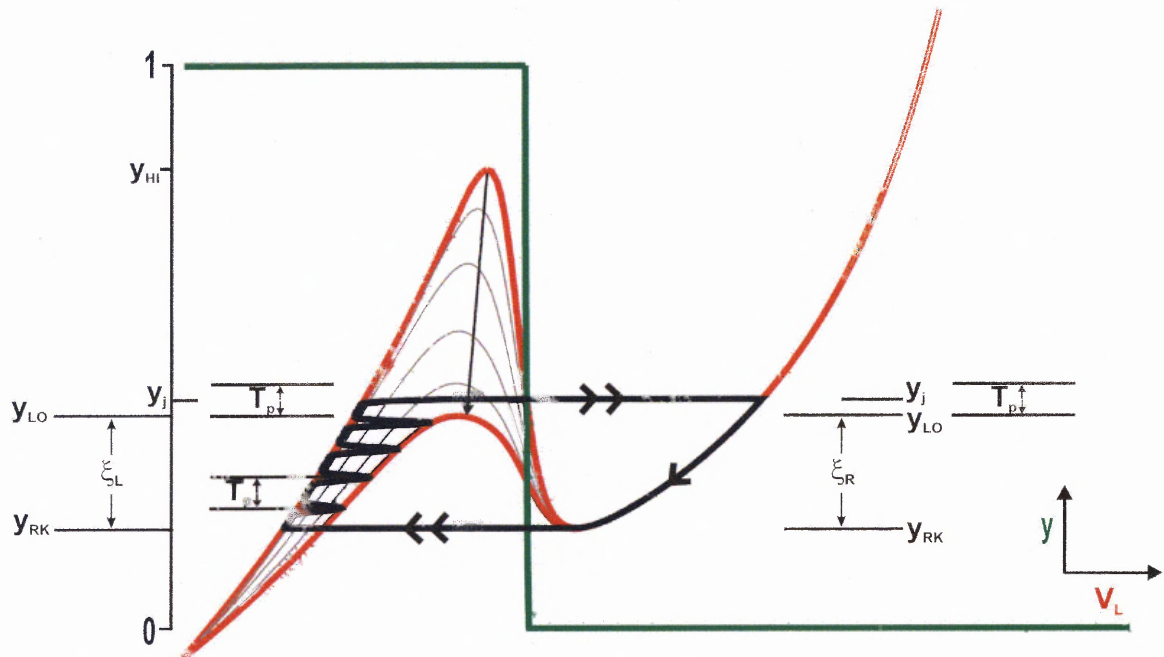


Figure 2.10 The Pyloric-Timed Input (P) Allows For Cycle-to-Cycle Variability in the Period of the Gastric Mill Rhythm. Beginning at the jump back to the left branch when $y=y_{RK}$, the shortest possible duration on the left branch (denoted by ζ_L) occurs when the y -coordinate of a phase point reaches y_{LO} at exactly the same time a pyloric forcing peak of P occurs to initiate the jump to the right branch. In this case, the duration on the right branch (denoted by ζ_R) is given by the time required to fall from $y=y_{LO}$ to $y=y_{RK}$. Thus, a lower bound for the gastric mill period (denoted by T_{min}) is given by $T_{min} = \zeta_L + \zeta_R$. However, if a forcing peak of P does not occur at exactly $y=y_{LO}$ on the left branch, then the phase point will continue to climb up the left branch until the next forcing peak lowers the V_L -nullcline below the phase point and initiates the jump to the right branch at $y=y_j$ (as in the figure). The jump at y_j can occur at most one pyloric period (T_P) after the phase point climbs above y_{LO} . As a result, the duration on the right branch is given by the time required to fall from $y=y_j$ to $y=y_{LO}$ (which takes at most one pyloric period T_P) plus the time ζ_R to fall down to $y=y_{RK}$. Thus, an upper bound for the gastric mill period is given by $T_{max} = T_{min} + 2T_P$.

CHAPTER 3

COMPARING PROJECTION NEURON AND NEUROMODULATORY EFFECTS ON NETWORK ACTIVITY USING A BIOPHYSICALLY-REALISTIC MODEL

3.1 Introduction

In this chapter, the MCN1-elicited and PK-elicited gastric mill rhythms are compared in the context of a more biophysically-realistic model. First, the mechanisms proposed in the reduced 2-dimensional model (previous chapter), which allow for PK to elicit a gastric mill rhythm that is similar to the MCN1-elicited rhythm, are assessed in the context of the more biophysically-realistic model. In each of the proposed mechanisms, PK elicits a gastric mill rhythm by boosting the activity of the LG neuron, via the induction of voltage-gated ionic currents, to balance the asymmetry within the INT1-LG reciprocally inhibitory pair (see Results, Figure 3.2). However, several details of the biological system were not included in the reduced 2-dimensional model. For example, INT1 and LG were treated as passive neurons so that action potential generation in them was ignored. Nonetheless, in the biophysically-realistic model of this chapter, all of the proposed PK mechanisms are still shown to elicit a gastric mill rhythm that is similar to the MCN1-elicited rhythm.

Next, the dorsal gastric (DG) neuron is added to the biophysically-realistic model. Physiologically, the DG neuron bursts in alternation with the LG neuron during both the MCN1-elicited and PK-elicited gastric mill rhythms (Figures 3.1, 3.2). During the MCN1-elicited rhythm, the DG neuron is an effective reporter of MCN1 activity within the STG (Coleman et al., 1995). However, the DG neuron does not have the same role in the PK-elicited rhythm, which occurs in the absence of MCN1 participation.

Consequently, the addition of the DG neuron to the biophysically-realistic model allows for a comparison of the cellular and network-level properties in both gastric mill rhythms.

First the cellular properties of both gastric mill rhythms are examined. Since the PK-elicited rhythm occurs in the absence of MCN1 participation, LG presynaptic inhibition of MCN1 is not involved in the PK-elicited rhythm. First, this chapter shows that PK elicits a similar gastric mill rhythm via the activation of plateau properties in the LG neuron. Then, using the same plateau properties in LG, this chapter assesses which aspects of the MCN1-elicited rhythm require the presence of the presynaptic inhibition.

Next, the two gastric mill rhythms are compared at the network level. Physiologically, the timing of activity in the DG neuron during the MCN1-elicited rhythm is determined by LG presynaptic inhibition of MCN1 (Coleman et al., 1995). Moreover, DG is only a follower neuron in the MCN1-elicited rhythm due to its lack of functional synaptic connections onto other STG neurons (Coleman et al., 1995). In contrast, bath application of PK strengthens an inhibitory synapse from the DG to LG neuron that is not functional in the MCN1-elicited rhythm (Hertzberg and Nusbaum, 2005). Therefore, the DG neuron may play a more active role in the PK-elicited rhythm, so its effect on network activity is examined using the biophysically-realistic model.

3.2 Methods

Previously, a conductance-based biophysical model of the MCN1-elicited gastric mill rhythm (Nadim et al., 1998) was used to show that a local synaptic input from the AB neuron of the pyloric circuit to INT1 strongly regulates the frequency of the MCN1-

elicited rhythm. INT1, LG, and MCN1 were treated as Hodgkin-and-Huxley type neurons in this biophysical model. Moreover, each neuron was modeled with a multi-compartment structure, where adjacent compartments were separated by an axial resistance, to separate the neuronal sites of synaptic input from that of action potential generation (Nadim et al., 1998). In addition, the local synapse from the AB neuron to INT1 was treated as an inhibitory periodic input in this model. However, this original biophysical model did not capture all of the features reported in the biological system for the MCN1-elicited rhythm. In particular, MCN1 still elicits a gastric mill rhythm of slower frequency when the AB to INT1 inhibition is removed in the biological system (Bartos et al., 1999), but the model did not produce a gastric mill rhythm in the absence of the AB to INT1 inhibition.

The original biophysical model has since been updated using insights gained from reduced mathematical modeling on the MCN1-elicited gastric mill rhythm (Manor et al., 1999; Ambrosio, 2005). In particular, in the updated model, MCN1 now elicits a slower gastric mill rhythm in the absence of the AB to INT1 inhibition, as occurs in the biological system. Moreover, the updated model was utilized in a recent study to investigate the effect of sensory feedback on the gastric mill rhythm (Beenhakker et al., 2005). All simulations of the biophysical model were performed with the software NETWORK, which is freely available at <http://stg.rutgers.edu/software/network/htm>.

3.2.1 Biophysically-Realistic Model of the MCN1-Elicited Gastric Mill Rhythm

Now, the updated conductance-based biophysical model of the MCN1-elicited gastric mill rhythm that is utilized in this chapter is described. Each neuron is modeled with

multiple compartments as shown in Figure 3.2. The membrane potential of a given compartment is obtained by numerical integration of a first-order differential equation of the form

$$C \frac{dV}{dt} = I_{Ext} - (I_{Leak} + \sum I_{axial} + \sum I_{ion} + \sum I_{syn}), \quad (3.1)$$

where V designates the membrane potential of the given compartment and the parameter C designates its membrane capacitance. I_{Ext} represents external (applied) current that can be injected into the neural compartment. I_{Leak} designates the leak current of the compartment, which models the passive flow of ions through the cell membrane. I_{Leak} is modeled by

$$I_{Leak} = g_{Leak} (V - E_{Leak}), \quad (3.2)$$

where the parameters g_{Leak} and E_{Leak} designate its conductance and reversal potential, respectively. Each I_{axial} represents an axial current which is induced in the given compartment due to a voltage difference with adjacent compartments. In particular, the i^{th} compartment of a neuron is influenced by axial currents from both the $(i+1)^{th}$ and $(i-1)^{th}$ compartments. Moreover, the sum of axial currents that affect the compartment in Equation (3.1) is modeled by

$$\sum I_{axial} = g^{i+1} (V - V^{i+1}) + g^{i-1} (V - V^{i-1}), \quad (3.3)$$

where V represents the membrane potential of the i^{th} compartment. Thus, g^{i+1} represents the axial conductance due to the voltage difference $(V - V^{i+1})$ with the adjacent compartment to the right. Similarly, g^{i-1} represents the axial conductance due to the voltage difference $(V - V^{i-1})$ with the adjacent compartment to the left. For terminal compartments, which have an adjacent neighbor only on one side, $g^{i+1} = 0$ for a right terminal compartment of a neuron while $g^{i-1} = 0$ for a left terminal compartment.

Next, each ionic current (I_{ion}) in Equation (3.1) is modeled by an equation of the form

$$I_{ion} = \bar{g}_{ion} m^p h^q (V - E_{ion}), \quad (3.4)$$

where \bar{g}_{ion} and E_{ion} designate its maximal conductance and equilibrium potential, respectively. Moreover, since the ionic conductance is voltage-gated, m and h designate activation and inactivation of the ionic conductance, respectively, where p and q are non-negative integers and $q = 0$ for a non-inactivating conductance. Both activation and inactivation are dependent upon the membrane potential of the compartment and are modeled by equations of the form

$$\tau_x(V) \frac{dx}{dt} = x_\infty(V) - x \quad x = m, h \quad (3.5)$$

$$x_\infty(V) = \frac{1}{1 + \exp(k(V - v_k))} \quad (3.6)$$

$$\tau_x(V) = \tau_1 + \frac{\tau_2}{1 + \exp(l(V - v_l))}. \quad (3.7)$$

In particular, the steady-state behavior for activation (or inactivation) of the ionic conductance is modeled by the sigmoidal function in Equation (3.6), where the parameters v_k and k represent the inflection point voltage and steepness of the sigmoid, respectively. Moreover, $k < 0$ for activation while $k > 0$ for inactivation. The corresponding time constant is described by the voltage-dependent sigmoid of Equation (3.7), where the parameters v_l and l similarly represent the inflection point voltage and steepness of the sigmoid, respectively. Moreover, the parameters τ_1 and τ_2 are used to model the extreme values of the time constant. For example, when $l < 0$ so that Equation (3.7) describes an increasing sigmoid, the minimum and maximum values of the sigmoid, which can be designated by τ_{LO} and τ_{HI} respectively, are given by $\tau_1 = \tau_{LO}$ and $\tau_2 = \tau_{HI} - \tau_{LO}$, so that Equation (3.7) describes a time constant for activation ($x = m$). On the other hand, when $l > 0$ so that Equation (3.7) describes a decreasing sigmoid, then $\tau_1 = \tau_{HI}$ and $\tau_2 = \tau_{LO} - \tau_{HI}$, and they describe a time constant for inactivation ($x = h$).

Then, each synaptic conductance in Equation (3.1) is modeled by an equation of the form

$$I_{syn} = \bar{g}_{syn} S(V - E_{syn}), \quad (3.8)$$

where the parameters \bar{g}_{syn} and E_{syn} designate its maximal conductance and reversal potential, respectively. The synaptic gating function, S , is dependent upon the membrane potential of the presynaptic compartment (V_{pre}), and the dynamics of the synapse are governed by equations of the form

$$\tau_S(V_{pre}) \frac{dS}{dt} = S_\infty(V_{pre}) - S \quad (3.9)$$

$$S_\infty(V_{pre}) = \frac{1}{1 + \exp(\alpha(V_{pre} - v_\alpha))} \quad (3.10)$$

$$\tau_S(V_{pre}) = \tau_3 + \frac{\tau_4}{1 + \exp(\beta(V_{pre} - v_\beta))}. \quad (3.11)$$

The steady-state behavior of the synapse is modeled by the sigmoid in Equation (3.10), whose inflection point voltage and steepness are given by the parameters v_α and α , respectively. Moreover, the synaptic time constant is modeled by the sigmoid in Equation (3.11), where v_β and β similarly model the inflection point voltage and steepness of the sigmoid while τ_3 and τ_4 model the voltage-dependent values of the time constant as described for the parameters τ_1 and τ_2 of Equation (3.7).

Finally, in the biological system, MCN1 axon terminals are electrically coupled to the LG neuron locally within the STG (Coleman et al., 1995). This fact is accounted for in the biophysical model by coupling the MCN1 axon terminal compartment and the LG

neurite compartment (see Figure 3.2). Moreover, electrical coupling between compartments is modeled by

$$I_{elec} = g_{elec} (V - V_{couple}), \quad (3.12)$$

where V designates the membrane potential of a given compartment while V_{couple} represents the membrane potential of the coupled compartment. The term in Equation (3.12) is subtracted from the right hand side of Equation (3.1) for the electrically coupled compartments. All parameter values for the MCN1-elicited gastric mill rhythm are given in Appendix A.

3.2.2 Building a Biophysically-Realistic Model of the PK-Elicited Gastric Mill Rhythm

Now, the biophysically-realistic model of the MCN1-elicited gastric mill rhythm is utilized to investigate how the neuromodulator PK can elicit a similar gastric mill rhythm. In the biological system, the gastric mill rhythm is not spontaneously active in the absence of MCN1 input (see Figure 1.2). Moreover, PK elicits a similar gastric mill rhythm when it is bath applied to the isolated STG (Figure 3.1); therefore, the PK-elicited rhythm occurs in the absence of MCN1 participation (Hertzberg and Nusbaum, 2005). Using the reduced 2-dimensional model in the previous chapter, three different mechanisms were proposed by which PK can elicit a gastric mill rhythm that is similar to the MCN1-elicited rhythm. Now, in this chapter, the efficacy of the proposed PK mechanisms is assessed in the context of the biophysically-realistic model.

For each of the mechanisms proposed in the previous chapter, PK elicits a similar gastric mill rhythm via the induction of voltage-gated ionic currents in the LG neuron. These PK-induced currents are denoted by I_{plat} , I_h , and $I_{Proc} + I_K$ for the three proposed mechanisms, respectively.

In the first mechanism, PK is proposed to induce a low-threshold, slowly-inactivating inward current in the LG neuron that is modeled by

$$I_{plat} = \bar{g}_{plat} m h (V - E_{plat}), \quad (3.13)$$

where the parameters \bar{g}_{plat} and E_{plat} designate the maximal conductance and equilibrium potential of the current, respectively. Moreover, as in Equation (3.4) m and h designate activation and inactivation, respectively, where $p = q = 1$ for I_{plat} . Moreover, the dynamics of activation and inactivation are modeled by Equations (3.5)-(3.7). In the case of I_{plat} which is a low-threshold slowly-inactivating current, inactivation (h) is modeled with a lower voltage threshold (v_k) and with a larger time constant (larger values of τ_1 and τ_2) than that of activation (m).

In the second mechanism, PK is proposed to induce a slow, hyperpolarization-activated, inward current in the LG neuron that is modeled by

$$I_h = \bar{g}_h m (V - E_h), \quad (3.14)$$

where the parameters \bar{g}_h and E_h designate the maximal conductance and equilibrium potential of the current, respectively. Physiologically, I_h is a slow, non-inactivating

current that is induced by hyperpolarization (Angstadt and Calabrese, 1989). Therefore, activation (m) of I_h is modeled with a relatively large time constant in Equation (3.7). Moreover, in the previous chapter I_h was used to show that PK-induction of a non-inactivating current in the LG neuron is sufficient to elicit a similar gastric mill rhythm.

In the final mechanism, PK is proposed to induce two non-inactivating currents in the LG neuron; in particular, a fast inward current (I_{proc}) for depolarization of the LG neuron plus a slow outward current (I_K) for repolarization of LG. Physiologically, several different neuropeptides have been shown to induce I_{proc} in STG neurons (Swensen and Marder, 2000, 2001). Accordingly, since PK is also a neuropeptide, it is assumed to induce I_{proc} in the LG neuron, which is modeled by

$$I_{proc} = \bar{g}_{proc} m (V - E_{proc}). \quad (3.15)$$

The parameters \bar{g}_{proc} and E_{proc} designate the maximal conductance and equilibrium potential of the current, respectively. Moreover, I_{proc} is modeled with small values of τ_1 and τ_2 in Equation (3.7) to model the fact that its activation (m) occurs with relatively fast kinetics in the biological system (Golowasch and Marder, 1992). The second proposed PK-induced current in this mechanism is a slow non-inactivating outward current that is modeled by

$$I_K = \bar{g}_K m (V - E_K), \quad (3.16)$$

where the parameters \bar{g}_K and E_K denote its maximal conductance and equilibrium potential, respectively. Physiologically, I_K is a slow outward current, and it is modeled with a relatively large time constant in Equation (3.7).

Parameter values for the proposed PK-induced currents in the LG neuron are given in Appendix A.

3.2.3 Including the Dorsal Gastric Neuron in the Biophysically-Realistic Model

The dorsal gastric (DG) neuron is included in the biophysically-realistic model of the MCN1-elicited and PK-elicited gastric mill rhythms. Physiologically, the DG neuron bursts in alternation with the LG neuron (see Figure 1.2). In the MCN1-elicited rhythm, the DG neuron is an effective reporter of MCN1 activity because it bursts in response to excitatory synaptic input from MCN1 axon terminals within the STG (Coleman et al., 1995). However, presynaptic inhibition of MCN1 (by the LG neuron) causes the DG neuron to become quiescent (Coleman et al., 1995). Therefore, the DG neuron bursts only when MCN1 axon terminals are uninhibited within the STG. In contrast, during the PK-elicited gastric mill rhythm which occurs in the absence of MCN1 participation, DG neuron bursts are generated by the neuromodulatory actions of PK. In this chapter, the biophysically-realistic model is used to compare the cellular mechanisms that drive DG activity in the MCN1-elicited and PK-elicited gastric mill rhythms.

3.2.3.1 *The DG Neuron is Modeled With the Intrinsic Currents I_h and I_K .* Two non-inactivating currents that contribute to the cellular properties of the DG neuron in the biological system are used for building a model of the DG neuron. In particular, a slow

hyperpolarization-activated inward current (I_h), which is described by Equation (3.14), and a slow outward current (I_K), which is described by Equation (3.16), are included in the model DG neuron. Physiologically, I_h and I_K are modulated in the DG neuron by synaptic input from the gastropyloric muscle stretch receptor (GPR) neurons, which project into the STG from the foregut (Katz and Harris-Warrick, 1989; Kiehn and Harris-Warrick, 1992a, b). In particular, GPR serotonin release enhances I_h but weakens I_K in the DG neuron (Katz, 1995b). Moreover, I_h contributes to the resting potential of the DG neuron in the biological system (Kiehn and Harris-Warrick, 1992a). In addition, although I_K in the DG neuron of the biological system is dependent upon both K^+ and Ca^{2+} ions (Kiehn and Harris-Warrick, 1992a), I_K in the model DG neuron is approximated by a voltage-dependent outward K^+ current in the form of Equation (3.16).

3.2.3.2 The Model DG Neuron Bursts in Response to I_{Proc} . In this work, bursting in the model DG neuron is generated by a proctolin-like current (I_{Proc}), as described by Equation (3.15). Experimental data from the biological system is used to support this role for I_{Proc} in the model DG neuron. First, in the MCN1-elicited gastric mill rhythm of the biological system, the DG neuron exhibits rhythmic bursting in response to synaptic input from MCN1 axon terminals. During the MCN1-elicited rhythm, MCN1 releases its neuropeptide co-transmitters proctolin and CabTRP Ia into the STG (Blitz et al., 1999). Physiologically, the DG neuron is not responsive to bath application of proctolin, but experimental data strongly suggests that MCN1 uses CabTRP Ia to excite the DG neuron (Wood et al., 2000). In particular, rhythmic bursting in the DG neuron is disrupted during the MCN1-elicited rhythm after bath application of Spantide I (Wood et al., 2000),

a tachykinin receptor antagonist that blocks the actions of CabTRP Ia (Christie et al., 1997). Specifically, bath application of Spantide switches the activity of the DG neuron from rhythmic bursting to tonic firing (Wood et al., 2000) (see also Results, Figure 3.6). Therefore, this strongly suggests that MCN1 uses its neuropeptide co-transmitter CabTRP Ia to generate rhythmic bursting in the DG neuron. In independent experiments, bath application of CabTRP Ia was shown to activate I_{proc} in many STG neurons (Swensen and Marder, 2000). As a result, this work assumes that MCN1-released CabTRP Ia induces I_{proc} in the DG neuron to facilitate rhythmic bursting.

On the other hand, in the PK-elicited gastric mill rhythm the DG neuron exhibits very similar bursting activity to that in the MCN1-elicited rhythm. However, the PK-elicited rhythm occurs in the absence of MCN1 participation (Hertzberg and Nusbaum, 2005). Therefore, MCN1 is not responsible for generating rhythmic bursts in the DG neuron during the PK-elicited rhythm. However, since PK is a neuropeptide, and several different neuropeptides have been shown to induce I_{proc} in STG neurons (Swensen and Marder, 2000), PK is assumed to induce I_{proc} in the DG neuron, as modeled by Equation (3.15), to generate rhythmic bursting in DG. It is noted that the neuropeptide PK was similarly assumed to induce I_{proc} in the LG neuron as part of the third proposed mechanism for the PK-elicited gastric mill rhythm (see Figure 3.2.C.3).

3.2.3.3 Incorporating the Model DG neuron in the MCN1-Elicited and PK-Elicited Gastric Mill Rhythms. The model DG neuron is included in the biophysically-realistic model of the MCN1-elicited and PK-elicited gastric mill rhythms. Physiologically, the two gastric mill rhythms are driven by different functional circuits, since the PK-elicited

rhythm occurs in the absence of MCN1 participation (Hertzberg and Nusbaum, 2005). In this work, the biophysically-realistic model is used to compare how network activity is coordinated in the MCN1-elicited and PK-elicited gastric mill rhythms. Furthermore, the inclusion of the DG neuron in the biophysically-realistic model allows for a more complete comparison with the MCN1-elicited and PK-elicited gastric mill rhythms of the biological system (Coleman et al., 1995; Bartos et al., 1999; Wood et al., 2000; Hertzberg and Nusbaum, 2005).

Parameter values for the model DG neuron are included in **Tables 3.1** and **3.2**.

3.3 Results

The biophysically-realistic model is now used to investigate the MCN1-elicited and PK-elicited gastric mill rhythms. Physiologically, it is believed that both excitatory synaptic input from MCN1 axon terminals within the STG plus presynaptic inhibition of these terminals by the LG neuron are necessary for eliciting a gastric mill rhythm (Coleman et al., 1995). Moreover, DG is a follower neuron during the MCN1-elicited rhythm due to its lack of functional synaptic connections onto other neurons within the STG (Coleman et al., 1995). In contrast, the PK-elicited rhythm, which occurs in the absence of MCN1 participation, involves a different functional circuit that elicits a similar gastric mill rhythm (Hertzberg and Nusbaum, 2005). Moreover, bath application of PK strengthens an inhibitory synapse from the DG to LG neuron (Figure 3.1) that is not functional during the MCN1-elicited rhythm (Hertzberg and Nusbaum, 2005). Therefore, the DG neuron may play a more active role in the PK-elicited rhythm.

First, the biophysically-realistic model is used to investigate the cellular properties that underlie the MCN1-elicited and PK-elicited gastric mill rhythms. In particular, the cellular mechanisms that were proposed for the PK-elicited gastric mill rhythm in the 2-dimensional model of the previous chapter are assessed in the context of the biophysically-realistic model. Next, since the PK-elicited rhythm does not involve presynaptic inhibition of MCN1 yet is still similar to the MCN1-elicited rhythm, the biophysically-realistic model is used to assess which aspects of the MCN1-elicited rhythm require the presence of the presynaptic inhibition. Then, the properties of the MCN1-elicited and PK-elicited gastric mill rhythms are compared at the network level. In particular, the biophysically-realistic model is used to examine which features of the MCN1-elicited rhythm are responsible for coordinating the timing of network activity. Similarly, the model is then used to investigate which features of the PK-elicited rhythm coordinate the timing of network activity. Finally, since the gastric mill rhythm controls food chewing in the biological system, the model is used to compare the types of chewing modes that may be activated during the MCN1-elicited and PK-elicited gastric mill rhythms.

3.3.1 The MCN1-Elicited Gastric Mill Rhythm in the Biophysically-Realistic Model

The frequency of the MCN1-elicited rhythm is driven by the slow excitatory synaptic input (s) from the MCN1 axon terminals to the LG neuron (Figure 3.2.B). Physiologically, MCN1 excitation of INT1 occurs on a faster time scale and does not drive the frequency of the MCN1-elicited rhythm, as confirmed by previous experiments (Bartos et al., 1999) and modeling (Nadim et al., 1998). Thus, during the inactive state of

the LG neuron, where it is inhibited by INT1, MCN1 excitation (s) slowly builds up in LG (Figure 3.2.B). The small-amplitude depolarizations in the LG membrane potential are due to the effect of the AB to INT1 inhibition (Figure 3.2.B). In particular, AB inhibition of INT1 in turn disrupts INT1 inhibition of the LG neuron, which effectively disinhibits the LG neuron from INT1. After a sufficient buildup of s excitation, the LG neuron escapes from INT1 inhibition and begins to burst. As a result, the LG neuron inhibits INT1 and presynaptically inhibits the MCN1 axon terminals (Figure 3.2.B). This presynaptic inhibition blocks MCN1 excitation to both INT1 and LG. However, since s decays slowly in the LG neuron (Figure 3.2.B), the LG burst phase continues during the presynaptic inhibition. Moreover, the electrical coupling between the LG neuron and the MCN1 axon terminals, which is not affected by presynaptic inhibition, is believed to prolong the LG burst phase (Coleman et al., 1995). However, the role of this electrical coupling during the MCN1-elicited rhythm is still not clearly understood. It is also noted that the AB to INT1 inhibition does not affect the LG burst phase, as occurs in the biological system (Bartos et al., 1999), because the INT1 to LG inhibitory synapse (inset of Figure 3.2.B) becomes inactive during the LG burst phase; as a result, the effect of the AB to INT1 inhibition is not effectively transmitted to the LG neuron through the inactive synapse. Subsequently, the LG burst phase terminates after a sufficient decay of s excitation in LG (Figure 3.2.B) and MCN1 is released from the presynaptic inhibition as the LG neuron falls back down into its inactive phase where it is inhibited by INT1. Then, the cycle begins again as s builds up in LG.

3.3.2 The PK-Elicited Gastric Mill Rhythm in the Biophysically-Realistic Model

Physiologically, the gastric mill rhythm is not spontaneously active in the absence of projection neuron input. In particular, the LG neuron rests in its inactive state while it is inhibited by INT1 which is active in the isolated STG (Bartos et al., 1999). In the biophysically-realistic model, the gastric mill rhythm is similarly not spontaneously active in the absence of MCN1 input (Figure 3.2.A). However, in the biological system bath application of the neuromodulator PK to the isolated STG elicits a gastric mill rhythm that is similar to the MCN1-elicited rhythm (Hertzberg and Nusbaum, 2005). Now, the biophysically-realistic model is used to assess the proposed mechanisms of the 2-dimensional model in the previous chapter that allowed for PK to elicit a similar gastric mill rhythm. Subsequently, we show that all three mechanisms proposed in the 2-dimensional model also allow for PK to elicit a similar gastric mill rhythm in the context of the biophysically-realistic model.

3.3.2.1 PK-Induction of a Slowly Inactivating Inward Current (I_{Plat}) in the LG Neuron Elicits a Similar Gastric Mill Rhythm. First, PK is shown to elicit a similar gastric mill rhythm via the induction of a low-threshold, slowly-inactivating inward current (I_{Plat}) in the LG neuron. This PK-induced current is modeled by Equation (3.13) with a fast activation plus a slow inactivation (see Methods). Thus, I_{Plat} is a regenerative current that, when induced by PK in the LG neuron, elicits a gastric mill rhythm that is similar to the MCN1-elicited rhythm. However, while the MCN1-elicited rhythm is controlled by the slow excitation from MCN1 to LG (s) plus the presynaptic inhibition from LG back to MCN1, this PK-elicited rhythm is instead controlled by the fast activation plus slow

inactivation of I_{Plat} in the LG neuron. Moreover, the frequency of this PK-elicited rhythm is driven by the slow inactivation of I_{Plat} , denoted by h (Figure 3.2.C.1). In particular, during the inactive state of the LG neuron where it is inhibited by INT1, I_{Plat} slowly de-inactivates in the LG neuron (increase of h – Figure 3.2.C.1), which allows for activation of I_{Plat} to occur (inset of Figure 3.2.C.1). As a result, I_{Plat} flows into and slowly depolarizes the LG neuron. Once again, the small-amplitude depolarizations in the LG membrane potential are due to the effect of the AB to INT1 inhibition, which disinhibits the LG neuron from INT1, as discussed for the MCN1-elicited rhythm. Moreover, since I_{Plat} inactivation is dependent upon the LG membrane potential (see Methods), each disinhibition of the LG neuron from INT1, which results in a small depolarization of LG, also results in a small inactivation of I_{Plat} (small decrease of h - Figure 3.2.C.1). After a sufficient buildup of I_{Plat} , the LG neuron escapes from INT1 inhibition and begins to burst. As a result, LG inhibits INT1 and I_{Plat} slowly inactivates in the LG neuron during its burst phase (decrease of h – Figure 3.2.C.1). It is noted that I_{Plat} activation occurs on a faster time scale and does not control the duration of the LG burst phase. Moreover, the AB to INT1 inhibition does not affect the LG burst phase as discussed for the MCN1-elicited rhythm. Subsequently, the LG burst phase terminates after a sufficient inactivation of I_{Plat} , and the LG neuron falls back down into its inactive state where it is inhibited by INT1. Then, the cycle begins again with the slow de-inactivation (increase in h) of I_{Plat} in the LG neuron. Thus, PK can elicit a gastric mill rhythm that is similar to the MCN1-elicited rhythm via the induction of I_{Plat} in the LG neuron.

3.3.2.2 *PK-Induction of a Slow, Hyperpolarization-Activated Inward Current (I_h) in the LG Neuron Elicits a Similar Gastric Mill Rhythm.* Next, it is shown that PK can elicit a similar gastric mill rhythm via the induction of a slow, hyperpolarization-activated inward current (I_h) in the LG neuron (Figure 3.2.C.2). I_h is a non-inactivating current modeled by Equation (3.14), (see Methods). In particular, activation of I_h occurs at low LG membrane potentials while de-activation of I_h occurs when LG reaches a high membrane potential (inset of Figure 3.2.C.2). Thus, as in the 2-dimensional model of the previous chapter, the biophysically-realistic model suggests that PK-induction of I_h in the LG neuron is sufficient to elicit a similar gastric mill rhythm. In particular, during the inactive state of the LG neuron where it is inhibited by INT1, I_h slowly activates in the LG neuron (increase in m – Figure 3.2.C.2). As a result, I_h flows into and slowly depolarizes the LG neuron. The fast, small-amplitude depolarizations in the LG membrane potential (Figure 3.2.C.2) are caused by the AB to INT1 inhibition which disinhibits the LG neuron from INT1, as discussed for the MCN1-elicited rhythm. Moreover, I_h undergoes a small de-activation (decrease in m – Figure 3.2.C.2) for each disinhibition in the LG neuron, since the conductance of I_h depends on the LG membrane potential (see Methods). Then, after a sufficient buildup of I_h , the LG neuron escapes from INT1 inhibition and begins to burst. As a result, LG inhibits INT1, and I_h slowly de-activates in the LG neuron during its burst phase (decrease in m – Figure 3.2.C.2). Moreover, the AB to INT1 inhibition does not affect the LG burst phase, as discussed for the MCN1-elicited rhythm. Subsequently, the LG burst terminates after sufficient de-activation of I_h , and the LG neuron falls back down into its inactive state where it is inhibited by INT1. Then, the cycle begins again with activation of I_h in the LG neuron.

Thus, in the second proposed mechanism, PK elicits a similar gastric mill rhythm via the induction of a non-inactivating current (I_h) in the LG neuron. This suggests that an inactivating current (such as I_{plat}) is not necessary for PK to elicit a similar gastric mill rhythm.

3.3.2.3 PK-Induction of Two Non-Inactivating Currents in the LG Neuron Elicits a Similar Gastric Mill Rhythm. A third mechanism by which PK can elicit a similar gastric mill rhythm is by the induction of two non-inactivating currents in the LG neuron; in particular, a fast inward current (I_{proc}), as modeled by Equation (3.15), plus a slow outward current (I_K), as modeled by Equation (3.16), (see Methods). I_{proc} and I_K play different roles in generating the gastric mill rhythm. In particular, I_{proc} depolarizes the LG neuron, which facilitates the transition to the LG burst phase, while I_K repolarizes the LG neuron, which causes the transition back to the inactive phase of LG. Both roles were performed by a single current in the previous two PK mechanisms. Moreover, the PK-induction of both I_{proc} and I_K in the LG neuron elicits a similar gastric mill rhythm whose frequency is controlled by the slow activation dynamics (m) of I_K (Figure 3.2.C.3). In particular, during the inactive state of the LG neuron where it is inhibited by INT1, I_K slowly de-activates (decrease in m – Figure 3.2.C.3), which restricts the flow of I_K out of the LG neuron. In addition, this allows for activation of the fast inward current (I_{proc}) to occur in the LG neuron (inset of Figure 3.2.C.3). As a result, I_{proc} flows into and depolarizes the LG neuron, but the duration of the inactive phase of the LG neuron is controlled by the slow dynamics (m) of I_K . In addition, the fast, small-amplitude depolarizations in the LG membrane potential are again due to the effect of the AB to

INT1 inhibition which disinhibits the LG neuron from INT1, as discussed for the MCN1-elicited rhythm. Then, after a sufficient de-activation of I_K (decrease in m – Figure 3.2.C.3), the LG neuron escapes from INT1 inhibition and begins to burst. As a result, LG inhibits INT1, and activation of I_K occurs in the LG neuron (slow increase in m – Figure 3.2.C.3). This allows I_K to flow out of and repolarize the LG neuron, so m slowly increases during the LG burst phase (Figure 3.2.C.3). The AB to INT1 inhibition does not affect the LG burst phase, as discussed for the MCN1-elicited rhythm. After a sufficient efflux of I_K , the LG burst terminates, and the LG neuron falls back down into its inactive state where it is inhibited by INT1. Then, the cycle begins again with a slow de-activation of I_K plus a fast activation of I_{proc} in the LG neuron. Thus, PK-induction of I_{proc} (for depolarization) plus I_K (for repolarization) in the LG neuron also elicits a gastric mill rhythm that is similar to the MCN1-elicited rhythm.

Testing if PK-Induction of I_{proc} in the LG neuron is Necessary to Elicit a Similar Gastric Mill Rhythm. In the last mechanism, PK induces I_{proc} for depolarization of the LG neuron, but the PK-elicited gastric mill rhythm is controlled by the slow dynamics (m) of the outward current, I_K (Figures 3.2.C.3 and equivalently Figure 3.3). Thus, one can ask if I_{proc} is necessary for PK to elicit a gastric mill rhythm. To answer this question, I_{proc} is first removed from the model by setting its maximal conductance \bar{g}_{proc} to zero in Equation (3.15) (see Methods). This disrupts bursting in the LG neuron, as only the slow outward current I_K is left for repolarization of LG (Figure 3.3.B). Next, to test if LG depolarization specifically by I_{proc} is required for PK to elicit a gastric mill rhythm, the LG neuron is instead depolarized with a constant applied current (I_{Ext}) to check if this

manual depolarization of LG will elicit a similar gastric mill rhythm. However, the PK-elicited rhythm where LG is depolarized by I_{Ext} (Figure 3.3.C) is different from the PK-elicited rhythm in which I_{Proc} depolarizes LG (Figure 3.3.A). Thus, Figure 3.3 suggests that although PK is still capable of eliciting a gastric mill rhythm in the absence of I_{Proc} , I_{Proc} plays an important role for generating a gastric mill rhythm that results in a similar pattern to the MCN1-elicited rhythm. In the biological system, there are no known pharmacological agents that effectively block proctolin receptors (M.P. Nusbaum, unpublished data). Therefore, an experiment to block I_{Proc} (as in Figure 3.3) would be difficult to do in the biological system. Moreover, Figure 3.3 supports Figure 2.7 of the previous chapter, which showed that a gastric mill rhythm can still be generated when PK only induces a slow, non-inactivating outward current, such as I_K , in the LG neuron. In particular, although I_{Ext} is used for depolarization of the LG neuron in Figure 3.3.C, the gastric mill rhythm is controlled by the slow dynamics (m) of PK-induced I_K .

3.3.3 PK Elicits a Similar Gastric Mill Rhythm via the Induction of Plateau Properties in the LG Neuron

Three different mechanisms have been proposed by which PK can elicit a gastric mill rhythm that is similar to the MCN1-elicited rhythm. Each mechanism involves PK-induction of voltage-gated ionic currents in the LG neuron to elicit a similar gastric mill rhythm.

However, in the biological system, PK also generates plateau properties in the LG neuron (Hertzberg and Nusbaum, 2004). In particular, a brief depolarizing current pulse in the LG neuron activates a prolonged depolarization in the LG membrane potential that

outlasts the brief pulse (Figure 3.4.A). Moreover, the plateau potential in the LG neuron is voltage-dependent as it can be terminated prematurely with a brief injection of negative current (Figure 3.4.A). This suggests that the mechanism by which PK elicits a gastric mill rhythm in the biological system must have slow kinetics in order to generate the prolonged depolarization in the LG plateau potential. Otherwise the depolarized state in LG would terminate with the brief current pulse. Moreover, Figure 3.4.A suggests that the mechanism by which PK elicits a gastric mill rhythm is voltage-dependent; otherwise, the plateau potential in LG would not be terminated by the brief negative current pulse. For each of the proposed mechanisms in the biophysically-realistic model of this work, the PK-elicited gastric mill rhythm is controlled by a slow, voltage-dependent PK-induced current in the LG neuron (Figure 3.2.C). As a result, the slow, voltage-dependent PK-induced current of each mechanism will allow for the generation of plateau properties in the LG neuron. The plateau potential generated by the first proposed mechanism (I_{Plat}) is shown in Figure 3.4.B. The other two proposed mechanisms (I_h and $I_{Proc}+I_K$) which elicit a similar gastric mill rhythm also generate a similar plateau potential in the LG neuron. Thus, the proposed PK mechanisms produce the plateau properties that PK generates in the LG neuron of the biological system.

3.3.4 The MCN1-Elicited and PK-Elicited Gastric Mill Rhythms are Distinguished by a Synaptic Input From AB to INT1

In the biological system, the MCN1-elicited and PK-elicited gastric mill rhythms are not similar in the absence of the AB to INT1 inhibition. In particular, MCN1 elicits a gastric mill rhythm of slower frequency in the absence of the AB to INT1 inhibition (Bartos et

al., 1999). In contrast, PK does not elicit a gastric mill rhythm in the absence of the AB to INT1 inhibition (Hertzberg and Nusbaum, 2005). This difference between the two gastric mill rhythms is reproduced in the biophysically-realistic model (Figure 3.5). In particular, MCN1 still generates a slower gastric mill rhythm when the AB to INT1 inhibition is removed from the model (Figure 3.5.A). In contrast, the PK-elicited rhythm is disrupted when the AB to INT1 inhibition is removed (Figure 3.5.B).

Thus, all three PK mechanisms proposed in this chapter reproduce the effects of the PK-elicited rhythm in the biological system. In particular, each proposed PK mechanism: **1** elicits a gastric mill rhythm that is similar to the MCN1-elicited rhythm, **2** generates plateau properties in the LG neuron, and **3** does not elicit a gastric mill rhythm in the absence of the AB to INT1 inhibition. Therefore, from the perspective of the biophysically-realistic model, all three of the proposed PK mechanisms are equivalent since they each elicit a gastric mill rhythm that has the same features. Thus, the PK mechanisms induced in the LG neuron are collectively designated by a generalized mechanism called " I_{PK} " (as in Figure 3.4) from hereon in the chapter since they all elicit a gastric mill rhythm that has the same features.

3.3.5 Including the Dorsal Gastric (DG) Neuron in the Biophysically-Realistic Model

Next, the DG neuron is included in the biophysically-realistic model of the MCN1-elicited and PK-elicited gastric mill rhythms. The model DG neuron was developed using experimental data from the biological system, where excitatory synaptic input from MCN1 axon terminals facilitates bursting in the DG neuron during the MCN1-elicited

rhythm (Coleman et al., 1995). To generate bursting in the model DG neuron, MCN1 is assumed to induce a proctolin-like current (I_{proc}) in DG (see Methods). Experimental data strongly suggests that MCN1 can indeed activate I_{proc} in the DG neuron. In particular, it is known that MCN1 uses its neuropeptide co-transmitter CabTRP Ia to excite the DG neuron (Wood et al., 2000), and bath application of CabTRP Ia has been shown to induce I_{proc} in STG neurons (Swensen and Marder, 2000). Therefore, in this chapter it is assumed that MCN1, through its co-transmitter CabTRP Ia, facilitates rhythmic bursting in the DG neuron via the induction of I_{proc} in DG.

To support this assumption with further biological data, rhythmic bursting in the DG neuron was disrupted during the MCN1-elicited rhythm when CabTRP Ia was pharmacologically blocked (Wood et al., 2000). In particular, during the MCN1-elicited rhythm, bath application of Spantide I, which blocks the actions of CabTRP Ia, switches the activity of the DG neuron from rhythmic bursting to tonic firing (Figure 3.6.A). Furthermore, the DG neuron becomes quiescent when MCN1 is inactive and therefore stops releasing CabTRP Ia (Figure 3.6.A). Thus, in the biological system Spantide application during the MCN1-elicited rhythm blocks MCN1-released CabTRP Ia and effectively weakens the response of the DG neuron to MCN1 stimulation, which suggested that MCN1 uses CabTRP Ia to influence the DG neuron (Wood et al., 2000).

This behavior in DG neuron activity is reproduced in the biophysically-realistic model, where MCN1 generates rhythmic bursting in the model DG neuron via the induction of I_{proc} . In particular, I_{proc} is induced by MCN1 in the model DG neuron based on the documented effects of the MCN1 co-transmitter CabTRP Ia on STG neurons in the biological system (Swensen and Marder, 2000, 2001). As a result, when I_{proc} is

weakened in the model DG neuron to mimic the effect of Spantide application in the biological system, the activity of the model DG neuron switches from rhythmic bursting to tonic firing (Figure 3.6.B). Then, in the absence of MCN1 activity I_{proc} is no longer induced in the model DG neuron so it becomes quiescent (Figure 3.6.B). This behavior in the model DG neuron also occurs in the PK-elicited rhythm of Figure 3.7.B, which does not involve the MCN1 circuitry. Thus, the biophysically-realistic model reproduces the cellular properties of the DG neuron in the biological system (Figure 3.6).

Next, the model DG neuron is added to the MCN1-elicited rhythm. In the biological system, the DG neuron bursts in alternation with the LG neuron, and it is an effective reporter of MCN1 activity within the STG (Coleman et al., 1995). In particular, during the LG interburst phase of the MCN1-elicited rhythm, excitatory synaptic input from MCN1 axon terminals facilitates rhythmic bursting in the DG neuron. However, during the LG burst phase, presynaptic inhibition of MCN1 axon terminals by the LG neuron blocks MCN1 excitation within the STG; therefore, the DG neuron becomes quiescent during the LG burst phase. This timing of DG neuron activity is reproduced in the biophysically-realistic model where the DG and LG neurons burst in alternation during the MCN1-elicited rhythm (Figure 3.7.A).

Next, the model DG neuron is added to the PK-elicited rhythm. Earlier, PK was shown to elicit a gastric mill rhythm by activating plateau properties in the LG neuron (see Figure 3.4). In the biological system, the timing of activity in the DG neuron is similar in both the MCN1-elicited and PK-elicited rhythms (Hertzberg and Nusbaum, 2005). Therefore, PK is also assumed to induce I_{proc} in the DG neuron to facilitate rhythmic bursting in DG (see Methods). In particular, PK is a neuropeptide, and, since

bath application of several different neuropeptides induces I_{Proc} in STG neurons (Swensen and Marder, 2000, 2001), PK is assumed to induce I_{Proc} in the model DG neuron, which facilitates rhythmic bursting in DG (as in Figure 3.6). As a result, the timing of activity in the model DG neuron is similar to that in the biological system, as the LG and DG neurons burst in alternation during both the MCN1-elicited and PK-elicited rhythms (Figure 3.7). Moreover, in the PK-elicited rhythm, an inhibitory synapse from the DG to LG neuron has been included in the model (Figure 3.7.B). In the biological system, PK strengthens this synapse, which is not functional during the MCN1-elicited rhythm (Hertzberg and Nusbaum, 2005). The effect of this synapse on the PK-elicited rhythm is examined later in the chapter. Thus, using physiological data, a biophysically-realistic model has been developed in this chapter that reproduces the activity of the DG neuron in both the MCN1-elicited and PK-elicited gastric mill rhythms.

3.3.6 Examining the Effects of Presynaptic Inhibition in the MCN1-Elicited Gastric Mill Rhythm

In the biological system, the MCN1-elicited and PK-elicited gastric mill rhythms appear similar, but they are generated by different functional circuits (Hertzberg and Nusbaum, 2005). In particular, the PK-elicited rhythm occurs in the absence of MCN1 participation. Therefore, the circuit components that are associated only with the MCN1-elicited rhythm, such as presynaptic inhibition of MCN1 by the LG neuron, do not play a role in the PK-elicited rhythm. However, the presynaptic inhibition is necessary for generating the MCN1-elicited rhythm in the biological system (Coleman et al., 1995). Therefore, we use the biophysically-realistic model to investigate which aspects of the

MCN1-elicited gastric mill rhythm require the presence of the presynaptic inhibition. We find that presynaptic inhibition of MCN1 is necessary for both **1** generating rhythmic bursting in the LG neuron and INT1 and **2** coordinating the timing of activity in the DG neuron during the MCN1-elicited rhythm (Figure 3.8).

In the MCN1-elicited rhythm of the biological system, excitatory synaptic input from MCN1 is slower in the LG neuron than in INT1 or DG (Coleman et al., 1995; Marder, 1996). Moreover, the presynaptic inhibition of MCN1 axon terminals by the LG neuron occurs during the LG burst phase of the rhythm (see Figure 1.2), and it causes a slow decay of MCN1 excitatory input in the LG neuron. In the biophysically-realistic model, the frequency of the MCN1-elicited rhythm is controlled by the slow dynamics of MCN1 excitation in the LG neuron (denoted by s – Figure 3.8.A). As a result, a weaker presynaptic inhibition in the model causes a slower decay of s , which prolongs the duration of the LG burst phase (Figure 3.8.B). In particular, the weaker presynaptic inhibition takes longer to terminate the LG burst. As a result, this prolongs the INT1 interburst phase, since the duration of the LG to INT1 inhibition (inset of Figure 3.8) increases with the duration of the LG burst phase. Furthermore, the DG interburst phase is also prolonged since the duration of the presynaptic inhibition also increases with the duration of the LG burst phase. In addition, as in the biological system, the model DG neuron becomes quiescent when LG presynaptically inhibits MCN1. In particular, the presynaptic inhibition (albeit weaker in Figure 3.8.B) disrupts MCN1-induction of I_{Proc} in the DG neuron so that DG becomes quiescent (see Figure 3.6). Thus, in the presence of a weaker presynaptic inhibition, the slow dynamics of s still have the dominant effect on

network oscillations; therefore, the slower decay of s prolongs the LG burst phase of this gastric mill rhythm.

When the presynaptic inhibition is made even weaker, the decay of s in LG becomes slow enough to disrupt rhythmic bursting between the LG neuron and INT1 (Figure 3.8.C). In particular, the decay of s is slowed to the point where the LG neuron settles to its burst phase. As a result, INT1 remains in its interburst phase since the LG to INT1 inhibition remains active throughout the prolonged LG burst phase. In addition, the DG neuron remains quiescent for the duration of the LG burst phase since the presynaptic inhibition of MCN1 continues for the duration of the LG burst phase. Thus, the weakened presynaptic inhibition of MCN1 still silences the DG neuron by disrupting the MCN1-induction of I_{proc} in DG. Moreover, the slow decay of s still has the dominant effect, and it is slow enough to cause the LG neuron to settle to its bursting phase. Therefore, only the LG burst phase of the gastric mill rhythm is exhibited in Figure 3.8.C.

When the presynaptic inhibition is removed from the model, the LG neuron and INT1 remain in their burst and interburst phases, respectively (Figure 3.8.D). However, in this case where there is no presynaptic inhibition (inset of Figure 3.8.D), there is no mechanism to cause a decay of s in the LG neuron; therefore, there is no mechanism to terminate the LG burst. As a result, the LG neuron remains in its bursting phase and never transitions to its interburst. This suggests that presynaptic inhibition is necessary for generating rhythmic bursting between the LG neuron and INT1 during the MCN1-elicited rhythm. Conversely, the DG neuron bursts rhythmically in the absence of the presynaptic inhibition in the model. In particular, the MCN1 synaptic input onto DG is now uninhibited by the LG neuron (inset of Figure 3.8.D), and the rhythmic bursting in

the DG neuron is controlled by its cellular properties (MCN1-induction of I_{Proc} - see Figure 3.6.B). However, in the absence of the presynaptic inhibition, the timing of DG neuron activity is no longer coordinated with the activity of the LG neuron. This suggests that the presynaptic inhibition is also necessary to coordinate the timing of activity between the LG and DG neurons so that they burst in alternation during the MCN1-elicited rhythm.

Thus, presynaptic inhibition of MCN1 axon terminals is necessary for both generating rhythmic bursting between the LG neuron and INT1 and for coordinating the timing of DG neuron activity in the MCN1-elicited gastric mill rhythm.

3.3.7 Assessing How Plateau Properties in the LG Neuron Would Affect the MCN1-Elicited Gastric Mill Rhythm

In the biological system, the PK-elicited gastric mill rhythm occurs in the absence of MCN1 participation and therefore does not involve presynaptic inhibition of projection neurons. Instead, PK elicits a gastric mill rhythm that is similar to the MCN1-elicited rhythm via the activation of plateau properties in the LG neuron (see Figure 3.4). Therefore, to investigate how a different functional circuit can still elicit a similar gastric mill rhythm, we use the biophysically-realistic model to assess which aspects of the MCN1-elicited rhythm would require the presence of presynaptic inhibition if the model LG neuron also included plateau properties. In the biological system, there is no substantial evidence to show that MCN1 induces plateau properties in the LG neuron (M.P. Nusbaum, unpublished data). However, we add plateau properties to the model LG neuron for the purpose of assessing the role of the presynaptic inhibition.

Earlier, three mechanisms were presented by which PK can elicit a similar gastric mill rhythm via the activation of plateau properties in the LG neuron (see Figure 3.4). All of the proposed PK mechanisms are equivalent from the perspective of the model since they all elicit a gastric mill rhythm with the same features (see Figures 3.5, 3.6); therefore, as mentioned earlier, we collectively refer to the PK mechanisms as “ I_{PK} ”. Thus, we assume that MCN1 activates the plateau properties of I_{PK} in the model LG neuron in order to assess which aspects of the MCN1-elicited gastric mill rhythm will still require presynaptic inhibition when plateau properties are included in the LG neuron. As a result, the conductance of I_{PK} (denoted by g_{PK} – Figure 3.9) oscillates with the LG neuron and helps control the frequency of the MCN1-elicited rhythm (Figure 3.9.A). Therefore, g_{PK} is an intrinsic property of the model LG neuron that is independent of the presynaptic inhibition and helps terminate the LG burst phase in Figure 3.9.

Now, when the presynaptic inhibition is weakened in the model, the duration of the LG burst phase does not change significantly, since g_{PK} facilitates the termination of the LG burst phase to preserve a similar oscillation frequency in LG (Figure 3.9). As a result, the frequency of the MCN1-elicited rhythm remains similar when the presynaptic inhibition is weakened in the model (Figures 3.9.B – 3.9.C). Then, when the presynaptic inhibition is removed, MCN1 synaptic input becomes uninhibited by the LG neuron (inset of Figure 3.9.D). Nevertheless, the intrinsic properties of g_{PK} in the LG neuron allows for the MCN1-elicited gastric mill rhythm to exhibit a similar frequency (Figure 3.9.D). This suggests that when I_{PK} is induced in the model LG neuron during the MCN1-elicited rhythm, presynaptic inhibition of MCN1 is not necessary for generating rhythmic bursting in the gastric mill neurons. However, the presynaptic inhibition of

MCN1 is still required to preserve the timing of activity among the network neurons. In particular, the LG and DG neurons become uncoordinated in the absence of presynaptic inhibition, as their burst phases overlap with each other instead of occurring in alternation (Figure 3.9.D). Therefore, this suggests that regardless of plateau property generation in the LG neuron, presynaptic inhibition of MCN1 is necessary for coordinating the timing of activity in the DG neuron during the MCN1-elicited gastric mill rhythm.

3.3.8 Investigating the Properties of the MCN1-Elicited Gastric Mill Rhythm at the Network Level

In the MCN1-elicited gastric mill rhythm, the timing of activity in the DG neuron is controlled by LG presynaptic inhibition of MCN1 (Figures 3.9 - 3.10). This has also been documented physiologically (Coleman et al., 1995). Now, the properties of the MCN1-elicited rhythm are further examined at the network level. First, we assess how a brief perturbation of the LG neuron affects the timing of activity in the other gastric mill neurons. In particular, a brief injection of positive current in the model LG neuron resets INT1 activity, via the LG to INT1 inhibition, and DG neuron activity, via LG presynaptic inhibition of MCN1 (Figure 3.10.B). Therefore, the MCN1-elicited gastric mill rhythm can be reset by the LG neuron.

In comparison, the DG neuron does not synapse onto the other gastric mill neurons. Therefore, a perturbation of the DG neuron has no effect on the activity of the LG neuron or INT1 (Figure 3.10.C). Thus, DG is only a follower neuron in the MCN1-elicited gastric mill rhythm, as it has no effect on the other gastric mill neurons.

In vivo, the gastric mill rhythm controls the rhythmic movements of three teeth that are responsible for food chewing in the animal (Figure 3.10.D). In particular, the LG neuron controls the protraction phase of the lateral gastric teeth, while the DG neuron controls the retraction phase of the medial gastric tooth (Heinzel et al., 1993). Using the biophysically-realistic model, it was shown that the LG neuron controls the timing of activity in the DG neuron during the MCN1-elicited rhythm (Figure 3.10.B). However, since DG is only a follower neuron in the MCN1-elicited rhythm, it has no effect on the LG neuron. Therefore, as a first approximation of behavioral significance (Figure 3.10.D), the model suggests that the protractor phase LG neuron controls the timing of network activity during the MCN1-elicited gastric mill rhythm.

3.3.9 Investigating the Effect of the DG to LG Synapse in the PK-Elicited Gastric Mill Rhythm

In the biological system, bath application of PK strengthens an inhibitory synapse from the DG to LG neuron which is not functional during the MCN1-elicited rhythm (Hertzberg and Nusbaum, 2005). The role of this PK-strengthened synapse is assessed using the biophysically-realistic model. In particular, the model suggests that the PK-strengthened synapse coordinates the timing of activity between the LG and DG neurons during the PK-elicited rhythm. Specifically, the PK-strengthened synapse ensures that the LG and DG neurons burst in alternation during the PK-elicited rhythm (Figure 3.11). In contrast, the timing of activity between the LG and DG neurons in the MCN1-elicited rhythm is coordinated by the presynaptic inhibition of MCN1 by the LG neuron (see Figures 3.11). Thus, the biophysically-realistic model suggests that, in the context of

coordinating the timing of activity between the LG and DG neurons, the PK-strengthened synapse in the PK-elicited rhythm parallels the function of the presynaptic inhibition in the MCN1-elicited rhythm. As a result, the PK-strengthened synapse allows for PK to elicit a gastric mill rhythm that is similar to the MCN1-elicited rhythm via a different functional circuit.

3.3.10 Investigating the Properties of the PK-Elicited Gastric Mill Rhythm at the Network Level

Next, the properties of the PK-elicited gastric mill rhythm are examined at the network level. Earlier, it was shown that the LG neuron can reset the MCN1-elicited rhythm through presynaptic inhibition of MCN1. However, presynaptic inhibition of projection neurons is not involved in the PK-elicited gastric mill rhythm, so the LG neuron will not have the same effect. In particular, a perturbation of the LG neuron only perturbs the activity of INT1, via the LG to INT1 inhibition, but has no effect on the DG neuron (Figure 3.12.B). Thus, the LG neuron has no mechanism with which to affect the activity of the DG neuron. Therefore, the LG neuron can not reset the PK-elicited gastric mill rhythm.

In comparison, while DG is only a follower neuron in the MCN1-elicited rhythm, the PK-strengthened inhibitory synapse from the DG to LG neuron allows for the DG neuron to play a more active role in the PK-elicited gastric mill rhythm. In particular, a brief current injection to perturb the DG neuron resets the timing of activity in the LG neuron, via the PK-strengthened synapse, which in turn resets INT1 activity, via the LG

to INT1 inhibition (Figure 3.12.C). Therefore the PK-strengthened synapse allows the DG neuron to reset and entrain the PK-elicited gastric mill rhythm.

Hence, during the PK-elicited gastric mill rhythm, the DG neuron controls the timing of activity in the LG neuron. However, the LG neuron has no effect on the DG neuron. *In vivo*, DG neuron activity controls the retraction phase of the medial gastric tooth, while LG neuron activity controls the protraction phase of the lateral gastric teeth (Heinzel et al., 1993). Therefore, as a first approximation of behavioral significance (Figure 3.12.D), the model suggests that the retractor phase DG neuron controls the timing of network activity during the PK-elicited gastric mill rhythm.

3.3.11 Summary of Results

In this chapter, the MCN1-elicited and PK-elicited gastric mill rhythms were compared using a biophysically-realistic model. First, each of the voltage-gated currents proposed to be induced by PK in the LG neuron was shown to elicit a gastric mill rhythm that is similar to the MCN1-elicited rhythm in the context of the biophysically-realistic model. Next, the coordination of network activity for both gastric mill rhythms was compared. In particular, although the MCN1-elicited and PK-elicited gastric mill rhythms appear similar, their locus of coordination is different.

In the MCN1-elicited gastric mill rhythm:

- The buildup and decay of MCN1 excitation in the LG neuron drives the network oscillations.

- Presynaptic inhibition of MCN1 axon terminals by the LG neuron coordinates network activity.
- The LG neuron can reset the timing of network activity.

In the PK-elicited gastric mill rhythm:

- The proposed PK-induced currents (which generate plateau properties in the LG neuron) drive the network oscillations.
- The PK-strengthened inhibitory synapse from the DG to LG neuron coordinates network activity.
- The DG neuron can reset the timing of network activity.

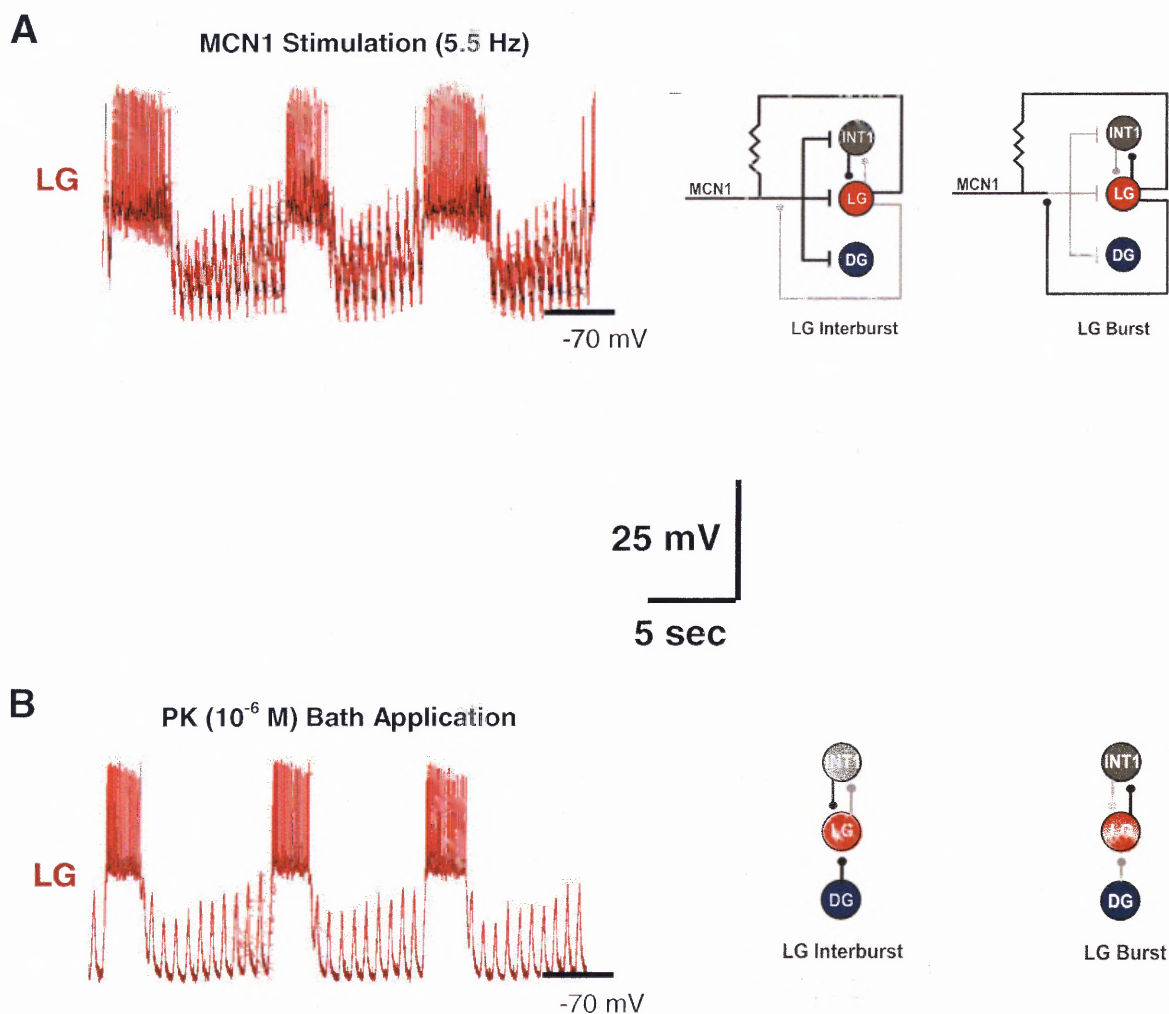


Figure 3.1 Bath Application of the Neuropeptide Pyrokinin (PK) Elicits a Gastric Mill Rhythm That is Similar to the MCN1-Elicited Rhythm (S. Saideman and M.P. Nusbaum, Unpublished Data). **A**, Recording of the LG neuron during the MCN1-elicited rhythm. **B**, Bath application of PK elicits very similar activity in LG. MCN1 and PK elicit similar gastric mill rhythms via different functional circuits (see circuitry diagrams in A and B). In particular, the PK-elicited rhythm occurs in the absence of MCN1 participation and therefore does not involve presynaptic inhibition of projection neurons. In addition, bath application of PK strengthens an inhibitory synapse from the DG to LG neuron which is not functional during the MCN1-elicited rhythm. However, the mechanism by which PK elicits a gastric mill rhythm is unknown.

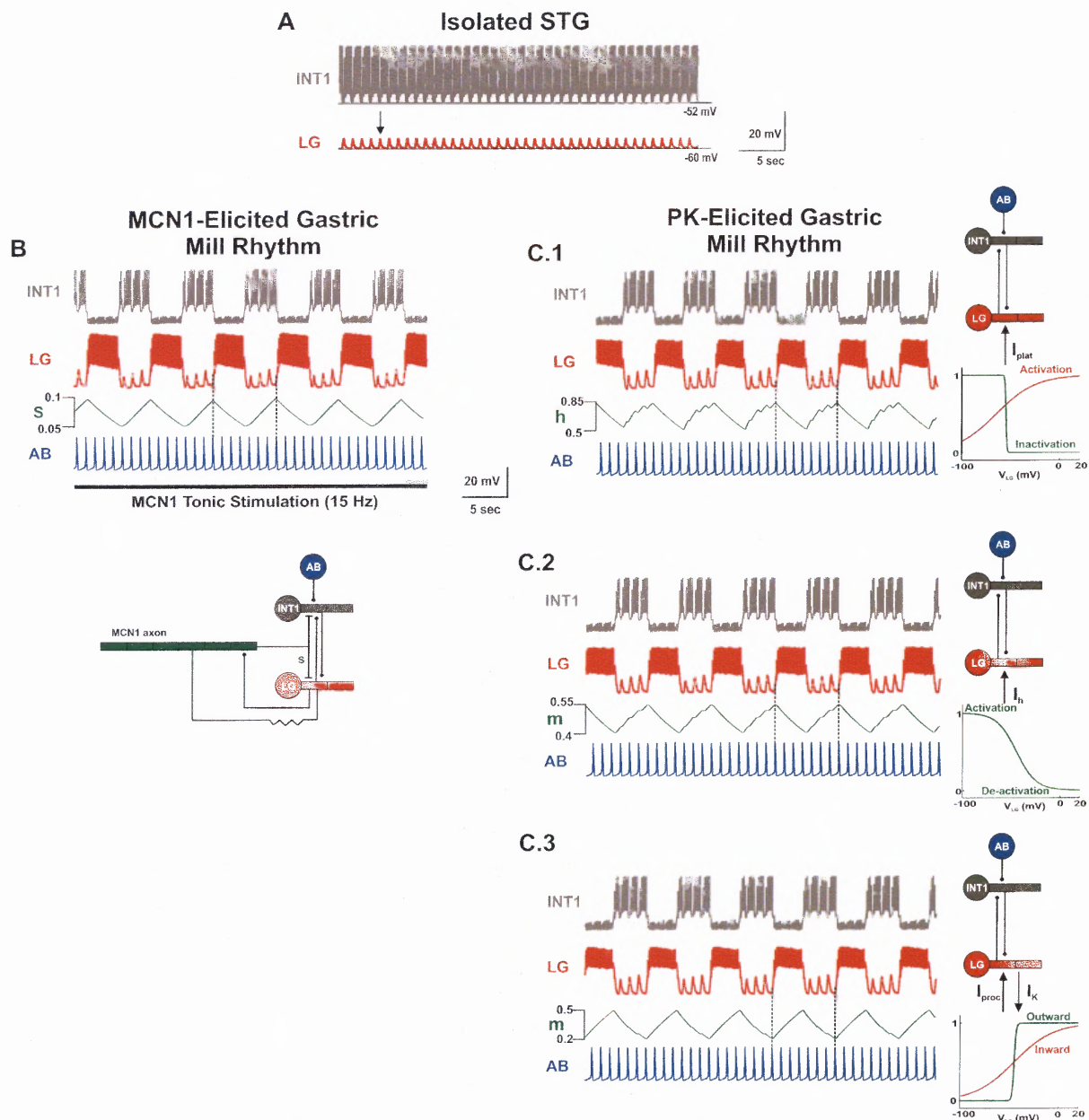


Figure 3.2 Biophysically-Realistic Model Used to Assess the Proposed PK Mechanisms. **A**, The gastric mill rhythm is not spontaneously active in the absence of MCN1. **B**, The MCN1-elicited rhythm is controlled by the slow excitatory input (s) from MCN1 to the LG neuron. The AB to INT1 inhibition triggers the LG burst onset. Most hyperpolarized membrane potentials: INT1 -60 mV; LG -55 mV; AB: -64 mV. **C1**, PK-induction of a slowly-inactivating inward current (I_{plat}) in LG elicits a similar gastric mill rhythm that is controlled by the slow inactivation (h) of I_{plat} . Most hyperpolarized potentials are the same as in **B**. **C2**, PK-induction of slow, hyperpolarization-activated inward current (I_h) in LG elicits a similar rhythm that is controlled by the slow dynamics (m) of I_h . Most hyperpolarized potentials: LG -52 mV; INT1 and AB same as in **B**. **C3**, PK-induction a fast inward current (I_{proc}) and a slow outward current (I_K) (both non-inactivating) in LG elicits a similar rhythm that is controlled by the slow dynamics (m) of I_K . Most hyperpolarized potentials are the same as in **B**.

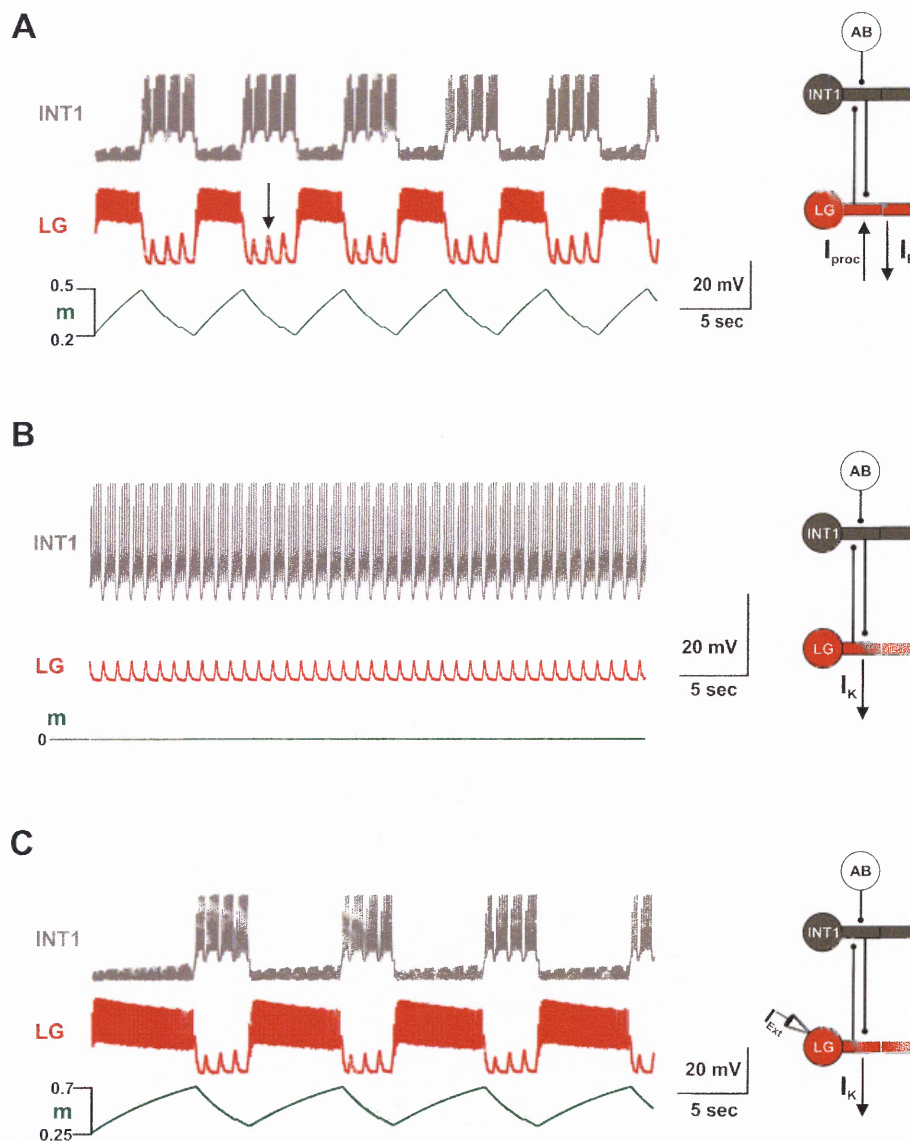


Figure 3.3 Investigating the Role of I_{proc} in the Last PK Mechanism. **A**, The gastric mill rhythm elicited by PK-induced ($I_{proc}+I_K$) in the LG neuron (same as Figure 3.2.C.3). The effect of the AB to INT1 inhibition is indicated by the arrow. Most hyperpolarized membrane potentials: INT1 -60 mV; LG -55 mV. **B**, Removal of I_{proc} disrupts the PK-elicited rhythm, as only the PK-induced outward current (I_K) is left for repolarization of LG. Most hyperpolarized membrane potentials: INT1 -53 mV; LG: -60 mV. **C**, The PK-induced outward current (I_K) controls the gastric mill rhythm that results after injecting external current (I_{Ext}) into the LG neuron. However, this gastric mill rhythm is different from that in A. Therefore, the model suggests that PK-induced I_{proc} is necessary to elicit a gastric mill rhythm that is similar to the MCN1-elicited rhythm. Most hyperpolarized membrane potentials: INT1 -61 mV; LG -16 mV.

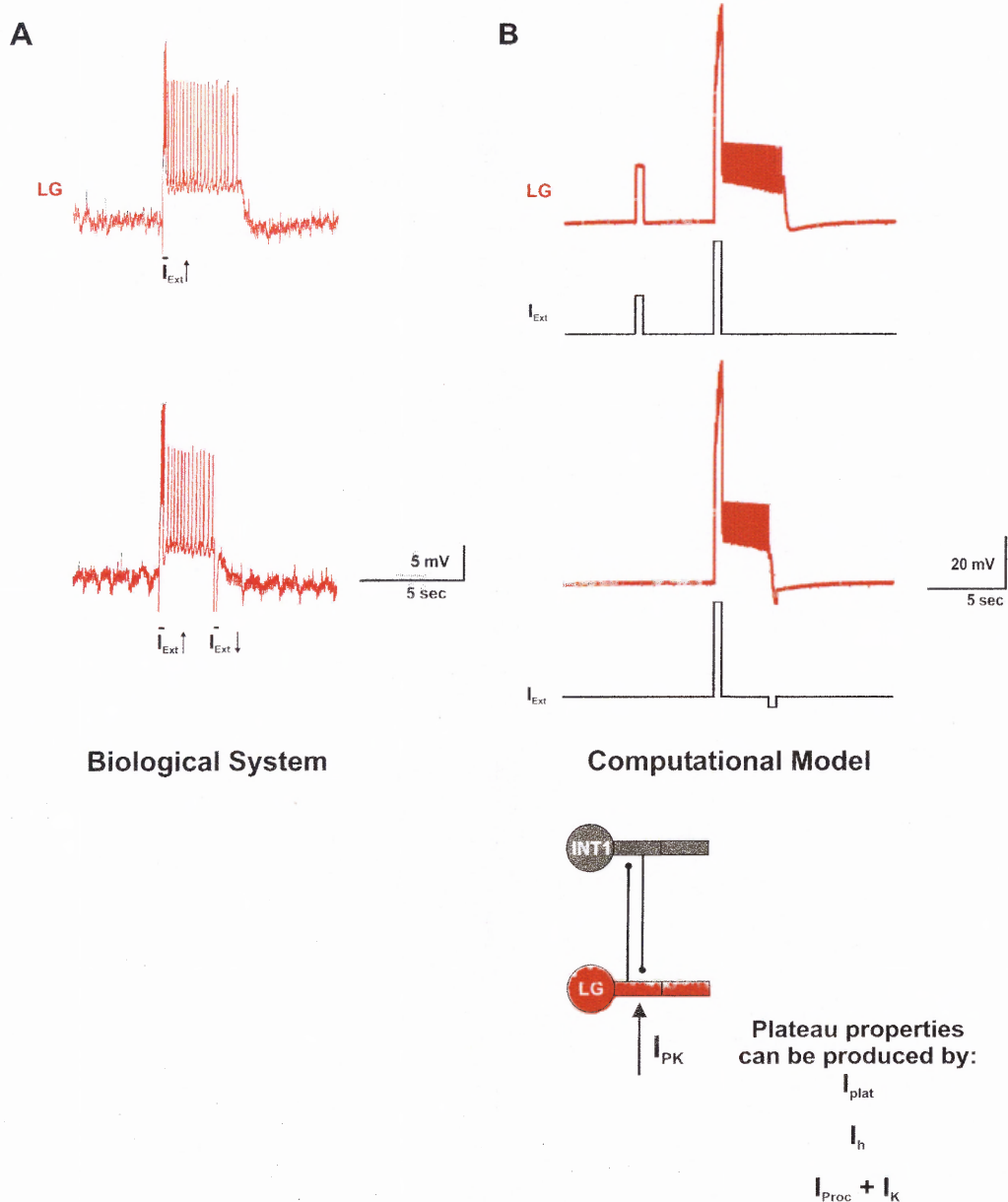


Figure 3.4 PK Elicits a Gastric Mill Rhythm via the Activation of Plateau Properties in the LG Neuron. **A**, In the biological system, bath application of PK induces a plateau potential in the LG neuron (S. Saideman and M.P. Nusbaum, unpublished data). In particular, a brief depolarizing current pulse activates a prolonged depolarization in the LG neuron that outlasts the brief pulse. The plateau potential is voltage dependent as it can be terminated prematurely with a brief injection of negative current. Most hyperpolarized LG membrane potential: -80 mV. **B**, The first proposed mechanism (I_{plat}) activates a similar plateau potential in the model LG neuron. Most hyperpolarized LG membrane potentials: top -55 mV; bottom -60 mV. The other proposed mechanisms (I_h and $I_{Proc}+I_K$) also activate similar plateau properties in the model LG neuron.

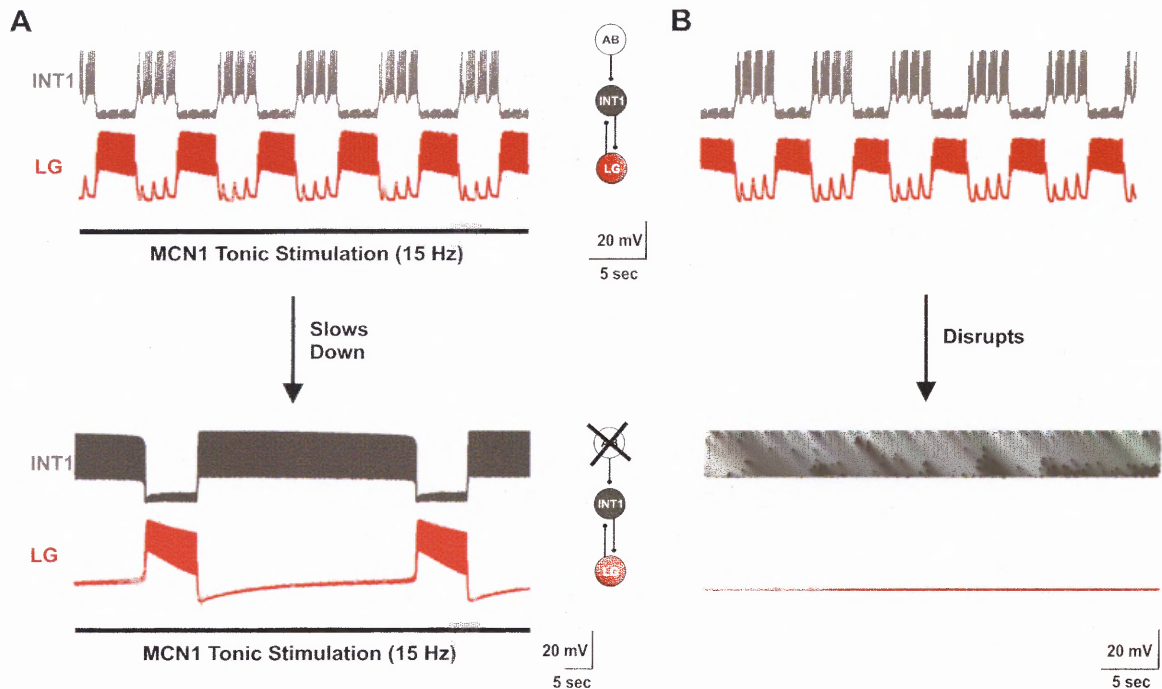


Figure 3.5 The MCN1-Elicited and PK-Elicited Gastric Mill Rhythms are Distinguished by the Effect of the AB to INT1 Inhibition. **A**, Removal of the AB to INT1 inhibition slows down the MCN1-elicited gastric mill rhythm. Most hyperpolarized membrane potentials: INT1 -60 mV; LG -55 mV (same top and bottom). This effect was also reported in the biological system (Bartos et al., 1999). **B**, In contrast, the PK-elicited gastric mill rhythm is disrupted when the AB to INT1 inhibition is removed. Most hyperpolarized membrane potentials: (top) INT1 -60 mV; LG -55 mV, (bottom) INT1 -48 mV; LG -52 mV. This effect was also reported in the biological system (Hertzberg and Nusbaum, 2005). Each of the proposed PK mechanisms produces the same result, and all three mechanisms are equivalent from the perspective of the model since they all elicit a gastric mill rhythm with the same features. The three PK mechanisms are collectively designated by I_{PK} (see Figure 3.4)

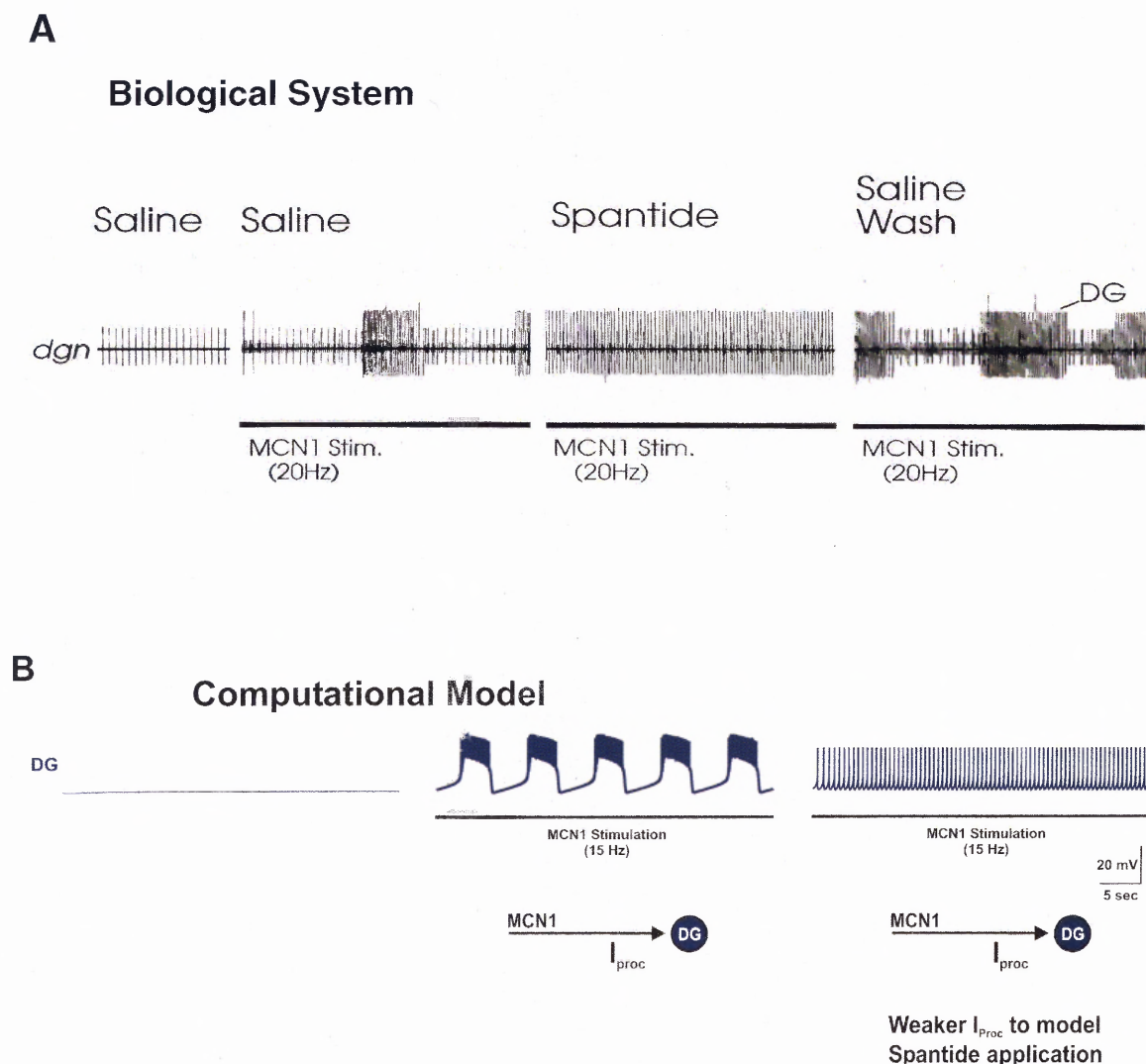


Figure 3.6 The Model DG Neuron Reproduces the Observed Behavior in the Biological System. **A**, Physiologically, MCN1 stimulation produces rhythmic bursting in the DG neuron. However, bath application of Spantide I changes DG activity from rhythmic bursting to tonic firing during MCN1 stimulation. Spantide I blocks the MCN1 neuropeptide co-transmitter CabTRP Ia. This suggests that MCN1 uses CabTRP Ia to excite the DG neuron (Adapted by permission from the Society for Neuroscience: Journal of Neuroscience (Wood et al., 20:8943-8953, 2000), copyright (2000)). **B**, In the model it is assumed that MCN1 activates a proctolin-like current (I_{proc}) in the DG neuron, since the MCN1 co-transmitter CabTRP Ia has been shown to activate I_{proc} in STG neurons. Consequently, MCN1-induced I_{proc} produces rhythmic bursting in the model DG neuron, whose activity switches to tonic firing when I_{proc} is weakened to model Spantide application. Most hyperpolarized membrane potentials: DG silent -46 mV; DG burst -51 mV; DG tonic -44 mV.

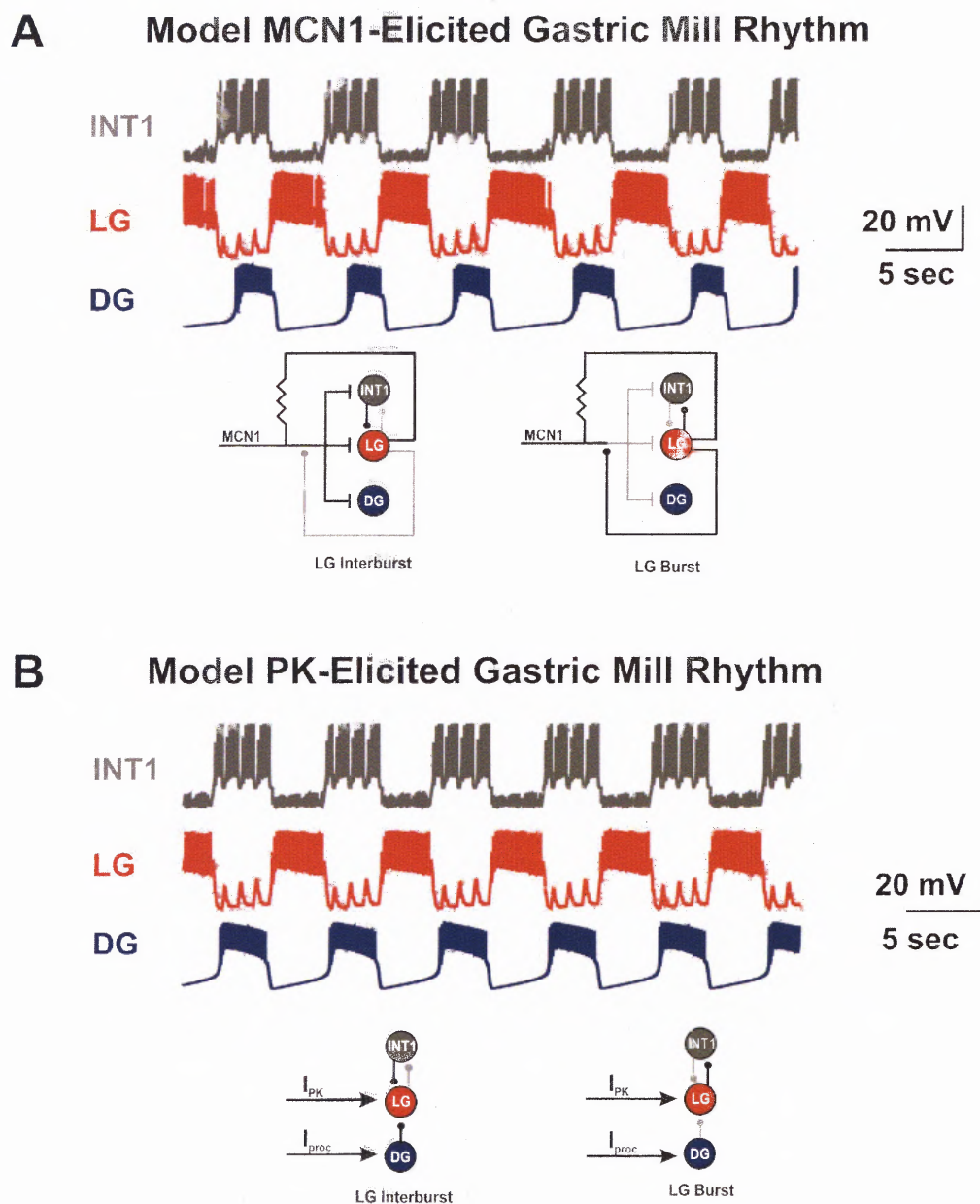


Figure 3.7 The Model DG Neuron is Included in the MCN1-Elicited and PK-Elicited Gastric Mill Rhythms. *A*, The LG and DG neurons burst in alternation during the MCN1-elicited rhythm. Most hyperpolarized membrane potentials: INT1 -60 mV; LG -55 mV; DG -51 mV. *B*, Similarly, the LG and DG neurons burst in alternation during the PK-elicited rhythm. PK elicits a similar gastric mill rhythm via a different functional circuit. The LG neuron bursts due to PK-induction of any one of the three plateau-generating mechanisms denoted by " I_{PK} " (see Figure 3.4). The DG neuron bursts during the PK-elicited rhythm due to PK-induction of I_{proc} . In particular, since PK is a neuropeptide, it is assumed to induce I_{proc} in the DG neuron. Most hyperpolarized membrane potentials are the same as in *A*.

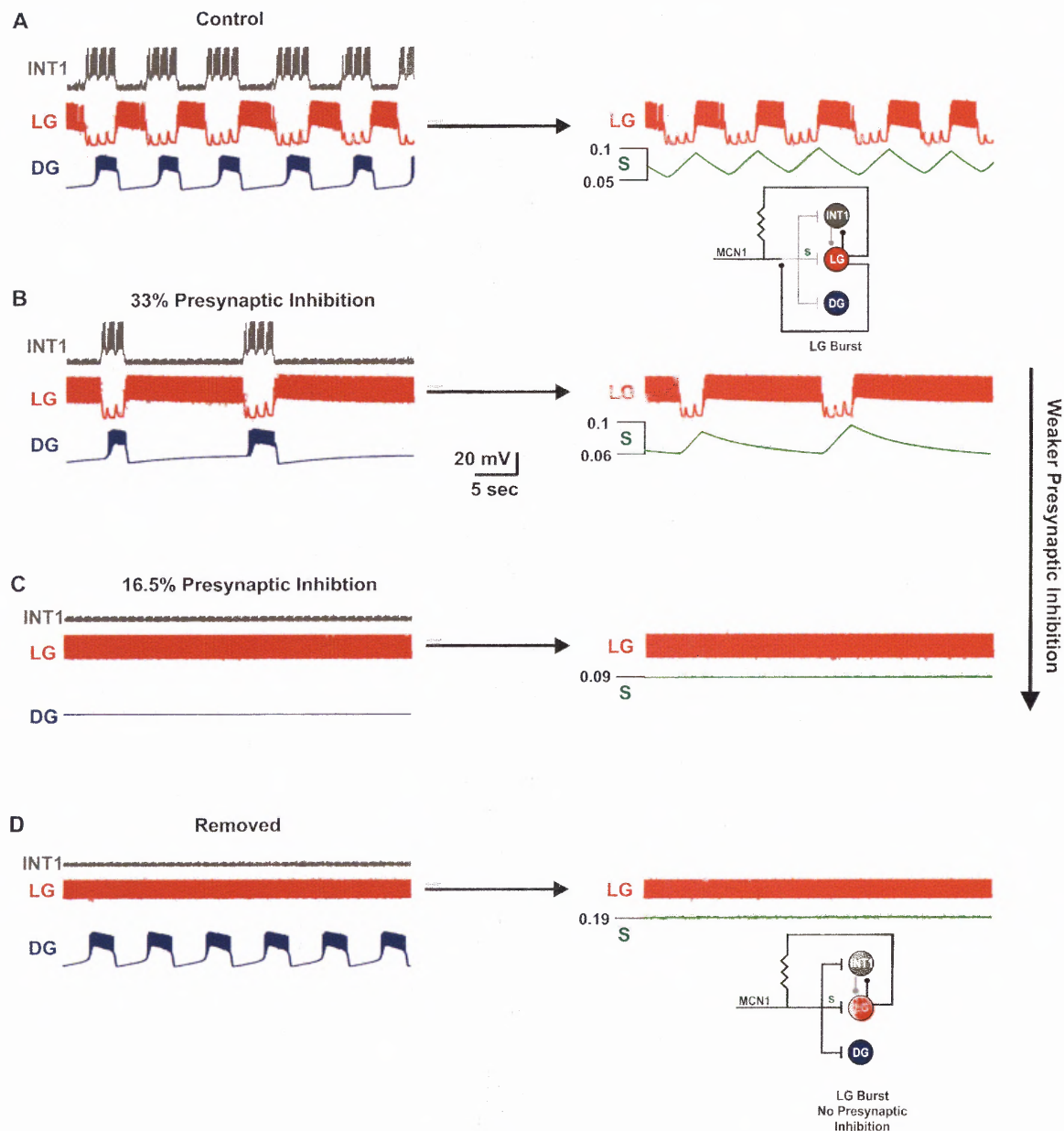


Figure 3.8 Effect of Presynaptic Inhibition in the MCN1-Elicited Gastric Mill Rhythm.

A, The slow modulatory excitation from MCN1 to the LG neuron (s) drives the MCN1-elicited gastric mill rhythm. **B**, A weaker presynaptic inhibition prolongs the LG burst phase, as the decay of MCN1 excitation (s) becomes slower in the LG neuron. **C**, An even weaker presynaptic inhibition disrupts rhythmic bursting. **D**, When the presynaptic inhibition is removed, no mechanism exists to terminate the LG burst. Therefore, the LG neuron is stuck in its burst phase while INT1 is stuck in its interburst, due to the LG to INT1 inhibition. However, LG has no influence over the DG neuron without the presynaptic inhibition, so the DG neuron bursts rhythmically due to MCN1-induced I_{Proc} in DG (see Figure 3.6). Most hyperpolarized membrane potentials **A**: INT1 -60 mV, LG -55 mV, DG -51 mV; **B**: INT1 (same as **A**), LG -54 mV, DG -50 mV; **C**: INT1 (same as **A**), LG -37 mV, DG -43 mV; **D**: INT1 (same as **A**), LG -27 mV, DG (same as **A**).

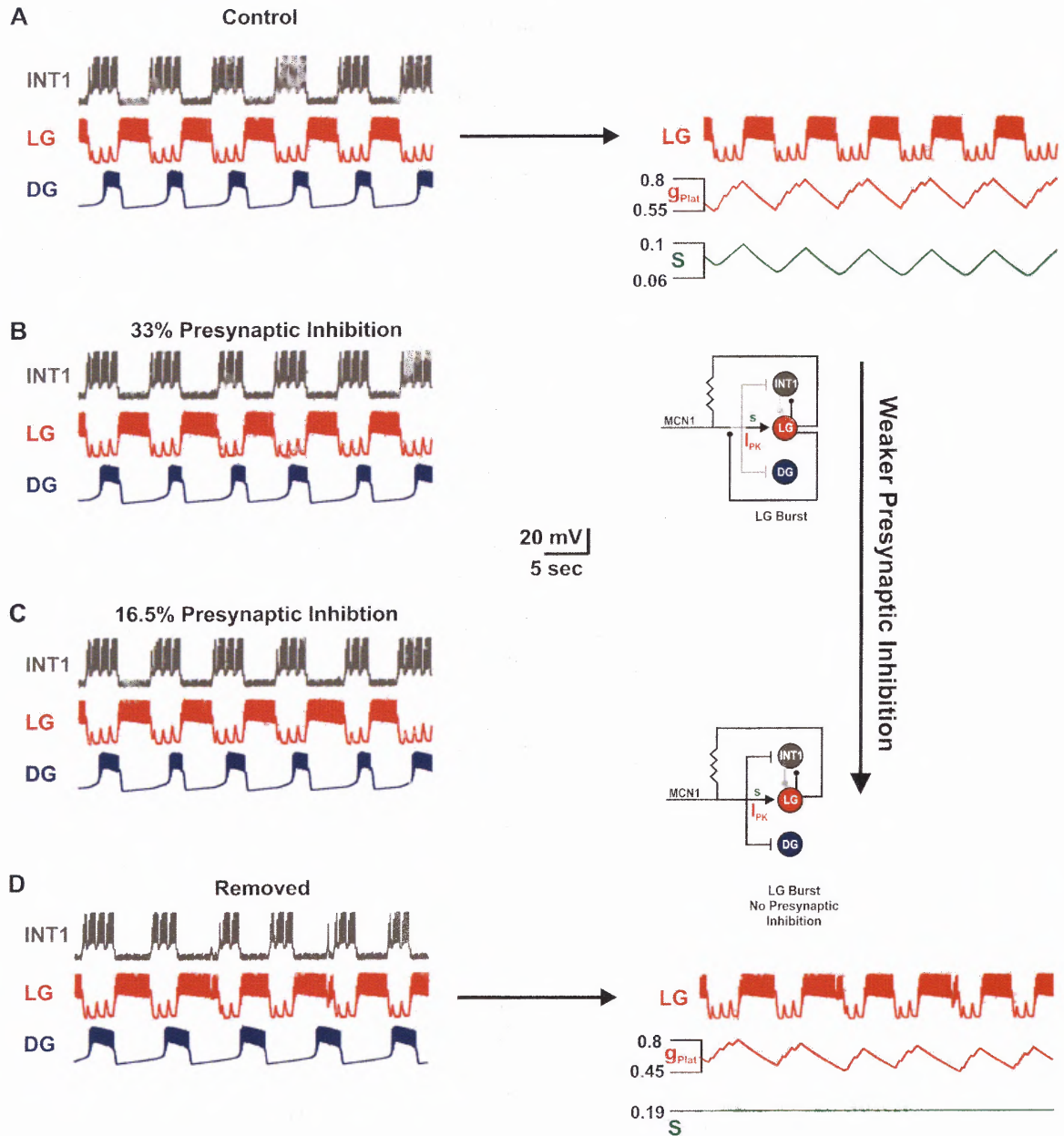


Figure 3.9 Assessing the Role of Presynaptic Inhibition if Plateau Properties are Included in the Model LG Neuron. *A*, Presynaptic inhibition is intact. The plateau properties of the model LG neuron help terminate the LG burst phase of this MCN1-elicited rhythm. *B-C*, As the presynaptic inhibition is weakened, the duration of the LG burst is not prolonged because the cellular properties of the model LG neuron terminate the LG burst phase independent of the presynaptic inhibition. *D*, Without the presynaptic inhibition, LG and INT1 continue to burst rhythmically due to the cellular properties in the LG neuron. However, the timing of activity between the LG and DG neurons becomes uncoordinated. In particular, the LG and DG neurons do not consistently burst in alternation without the presynaptic inhibition. Most hyperpolarized membrane potentials: INT1 -60 mV; LG -55 mV; DG -51 mV (same for all traces).

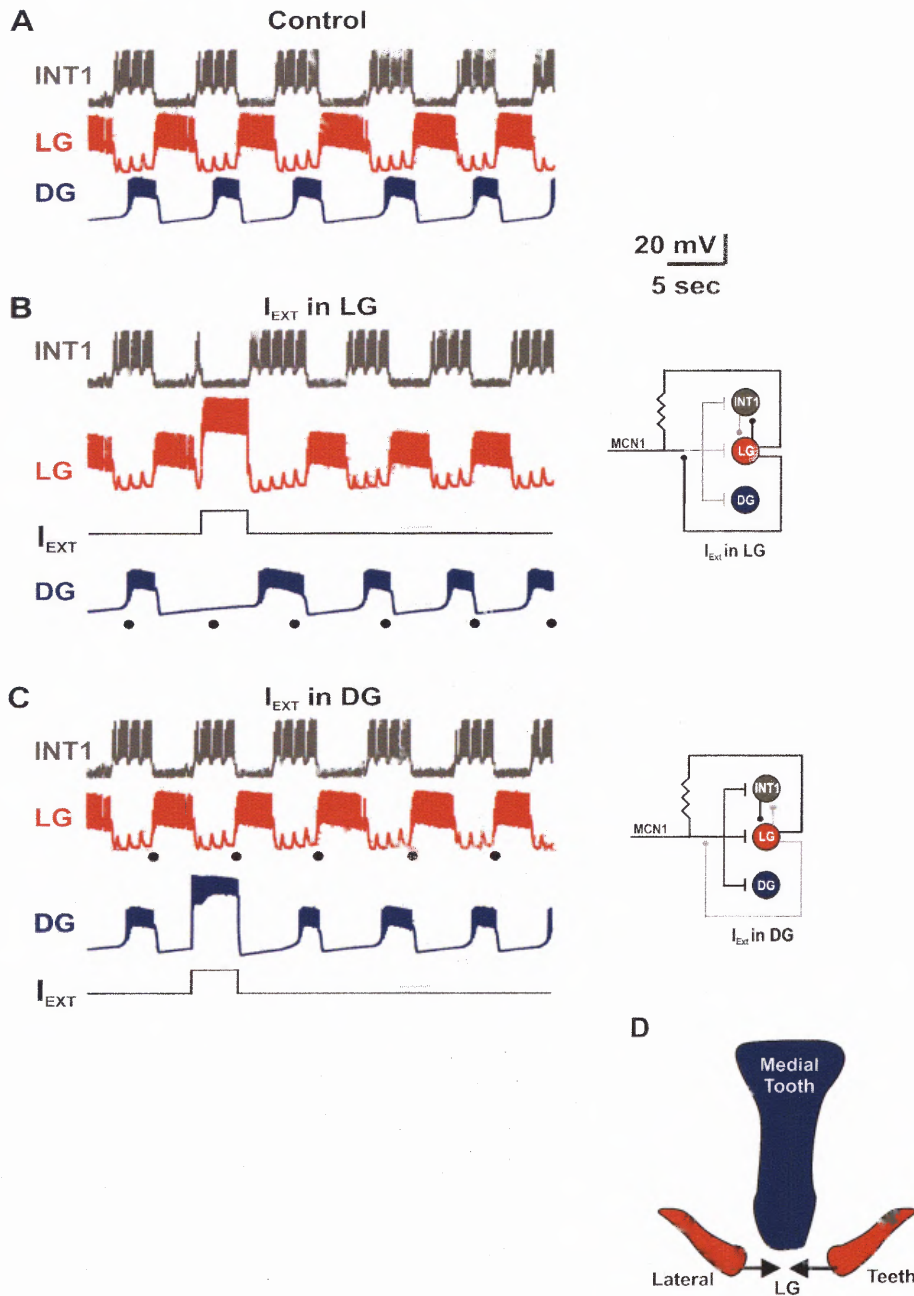


Figure 3.10 Network-Level Properties of the MCN1-Elicited Gastric Mill Rhythm. *A*, Control conditions. *B*, The LG neuron can reset the MCN1-elicited rhythm. Perturbing the model LG neuron via a brief depolarizing current injection resets the timing of activity in INT1, via the LG to INT1 inhibition, and the timing of DG activity, via presynaptic inhibition of MCN1. Filled circles indicate the DG burst onset in *A*. *C*, The DG neuron, since it has no functional synapses, can not reset the MCN1-elicited rhythm. Filled circles indicate the LG burst onset in *A*. *D*, The LG neuron (lateral tooth protractor) controls the timing of DG activity (medial tooth retractor). This suggests that the LG protractor phase controls the MCN1-elicited rhythm. Most hyperpolarized membrane potentials *A*: INT1 -60 mV; LG -55 mV; DG -51 mV, *B*: INT1 -61 mV; LG -57 mV; DG (same as *A*), *C*: INT1, LG (same as *A*), DG -52 mV.

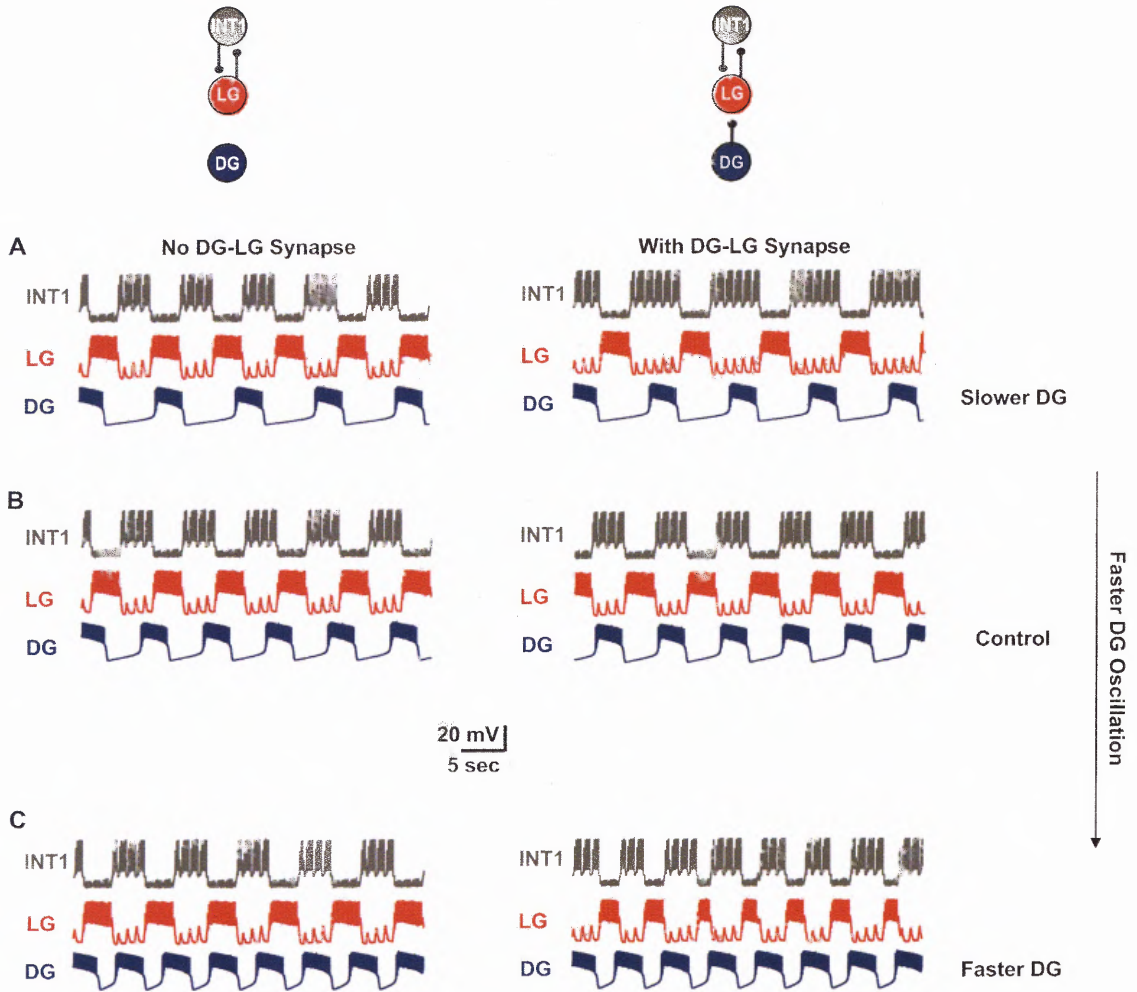


Figure 3.11 Investigating the Role of the PK-Strengthened DG to LG Synapse During the PK-Elicited Gastric Mill Rhythm. A-C, The PK-strengthened synapse regulates the timing of activity between the LG and DG neurons during the PK-elicited rhythm. In particular, the PK-strengthened synapse ensures that the LG and DG neurons burst in alternation. Moreover, as the speed of oscillations in the model DG neuron increases from A to C, the PK-strengthened synapse continues to ensure that the LG and DG neurons burst in alternation. Most hyperpolarized membrane potentials, Top and Middle: INT1 -60 mV, LG -55 mV, DG -51 mV; Bottom: INT1, LG (same as Top), DG -50 mV.

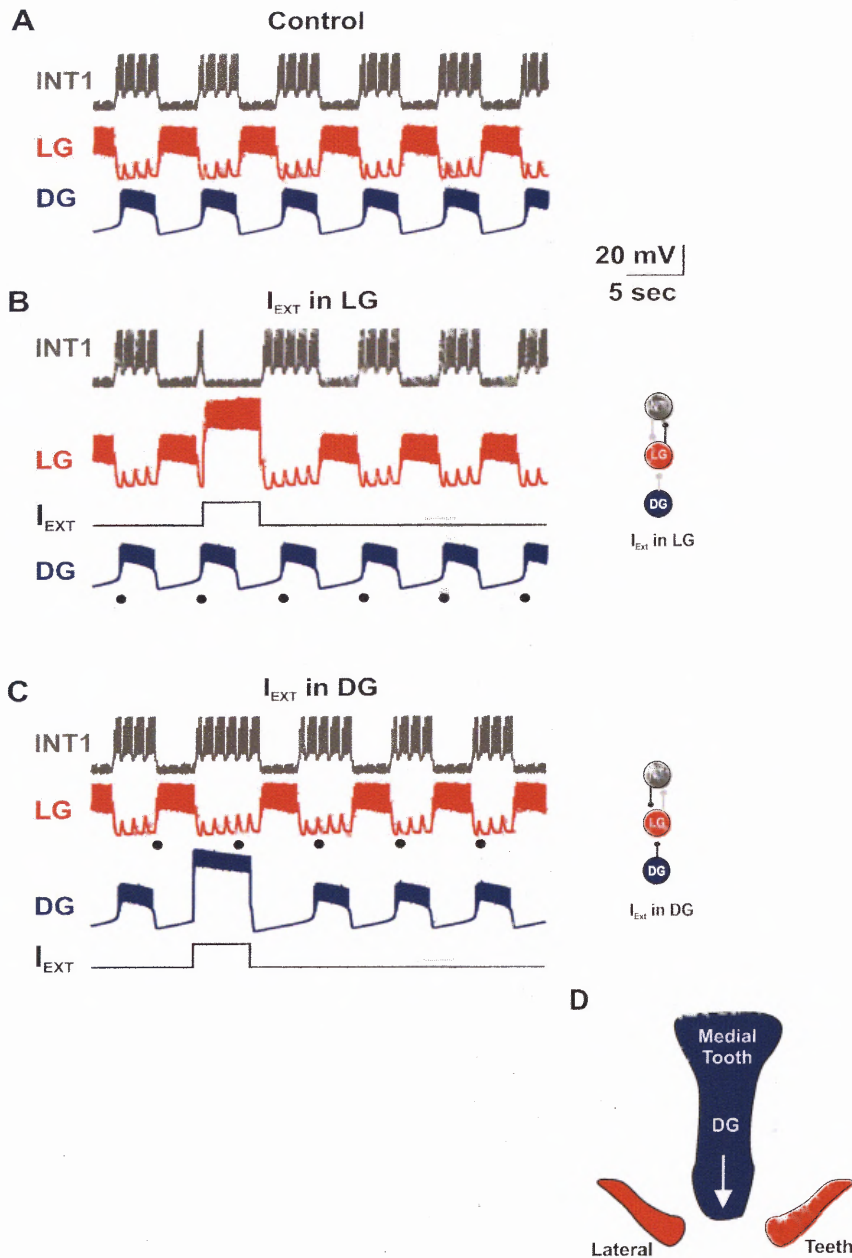


Figure 3.12 Network-Level Properties of the PK-Elicited Gastric Mill Rhythm. *A*, Control conditions. *B*, The LG neuron can not reset the PK-elicited rhythm. In particular, a perturbation of the LG neuron perturbs the activity of INT1, via the LG to INT1 inhibition, but has no effect on the DG neuron. *C*, The DG neuron resets the PK-elicited rhythm. A perturbation of the DG neuron perturbs the activity of LG, via the DG to LG synapse, which in turn perturbs INT1, via removal of the LG to INT1 synapse. *D*, The DG neuron (medial tooth retractor) controls the timing of activity in the LG neuron (lateral tooth protractor). This suggests that the DG retractor phase controls the PK-elicited rhythm, which could involve a different chewing mode than the MCN1-elicited rhythm. Most hyperpolarized membrane potentials, *A*: INT1 -60 mV, LG -55 mV, DG -51 mV; *B*: INT1 -61 mV, LG -57 mV, DG (same as *A*); *C*: INT1, LG (same as *A*), DG -53 mV.

CHAPTER 4

INVESTIGATING HOW FEEDBACK TO PROJECTION NEURONS SHAPES ACTIVITY IN A RHYTHMIC NETWORK: A MODELING STUDY

4.1 Introduction

Projection neuron pathways play an important role in shaping rhythmic pattern generation. In mammals, for example, descending pathways from the cerebellum and brainstem influence the rhythmic circuits that generate locomotor activity in the spinal cord (Burke, 2001; Matsuyama et al., 2004; Yamaguchi, 2004). Generally, rhythmic networks are studied assuming of a feed-forward architecture, in which descending projection neuron pathways initiate, terminate, or modify network activity (Kasicki and Grillner, 1986; Deliagina et al., 2002; Blitz et al., 2004; Rossignol et al., 2006). In reality, however, the circuitry is more complex in that projection neurons in turn receive rhythmic feedback from their target networks (Perreault et al., 1993; Norris et al., 1996; Wood et al., 2004; Zelenin, 2005). Such feedback can influence the pattern of projection neuron inputs, but the role of rhythmic feedback in shaping network activity is not well-understood.

This dissertation addresses these issues using the gastric mill rhythm of the crab, *C. borealis* (Harris-Warrick et al., 1992; Marder and Calabrese, 1996; Nusbaum and Beenhakker, 2002). Physiologically, the gastric mill circuit is located in the stomatogastric ganglion (STG) (see Figure 1.2), where it receives a local synaptic input from the coactive pyloric circuit (Bartos et al., 1999). In addition, the STG circuitry is innervated by descending neuronal input from ~20 projection neurons (Nusbaum and Beenhakker, 2002). Although the gastric mill rhythm is generally not spontaneously

active, tonic stimulation of the projection neuron MCN1 readily elicits a gastric mill rhythm *in vitro* (Coleman et al., 1995). However, co-stimulation of MCN1 plus a second projection neuron, the commissural projection neuron 2 (CPN2), elicits a distinct gastric mill rhythm (Blitz and Nusbaum, 1997; Beenhakker and Nusbaum, 2004). In addition, the projection neurons MCN1 and CPN2 receive rhythmic feedback from STG circuits (Norris et al., 1994; Wood et al., 2004). However, the role of this feedback in shaping the gastric mill rhythm is not well understood.

This dissertation uses a reduced mathematical model to investigate how (1) feed-forward inputs from the projection neurons MCN1 and CPN2 and (2) feedback to these projection neurons shapes the gastric mill rhythm. Previously, a 3-dimensional model was used to analyze the synaptic properties that underlie the MCN1-elicited gastric mill rhythm (Manor et al., 1999). Then, a second reduced model was used to investigate how feedback from the pyloric circuit affects the frequency of the MCN1-elicited rhythm, and it showed that the timing of pyloric feedback is crucial for generating an MCN1-elicited rhythm with the observed frequency in the biological system (Ambrosio-Mouser et al., 2006). Now, this dissertation develops a reduced 2-dimensional model to analyze the synaptic properties that underlie the MCN1/CPN2-elicited gastric mill rhythm. The network dynamics of this 2-dimensional model are readily examined via a phase-plane analysis. As a result, this allows for an investigation of how both feed-forward inputs from MCN1 and CPN2 and how feedback to these projection neurons shapes the gastric mill rhythm.

4.2 Methods

This chapter develops a 2-dimensional model of the MCN1/CPN2-elicited gastric mill rhythm, where MCN1 and CPN2 are two coactive projection neurons. First, a reduction of the 3-dimensional model of (Manor et al., 1999) down to a 2-dimensional model of the MCN1-elicited rhythm that was performed in Chapter 2 is reviewed. Then, CPN2 is added to this model, which is kept in 2 dimensions by exploiting the difference in synaptic time scales.

4.2.1 Three-Dimensional Model of the MCN1-Elicited Gastric Mill Rhythm

In the 3-dimensional model of the MCN1-elicited rhythm (Manor et al., 1999), INT1 and LG were treated as passive neurons so that action potential generation in them could be ignored. As a result, only the slow envelope of network oscillations was considered by (Manor et al., 1999) in order to simplify the network dynamics and perform a mathematical analysis. This 3-dimensional model was already described in detail in Chapter 2, where it is given by Equations (2.1) - (2.3). Therefore, only a brief overview of the 3-dimensional model is given in this chapter. First, the 3-dimensional model of (Manor et al., 1999) is rewritten in this chapter for clarity

$$C_I \frac{dV_I}{dt} = - \underbrace{g_{Leak,I} (V_I - E_{Leak,I})}_{I_{Leak,I}} - \underbrace{\bar{g}_{L \rightarrow I} m_{L \rightarrow I} (V_L) (V_I - E_{L \rightarrow I})}_{I_{L \rightarrow I}} - \underbrace{\bar{g}_P P(t) (V_I - E_P)}_{I_P} \quad (4.1)$$

$$C_L \frac{dV_L}{dt} = - \underbrace{g_{Leak,L} (V_L - E_{Leak,L})}_{I_{Leak,L}} - \underbrace{\bar{g}_{I \rightarrow L} m_{I \rightarrow L} (V_I) (V_L - E_{I \rightarrow L})}_{I_{I \rightarrow L}} - \underbrace{\bar{g}_S S (V_L - E_S)}_{I_S} \quad (4.2)$$

$$\frac{ds}{dt} = \begin{cases} \frac{1-s}{\tau_{LO}}, & V_L \leq v_{pre} \\ \frac{-s}{\tau_{HI}}, & V_L > v_{pre} \end{cases}. \quad (4.3)$$

The state variables V_I , V_L , and s represent the membrane potential of INT1, the membrane potential of the LG neuron, and the slow, excitatory synaptic input from MCN1 to the LG neuron, respectively. The terms $\mathbf{I}_{Leak,I}$ and $\mathbf{I}_{Leak,L}$ in Equations (4.1) and (4.2) model the leak current in each neuron and are described in more detail in Chapter 2. The terms $\mathbf{I}_{L \rightarrow I}$ and $\mathbf{I}_{I \rightarrow L}$ in Equations (4.1) and (4.2), respectively, model the reciprocally inhibitory synapses between INT1 and the LG neuron. The synaptic gating functions $m_{L \rightarrow I}(V_L)$ and $m_{I \rightarrow L}(V_I)$ depend only on the membrane potential of the presynaptic neuron and are modeled by the sigmoidal functions in Equations (2.4) and (2.5), respectively, in Chapter 2. The term \mathbf{I}_P in Equation (4.1) models the local inhibitory synapse from the pacemaker of the pyloric circuit (the AB neuron) to INT1. In the biological system, the frequency of the pyloric rhythm ($\sim 1\text{Hz}$) is much faster than the frequency of the gastric mill rhythm ($\sim 10\text{Hz}$) (Bartos et al., 1999). Therefore, in the 3-dimensional model of (Manor et al., 1999), the synaptic input $P(t)$ is modeled by a fast, periodic forcing function given by

$$P(t) = \sin\left(\frac{\pi \text{mod}(t, per)}{dur}\right) H(dur - \text{mod}(t, per)), \quad (4.4)$$

which oscillates in $[0,1]$ and whose period and duty cycle are given by the parameters *per* and *dur*, respectively. Finally, the term \mathbf{I}_s in Equation (4.2) models the slow, excitatory synaptic input from MCN1 to the LG neuron. This slow input is gated by the membrane potential of the LG neuron, via presynaptic inhibition of MCN1, as described by Equation (4.3). In particular, MCN1 excitation (s) builds up in the LG neuron with time constant τ_{LO} when V_L is below the synaptic threshold voltage v_{pre} for presynaptic inhibition of MCN1. As a result, V_L slowly rises as s builds up in the LG neuron (see Figure 4.1). When V_L exceeds v_{pre} , s decays in the LG neuron with time constant τ_{HI} due to LG presynaptic inhibition of MCN1. As a result, V_L slowly falls when s decays in the LG neuron (see Figure 4.1). In the biological system, the frequency of the MCN1-elicited rhythm is controlled by the excitatory synapse from MCN1 to the LG neuron, which acts on a slower time scale than that of all other synapses in the network (Coleman et al., 1995). Therefore, the time constants τ_{LO} and τ_{HI} in Equation (4.3) are assigned with large values to model the slow synaptic time scale of the MCN1 to LG synapse. Moreover, this slow time scale is revealed when Equation (4.3) is rewritten in the form

$$\frac{ds}{dt} = \frac{H(v_{pre} - V_L) - s}{\tau_{HI} + (\tau_{LO} - \tau_{HI})H(v_{pre} - V_L)} = \varepsilon \left(\frac{H(v_{pre} - V_L) - s}{1 + (\tilde{\tau} - 1)H(v_{pre} - V_L)} \right), \quad (4.5)$$

where $0 < \varepsilon = \frac{1}{\tau_{HI}} \ll 1$ and $\tilde{\tau} = \frac{\tau_{LO}}{\tau_{HI}}$. Therefore, the state variable s evolves much more slowly than the other state variables since ε is small in Equation (4.5), and s drives the network oscillations (see Figure 4.1).

4.2.2 Reduction to a 2-Dimensional Model of the MCN1-Elicited Gastric Mill Rhythm

In the 3-dimensional model, INT1 is only influenced by synaptic inputs that occur on a fast time scale, but the LG neuron, on the other hand, is influenced by the slow excitatory synapse from MCN1 (see Figure 4.1). This difference in synaptic time scales can be exploited to reduce the 3-dimensional model of (Manor et al., 1999) down to 2 dimensions involving the state variables V_L and s . In particular, the membrane potential of INT1 (V_I) can be assumed to adjust instantaneously to its steady for each value of V_L and s , since INT1 is only influenced by fast synaptic inputs. Thus, dividing through Equation (4.1) by the leak conductance $g_{Leak,I}$ gives

$$\tau_I \frac{dV_I}{dt} = -(V_I - E_{Leak,I}) - \frac{\bar{g}_{L \rightarrow I}}{g_{Leak,I}} m_{L \rightarrow I}(V_L)(V_I - E_{L \rightarrow I}) - \frac{\bar{g}_P}{g_{Leak,I}} P(t)(V_I - E_P), \quad (4.6)$$

where $\tau_I = \frac{C_I}{g_{Leak,I}}$ is the membrane time constant of INT1. Then, setting $\tau_I = 0$ sets the left hand side of Equation (4.6) to zero and allows for an explicit solution of the INT1 membrane potential

$$V_I = u(V_L; P(t)) = \frac{g_{Leak,I} E_{Leak,I} + \bar{g}_{L \rightarrow I} m_{L \rightarrow I}(V_L) E_{L \rightarrow I} + \bar{g}_P P(t) E_P}{g_{Leak,I} + \bar{g}_{L \rightarrow I} m_{L \rightarrow I}(V_L) + \bar{g}_P P(t)}. \quad (4.7)$$

As a result, V_I is now expressed in terms of the state variable V_L and the pyloric-timed forcing function $P(t)$ (see also Figure 4.2). It is noted that V_L affects INT1 via the LG to

INT1 inhibitory synapse $m_{L \rightarrow I}(V_L)$ while $P(t)$ models the fast inhibition of INT1 by the pyloric circuit (Figure 4.2). However, in the biological system, the pyloric inhibition of INT1 does not affect the gastric mill rhythm during the active state of the LG neuron (Bartos et al., 1999). This biological fact is incorporated into the model by making the pyloric-timed forcing function dependent upon the LG membrane potential as well

$$P(t, V_L) = P(t)q(V_L). \quad (4.8)$$

In particular, $P(t)$ is the same forcing function of Equation (4.4) while $q(V_L)$ is a decreasing sigmoid of V_L that is modeled by Equation (2.12) of Chapter 2. Thus, the pyloric-timed forcing term of Equation (4.8) only affects the gastric mill rhythm during the inactive state of the LG neuron (see Results).

After replacing $P(t)$ with the $P(t, V_L)$ term of Equation (4.8), the expression for the membrane potential of INT1 in Equation (4.7) becomes $V_I = u(V_L; P(t, V_L))$. Then, substitution of this V_I expression into the $m_{I \rightarrow L}(V_I)$ term of Equation (4.2) gives a 2-dimensional model of the MCN1-elicited gastric mill rhythm

$$\begin{aligned} \frac{dV_L}{dt} = & - \underbrace{g_{Leak,L}(V_L - E_{Leak,L})}_{I_{Leak,L}} - \underbrace{\bar{g}_{I \rightarrow L} m_{I \rightarrow L}(u(V_L; P(t, V_L))) (V_L - E_{I \rightarrow L})}_{I_{I \rightarrow L}} \\ & - \underbrace{\bar{g}_s s (V_L - E_s)}_{I_s} \end{aligned} \quad (4.9)$$

$$\frac{ds}{dt} = \begin{cases} \frac{1-s}{\tau_{LO}}, & V_L \leq v_{pre} \\ \frac{-s}{\tau_{HI}}, & V_L > v_{pre} \end{cases} \quad (4.10)$$

Thus, the dynamics of INT1 have been absorbed into the dynamics of the state variable V_L (Figure 4.2). As a result, the effects of the fast inhibitory synapses that influence INT1 are absorbed into the INT1 to LG synapse, as indicated by the $m_{I \rightarrow L}(u(V_L; P(t, V_L)))$ term of Equation (4.9) (see also Figure 4.2). Thus, the 3-dimensional model of (Manor et al., 1999) has been reduced to 2 dimensions where both state variables are directly involved in generating network oscillations. This allows for a complete examination of the network dynamics of the MCN1-elicited gastric mill rhythm via a phase-plane analysis in the V_L - s plane.

Next, the phase-plane geometry of the 2-dimensional model is examined. First, the V_L - and s -nullclines are computed, which designate the curves in the V_L - s phase plane where $dV_L/dt = 0$ and $ds/dt = 0$, respectively. The V_L -nullcline is computed by setting $dV_L/dt = 0$ in Equation (4.9) and solving for s . However, since the 2-dimensional model is non-autonomous due to the pyloric forcing term $P(t, V_L)$ of Equation (4.9), a family of V_L -nullclines will exist in the phase plane. In particular, a one-parameter family of cubic V_L -nullclines indexed by the values p in $[0, 1]$ of $P(t, V_L)$ exists in the V_L - s phase plane given by

$$s(V_L; p) = - \frac{g_{Leak,L}(V_L - E_{Leak,L}) + \bar{g}_{I \rightarrow L} m_{I \rightarrow L}(u(V_L; p))(V_L - E_{I \rightarrow L})}{\bar{g}_s(V_L - E_s)}, \quad (4.11)$$

where the extreme values $p = 0$ ($p = 1$) correspond to the unforced (maximally forced) system. The s -nullcline, on the other hand, is computed by setting $ds/dt = 0$ in Equation (4.10) and solving for s to obtain the step function

$$s = \begin{cases} 0, & V_L \leq v_{pre} \\ 1, & V_L > v_{pre} \end{cases}. \quad (4.12)$$

In the unforced system where $p = 0$ in Equation (4.11), a single cubic V_L -nullcline exists in the phase plane, given by $s(V_L; 0)$. This corresponds to when $P(t, V_L) = 0$ in Equation (4.9), so that the 2-dimensional system becomes autonomous and only one V_L -nullcline exists in the phase plane. Within the V_L - s phase plane, $dV_L/dt > 0$ (< 0) above (below) the V_L -nullcline while $ds/dt > 0$ (< 0) below (above) the s -nullcline. Therefore, the outer branches of the cubic V_L -nullcline are stable (attracting) while its middle branch is unstable (repelling). In addition, the V_L - and s -nullclines intersect along the unstable middle branch of the cubic, which allows the system to exhibit oscillations (Rinzel and Ermentrout, 1998). Furthermore, the time constants of MCN1 excitation (τ_{LO} , τ_{HI}) are chosen to be large in order to put the system in a relaxation regime. As a result, the periodic orbit in the V_L - s phase plane consists of two fast and two slow portions (Figure 4.3.A.1), where the slow portions track the outer branches of the cubic to which they are strongly attracted by the fast horizontal flow. Furthermore, the periodic orbit in the V_L - s phase plane describes the oscillation in the LG membrane potential (Figure 4.3.A.2) during the gastric mill rhythm (see Results).

In the forced system where $0 \leq p \leq 1$ in Equation (4.11), a family of cubic V_L -nullclines exists in the phase plane. Two members of this family are shown in Figure 4.3.B.1. In particular, the higher cubic occurs when $p = 0$ and corresponds to the unforced system of Figure 4.3.A.1, while the lower cubic occurs when $p = 1$ and corresponds to the maximally forced system at the peak of the pyloric forcing. Thus, the pyloric forcing term shifts the V_L -nullcline as p varies in $[0,1]$, which causes the trajectory to shift back and forth between the higher and lower cubics (Figure 4.3.B.1). The transitions between cubics are impulsive since the pyloric forcing peak is small compared to the pyloric period. Therefore, when $p = 0$ in Equation (4.11), the trajectory in the V_L - s phase plane tracks the higher (unforced) cubic (Figure 4.3.B.1), then shifts through a family of lower cubics for nonzero values of p and touches the lowest (maximally forced) cubic at $p = 1$ (Figure 4.3.B.1). Physiologically, the pyloric forcing term models the effect of the inhibitory synapse from the pyloric circuit to INT1 (inset of Figure 4.3) on the network dynamics of the gastric mill rhythm. In particular, the pyloric-timed inhibition of INT1 in turn disrupts the INT1 to LG inhibition (inset of Figure 4.3), which effectively disinhibits the LG neuron from INT1, as illustrated by the periodic subthreshold depolarizations in the LG membrane potential (Figure 4.3.B.2) (see Results). Moreover, as modeled by Equation (4.8), the pyloric forcing only affects the inactive state of the LG neuron and therefore only shifts the left branch of the V_L -nullcline. The right branch of the V_L -nullcline, which corresponds to the active state of the LG neuron, remains stationary since the effect of the pyloric forcing is not effectively transmitted through the INT1 to LG synapse during the active state of the LG neuron (see Results).

4.2.3 A 2-Dimensional Model of the MCN1-Elicited Gastric Mill Rhythm that Includes the Effect of Rhythmic Feedback

Physiologically, MCN1 is rhythmically active in the presence of inhibitory feedback from the pyloric circuit (Coleman and Nusbaum, 1994). In particular, in the intact biological system, the pacemaker of the pyloric circuit (the AB neuron) inhibits the cell body of MCN1 in the commissural ganglion (CoG). In the absence of this inhibitory feedback connection (as in Figure 4.1), tonic stimulation of MCN1 elicits a gastric mill rhythm whose frequency is regulated by the local AB to INT1 inhibition in the STG (Nadim et al., 1998; Bartos et al., 1999). The 2-dimensional model in Equations (4.9) and (4.10) describes this gastric mill rhythm. However, recent experiments showed that in the presence of the AB to MCN1 feedback inhibition, the MCN1-elicited gastric mill rhythm exhibits distinct network properties (Wood et al., 2004). In particular, rhythmic stimulation of MCN1 elicits a gastric mill rhythm whose frequency is insensitive to the effect of the local AB to INT1 inhibition in the STG (Wood et al., 2004). A mathematical model was recently used to show that the frequency of this gastric mill rhythm is critically dependent upon the relative timing between the local AB to INT1 inhibition and that of the AB to MCN1 feedback inhibition (Ambrosio, 2005; Ambrosio-Mouser et al., 2006). In particular, the AB to INT1 inhibition (in the STG) must occur at nearly the same phase of the pyloric rhythm as the AB to MCN1 feedback inhibition (in the CoG) in order to elicit a gastric mill rhythm with the observed frequency of the biological system (Ambrosio-Mouser et al., 2006).

In this chapter, the findings of (Ambrosio-Mouser et al., 2006) are used to develop a reduced 2-dimensional model of the MCN1-elicited gastric mill rhythm that includes the effect of the AB to MCN1 feedback inhibition. Moreover, the biological fact that the AB to MCN1 feedback inhibition rhythmically interrupts the excitatory feed-forward synapse from MCN1 to the LG neuron (Wood et al., 2004) is used to develop the 2-dimensional model. This excitatory feed-forward synapse is modeled by the I_s term of Equation (4.9). Thus, to model the effect of the pyloric feedback inhibition on the MCN1 to LG synapse, a periodic forcing function is included in the I_s term given by

$$\sigma(t) = 1 + \bar{g}_\sigma \sin\left(\frac{\pi \text{mod}(t, per)}{dur}\right) H(dur - \text{mod}(t, per)). \quad (4.13)$$

In particular, $\sigma(t)$ oscillates in $[0,1]$ and models the pyloric-timed inhibition of the excitatory MCN1 to LG synapse by the AB to MCN1 feedback inhibition (Figure 4.4). The parameter \bar{g}_σ designates the maximal conductance of $\sigma(t)$, whose period and duty cycle, given by the parameters per and dur respectively, are the same as that for the AB to INT1 inhibition modeled by Equation (4.4). Moreover, the pyloric-timed oscillation of $\sigma(t)$ is such that $(1 - \bar{g}_\sigma) \leq \sigma(t) \leq 1$, where $\sigma(t) = (1 - \bar{g}_\sigma) > 0$ represents the maximum inhibition of the MCN1 to LG synapse while $\sigma(t) = 1$ represents the unforced synapse. Thus, a 2-dimensional model of the MCN1-elicited gastric mill rhythm that includes the effect of the pyloric feedback inhibition to MCN1 is given by

$$\begin{aligned} \frac{dV_L}{dt} = & -g_{Leak,L}(V_L - E_{Leak,L}) - \bar{g}_{I \rightarrow L} m_{I \rightarrow L}(u(V_L; P(t)))(V_L - E_{I \rightarrow L}) \\ & - \underbrace{\bar{g}_s s \sigma(t)}_{\mathbf{I}_{s(\text{rhythmic})}}(V_L - E_s) \end{aligned} \quad (4.14)$$

$$\frac{ds}{dt} = \begin{cases} \frac{1-s}{\tau_{LO}}, & V_L \leq v_{pre} \\ \frac{-s}{\tau_{HI}}, & V_L > v_{pre} \end{cases} \quad (4.15)$$

The $\mathbf{I}_{s(\text{rhythmic})}$ term in Equation (4.14) now includes both a fast and a slow process. In particular, the state variable s , whose dynamics are governed by Equation (4.15) (which equivalent to Equation (4.10)) oscillates on a slow time scale (as shown previously in Equation (4.5)), while in comparison the $\sigma(t)$ oscillation that is governed by Equation (4.13) is fast (Figure 4.4). However, the network oscillations are still driven by the slow dynamics of the state variable s , while $\sigma(t)$ acts as a forcing function (see Results). Physiologically, s again describes the slow buildup and decay of the presynaptically-gated MCN1 excitation in the LG neuron.

The forcing function $P(t)$ in Equation (4.14), which models the local AB to INT1 inhibition in the STG, is only time-dependent in this model. Previously in the 2-dimensional model of Equations (4.9) and (4.10), $P(t)$ was also made dependent upon the LG membrane potential. This was done in order to model the biological fact that the active state of the LG neuron is not affected by the local AB to INT1 inhibition during the gastric mill rhythm that elicited by tonic MCN1 stimulation (Bartos et al., 1999). In contrast, rhythmic stimulation of MCN1 elicits a gastric mill rhythm in which the active

state of LG is indeed affected by the AB to INT1 inhibition (Wood et al., 2004), (Figure 4.5). Therefore, $P(t)$ is only time-dependent in Equation (4.14) so that it continues to affect the active state of the LG neuron (see Results).

Next, the phase-plane geometry of the 2-dimensional model in Equations (4.14) and (4.15) is examined. It is noted that Equation (4.14) includes the two forcing functions $P(t)$ and $\sigma(t)$. Therefore, setting $dV_L/dt = 0$ and solving for s gives the 2-parameter family of cubic V_L -nullclines

$$s(V_L; p, \sigma) = -\frac{g_{Leak,L}(V_L - E_{Leak,L}) + \bar{g}_{I \rightarrow L} m_{I \rightarrow L}(u(V_L; p))(V_L - E_{I \rightarrow L})}{\bar{g}_s \sigma (V_L - E_s)} \quad (4.16)$$

that is indexed by the forcing parameters p of $P(t)$ and σ of $\sigma(t)$. In particular, p again varies in $[0,1]$ and models the effect of the local AB to INT1 inhibition in the STG, where the extreme values $p = 0$ ($p = 1$) again correspond to the minimum (maximum) forcing due to $P(t)$. On the other hand, σ varies in $[(1 - \bar{g}_\sigma), 1]$ and models the effect of the AB to MCN1 feedback inhibition. The extreme values $\sigma = 1 - \bar{g}_\sigma$ ($\sigma = 1$) correspond to the maximum (minimum) inhibition of the MCN1 to LG synapse due to the $\sigma(t)$ forcing function. The s -nullcline is computed by setting $ds/dt = 0$ in Equation (4.15) to obtain the same step function as in Equation (4.12).

To simplify the network dynamics in the V_L - s phase plane, the AB to INT1 inhibition (in the STG) is assumed to occur at the same phase of the pyloric rhythm as the AB to MCN1 feedback inhibition (in the CoG), which is a reasonable assumption in the biological system (see Results, Figure 4.5). As a result, the oscillations in $P(t)$ and $\sigma(t)$,

modeled by Equations (4.4) and (4.13) respectively, occur in phase so that the forcing parameter values p and σ of Equation (4.16) simultaneously affect the network dynamics in the V_L - s phase plane. Furthermore, the net effect of the simultaneous forcing parameters shifts the cubic V_L -nullcline up in the phase plane, which corresponds to the pyloric-timed hyperpolarizations in the LG membrane potential (see Results, Figure 4.6). Subsequently, the geometrical properties in the V_L - s phase plane are used to investigate how the added effect of the AB to MCN1 feedback inhibition changes the network dynamics of the MCN1-elicited gastric mill rhythm (see Results, Figures 4.7 and 4.8).

4.2.4 Building a Mathematical Model of the MCN1/CPN2-Elicited Gastric Mill Rhythm

A reduced mathematical model is developed to study the gastric mill rhythm that is elicited by co-stimulation of the CoG projection neurons MCN1 and CPN2 (Figure 4.8). Physiologically, the axon of CPN2 descends into the STG where its terminals excite the LG neuron (Norris et al., 1994). This excitation is believed to occur via a local electrical coupling within the STG (M.P. Nusbaum, personal communication). In addition, the cell body of CPN2 is strongly inhibited by INT1 in the CoG (Norris et al., 1994). Although stimulation of CPN2 alone is generally not sufficient to elicit a gastric mill rhythm (Norris et al., 1994), co-stimulation of MCN1 and CPN2 elicits a distinct gastric mill rhythm from that elicited by MCN1 stimulation alone (Blitz and Nusbaum, 1997). Thus, this chapter develops a reduced model of the MCN1/CPN2-elicited gastric mill rhythm to investigate how the addition of a second projection neuron (CPN2) changes the network dynamics of the MCN1-elicited rhythm. First, the case in which MCN1 is tonically

active is considered, which occurs in the absence of the AB to MCN1 feedback inhibition, as in the 2-dimensional model of Equations (4.9) and (4.10). The addition of CPN2 to this system gives a 3-dimensional model of the MCN1/CPN2-elicited gastric mill rhythm given by

$$\begin{aligned} \frac{dV_L}{dt} = & -g_{Leak,L}(V_L - E_{Leak,L}) - \bar{g}_{I \rightarrow L} m_{I \rightarrow L} (u(V_L; P(t, V_L))) (V_L - E_{I \rightarrow L}) \\ & - \underbrace{\bar{g}_s s (V_L - E_s)}_{I_s} - \underbrace{g_e (V_L - V_C)}_{I_e} \end{aligned} \quad (4.17)$$

$$\frac{dV_C}{dt} = - \underbrace{g_{Leak,C}(V_C - E_{Leak,C})}_{I_{LeakC}} - \underbrace{\bar{g}_{I \rightarrow C} m_{I \rightarrow C} (u(V_L; P(t, V_L))) (V_C - E_{I \rightarrow C})}_{I_{I \rightarrow C}} \quad (4.18)$$

$$\frac{ds}{dt} = \begin{cases} \frac{1-s}{\tau_{LO}}, & V_L \leq v_{pre} \\ -\frac{s}{\tau_{HI}}, & V_L > v_{pre} \end{cases} \quad (4.19)$$

The dynamics of the LG neuron in this system are modeled by Equation (4.17), where the only change from Equation (4.9) is the additional I_e term that describes the local electrical coupling between the CPN2 axon and the LG neuron in the STG (Figure 4.8.A). The parameter g_e represents the conductance of this synapse while the variable V_C represents the membrane potential of CPN2. This electrical coupling is modeled as a one-way (feed-forward) synapse from CPN2 to LG since it occurs locally within the STG and does not involve the CPN2 cell body in the CoG.

The dynamics of CPN2 are modeled by Equation (4.18), where it is treated as a passive neuron. The term $\mathbf{I}_{Leak,C}$ models the leak current of CPN2, where the parameters $g_{Leak,C}$ and $E_{Leak,C}$ designate the leak conductance and reversal potential, respectively. In the biological system, the membrane potential of CPN2 remains depolarized in the absence of INT1 inhibition (Norris et al., 1994). This biological fact is modeled by assigning a high value to $E_{Leak,C}$ (see Table B.2 of Appendix B).

The term $\mathbf{I}_{I \rightarrow C}$ in Equation (4.18) models the inhibitory feedback synapse from INT1 to CPN2 (see Figure 4.8.A), where the parameters $\bar{g}_{I \rightarrow C}$ and $E_{I \rightarrow C}$ designate its maximal conductance and reversal potential, respectively. Moreover, this inhibitory feedback synapse is controlled by the instantaneous sigmoidal gating function

$$m_{I \rightarrow C}(u) = \frac{1}{1 + \exp((v_{I \rightarrow C} - u)/k_{I \rightarrow C})}, \quad (4.20)$$

which depends only on the presynaptic membrane potential of INT1 that is given by $V_I = u(V_L; P(t, V_L))$, as derived earlier in Equations (4.7) and (4.8). The parameters $v_{I \rightarrow C}$ and $k_{I \rightarrow C}$ designate the synaptic inflection point voltage and steepness of this sigmoid, respectively. Moreover, since the above sigmoid is a function of $u(V_L; P(t, V_L))$, the effect of the AB to INT1 inhibition, modeled by $P(t, V_L)$ in Equation (4.8), is transmitted to CPN2 via the inhibitory feedback synapse from INT1. Consequently, the transmission of the $P(t, V_L)$ forcing function induces pyloric-timed depolarizations in the membrane potential of CPN2 (see Results Figure 4.9). Furthermore, as discussed for the 2-dimensional model in Equations (4.9) and (4.10),

$P(t, V_L)$ depends upon the LG membrane potential in order to prevent the AB to INT1 inhibition from affecting the active state of the LG neuron when MCN1 is tonically active (see Results).

The slow dynamics of the state variable s are governed by Equation (4.19), which is equivalent to Equation (4.10), and s models the slow, presynaptically-gated excitation from MCN1 to the LG neuron. Hence, as in the MCN1-elicited rhythm, MCN1 excitation (s) builds up in the LG neuron with time constant τ_{LO} when V_L is below the synaptic threshold voltage v_{pre} for presynaptic inhibition, while s decays in LG with time constant τ_{HI} when V_L exceeds v_{pre} .

4.2.5 Reduction to a 2-Dimensional Model of the MCN1/CPN2-Elicited Gastric Mill Rhythm

The 3-dimensional model of the MCN1/CPN2-elicited gastric mill rhythm is now reduced to 2 dimensions by exploiting the difference in synaptic time scales, as was done for the derivation of Equations (4.9) and (4.10). In particular, CPN2 is only affected by the fast inhibitory synapse from INT1 which is gated by the instantaneous sigmoid of Equation (4.20). In contrast, the LG neuron is affected by the slow excitatory synapse from MCN1, which acts on a slower time scale than that of all other synapses in the network (see Equation (4.5)). Therefore, since CPN2 is only affected by a fast synapse in the model, its membrane potential (V_C) can be assumed to adjust instantaneously to its steady-state for each value of the state variables V_L and s . In particular, dividing through Equation (4.18) by the leak conductance $g_{Leak,C}$ gives

$$\tau_C \frac{dV_C}{dt} = -(V_C - E_{Leak,C}) - \frac{\bar{g}_{I \rightarrow C}}{g_{Leak,C}} m_{I \rightarrow C} (u(V_L; P(t, V_L))) (V_C - E_{I \rightarrow C}), \quad (4.21)$$

where $\tau_C = \frac{C_C}{g_{Leak,C}}$ is the membrane time constant of CPN2 and $C_C = 1$ is the membrane

capacitance of CPN2 in Equation (4.18). Then, setting the time constant $\tau_C = 0$ sets the left hand side of Equation (4.21) to zero and allows for an explicit solution of the CPN2 membrane potential given by

$$V_C = r \left(\underbrace{u(V_L; P(t, V_L))}_{\hat{v}_i} \right) = \frac{g_{Leak,C} E_{Leak,C} + \bar{g}_{I \rightarrow C} m_{I \rightarrow C} (u(V_L; P(t, V_L))) E_{I \rightarrow C}}{g_{Leak,C} + \bar{g}_{I \rightarrow C} m_{I \rightarrow C} (u(V_L; P(t, V_L)))}. \quad (4.22)$$

As a result, the membrane potential of CPN2 is now expressed in terms of the state variable V_L and the forcing function $P(t, V_L)$ (see Figure 4.8.B). Substitution of Equation (4.22) into V_C of the \mathbf{I}_e term in Equation (4.17) then gives a 2-dimensional model of the MCN1/CPN2-elicited gastric mill rhythm

$$\begin{aligned} \frac{dV_L}{dt} = & -g_{Leak,L} (V_L - E_{Leak,L}) - \bar{g}_{I \rightarrow L} m_{I \rightarrow L} (u(V_L; P(t, V_L))) (V_L - E_{I \rightarrow L}) \\ & - \underbrace{\bar{g}_s s (V_L - E_s)}_{\hat{v}_i} - \underbrace{g_e (V_L - r(u(V_L; P(t, V_L))))}_{\hat{v}_e} \end{aligned} \quad (4.23)$$

$$\frac{ds}{dt} = \begin{cases} \frac{1-s}{\tau_{LO}}, & V_L \leq v_{pre} \\ \frac{-s}{\tau_{HI}}, & V_L > v_{pre} \end{cases}. \quad (4.24)$$

Therefore, in reducing the 3-dimensional model to 2 dimensions, the dynamics of CPN2 are absorbed into the dynamics of the state variable V_L (Figure 4.8.B). Moreover, the effect of the INT1 to CPN2 feedback inhibition is absorbed in the electrical synapse from CPN2 to the LG neuron (Figure 4.8.B). Thus, the network dynamics of the MCN1/CPN2-elicited gastric mill rhythm are described in terms of the 2 state variables V_L and s , which are directly involved in generating network oscillations. As a result, this allows for a complete examination of the network dynamics in the MCN1/CPN2-elicited gastric mill rhythm via the geometrical properties in the V_L - s phase plane.

Next, the phase-plane geometry of this 2-dimensional model is examined, where only one forcing function given by $P(t, V_L)$ exists in the model. Thus, setting $dV_L/dt = 0$ in Equation (4.23) and solving for s gives the 1-parameter family of cubic V_L -nullclines that is indexed by the values p of $P(t, V_L)$

$$s(V_L; p) = - \frac{\left\{ g_{Leak,L} (V_L - E_{Leak,L}) + \bar{g}_{I \rightarrow L} m_{I \rightarrow L} (u(V_L; p)) (V_L - E_{I \rightarrow L}) \right\} + g_e (V_L - r(u(V_L; p)))}{\bar{g}_s (V_L - E_s)}. \quad (4.25)$$

As in the family of cubic V_L -nullclines for the MCN1-elicited rhythm modeled by Equation (4.11), the parameter p in Equation (4.25) varies in $[0,1]$ where $p = 0$ ($p = 1$) corresponds to the minimum (maximum) forcing due to $P(t, V_L)$. The s -nullcline is

computed by setting $ds/dt = 0$ in Equation (4.24) and solving for s to obtain the same step function as in Equation (4.12).

Physiologically, the parameter p models the effect of the local AB to INT1 inhibition on the network dynamics of the MCN1/CPN2-elicited gastric mill rhythm. Moreover, Equation (4.25) indicates that the forcing parameter p affects the LG neuron via two pathways; the INT1 to LG inhibitory synapse and the CPN2 to LG electrical synapse (see Results). In contrast, the forcing parameter p in the MCN1-elicited rhythm only affects the LG neuron through the former pathway (see Equation (4.11)). Subsequently, the geometrical properties in the V_L - s phase plane are used to investigate how the addition of CPN2 changes the network dynamics of the MCN1-elicited rhythm (see Results Figures 4.9 – 4.13).

4.2.6 A 2-Dimensional Model of the MCN1/CPN2-Elicited Gastric Mill Rhythm That Includes the Effect of Rhythmic Feedback to MCN1

Next, a 2-dimensional model of the MCN1/CPN2-elicited gastric mill rhythm is developed that includes the effect of the inhibitory feedback connection from AB to MCN1 (Figure 4.14). The effect of this feedback connection was included in the MCN1-elicited rhythm modeled by Equations (4.14) and (4.15). In particular, the fast, periodic forcing function $\sigma(t)$ (see Equation (4.13)) was used to model the pyloric-timed interruption of the excitatory MCN1 to LG synapse by the AB to MCN1 feedback inhibition. Now, this pyloric-timed interruption of the MCN1 to LG synapse is included in a 2-dimensional model of the MCN1/CPN2-elicited gastric mill rhythm given by

$$\begin{aligned} \frac{dV_L}{dt} = & -g_{Leak,L} (V_L - E_{Leak,L}) - \bar{g}_{l \rightarrow L} m_{l \rightarrow L} (u(V_L; P(t))) (V_L - E_{l \rightarrow L}) \\ & - \underbrace{\bar{g}_s s \sigma(t) (V_L - E_s)}_{\mathbf{I}_{s(\text{rhythmic})}} - \underbrace{g_e (V_L - r(u(V_L; P(t))))}_{\mathbf{I}_e} \end{aligned} \quad (4.26)$$

$$\frac{ds}{dt} = \begin{cases} \frac{1-s}{\tau_{LO}}, & V_L \leq v_{pre} \\ \frac{-s}{\tau_{HI}}, & V_L > v_{pre} \end{cases}. \quad (4.27)$$

In particular, the $\mathbf{I}_{s(\text{rhythmic})}$ term of Equation (4.26) includes the effect of the $\sigma(t)$ forcing function, which inhibits the MCN1 to LG synapse to model the effect of the AB to MCN1 feedback inhibition (see Results). In addition, it is noted that the forcing term $P(t)$ is only time-dependent in Equation (4.26) in order to model the biological fact that the AB to INT1 inhibition continues to affect the active state of the LG neuron when MCN1 is rhythmically active, as was described in the derivation of Equations (4.14) and (4.15). Nevertheless, outside of the $\sigma(t)$ and $P(t)$ forcing functions, the remainder of the model MCN1/CPN2-elicited gastric mill rhythm in Equations (4.26) and (4.27) is equivalent to that in Equations (4.23) and (4.24).

Next, the phase-plane geometry of the above system is examined. Since Equation (4.26) includes two forcing functions, setting $dV_L/dt = 0$ and solving for s gives the 2-parameter family of cubic V_L -nullclines that is indexed by the values p of $P(t)$ and σ of $\sigma(t)$

$$s(V_L; p, \sigma) = - \frac{\left\{ \begin{aligned} &g_{Leak,L}(V_L - E_{Leak,L}) + \bar{g}_{l \rightarrow L} m_{l \rightarrow L}(u(V_L; p))(V_L - E_{l \rightarrow L}) \\ &+ g_e(V_L - r(u(V_L; p))) \end{aligned} \right\}}{\bar{g}_s \sigma (V_L - E_s)}. \quad (4.28)$$

where p varies in $[0,1]$ while σ varies in $[(1 - \bar{g}_\sigma), 1]$. Moreover, as in the family of cubics for the MCN1-elicited rhythm that is modeled by Equation (4.16), the value $p = 0$ ($p = 1$) represents the minimum (maximum) forcing due to $P(t)$, while $\sigma = 1 - \bar{g}_\sigma$ ($\sigma = 1$) represents the maximum (minimum) forcing due to $\sigma(t)$. However, the forcing effect of p is transmitted to the LG neuron via 2 pathways, as occurs for the cubics of the previous system modeled by Equation (4.25). Meanwhile, the s -nullcline is given by the step function of Equation (4.12).

To simplify the network dynamics in the V_L - s phase plane, the forcing functions $P(t)$ and $\sigma(t)$ are assumed to oscillate in phase so that the forcing parameter values of p and σ in Equation (4.28) simultaneously affect the network dynamics. The same assumption was made for the family of cubics in the MCN1-elicited rhythm modeled by Equation (4.16). Subsequently, the net effect of the simultaneous forcing parameters σ and p in Equation (4.28) shifts up the cubic V_L -nullcline in the phase plane, which corresponds to the pyloric-timed hyperpolarizations in the LG membrane potential (see Results, Figure 4.15). Thus, the above system is used to investigate how the addition of the AB to MCN1 feedback inhibition affects the network dynamics of the MCN1/CPN2-elicited gastric mill rhythm (see Results, Figures 4.15, 4.16).

4.2.7 A 2-Dimensional Model of the VCN-Influenced MCN1/CPN2-Elicited Gastric Mill Rhythm

In the biological system, the ventral cardiac neurons (VCN) are a group of sensory neurons that elicit a gastric mill rhythm via their projections into the CoGs. In particular, VCN stimulation co-activates several CoG projection neurons, including MCN1 and CPN2, which in turn elicits a gastric mill rhythm in the STG (Beenhakker and Nusbaum, 2004). Recent experiments showed that this VCN-elicited gastric mill rhythm can be closely approximated by co-stimulation of MCN1 and CPN2 in their VCN-influenced activity patterns (Beenhakker and Nusbaum, 2004). However, while CPN2 exhibits similar activity, MCN1 is rhythmically active during the LG interburst phase of the VCN-elicited rhythm but tonically active during the LG burst phase (see Figure 4.17).

Thus, a 2-dimensional model of the MCN1/CPN2-elicited gastric mill rhythm is developed in which MCN1 and CPN2 exhibit their VCN-influenced activity. To model the alternating (rhythmic/tonic) activity in MCN1, a forcing function that is similar to that of $\sigma(t)$ in Equation (4.13) is used. However, while $\sigma(t)$ inhibits the MCN1 to LG synapse throughout the gastric mill rhythm, the forcing function

$$\sigma(t, V_L) = \underbrace{1 + \bar{g}_\sigma \sin\left(\frac{\pi \text{mod}(t, per)}{dur}\right) H(dur - \text{mod}(t, per)) H(v_{pre} - V_L)}_{\sigma(t)} \quad (4.29)$$

is used to inhibit the MCN1 to LG synapse only during the LG interburst phase. In particular, the above $\sigma(t, V_L)$ forcing function is equivalent to $\sigma(t)$ in Equation (4.13) whenever $V_L \leq v_{pre}$, but $\sigma(t, V_L) = 1$ when $V_L > v_{pre}$. Thus, an MCN1/CPN2-elicited

gastric mill rhythm in which MCN1 exhibits alternating (rhythmic/tonic) activity is modeled by the 2-dimensional system

$$\begin{aligned} \frac{dV_L}{dt} = & -g_{Leak,L}(V_L - E_{Leak,L}) - \bar{g}_{l \rightarrow L} m_{l \rightarrow L} (u(V_L; P(t, V_L))) (V_L - E_{l \rightarrow L}) \\ & - \underbrace{\bar{g}_s s \sigma(t, V_L) (V_L - E_s)}_{\mathbf{I}_{s(\text{alternating})}} - \underbrace{g_e (V_L - r(u(V_L; P(t - \mu, V_L))))}_{\mathbf{I}_{e(\text{delayP})}} \end{aligned} \quad (4.30)$$

$$\frac{ds}{dt} = \begin{cases} \frac{1-s}{\tau_{LO}}, & V_L \leq v_{pre} \\ \frac{-s}{\tau_{HI}}, & V_L > v_{pre} \end{cases}. \quad (4.31)$$

In particular, the $\mathbf{I}_{s(\text{alternating})}$ term of Equation (4.30) includes the effect of $\sigma(t, V_L)$, which oscillates in $[(1 - \bar{g}_\sigma), 1]$ when $V_L \leq v_{pre}$ to periodically inhibit the MCN1 to LG synapse during the inactive state of the LG neuron. However, $\sigma(t, V_L) = 1$ when $V_L > v_{pre}$ so that the MCN1 to LG synapse is unforced during the active state of the LG neuron. In addition, the $P(t, V_L)$ forcing function in Equation (4.30) is dependent upon the LG membrane potential so that the AB to INT1 inhibition does not affect the active state of the LG neuron when MCN1 is tonically active (when the MCN1 to LG synapse is unforced), as discussed in the derivation of Equations (4.9) and (4.10). Furthermore, as in the previous models of the MCN1/CPN2-elicited gastric mill rhythm, the forcing effect of $P(t, V_L)$ is transmitted to the LG neuron via both the INT1 to LG inhibitory synapse and the CPN2 to LG electrical synapse. However, in this model we investigate how a timing delay in the transmission of the $P(t, V_L)$ forcing effect through the latter CPN2 to LG

pathway affects the network dynamics. In the biological system, such a delay can be approximated by $\frac{1}{2}$ of a pyloric period (see Results, Figure 4.20). This delay is modeled by the forcing function $P(t-\mu, V_L)$ in the $\mathbf{I}_{e(\text{delay}P)}$ term of Equation (4.30). In particular, the forcing effect of $P(t, V_L)$ is delayed by the parameter μ when transmitted to the LG neuron via the CPN2 pathway (see Results).

Next, the phase-plane geometry of this 2-dimensional model is examined. Setting $dV_L/dt = 0$ in Equation (4.30) and solving for s gives the 3-parameter family of cubic V_L -nullclines that is indexed by the values σ of $\sigma(t, V_L)$, p of $P(t, V_L)$ and p_μ of $P(t-\mu, V_L)$

$$s(V_L; \sigma, p, p_\mu) = - \frac{\left\{ \begin{array}{l} g_{Leak,L} (V_L - E_{Leak,L}) + \bar{g}_{l \rightarrow L} m_{l \rightarrow L} (u(V_L; p)) (V_L - E_{l \rightarrow L}) \\ + g_e (V_L - r(u(V_L; p_\mu))) \end{array} \right\}}{\bar{g}_s \sigma (V_L - E_s)}. \quad (4.32)$$

In particular, the parameter σ varies in $[(1 - \bar{g}_\sigma), 1]$ when $V_L \leq v_{pre}$ and models the pyloric-timed interruption of the MCN1 to LG synapse during the LG interburst phase of this gastric mill rhythm. However, $\sigma = 1$ when $V_L > v_{pre}$ so that the MCN1 to LG synapse is unforced during the LG burst phase. In addition, the parameters p and p_μ both vary in $[0, 1]$ and model the effect of the AB to INT1 inhibition. When $\mu = 0$, the forcing functions $P(t, V_L) = P(t-\mu, V_L)$ and the forcing effects of p and p_μ simultaneously affect the network dynamics. However, their forcing effects occur at different phases of the pyloric rhythm when $\mu \neq 0$. We first investigate how the alternating (rhythmic/tonic) activity in the MCN1 to LG synapse affects the network dynamics of this gastric mill rhythm (see Results Figures 4.18, 4.19). Then, we investigate how a timing delay in the transmission

of the $P(t, V_L)$ forcing effect through the CPN2 to LG pathway affects the network dynamics (see Results Figures 4.21, 4.22).

4.3 Results

The 2-dimensional models that were developed in Methods are now used to investigate how the projection neurons MCN1 and CPN2 shape the gastric mill rhythm. In addition, the models developed in this chapter also include the effects of inhibitory rhythmic feedback to the projection neurons. Therefore, this also allows for investigating how such feedback influences the gastric mill rhythm. In particular, as the state variables of each 2-dimensional model are directly involved in generating network oscillations, the network dynamics of each model are fully described via the geometrical properties in the V_L - s phase. First the MCN1-elicited rhythm is studied. Then, the network properties of the MCN1/CPN2-elicited gastric mill rhythm are investigated.

4.3.1 Investigating the Network Dynamics of the MCN1-Elicited Gastric Mill Rhythm

First, the MCN1-elicited gastric mill rhythm that is modeled by the 2-dimensional system in Equations (4.9) and (4.10) is studied via its geometrical properties in the V_L - s phase plane. Since the network dynamics of this gastric mill rhythm were already described in detail in Section 2.3.1 (see Chapter 2), only a brief overview of the MCN1-elicited rhythm is given in this section. The state variable s , which describes the slow presynaptically-gated excitation from MCN1 to the LG neuron, drives the network

oscillations in this system. Moreover, the time constants of s in Equation (4.10) are chosen to be large so that the system operates in a relaxation regime (see Methods). Physiologically, the left branch of the V_L -nullcline corresponds to the inactive state of the LG neuron, while the right branch corresponds to the active state of LG. Moreover, the forcing function $P(t, V_L)$ in Equation (4.9), which models the local AB to INT1 inhibition, makes the 2-dimensional system non-autonomous so that a family of cubic V_L -nullclines exists in the phase plane (see Methods). This family of cubics is modeled by Equation (4.11), while the s -nullcline is modeled by Equation (4.12).

First, the unforced MCN1-elicited gastric mill rhythm is described, which corresponds to when the forcing function $P(t, V_L) = 0$ in Equation (4.9). Since the 2-dimensional model is autonomous in the absence of this forcing function, a single cubic V_L -nullcline, given by $s(V_L; 0)$ in Equation (4.11), exists in the phase plane (see Methods). During the inactive state of the LG neuron where it is inhibited by INT1, the slow excitation from MCN1 (s) slowly builds up in the LG neuron. As a result, a phase point slowly climbs up the left branch of the cubic V_L -nullcline from the point 1 to the point 2 as s increases in LG (Figure 4.3.A.1), and the slow buildup of s excitation causes the LG membrane potential to slowly rise (Figure 4.3.A.2). When the phase point reaches the left knee of the cubic at the point 2 (Figure 4.3.A.1), it becomes unstable and undergoes a saddle-node bifurcation. As a result, the phase point jumps to the stable right branch of the cubic at the point 3 (Figure 4.3.A.1), since $dV_L/dt > 0$ above the V_L -nullcline (see Methods). Physiologically, this jump corresponds to when enough MCN1 excitation builds up in the LG neuron to allow it to overcome its inhibition by INT1. Then, during the active state of the LG neuron where it inhibits INT1 and presynaptically inhibits

MCN1, the presynaptic inhibition causes s to slowly decay in LG so that the phase point slowly falls down the right branch of the cubic and V_L slowly falls toward its resting potential (Figure 4.3.A.2). When the phase point reaches the right knee of the cubic at the point 4 (Figure 4.3.A.1), it becomes unstable and undergoes another saddle node bifurcation. As a result, the phase point jumps back to the stable left branch of the cubic at the point 1 (Figure 4.3.A.1), since $dV_L/dt < 0$ below the V_L -nullcline (see Methods). Physiologically, this jump corresponds to when the LG neuron falls back down into its inactive state due to the graded inhibition from INT1, which in turn removes the LG presynaptic inhibition of MCN1. Then, the cycle begins again as the phase point slowly climbs up the left branch of the cubic and s slowly builds up in the LG neuron.

Next, the forced MCN1-elicited gastric mill rhythm is described, where $0 \leq P(t, V_L) \leq 1$ in Equation (4.9) so that a family of cubic V_L -nullclines exists in the phase plane (see Methods). Two members of this family are shown in Figure 4.3.B.1, where the higher (unforced) cubic occurs when $p = 0$ in Equation (4.11) while the lower (maximally forced) cubic occurs when $p = 1$ and corresponds to the maximally forced system at the peak of the pyloric oscillation (see Methods). During the inactive state of the LG neuron where s slowly builds up in LG, the phase point slowly climbs up the left branch of the V_L -nullcline as it is bounced back and forth between the unforced and maximally forced cubics (Figure 4.3.B.1). Each pyloric peak shifts the unforced cubic down to the maximally forced cubic, and the pyloric-timed transitions between left branches of the V_L -nullcline correspond to the small-amplitude depolarizations in V_L during the inactive state of the LG neuron (Figure 4.3.B.2). In particular, the AB to INT1 inhibition interrupts the INT1 to LG inhibition (inset of Figure 4.3), which effectively

disinhibits the LG neuron from INT1 and causes the small pyloric-timed depolarizations in V_L . When the phase point reaches the level of the lower left knee, the next forcing peak shifts the cubic below the phase point and initiates the jump to the stable right branch at the point 2 (Figure 4.3.B.1), since $dV_L/dt > 0$ above the V_L -nullcline (see Methods). Thus, the pyloric-timed forcing allows the jump to the right branch to occur below the higher left knee of the unforced cubic, so less MCN1 excitation is required to build up in the LG neuron before it jumps to the right branch. Then, during the active state of the LG neuron, the phase point slowly falls down the right branch of the cubic as s slowly decays in LG due to its presynaptic inhibition of MCN1 (Figure 4.3.B.1). There is only one right branch of the V_L -nullcline since the pyloric forcing function $P(t, V_L)$ does not affect the active state of the LG neuron (see Methods). When the phase point reaches the right knee of the cubic at the point 4, it becomes unstable and undergoes a saddle-node bifurcation, where it jumps back to the point 1 on the stable left branch (Figure 4.3.B.1). This jump corresponds to when the LG neuron falls back down into its inactive state, which removes the presynaptic inhibition of MCN1. Then, the cycle begins again as the phase point slowly climbs up the left branch.

Hence, the jump to the right branch of the V_L -nullcline is initiated by a pyloric forcing peak. Physiologically, this means that the onset of the LG burst phase is triggered by the AB to INT1 inhibition (Figure 4.3.B.2). In addition, the pyloric-timed forcing shortens the duration on the left branch of the V_L -nullcline, which in turn shortens the duration on the right branch since the jump from the point 2 to the point 3 occurs at a lower value of s than in the unforced system (Figure 4.3.B.1). Thus, the AB to INT1

inhibition also increases the frequency of network oscillations in this gastric mill rhythm (Figure 4.3.B.2).

4.3.2 Including the Effect of Rhythmic Feedback in the MCN1-Elicited Gastric Mill Rhythm

The previous model showed that, in the absence of feedback to MCN1, the local AB to INT1 inhibition (in the STG) increases the frequency of the MCN1-elicited gastric mill rhythm. Now, we examine how the inhibitory feedback connection from AB to MCN1 (in the CoG) affects the network dynamics. Recent experiments (Wood et al., 2004) showed that the local AB to INT1 inhibition (in the STG) no longer affects the frequency of the MCN1-elicited gastric mill rhythm but prolongs the duration of the LG phase when the AB to MCN1 feedback inhibition (in the CoG) is present. The 2-dimensional model of Equations (4.14) and (4.15) is used to investigate how the addition of this inhibitory feedback connection changes the network dynamics. In particular, the forcing function $\sigma(t)$ in the $\mathbf{I}_{s(\text{rhythmic})}$ term of Equation (4.14) is used to model the effect of the AB to MCN1 feedback inhibition, which causes a pyloric-timed interruption of the excitatory MCN1 to LG synapse (see Methods). In addition, the forcing function $P(t)$ in Equation (4.14) is used to model the effect of the local AB to INT1 inhibition in the STG (see Methods).

The effect of the AB to MCN1 feedback inhibition on the network dynamics of the MCN1-elicited gastric mill rhythm is examined using the geometrical properties in the V_L - s phase plane. The 2-dimensional model in Equations (4.14) and (4.15) contains 2 forcing functions; therefore, a 2-parameter family of cubic V_L -nullclines that is indexed

by the values σ of $\sigma(t)$ and p and $P(t)$ exists in the phase plane, as described by Equation (4.16) (see Methods). To simplify the network dynamics in this system, $\sigma(t)$ and $P(t)$ are assumed to oscillate in phase (see Methods). Physiologically, this means that the AB to MCN1 feedback inhibition (in the CoG) occurs at the same phase of the pyloric rhythm as the local AB to INT1 inhibition (in the STG), which is a reasonable assumption in the biological system (see Figure 4.5). Meanwhile, the s -nullcline is again modeled by Equation (4.12) (see Methods).

4.3.2.1 Network Dynamics in the Absence of the Local AB to INT1 Inhibition. First, as was done in the previous system, the forcing effect of the local AB to INT1 inhibition is removed (inset of Figure 4.6.A) by setting $p = 0$ in Equation (4.16). As a result, only the AB to MCN1 feedback inhibition, whose effect is modeled by σ , forces the system. The value of σ in Equation (4.16) varies in $[(1 - \bar{g}_\sigma), 1]$, where $0 < (1 - \bar{g}_\sigma) < 1$ (see Methods). Two members of the family of cubic V_L -nullclines in this system are shown in Figure 4.6.A.1. The lower cubic occurs when $\sigma = 1$ in Equation (4.16) and corresponds to the unforced system, where the MCN1 to LG synapse, that is modeled by the $\mathbf{I}_{s(\text{rhythmic})}$ term of Equation (4.14), is unforced by the effect of $\sigma(t)$. In addition, the unforced cubic in Figure 4.6.A.1 is equivalent to the unforced cubic of Figure 4.3. On the other hand, the higher cubic in Figure 4.6.A.1 occurs when $\sigma = 1 - \bar{g}_\sigma$ in Equation (4.16) and corresponds to the maximally forced system at the trough of the pyloric-timed $\sigma(t)$ oscillation (see Methods, Figure 4.4). In particular, each trough of $\sigma(t)$, which inhibits the MCN1 to LG synapse, shifts the unforced (lower) cubic up to the maximally forced

(higher) cubic, whose outer branches sit at more hyperpolarized values of V_L than that of the unforced cubic (Figure 4.6.A.1).

Thus, during the inactive state of the LG neuron where s slowly builds up in LG, a phase point slowly climbs up the left branch of the V_L -nullcline as it is bounced back and forth between the higher (maximally forced) and lower (unforced) cubics. In particular, the fast, pyloric-timed forcing $\sigma(t)$ shifts the trajectory from the lower cubic to the higher (maximally forced) cubic (Figure 4.6.A.1), which hyperpolarizes the LG membrane potential. Physiologically, these hyperpolarizations in the LG neuron are due to the effect of the pyloric-timed AB to MCN1 feedback inhibition which interrupts the excitatory MCN1 to LG synapse (Figure 4.6.A.2). When the phase point reaches the level of the lower (unforced) left knee, the next value of $\sigma = 1$ in Equation (4.16) brings the unforced cubic below the phase point and initiates the jump to the stable right branch at the point 2 (Figure 4.6.A.1). Geometrically, the jump to the right branch is initiated when the system is unforced ($\sigma = 1$), where the trajectory tracks the lower (unforced) cubic and $dV_L/dt > 0$ above the V_L -nullcline (see Methods). In contrast, the jump to the right branch does not occur when the system is forced ($(1 - \bar{g}_\sigma) \leq \sigma < 1$), where the trajectory no longer tracks the lower cubic and $dV_L/dt < 0$ in the region between the lower (unforced) left knee and the higher (maximally forced) left branch (Figure 4.6.A.1). Hence, the jump to the right branch is initiated during an episode in which the MCN1 to LG synapse is unforced by the AB to MCN1 feedback inhibition, as is similarly reported in the biological system (Wood et al., 2004).

During the active state of the LG neuron, s slowly decays in LG due to the presynaptic inhibition of MCN1, so the phase point slowly falls down the right branch of

the V_L -nullcline from the point 3 to the point 4 (Figure 4.6.A.1). However, $\sigma(t)$ continues to force the system, so the phase point is bounced back and forth between the higher (maximally forced) and lower (unforced) cubics as it falls down the right branch. In particular, each forcing trough of $\sigma(t)$ again shifts the unforced (lower) cubic up to the maximally forced (higher) cubic, which causes the pyloric-timed hyperpolarizations during the active state of the LG neuron (Figure 4.6.A.2). When the phase point reaches the level of the higher right knee, the next trough of $\sigma(t)$ (where $\sigma = 1 - \bar{g}_\sigma$ in Equation (4.16)) shifts the cubic above the phase point and initiates the jump back to the stable left branch at the point 4 (Figure 4.6.A.1), since $dV_L/dt < 0$ below the higher V_L -nullcline when the system is forced. Thus, the jump back to the left branch is initiated by a $\sigma(t)$ forcing trough. Then, the cycle begins again as the phase point climbs up the left branch. It is noted that the jump back to the left branch occurs before the phase point falls to the lower (unforced) right knee (Figure 4.6.A.1); therefore, less decay of MCN1 excitation (s) is required to push the LG neuron back down into its inactive state in the presence of the AB to MCN1 feedback inhibition.

Hence, in this system, the jump to the right branch is initiated when the system is unforced, while the jump back to the left branch is initiated by a $\sigma(t)$ forcing trough. Physiologically, this means that in the presence of the AB to MCN1 feedback inhibition, the onset of the LG burst phase occurs during an episode of the MCN1 to LG excitation that is uninterrupted by the AB to MCN1 feedback inhibition, as reported in the biological system (Wood et al., 2004). However, the termination of the LG burst phase is triggered by the AB to MCN1 feedback inhibition. It is also noted that in the presence of the AB to MCN1 feedback inhibition, the termination of the LG burst phase is not

initiated by the graded inhibition from INT1, since the phase point jumps back to the left branch before reaching the lower (unforced) right knee (Figure 4.6.A.1).

4.3.2.2 *Including the Effect of the Local AB to INT1 Inhibition.* Next, the network dynamics of the full system are investigated, which includes the effect of the local AB to INT1 inhibition that is modeled by the value p in Equation (4.16). The forcing functions $\sigma(t)$ and $P(t)$ oscillate in phase (see Methods), so they simultaneously affect the network dynamics. The unforced (lower) cubic of this system (Figure 4.6.B.1) occurs when $\sigma = 1$ and $p = 0$ in Equation (4.16). This means that the system is unforced when the MCN1 to LG excitation is uninterrupted by the $\sigma(t)$ forcing, which simultaneously corresponds to when INT1 is uninhibited by the $P(t)$ forcing (inset of Figure 4.6.B). Moreover, the unforced cubic in Figure 4.6.B.1 is equivalent to that of Figure 4.6.A.1. In contrast, the maximally forced (higher) cubic in Figure 4.6.B.1 occurs when $\sigma = 1 - \bar{g}_\sigma$ and $p = 1$ in Equation (4.16) (see Methods). This means that the system is maximally forced at the peak inhibition of the MCN1 to LG synapse by $\sigma(t)$ and the simultaneous peak inhibition of INT1 by $P(t)$ (inset of Figure 4.6.B). However, the added effect of $P(t)$ disrupts the INT1 to LG inhibitory synapse, which initiates small depolarizations in the membrane potential of the LG neuron (see Figure 4.3.B.2). Therefore, the depolarizing effect of $P(t)$ on the LG membrane potential interferes with the hyperpolarizing effect of $\sigma(t)$ that interrupts the MCN1 to LG synapse. As a result, the net effect of the simultaneous $\sigma(t)$ and $P(t)$ forcing functions causes smaller hyperpolarizations in the LG membrane potential compared to that caused by $\sigma(t)$ alone. In particular, the outer branches of the

maximally forced (higher) cubic in Figure 4.6.B.1 sit at less hyperpolarized values of V_L than that of the maximally forced cubic in Figure 4.6.A.1.

Now, we investigate the added effect of the local AB to INT1 inhibition on the network dynamics of this system. First, during the inactive state of the LG neuron where s slowly builds up in LG, a phase point slowly climbs up the left branch of the V_L -nullcline as it is bounced back and forth between the higher (maximally forced) and lower (unforced) cubics (Figure 4.6.B.1). Since the depolarizing effect of $P(t)$ interferes with the hyperpolarizing effect of the $\sigma(t)$ forcing, the LG membrane potential exhibits smaller pyloric-timed hyperpolarizations (Figure 4.6.B.2) compared to the case in which $P(t)$ is absent (Figure 4.6.A.2). Then, the jump to the right branch of the V_L -nullcline is again initiated when the system is unforced at the point 2 (Figure 4.6.B.1). Geometrically, the jump to the right branch again occurs when the system is unforced, where the trajectory tracks the lower cubic and $dV_L/dt > 0$ above the V_L -nullcline. Thus, in the presence of $P(t)$, the jump to the right branch is still not initiated when the system is forced, since $dV_L/dt < 0$ in the region between the lower (unforced) left knee and higher (maximally forced) left knee (Figure 4.6.B.1). Hence, the LG burst onset occurs when the system is unforced by both the AB to MCN1 feedback inhibition and the local AB to INT1 inhibition.

During the active state of the LG neuron where s slowly decays in LG due to the presynaptic inhibition of MCN1, the phase point slowly falls down the right branch of the V_L -nullcline as it is bounced back and forth between the higher (maximally forced) and lower (unforced) cubics. The $P(t)$ forcing again interferes with the effect of the $\sigma(t)$ forcing, which causes smaller pyloric-timed hyperpolarizations during the active state of

the LG neuron. As a result, in the presence of the $P(t)$ forcing, the duration on the right branch increases, and one more pyloric-timed transition is required before the phase point can jump back to the left branch (Figure 4.6.B.1) as compared to the case in which $P(t)$ is absent (Figure 4.6.A.1). The significance of this increased duration on the right branch will be discussed shortly in section 4.3.2.3. When the phase point reaches the level of the higher right knee, the next forcing peak shifts the cubic above the phase point and initiates the jump back to the stable left branch at the point 4 (Figure 4.6.B.1), since $dV_L/dt < 0$ below the higher V_L -nullcline when the system is forced. Thus, the jump back to the left branch is still initiated by a $\sigma(t)$ forcing trough. Then, the cycle begins again as the phase point slowly climbs up the left branch.

Hence, in the presence of both the AB to MCN1 feedback inhibition and the local AB to INT1 inhibition, the LG burst onset of this gastric mill rhythm (Figure 4.6.B.2) is still initiated during an episode of the MCN1 to LG excitation that is uninterrupted by the AB to MCN1 feedback, since the jump to the right branch of the V_L -nullcline occurs when the system is unforced (Figure 4.6.B.1). This result is also reported in the biological system (Wood et al., 2004). Meanwhile, the termination of the LG burst phase is still triggered by the AB to MCN1 feedback inhibition (Figure 4.6.B.2), as the jump back to the left branch is initiated by a forcing trough of $\sigma(t)$ (Figure 4.6.B.1). Furthermore, it is noted that, in the presence of the AB to MCN1 feedback inhibition, a greater buildup of MCN1 excitation (s) is required to trigger the LG burst onset, since a phase point must climb up to a higher left knee before jumping to the right branch (compare Figures 4.6.B.1 and 4.3.B.1). However, less decay of s is required to terminate the LG burst phase when the AB to MCN1 feedback inhibition is present, since the jump

back to the left branch is initiated by a forcing trough of $\sigma(t)$ when the phase point falls below the higher (forced) right knee (compare Figures 4.6.B.1 and 4.3.B.1).

4.3.2.3 *AB to INT1 Inhibition Prolongs the Duration of the LG Burst Phase.* As the forcing functions $P(t)$ and $\sigma(t)$ oscillate in phase, the depolarizing effect of $P(t)$ on the LG membrane potential interferes with the hyperpolarizing effect of $\sigma(t)$. In particular, the outer branches of the higher (maximally forced) cubic sit at less hyperpolarized values of V_L in the presence of $P(t)$ (Figure 4.6.B.1) than when $P(t)$ is absent (Figure 4.6.A.1). As a result, smaller pyloric-timed hyperpolarizations occur in the LG membrane potential when the local AB to INT1 inhibition is present (Figure 4.7). In addition, in the presence of the $P(t)$ forcing, the right knee of the higher (maximally forced) cubic (Figure 4.6.B.1) sits at a lower value of s compared to when $P(t)$ is absent (Figure 4.6.A.1). Physiologically, this means that, when the local AB to INT1 inhibition is present, a greater decay of MCN1 excitation (s) is required before the AB to MCN1 feedback inhibition can terminate the LG burst. As a result, an additional pyloric-timed hyperpolarization occurs during the LG burst phase in the presence of the AB to INT1 inhibition (Figure 4.7); therefore, the local AB to INT1 inhibition prolongs the duration of the LG burst phase during this gastric mill rhythm. A similar result was reported in the biological system (Wood et al., 2004). Furthermore, with the prolonged LG burst phase, the local AB to INT1 inhibition slows the frequency of network oscillations during this gastric mill rhythm (Figure 4.7).

In addition, as was reported in the biological system (Wood et al., 2004), a smaller latency exists between the onset of the preceding episode of the MCN1 to LG

excitation and the onset of the LG burst phase when the local AB to INT1 inhibition is present (Figure 4.6.B.1). In particular, since the jump back to the left branch occurs at a lower value of s when the $P(t)$ forcing is present (Figure 4.6.B.1), the phase point starts at a lower value of s on the left branch of the V_L -nullcline compared to when $P(t)$ is absent (Figure 4.6.A.1). Therefore, although the phase point undergoes the same number of pyloric-timed transitions on the left branch (Figures 4.6.A.1 and 4.6.B.1), it starts with a lower value of s when $P(t)$ is present and jumps to the right branch after rounding the unforced left knee (Figure 4.6.B.1). As a result, in the presence of $P(t)$, the onset of the LG burst phase occurs in the middle of an uninterrupted episode of the MCN1 to LG excitation (Figure 4.6.B.2) instead of at the beginning of such an episode when the $P(t)$ forcing is absent (Figure 4.6.A.2). Therefore, there is a smaller latency between the onset of the preceding episode of the MCN1 to LG excitation and the onset of the LG burst phase when the local AB to INT1 inhibition is present (Figure 4.6.B.1), as was also reported in the biological system (Wood et al., 2004).

4.3.3 Investigating the Network Dynamics of the MCN1/CPN2-Elicited Gastric Mill Rhythm

Next, the gastric mill rhythm that is elicited by co-stimulation of MCN1 and CPN2 is studied. In the biological system, co-stimulation of these two projection neurons elicits a distinct gastric mill rhythm from that elicited by MCN1 stimulation alone (Blitz and Nusbaum, 1997). Now, the 2-dimensional model of Equations (4.23) and (4.24) (see Methods) is used to investigate how CPN2 changes the network dynamics of the MCN1-elicited rhythm. The addition of CPN2 adds two new synapses to the network (see

Methods); in particular, (1) a local electrical synapse from the CPN2 axon to the LG neuron in the STG plus (2) an inhibitory feedback connection from INT1 to the CPN2 cell body in the CoG (inset of Figure 4.9). First, the effect of the AB to MCN1 feedback inhibition is ignored in order to consider the case in which MCN1 is tonically active during the MCN1/CPN2-elicited gastric mill rhythm. Therefore, the network dynamics of the MCN1/CPN2-elicited gastric mill rhythm, modeled by Equations (4.23) and (4.24), are compared with that of the MCN1-elicited rhythm, modeled by Equations (4.9) and (4.10) (see Methods), by using the geometrical properties in the V_L - s phase plane.

Only one forcing function, given by $P(t, V_L)$ in Equation (4.23), is contained in this model of the MCN1/CPN2-elicited gastric mill rhythm. However, the effect of this forcing function, which models the local AB to INT1 inhibition in the STG, is transmitted to the LG neuron via two pathways (see Methods); in particular, (1) the INT1 to LG inhibitory synapse and (2) the CPN2 to LG electrical synapse (inset of Figure 4.9). Only the first pathway exists in the MCN1-elicited rhythm, while the second pathway, which is contained in the I_e term of Equation (4.23), facilitates the pyloric-timed depolarizations in CPN2 (Figure 4.9.B). Hence, a 1-parameter family of cubic V_L -nullclines indexed by the values p of $P(t, V_L)$ in Equation (4.25) exists in the V_L - s phase plane (see Methods). The value of p varies in $[0,1]$, where $p = 0$ ($p = 1$) again corresponds to the unforced (maximally forced) system. Moreover, the V_L -nullclines corresponding to these extreme values of p are shown in Figure 4.9.A, where the higher cubic corresponds to unforced ($p = 0$) system while the lower cubic corresponds to the maximally forced ($p = 1$) system. For purposes of comparison, the maximally forced ($p = 1$) cubic of the MCN1-elicited

rhythm from Figure 4.3.B.1 is also shown in the V_L - s phase plane of Figure 4.9.A. Meanwhile the s -nullcline is again modeled by Equation (4.12).

4.3.3.1 *The Addition of CPN2 Slows the Frequency of Network Oscillations.* Although the dynamics in the V_L - s phase plane are similar to that of the MCN1-elicited rhythm from Figure 4.3.B.1, the addition of CPN2 slows the frequency of network oscillations. In particular, during the inactive state of the LG neuron where MCN1 excitation (s) slowly builds up in LG, a phase point slowly climbs up the left branch of the V_L -nullcline as it is bounced back and forth between the higher (unforced) and lower (maximally forced) cubics by the pyloric-timed forcing. However, in the presence of CPN2, the phase point must climb up to a higher maximally forced left knee compared to that of the MCN1-elicited rhythm (Figure 4.9.A). More is explained about this higher left knee shortly. As a result, more s excitation is required to build up in the LG neuron before it can jump into its active state (Figure 4.9.B). Then, at the point 2 (Figure 4.9.A), a $P(t, V_L)$ forcing peak shifts the V_L -nullcline below the phase point and initiates the jump to the stable right branch, since $dV_L/dt > 0$ above the lower V_L -nullcline when the system is forced. Next, during the active state of the LG neuron, the phase point slowly falls down the right branch of the V_L -nullcline as s slowly decays in LG due to the presynaptic inhibition of MCN1. Again, there is only one right branch of the V_L -nullcline since $P(t, V_L)$ does not affect the active state of LG when MCN1 is tonically active (see Methods). However, in the presence of CPN2, the phase point must fall to a lower right knee compared to that of the MCN1-elicited rhythm before it can jump back to the stable left branch (Figure 4.9.A). More is explained about this lower right knee shortly. As a

result, a greater decay of s excitation is required before the LG neuron can fall back down into its inactive state (Figure 4.9.B). Then, at the point 4 (Figure 4.9.A), the phase point becomes unstable and undergoes a saddle-node bifurcation where it jumps back to the stable left branch since $dV_L/dt < 0$ below the V_L -nullcline. The cycle then begins again as s slowly builds up in the LG neuron and the phase point slowly climbs up the left branch.

Hence, the addition of CPN2 slows the frequency of the gastric mill rhythm. First, during the LG interburst phase, INT1 feedback inhibition to CPN2 hyperpolarizes the CPN2 membrane potential, (V_C) (see Methods). As a result, V_C becomes more hyperpolarized than the LG membrane potential (V_L) (Figure 4.9.B) so that $V_L > r\left(\underbrace{u(V_L; P(t, V_L))}_{V_C}\right)$ in the \mathbf{I}_e term of Equation (4.23). Since the rest of the terms on the right hand side of this equation are equivalent to that of the MCN1-elicited rhythm in Equation (4.9), \mathbf{I}_e makes the right hand side of Equation (4.23) more negative. Thus, as V_L increases up the left branch of the V_L -nullcline, CPN2 pulls down V_L via its electrical coupling with LG. As a result, the LG neuron requires a greater buildup of MCN1 excitation (s) before jumping into its active state, which raises the left knee of the V_L -nullcline. Moreover, since the jump to the right branch occurs at higher values of V_L and s (Figure 4.9.A), the peak LG membrane potential in the MCN1/CPN2-elicited gastric mill rhythm is more depolarized than that of the MCN1-elicited rhythm (Figure 4.9.B).

During the LG burst phase, V_C becomes more depolarized than V_L since CPN2 is uninhibited by INT1 (see Methods), so $V_L < r\left(\underbrace{u(V_L; P(t, V_L))}_{V_C}\right)$ in the \mathbf{I}_e term of Equation (4.23). Moreover, as V_L falls when the phase point slowly falls down the right branch of the V_L -nullcline, $dV_L/dt < 0$ during the LG burst phase. However, \mathbf{I}_e now makes the right

hand side of Equation (4.23) more positive since $V_L < V_C$. Therefore, during the LG burst phase, CPN2 pulls up V_L via its electrical coupling with LG. As a result, a greater decay of s excitation is required in the LG neuron before it can fall back down into its inactive state; thus, the right knee of the V_L -nullcline is lower in the presence of CPN2 (Figure 4.9.A). This prolongs the LG burst phase of the MCN1/CPN2-elicited gastric mill rhythm compared to that of the MCN1-elicited rhythm (Figure 4.9.B). Moreover, as the jump back to the left branch occurs at lower values of V_L and s (Figure 4.9.A), the minimum LG membrane potential in the MCN1/CPN2-elicited gastric mill rhythm is more hyperpolarized than that of the MCN1-elicited rhythm (Figure 4.9.B). Furthermore, since the trajectory on the left branch of the V_L -nullcline begins at a lower value of s and the phase point must climb to a higher left knee, the LG interburst phase of the MCN1/CPN2-elicited gastric mill rhythm is also prolonged compared to that of the MCN1-elicited rhythm (Figure 4.9.B). Hence, the addition of CPN2 slows the frequency of network oscillations in the gastric mill rhythm.

4.3.3.2 Effect of the Local AB to INT1 Inhibition. The AB to INT1 inhibition, which is modeled by the forcing function $P(t, V_L)$ in Equation (4.23) (see Methods), has similar effects on the MCN1/CPN2-elicited gastric mill rhythm as on the MCN1-elicited rhythm of Equations (4.9) and (4.10). In particular, the AB to INT1 inhibition triggers the onset of the LG burst phase during the MCN1/CPN2-elicited gastric mill rhythm (Figure 4.10.B), since the jump to the right branch of the V_L -nullcline is initiated by a $P(t, V_L)$ forcing peak (Figure 4.10.A). Moreover, the AB to INT1 inhibition increases the frequency of network oscillations. In particular, when the AB to INT1 inhibition is

absent (inset of Figure 4.11) the network oscillations are slower (Figure 4.11.B). Specifically, in the absence of the $P(t, V_L)$ forcing function, the system in Equations (4.23) and (4.24) (see Methods) becomes autonomous so that a single (unforced) V_L -nullcline exists in the phase plane. However, network oscillations in the unforced system are slower since the phase point must climb up to the higher (unforced) left knee before jumping to the right branch (Figure 4.11.A). Furthermore, the left knee (right knee) of the V_L -nullcline is higher (lower) in the presence of CPN2, so the frequency of network oscillations in the unforced MCN1/CPN2-elicited gastric mill rhythm is slower than that of the MCN1-elicited rhythm (Figure 4.11.B). Hence, the AB to INT1 inhibition triggers the onset of the LG burst phase and increases the frequency of network oscillations during this MCN1/CPN2-elicited gastric mill rhythm.

4.3.3.3 Effect of the INT1 to CPN2 Feedback Inhibition. The INT1 to CPN2 feedback inhibition facilitates the prolonged LG interburst phase of the MCN1/CPN2-elicited gastric mill rhythm. In particular, when CPN2 is inhibited by INT1, its membrane potential (V_C) becomes more hyperpolarized than V_L during the LG interburst phase (see Figure 4.9.B). Thus, $V_L > V_C$ in the \mathbf{I}_e term of Equation (4.23) (see Methods), which makes the right hand side of this equation more negative. As a result, CPN2 pulls down V_L , via its electrical coupling with the LG neuron, and prolongs the LG interburst phase of the gastric mill rhythm (see Figure 4.9.B).

In contrast, when the INT1 to CPN2 feedback inhibition is absent, V_C is never hyperpolarized (Figure 4.12.B) and it sits at its resting potential (see Methods). As a result, $V_L < V_C$ in the \mathbf{I}_e term of Equation (4.23), which makes the right hand side of this

equation more positive so that CPN2 now pulls up V_L during the LG interburst phase. Consequently, this lowers the left knee of the V_L -nullcline below that of the MCN1-elicited rhythm, which shortens the duration on the left branch of the V_L -nullcline (Figure 4.12.A) since the phase point jumps to the right branch sooner. Thus, in the absence of the INT1 to CPN2 feedback inhibition, the duration of the LG interburst phase becomes even shorter than that of the MCN1-elicited rhythm (Figure 4.12.B). On the other hand, the INT1 to CPN2 feedback inhibition is not active during the LG burst phase, so its absence does not significantly affect the duration of the LG burst phase (Figure 4.12.B). Hence, the INT1 to CPN2 feedback inhibition only prolongs LG interburst phase of the MCN1/CPN2-elicited gastric mill rhythm.

4.3.3.4 Network Oscillations Persist Without the INT1 to LG Inhibitory Synapse. During the gastric mill rhythm, INT1 and the LG neuron oscillate in anti-phase due to their reciprocal inhibition. In the biological system, the INT1 to LG inhibitory synapse is necessary for the MCN1-elicited rhythm to occur (Bartos et al., 1999). However, the MCN1/CPN2-elicited gastric mill rhythm in the biological system still persists when the INT1 to LG synapse is pharmacologically removed (Akay et al., 2004). We show that when the INT1 to LG synapse is removed, the INT1 to CPN2 feedback inhibition still facilitates network oscillations during the MCN1/CPN2-elicited gastric mill rhythm (Figure 4.13).

In particular, during the MCN1/CPN2-elicited gastric mill rhythm, INT1 inhibits the LG neuron both directly, via the INT1 to LG synapse, and indirectly, via the INT1 to CPN2 feedback synapse (inset of Figure 4.13). The addition of the latter feedback

pathway was shown to prolong the duration of the LG interburst phase (see Figure 4.12). In particular, CPN2 pulls down V_L which raises the left knee of the V_L -nullcline, so that more MCN1 excitation (s) is required to build up in the LG neuron before it can jump into its active state (see Figure 4.9). However, when the direct INT1 to LG synapse is removed, INT1 only indirectly inhibits the LG neuron via the latter feedback pathway to CPN2 (inset of Figure 4.13). Yet, network oscillations still persist in the absence of the direct INT1 to LG synapse (Figure 4.13.B). However, INT1 inhibits the LG neuron more weakly when only the indirect CPN2 pathway is present. As a result, the left knee of the V_L -nullcline is lower when only the INT1 to CPN2 feedback pathway is present, so less buildup of s excitation is required for the LG neuron to jump into its active state (Figure 4.13.A). Therefore, the duration of the LG interburst phase becomes shorter when the direct INT1 to LG synapse is removed (Figure 4.13.B).

On the other hand, since the INT1 to LG synapse is not active during the LG burst phase, its removal does not significantly affect the duration of the LG burst phase during this gastric mill rhythm (Figure 4.13.B). Moreover, although the phase point traverses a smaller distance down the right branch of the V_L -nullcline (Figure 4.13.A), the duration of the LG burst phase remains similar in the absence of the INT1 to LG synapse. This is because the trajectory in the V_L - s phase plane slows down when the right knee of the V_L -nullcline approaches the s -nullcline. It is noted that if the V_L - and s -nullclines intersect along the stable right branch of the cubic, then this forms a stable (attracting) fixed point, since $dV_L/dt > 0$ (< 0) above (below) the V_L -nullcline (see Methods). We also note that the right knee of the V_L -nullcline becomes lower when the INT1 to LG synapse is removed. In particular, after setting the conductance of the INT1 to LG synapse to

$\bar{g}_{I \rightarrow L} = 0$ (see Methods), the magnitude of s in Equation (4.25) becomes smaller for values of V_L near the right knee of the V_L -nullcline. Subsequently, the duration of the LG burst phase remains similar when the INT1 to LG synapse is removed since the trajectory is slower near the right knee of the V_L -nullcline. Moreover, network oscillations persist during the MCN1/CPN2-elicited gastric mill rhythm when the INT1 to LG synapse is absent.

4.3.4 Investigating How Rhythmic Feedback to MCN1 Affects the Network Dynamics of the MCN1/CPN2-Elicited Gastric Mill Rhythm

The inhibitory feedback connection from the AB neuron causes MCN1 to be rhythmically active in the biological system (see Methods). The effects of the AB to MCN1 feedback inhibition on the MCN1-elicited rhythm were shown earlier (see Figures 4.6-4.7). Now the 2-dimensional model of Equations (4.26) and (4.27) (see Methods) is used to investigate how the addition of the AB to MCN1 feedback inhibition changes the network dynamics of the MCN1/CPN2-elicited gastric mill rhythm.

Two forcing functions given by $P(t)$ and $\sigma(t)$ in Equation (4.26) exist in this model of the MCN1/CPN2-elicited gastric mill rhythm (see Methods). The $P(t)$ forcing function describes the local AB to INT1 inhibition in STG. As was shown in the previous model of Equations (4.23) and (4.24), the effect of $P(t)$ is transmitted to the LG neuron via both the INT1 to LG inhibitory synapse and the CPN2 to LG electrical synapse (see Methods). In addition, $P(t)$ is only time-dependent in Equation (4.26) to model the fact that the local AB to INT1 inhibition continues to affect the active state of the LG neuron when MCN1 is rhythmically active (see Methods). Meanwhile, the $\sigma(t)$

forcing function in the $\mathbf{I}_{s(\text{rhythmic})}$ term of Equation (4.26) describes the effect of the AB to MCN1 feedback inhibition, which periodically interrupts the excitatory MCN1 to LG synapse (see Methods). This $\sigma(t)$ forcing function was used earlier in the MCN1-elicited rhythm of Equations (4.14) and (4.15) (see Methods).

A 2-parameter family of cubic V_L -nullclines, which is indexed by the values p of $P(t)$ and σ of $\sigma(t)$ and is modeled by Equation (4.28), exists in the V_L - s phase plane (see Methods). Moreover, as occurs in the family of cubics for the MCN1-elicited rhythm of Equation (4.16), the value of p varies in $[0,1]$ while the value of σ varies in $[(1-\bar{g}_\sigma),1]$. In addition, $P(t)$ and $\sigma(t)$ are again assumed to oscillate in phase in order to simplify the network dynamics in the V_L - s phase plane (see Methods). Physiologically, this means that the AB to INT1 inhibition (in the STG) occurs at the same phase of the pyloric rhythm as the AB to MCN1 feedback inhibition (in the CoG). Thus, the unforced system occurs when $p = 0$ and $\sigma = 1$ in Equation (4.28), while the maximally forced system occurs when $p = 1$ and $\sigma = 1 - \bar{g}_\sigma$ (see Methods). Meanwhile, the s -nullcline is again modeled by Equation (4.12).

4.3.4.1 *CPN2 Slows the Frequency of Network Oscillations.* When MCN1 is rhythmically active, the addition of CPN2 still slows the frequency of network oscillations (Figure 4.15). In particular, during the LG interburst phase, the INT1 to CPN2 feedback inhibition hyperpolarizes the CPN2 membrane potential (V_C) (Figure 4.15.B) so that $V_L > r\left(\underbrace{u(V_L; P(t))}_{V_c}\right)$ in the \mathbf{I}_e term of Equation (4.26). As in the previous

model of the MCN1/CPN2-elicited rhythm, this makes the right hand side of Equation

(4.26) more negative, which prolongs the LG interburst phase of this gastric mill rhythm (Figure 4.15). In particular, CPN2 pulls down V_L via its electrical coupling with the LG neuron, which raises the left knee of the V_L -nullcline so that more MCN1 excitation (s) is required to build up in the LG neuron before it can jump into its active state (Figure 4.15.A). Then, during the LG burst phase where INT1 no longer inhibits CPN2,

$$V_L < \underbrace{r(u(V_L; P(t)))}_{v_c}$$

and prolongs the LG burst phase of this gastric mill rhythm (Figure 4.15). In particular, CPN2 pulls up V_L during the LG burst phase, which lowers the right knee of the V_L -nullcline so that a greater decay of s excitation is required before the LG neuron can fall back down into its inactive state (Figure 4.15.A). Hence, CPN2 slows the frequency of network oscillations in the presence of the AB to MCN1 feedback inhibition.

4.3.4.2 Onset of LG Burst Phase is Triggered by the MCN1 to LG Excitation. When MCN1 is rhythmically active during the MCN1-elicited rhythm, the onset of the LG burst phase was shown to occur during an episode of the MCN1 to LG excitation that is uninterrupted by the AB to MCN1 feedback inhibition (see Figure 4.6). Now, in the MCN1/CPN2-elicited gastric mill rhythm, the onset of the LG burst phase occurs under the same conditions when MCN1 is rhythmically active (Figure 4.15). In particular, during the inactive state of the LG neuron where s slowly builds up in LG, a phase point slowly climbs up the left branch of the V_L -nullcline as it is bounced back and forth between the higher (maximally forced) and lower (unforced) cubics (Figure 4.15.A). The lower cubic, which occurs when $p = 0$ and $\sigma = 1$ in Equation (4.28) (see Methods), corresponds to the unforced system. Physiologically, the system is unforced when the

AB to INT1 inhibition is absent ($p = 0$) and when the MCN1 to LG synapse is uninterrupted ($\sigma = 1$) by the AB to MCN1 feedback inhibition. In contrast, the higher cubic, which occurs when $p = 1$ and $\sigma = 1 - \bar{g}_\sigma$ in Equation (4.28) (see Methods), corresponds to the maximally forced system. Physiologically, the system is maximally forced at the peak of the AB to INT1 inhibition ($p = 1$) and at the peak inhibition of the MCN1 to LG synapse ($\sigma = 1 - \bar{g}_\sigma$) by the AB to MCN1 feedback connection.

The jump to the right branch of the V_L -nullcline occurs when the system is unforced at the point 2 (Figure 4.15.A). Geometrically, the trajectory tracks the lower cubic only when the system is unforced. In contrast, when the system is forced, the trajectory no longer tracks the lower cubic, and $dV_L/dt < 0$ in the region between the left knee of the lower (unforced) cubic and the left branch of the higher (maximally forced) cubic (Figure 4.15.A). Thus, since the phase point can not jump to the right branch when $dV_L/dt < 0$, the jump at the point 2 occurs when the system is unforced, where $dV_L/dt > 0$ above the lower V_L -nullcline (Figure 4.15.A). Physiologically, this means that the LG neuron jumps into its active state during an episode of the MCN1 to LG excitation that is uninterrupted by the AB to MCN1 feedback inhibition (Figure 4.15.B). Moreover, since $P(t)$ and $\sigma(t)$ oscillate in phase, this also means that the AB to INT1 inhibition does not trigger the onset of the LG burst phase during this gastric mill rhythm.

4.3.4.3 *LG Burst Termination is Triggered by the AB to MCN1 Feedback Inhibition.*

Unlike the jump to the right branch which occurs when the system is unforced, the jump back to the left branch of the V_L -nullcline is initiated when the system is forced (Figure 4.15). In particular, during the active state of the LG neuron where s slowly decays in

LG due to the presynaptic inhibition of MCN1, the phase point slowly falls down the right branch of the V_L -nullcline as it bounced back and forth between the unforced (lower) and maximally forced (higher) cubics (Figure 4.15.A). When the phase point reaches the level of the higher right knee, the next peak of the forcing, where $p = 1$ and $\sigma = 1 - \bar{g}_\sigma$ in Equation (4.28), shifts the cubic above the phase point and initiates the jump back to the left branch at the point 4 (Figure 4.15.A), since $dV_L/dt < 0$ below the higher V_L -nullcline when the system is forced. Thus, similar to that of the MCN1-elicited rhythm (see Figure 4.6), this means that the jump back to the left branch is initiated by a $\sigma(t)$ forcing trough, which causes the pyloric-timed hyperpolarizations in V_L during the active state of the LG neuron (Figure 4.15.B). Physiologically, this means that the LG burst phase is terminated by the AB to MCN1 feedback inhibition during this MCN1/CPN2-elicited gastric mill rhythm (Figure 4.15.B). However, the LG burst termination occurs after a greater decay of s (Figure 4.15), compared to that of the MCN1-elicited rhythm (see Figure 4.6), due to the effect of CPN2, which lowers the right knee of the V_L -nullcline and prolongs the duration of the LG burst phase.

4.3.4.4 AB to INT1 Inhibition Prolongs the Duration of the LG Burst Phase. Since the forcing functions $P(t)$ and $\sigma(t)$ oscillate in phase, the effect of $P(t)$, which depolarizes the LG membrane potential, interferes with the hyperpolarizing effect of $\sigma(t)$. Therefore, similar to that which occurs during the MCN1-elicited rhythm (see Figure 4.7), the LG membrane potential exhibits smaller pyloric-timed hyperpolarizations in the presence of the local AB to INT1 inhibition during this MCN1/CPN2-elicited gastric mill rhythm (Figure 4.16). Moreover, since the right knee of the maximally forced (higher) cubic sits

at a lower value of s in the presence of $P(t)$ (Figure 4.16), a greater decay of MCN1 excitation (s) is required before the phase point can jump back to the left branch when $P(t)$ is present. Physiologically, this means that the AB to MCN1 feedback inhibition becomes less effective at terminating the LG burst phase when the local AB to INT1 inhibition is present. In particular, the LG burst phase is terminated (jump back to the left branch) only after additional pyloric-timed hyperpolarizations, since the phase point must fall to a lower forced right knee when the AB to INT1 inhibition is present (Figure 4.16). Hence, similar to that which occurs during the MCN1-elicited rhythm (see Figure 4.7), the AB to INT1 inhibition prolongs the LG burst phase of this MCN1/CPN2-elicited gastric mill rhythm, which in turn slows the frequency of network oscillations (Figure 4.16). However, it is noted that CPN2 has a greater effect in slowing the network oscillations (see Figure 4.9) than that of the local AB to INT1 inhibition.

4.3.5 Investigating the Network Dynamics of the VCN-Influenced MCN1/CPN2-Elicited Gastric Mill Rhythm

Next, this section investigates how pyloric-timed activity in MCN1 during only the LG interburst phase affects the network dynamics of the MCN1/CPN2-elicited gastric mill rhythm. In the biological system, stimulation of the ventral cardiac neurons (VCN) co-activates MCN1 and CPN2 in the CoG, which in turn elicits a gastric mill rhythm in the STG (Beenhakker and Nusbaum, 2004). During this VCN-elicited gastric mill rhythm, MCN1 is rhythmically active during the LG interburst phase (due to feedback from AB) but tonically active during the LG burst phase (Figure 4.17). Meanwhile, CPN2 exhibits a similar activity pattern as that in the previous MCN1/CPN2-elicited rhythms. Recently

in the biological system, co-stimulation of MCN1 and CPN2 in their VCN-influenced activity patterns was shown to elicit a gastric mill rhythm that closely approximates the VCN-elicited rhythm (Beenhakker and Nusbaum, 2004). As a result, we use the 2-dimensional model of Equations (4.30) and (4.31) (see Methods) to investigate how the VCN-influenced activity patterns in MCN1 and CPN2 affect the network dynamics of the MCN1/CPN2-elicited gastric mill rhythm.

The VCN-influenced activity in MCN1 is modeled by using the forcing function $\sigma(t, V_L)$ in the $\mathbf{I}_{s(\text{alternating})}$ term of Equation (4.30) (see Methods). As in the previous MCN1/CPN2-elicited rhythm, $\sigma(t, V_L)$ is used to model the pyloric-timed interruption of the excitatory MCN1 to LG synapse by the AB to MCN1 feedback inhibition. However, in this system, $\sigma(t, V_L)$ is voltage-dependent in Equation (4.29) so that it only interrupts the MCN1 to LG synapse during the LG interburst phase of the gastric mill rhythm (see Methods). Next, the AB to INT1 inhibition is modeled by the forcing function $P(t, V_L)$ in Equation (4.30). The voltage dependence of $P(t, V_L)$ is used to model the fact that the AB to INT1 inhibition does not affect the LG burst phase of the gastric mill rhythm whenever MCN1 is tonically active (see Methods). In addition, as in the previous models of the MCN1/CPN2-elicited rhythm, the forcing effect of the AB to INT1 inhibition is transmitted to the LG neuron via two pathways: (1) the INT1 to LG inhibitory synapse and (2) the CPN2 to LG electrical synapse (inset of Figure 4.18). We first assume that, as in the previous models, the forcing effect of the AB to INT1 inhibition is transmitted through both pathways simultaneously (Figures 4.18, 4.19). Afterward, we investigate how a timing delay in transmitting the forcing effect of the AB to INT1 inhibition

through the latter CPN2 pathway affects the network dynamics; as such a delay seems to occur in the biological system (Figure 4.20).

Thus, in the first case, where the forcing effect of the AB to INT1 inhibition is transmitted simultaneously through both pathways, the forcing functions $P(t, V_L) = P(t - \mu, V_L)$ in Equation (4.30), since $\mu = 0$ in the case of no delay through the CPN2 pathway (see Methods). As a result, the network dynamics of this system are only forced by $\sigma(t, V_L)$ and $P(t, V_L)$ which oscillate in phase, as occurs in the previous models of the MCN1/CPN2-elicited rhythm (see Methods). Furthermore, in this case of no timing delay, $p = p_\mu$ in Equation (4.32) so that the family of cubic V_L -nullclines depends only on 2 forcing parameter values (see Methods), where σ varies in $[(1 - \bar{g}_\sigma), 1]$ and p varies in $[0, 1]$, as occurs in the previous model of the MCN1/CPN2-elicited rhythm. Hence, the unforced system occurs when $\sigma = 1$ and $p = 0$ in Equation (4.32), while the maximally forced system occurs when $\sigma = 1 - \bar{g}_\sigma$ and $p = 1$ (see Methods).

4.3.5.1 LG Burst Onset is Triggered by the MCN1 to LG Excitation (No Delay in Transmission of AB to INT1 Forcing). In the first case, where the forcing effect of the AB to INT1 inhibition is transmitted simultaneously through both pathways (inset of Figure 4.18), the onset of the LG burst phase occurs during an episode of the MCN1 to LG excitation that is uninterrupted by the AB to MCN1 feedback inhibition (Figure 4.18). In particular, during the inactive state of the LG neuron where s slowly builds up in LG, a phase point slowly climbs up the left branch of the V_L -nullcline as it is bounced back and forth between the higher (maximally forced) and lower (unforced) cubics (Figure 4.18A). Physiologically, the system is unforced when the MCN1 to LG synapse

is uninterrupted by the AB to MCN1 feedback inhibition ($\sigma = 1$ in Equation (4.32)) and when the AB to INT1 inhibition is absent ($p = 0$ in Equation (4.32)) (see Methods). In contrast, the system is maximally forced at the peak inhibition of the MCN1 to LG synapse by the AB to MCN1 feedback ($\sigma = 1 - \bar{g}_\sigma$) and at the peak of the local AB to INT1 inhibition ($p = 1$) (see Methods).

Then, the jump to the right branch of the V_L -nullcline occurs at the point 2 when the system is unforced (Figure 4.18.A). In particular, as was shown in the previous system (Figure 4.17.A), the jump to the right branch does not occur when the system is forced since the trajectory no longer tracks the lower cubic and $dV_L/dt < 0$ in the region between the lower (unforced) left knee and the higher (maximally forced) left branch (Figure 4.18.A). Instead, the jump to the right branch occurs when the system is unforced, where the trajectory tracks the lower cubic and $dV_L/dt > 0$ in the region above the lower left knee (Figure 4.18.A). Physiologically, this means that the onset of the LG burst phase during this gastric mill rhythm occurs during an episode of the MCN1 to LG excitation that is uninterrupted by the AB to MCN1 feedback inhibition (Figure 4.18.B). Furthermore, since $\sigma(t, V_L)$ and $P(t, V_L)$ oscillate in phase, the LG burst onset is not triggered by the AB to INT1 inhibition.

4.3.5.2 *LG Burst Termination is Not Triggered by the AB to MCN1 Feedback Inhibition.*

Since MCN1 is tonically active during the LG burst phase of this gastric mill rhythm, the MCN1 to LG synapse is not affected by the AB to MCN1 feedback inhibition during the LG burst phase. In particular, $\sigma(t, V_L) = 1$ (see Methods) so that the MCN1 to LG synapse remains uninterrupted for the duration of the LG burst phase (Figure 4.18.B). In addition,

the local AB to INT1 inhibition, modeled by $P(t, V_L)$, has no effect on the LG burst phase of the gastric mill rhythm when MCN1 is tonically active (see Methods). Therefore, the system is unforced during the active state of the LG neuron so that the trajectory in the V_L - s phase plane only tracks the unforced right branch of the V_L -nullcline (Figure 4.18.A). In particular, the phase point falls down the unforced right branch as s slowly decays in LG due to the presynaptic inhibition of MCN1. Then, when the phase point reaches the unforced (lower) right knee at the point 4 (Figure 4.18.A), it undergoes a saddle-node bifurcation and jumps back to the left branch of the V_L -nullcline since $dV_L/dt < 0$ below the right knee. Hence, the AB to MCN1 feedback inhibition does not terminate the LG burst phase of this gastric mill rhythm, since the jump back to the left branch occurs at the unforced right knee. Physiologically, this means that the LG burst phase is terminated by the graded inhibition from INT1.

4.3.5.3 *AB to INT1 Inhibition Has No Effect on the Frequency of Network Oscillations.*

In this first case where the forcing effect of $P(t, V_L)$ is transmitted simultaneously through both (1) the INT1 to LG synapse and (2) the CPN2 to LG synapse (inset of Figure 4.18), the AB to INT1 inhibition has no effect on the frequency of network oscillations. In particular, network oscillations occur with the same frequency in the absence of the local AB to INT1 inhibition (Figure 4.19). The only effect of the AB to INT1 inhibition is that it causes the LG membrane potential to exhibit smaller pyloric-timed hyperpolarizations during the LG interburst phase of this gastric mill rhythm (Figure 4.19). In particular, since the $\sigma(t, V_L)$ and $P(t, V_L)$ forcing functions oscillate in phase (see Methods), the effect of $P(t, V_L)$, which depolarizes the LG membrane potential, interferes with the

hyperpolarizing effect of $\sigma(t, V_L)$ (see Methods) so that smaller pyloric-timed hyperpolarizations occur during the LG interburst phase when the AB to INT1 inhibition is present.

4.3.5.4 A Timing Delay in Transmitting the Forcing Effect of the AB to INT1 Inhibition Changes the Network Dynamics. During the MCN1/CPN2-elicited gastric mill rhythm, AB inhibition of INT1 in turn removes INT1 inhibition of CPN2 (inset of Figure 4.18). As a result, the CPN2 membrane potential exhibits pyloric-timed depolarizations, due to the removal of INT1 inhibition, during the LG interburst phase of the gastric mill rhythm (Figure 4.18.B). Hence, the pyloric-timed depolarizations in CPN2 are due to the effect of the AB to INT1 inhibition. Thus far, it has been assumed that the forcing effect of the AB to INT1 inhibition through this CPN2 pathway is simultaneous with the forcing effect through the INT1 to LG synapse (see Methods). As a result, the pyloric-timed depolarizations in CPN2 occur in phase with the pyloric-timed hyperpolarizations in the LG neuron and interruptions of the MCN1 to LG synapse (Figure 4.18.B). However, in the biological system, these pyloric-timed depolarizations in CPN2 are out of phase with the pyloric-timed activity in the LG neuron and MCN1 (Figure 4.20). This suggests that the forcing effect of the AB to INT1 inhibition through the CPN2 pathway is delayed (inset of Figure 4.20).

In the 2-dimensional model of Equations (4.30) and (4.31), the forcing effect of the AB to INT1 inhibition that is transmitted through the CPN2 pathway is modeled by the forcing function $P(t-\mu, V_L)$ (see Methods). Thus far, it has been assumed that $P(t-\mu, V_L) = P(t, V_L)$, where $\mu = 0$ in Equation (4.30) (see Methods). Now, we assume that $\mu \neq 0$ so

that the forcing effect of the AB to INT1 inhibition is delayed through the CPN2 pathway. In particular, $P(t-\mu, V_L)$ is modeled with a delay of $\frac{1}{2}$ of a pyloric period so that it oscillates in anti-phase with the forcing functions $P(t, V_L)$ and $\sigma(t, V_L)$ of Equation (4.30) (see Methods). This is a reasonable approximation of the biological system (Figure 4.20), where the pyloric-timed depolarizations in CPN2 occur nearly in anti-phase with the pyloric-timed hyperpolarizations in the LG neuron and interruptions of MCN1 activity. Subsequently, the family of cubic V_L -nullclines modeled by Equation (4.32) is forced by 3 parameter values, where p and p_μ vary in $[0,1]$ with $p \neq p_\mu$ while σ varies in $[(1-\bar{g}_\sigma), 1]$ (see Methods).

4.3.5.5 LG Burst Onset is Triggered by the AB to INT1 Inhibition (Via its Delayed Effect Through the CPN2 Pathway). In the case where the forcing effect of the AB to INT1 inhibition is delayed through the CPN2 pathway (inset of Figure 4.21), it triggers the onset of the LG burst phase during this gastric mill rhythm (Figure 4.21). In particular, during the inactive state of the LG neuron where s slowly builds up in LG, a phase point slowly climbs up the left branch of the V_L -nullcline as it is bounced back and forth between cubics in the V_L - s phase plane of this system (Figure 4.21.A). The higher cubic (Figure 4.21.A) corresponds to when the system is maximally forced by the $\sigma(t, V_L)$ and $P(t, V_L)$ forcing functions but unforced by $P(t-\mu, V_L)$, which occurs when $\sigma = 1 - \bar{g}_\sigma$, $p = 1$, and $p_\mu = 0$ in Equation (4.32) (see Methods). Physiologically, this occurs at the peak inhibition of the MCN1 to LG synapse by the AB to MCN1 feedback ($\sigma = 1 - \bar{g}_\sigma$) and when the AB to INT1 inhibition is at its peak in the STG ($p = 1$) but at its minimum in the CPN2 pathway ($p_\mu = 0$) (see Methods). In contrast, the lower cubic (Figure 4.21.A)

corresponds to when the system is unforced by $\sigma(t, V_L)$ and $P(t, V_L)$ but maximally forced by $P(t-\mu, V_L)$. Physiologically, this occurs when the MCN1 to LG synapse is uninterrupted by the AB to MCN1 feedback inhibition ($\sigma = 1$) and when the AB to INT1 inhibition is at its minimum in the STG ($p = 0$) but at its peak in the CPN2 pathway ($p_\mu = 1$) (see Methods). The middle cubic corresponds to the unforced system, which occurs when the MCN1 to LG synapse is uninterrupted by the AB to MCN1 feedback inhibition ($\sigma = 1$) and when the AB to INT1 inhibition is absent ($p = p_\mu = 0$).

Thus, the forcing functions $\sigma(t, V_L)$ and $P(t, V_L)$ again oscillate in phase, and their net effect shifts the trajectory to the higher cubic in the V_L - s phase plane (Figure 4.21.A), which produces a hyperpolarization in the LG neuron (Figure 4.21.B). In contrast, the forcing function $P(t-\mu, V_L)$ oscillates in anti-phase and shifts the trajectory to the lower cubic (Figure 4.21.A), which produces a depolarization in the LG neuron (Figure 4.21.B). Thus, when the phase point reaches the level of the lower left knee, the next forcing peak of $P(t-\mu, V_L)$ shifts the V_L -nullcline below the phase point and initiates the jump to the right branch, since $dV_L/dt > 0$ above the V_L -nullcline. Physiologically, this means that the AB to INT1 inhibition, via its delayed forcing effect through the CPN2 pathway, triggers the onset of the LG burst phase during this gastric mill rhythm. Therefore, the MCN1 to LG excitation no longer initiates the LG burst onset when the forcing effect of the AB to INT1 inhibition is delayed through the CPN2 pathway (Figure 4.21.B).

4.3.5.6 AB to INT1 Inhibition Increases the Frequency of Network Oscillations (Via its Delayed Effect Through the CPN2 Pathway). In the case where the forcing effect of the AB to INT1 inhibition is delayed through the CPN2 pathway, it increases the frequency

of network oscillations. In particular, the network oscillations occur with slower frequency when the AB to INT1 inhibition is removed (Figure 4.22). Moreover, when the AB to INT1 inhibition is absent, a phase point can not jump to the right branch of the V_L -nullcline until it reaches the level of the middle (unforced) left knee (Figure 4.22.A). In contrast, when the AB to INT1 inhibition is present, the jump to the right branch is initiated by a peak of $P(t-\mu, V_L)$ (see Methods) before the phase point climbs up to the middle (unforced) left knee (Figure 4.22.B). As a result, the frequency of this gastric mill rhythm increases in the presence of the AB to INT1 inhibition (Figure 4.22.C) since the jump to the right branch occurs at a lower value of s . Similarly, recent experiments in the biological system showed that the AB to INT1 inhibition increases the frequency of this MCN1/CPN2-elicited gastric mill rhythm (M. Kirby and M.P. Nusbaum, unpublished data). Therefore, this suggests that the AB to INT1 inhibition plays an important role only when its forcing effect is transmitted with a delay through the INT1 to CPN2 feedback pathway during this MCN1/CPN2-elicited gastric mill rhythm.

4.3.6 Summary of Results

Using a 2-dimensional model, this chapter investigated how the motor pattern of the gastric mill rhythm is shaped by (1) feed-forward synaptic inputs from MCN1 and CPN2 and (2) rhythmic feedback to these projection neurons.

First, the network dynamics of the MCN1-elicited rhythm were examined when there is no feedback to MCN1. In this case, it was shown that the local AB→INT1 inhibition:

- Increases the frequency of network oscillations.

- Determines the onset of the LG burst phase.

Next, pyloric-timed feedback to MCN1 (AB→MCN1 feedback inhibition) was shown to change the network dynamics of the MCN1-elicited rhythm.

In particular, the onset of the LG burst phase is:

- Not determined by the local AB→INT1 inhibition.
- Triggered during an episode of the MCN1→LG excitation that is not interrupted by the AB→MCN1 feedback inhibition.

The termination of the LG burst phase is:

- Determined by the AB→MCN1 feedback inhibition.

The local AB→INT1 inhibition:

- Prolongs the duration of the LG burst phase.
- Slows the frequency of network oscillations.
- Decreases the latency between the onset of the LG burst phase and the onset of the preceding episode of the MCN1→LG excitation.

Then, the network dynamics of the MCN1/CPN2-elicited rhythm were examined.

The addition of CPN2 to the system:

- Slows the frequency of network oscillations.
- Changes the locus of pattern generation (allows for network oscillations to persist without reciprocal inhibition between INT1 and the LG neuron).

In the absence of feedback to MCN1:

- The local $AB \rightarrow INT1$ inhibition (1) increases the frequency of network oscillations and (2) determines the onset of the LG burst phase.

In the presence of the pyloric-timed feedback to MCN1:

- The onset of the LG burst phase is triggered during an episode of the $MCN1 \rightarrow LG$ excitation (that is not interrupted by $AB \rightarrow MCN1$).
- The termination of the LG burst phase is determined by the local $AB \rightarrow INT1$ inhibition.
- The local $AB \rightarrow INT1$ inhibition (1) prolongs the duration of the LG burst phase (2) slows the frequency of network oscillations.

During a VCN-influenced activity pattern in MCN1:

- If the effect of the $AB \rightarrow INT1$ inhibition is transmitted simultaneously through the $INT1 \rightarrow LG$ synapse and the $INT1 \rightarrow CPN2$ feedback pathway, then (1) the onset of the LG burst phase is triggered by the $MCN1 \rightarrow LG$ excitation (2) the $AB \rightarrow INT1$ inhibition has no effect on the frequency of network oscillations
- If the effect of the $AB \rightarrow INT1$ inhibition is transmitted in anti-phase through the $INT1 \rightarrow LG$ synapse and the $INT1 \rightarrow CPN2$ feedback pathway, then the $AB \rightarrow INT1$ inhibition (1) determines the onset of the LG burst phase (2) increases the frequency of network oscillations.

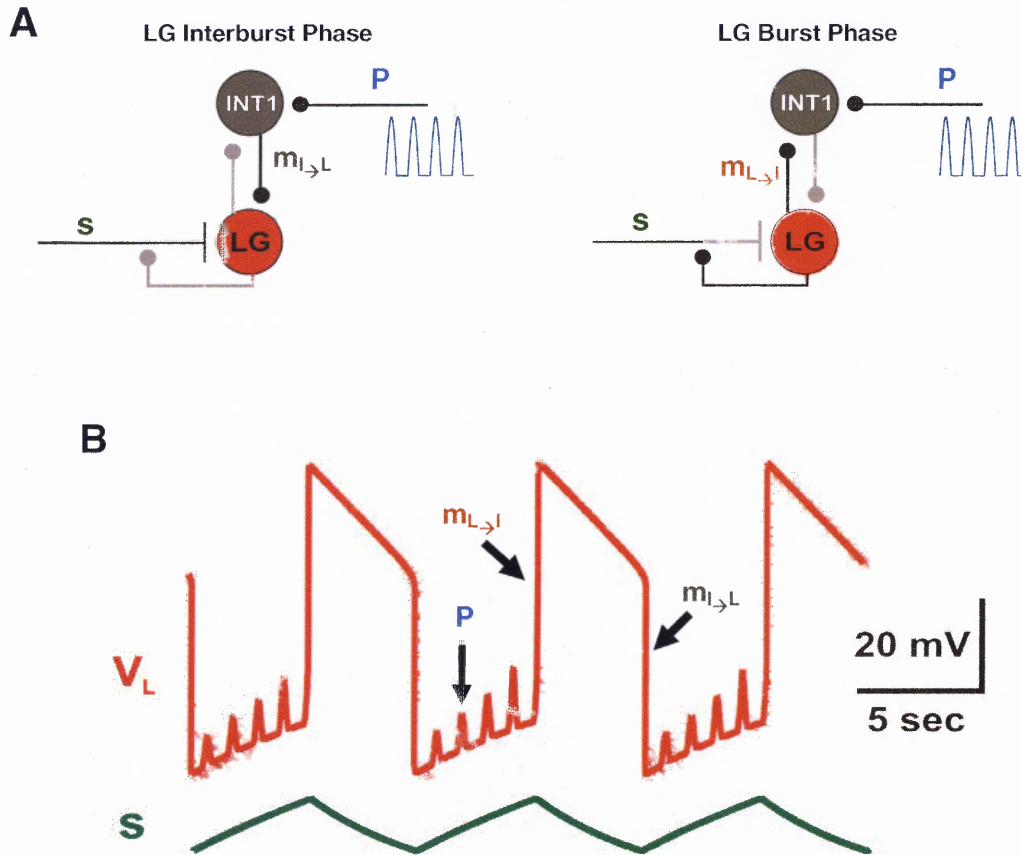


Figure 4.1 Reduced (3-Dimensional) Model of the MCN1-Elicited Gastric Mill Rhythm. **A**, Circuit diagram showing both phases of the gastric mill rhythm in this reduced model. INT1 and the LG neuron are treated as passive neurons that are connected by a graded reciprocal inhibition. In addition, the LG neuron receives a slow modulatory excitation from MCN1 (s), which is gated by the LG membrane potential via presynaptic inhibition of MCN1. INT1 receives a fast periodic inhibition from the AB neuron (P). **B**, MCN1 excitation of the LG neuron (s) evolves on a much slower time scale than that of all other synapses in this network and drives the frequency of network oscillations. In particular, s slowly builds up during the LG interburst phase when MCN1 excites the LG neuron, and s slowly decays during the LG burst phase due to LG presynaptic inhibition of MCN1. Transitions between the LG interburst and burst phases are controlled by the reciprocal inhibition between INT1 and the LG neuron. The periodic inhibition of INT1 (P) releases the LG neuron from INT1 inhibition and facilitates the subthreshold depolarizations in LG. However, P does not affect the LG burst phase since the INT1 to LG inhibition is inactive.

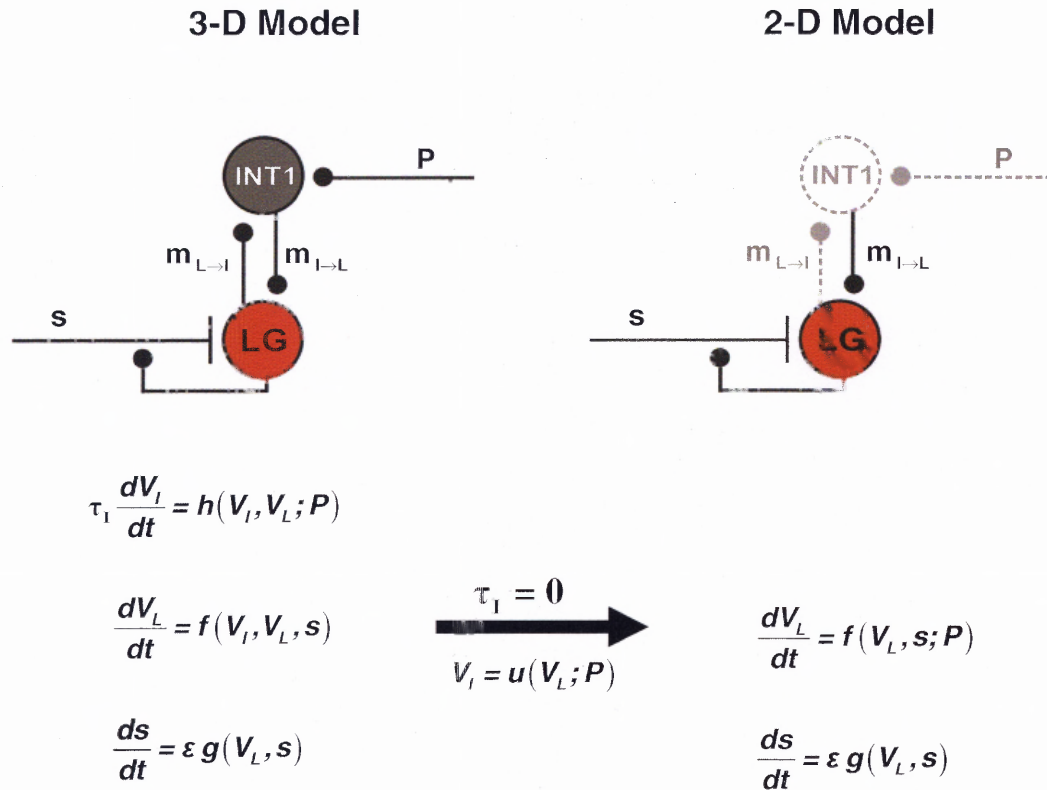


Figure 4.2 Reduction to a 2-Dimensional Model of the MCN1-Elicited Gastric Mill Rhythm. The LG neuron is influenced by the slow modulatory excitation from MCN1, which is much slower than all other synapses in the network. INT1, on the other hand, is only influenced by fast synapses in this model, so its membrane potential (V_I) can be assumed to adjust instantaneously to its steady state for each value of the state variables V_L and s . This is done by setting the membrane time constant of INT1 to zero. As a result, the dynamics of INT1 are absorbed into the dynamics of the state variable V_L . Moreover, the effects of the inhibitory synapses onto INT1 are absorbed into the INT1 to LG synapse in the 2-dimensional model.

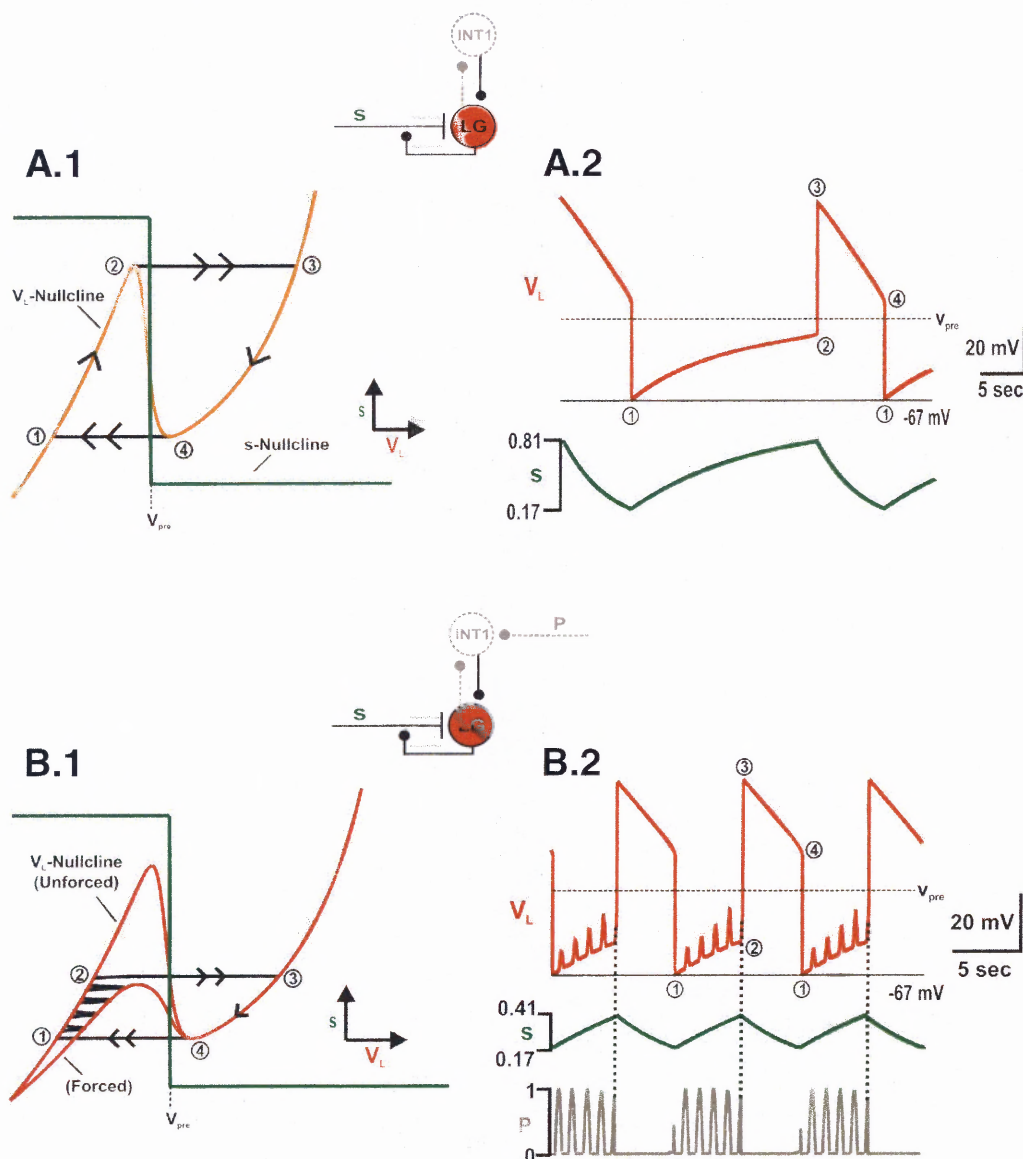


Figure 4.3 Network Dynamics of the MCN1-Elicited Gastric Mill Rhythm. *A.1*, Phase plane diagram of the 2-dimensional model of the MCN1-elicited gastric mill rhythm. During the LG interburst phase, a phase point slowly climbs up the left branch of the V_L -nullcline as MCN1 excitation (s) slowly builds up in the LG neuron. During the LG burst phase, the phase point slowly falls down the right branch of the V_L -nullcline as s decays in LG due to presynaptic inhibition of MCN1. Jumps between the outer branches of the V_L -nullcline correspond to the transitions between the LG interburst and burst phases. *A.2*, Network oscillations are described by the periodic trajectory in *A.1*. The synaptic voltage threshold v_{pre} separates the LG interburst and burst phases. *B.1*, Phase plane diagram in the presence of the AB to INT1 inhibition (P). The higher cubic corresponds to the unforced system in *A.1* while the lower cubic corresponds to the maximally forced system at the peak of P . *B.2*, The AB to INT1 inhibition increases the frequency of network oscillations and triggers the onset of the LG burst phase.

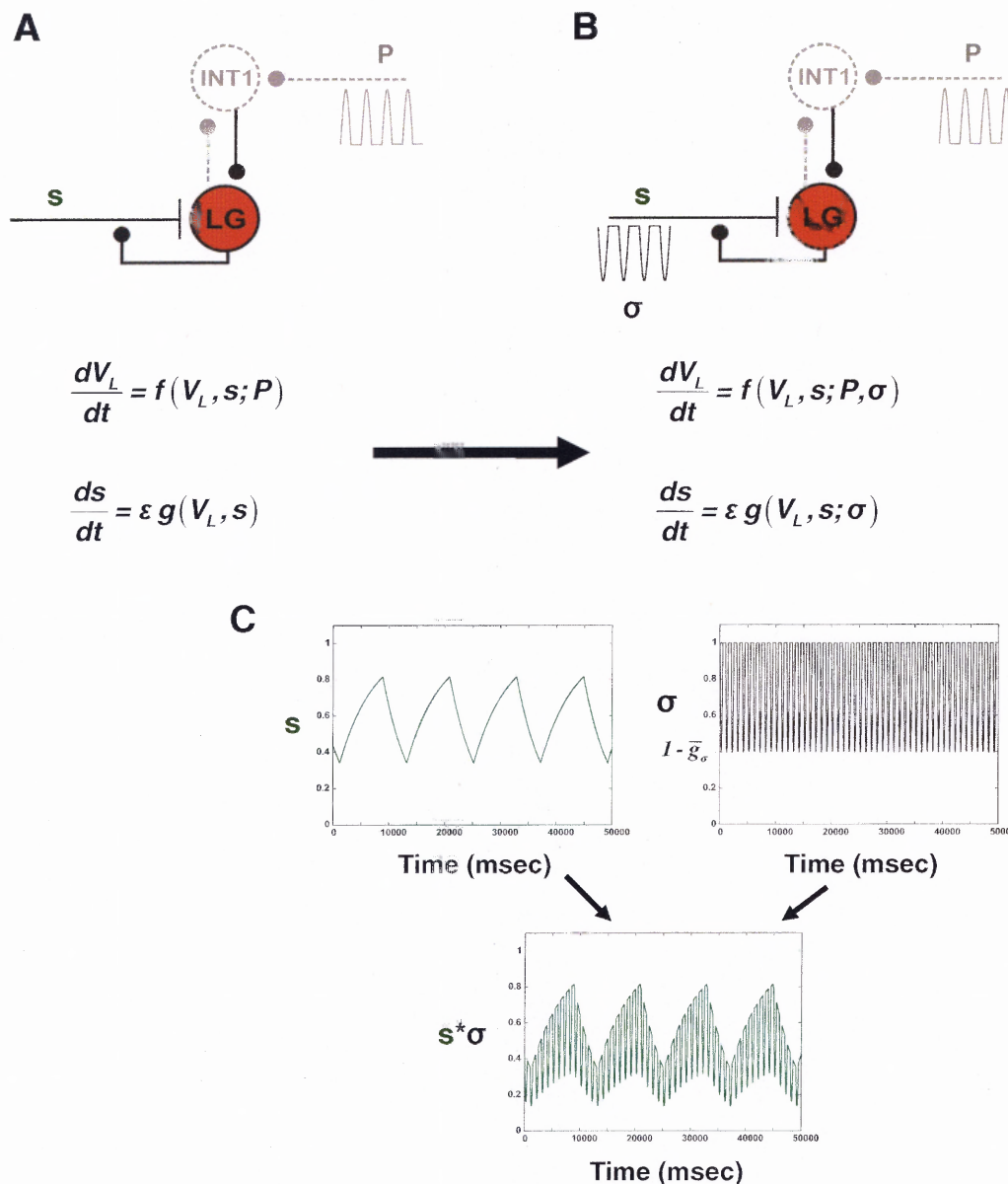


Figure 4.4 Adding the Effect of the AB to MCN1 Feedback Inhibition to the 2-Dimensional Model. *A*, The 2-dimensional model from the previous figure. *B*, The effect of the AB to MCN1 feedback inhibition is added to the 2-dimensional model. In the biological system, this feedback connection causes pyloric-timed interruptions in the activity of MCN1 (see Figure 4.5). Therefore, the effect of the AB to MCN1 feedback inhibition is modeled by a periodic forcing function (σ) that interrupts the feed-forward MCN1 to LG excitatory synapse. The forcing functions P and σ oscillate in phase in this 2-dimensional model. *C*, The state variable s describes the slow, presynaptically-gated buildup of decay of MCN1 excitation in LG that drives the network oscillations. The forcing function σ shapes the network oscillations via its periodic interruption of s .

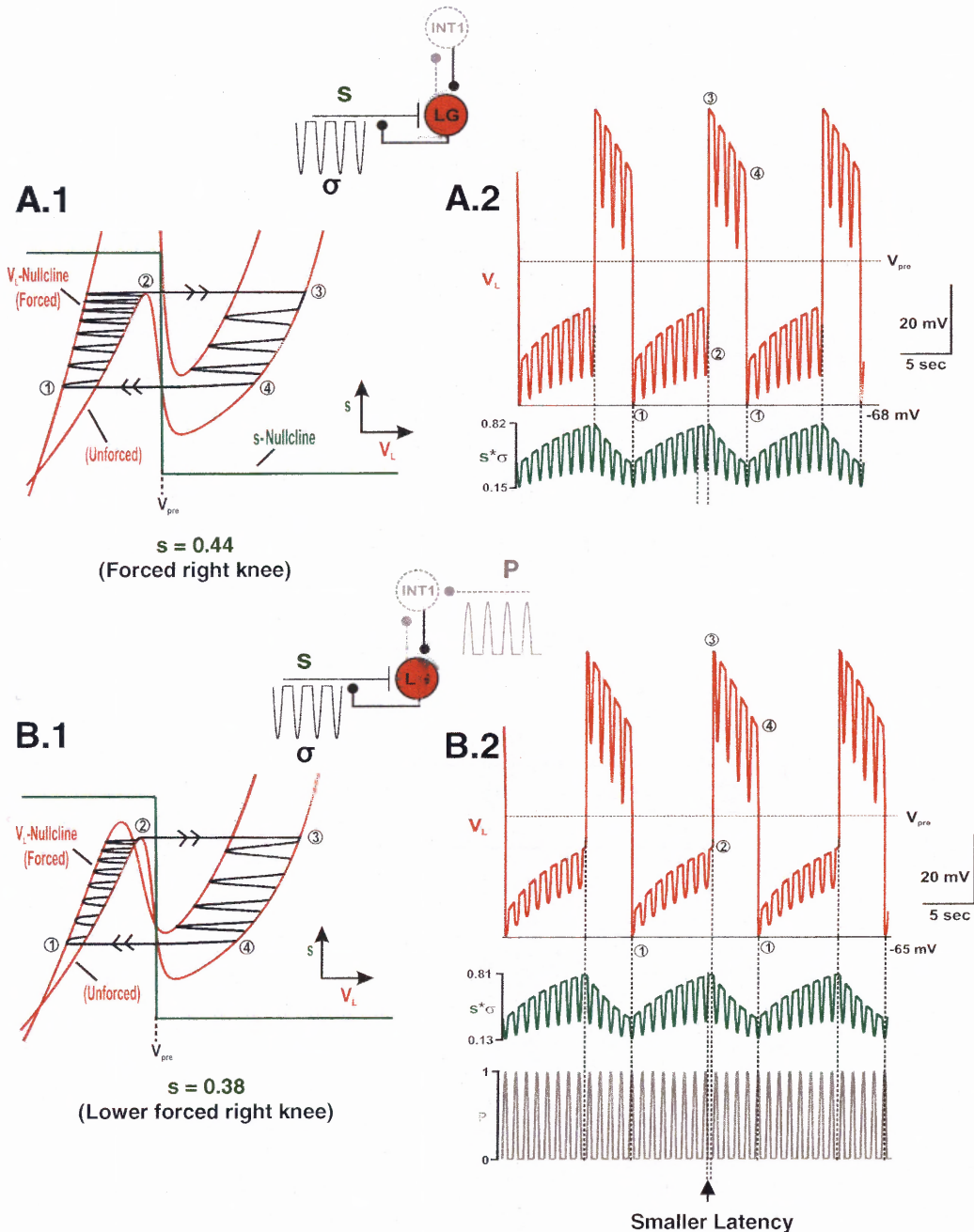


Figure 4.6 Investigating How the AB to MCN1 Feedback Inhibition Changes the Network Dynamics of the MCN1-Elicited Rhythm. *A.1*, Phase plane diagram when only σ forces the system (periodically disrupts MCN1 to LG synapse). The lower (higher) cubic corresponds to the unforced (maximally forced) system. *A.2*, The onset of the LG burst phase is initiated during an uninterrupted episode of the MCN1 to LG excitation (jump to the right branch in *A.1* occurs when system is unforced). The termination of the LG burst phase is triggered by the AB to MCN1 feedback inhibition (jump back to left branch in *A.1* triggered by a forcing trough of σ). *B.1*, Phase plane diagram when both σ and P force the system. The jump back to the left branch occurs after a greater decay in s . *B.2*, A smaller latency exists between the onset of the previous episode of the MCN1 to LG excitation and the onset of the LG burst phase, as reported in the biological system.

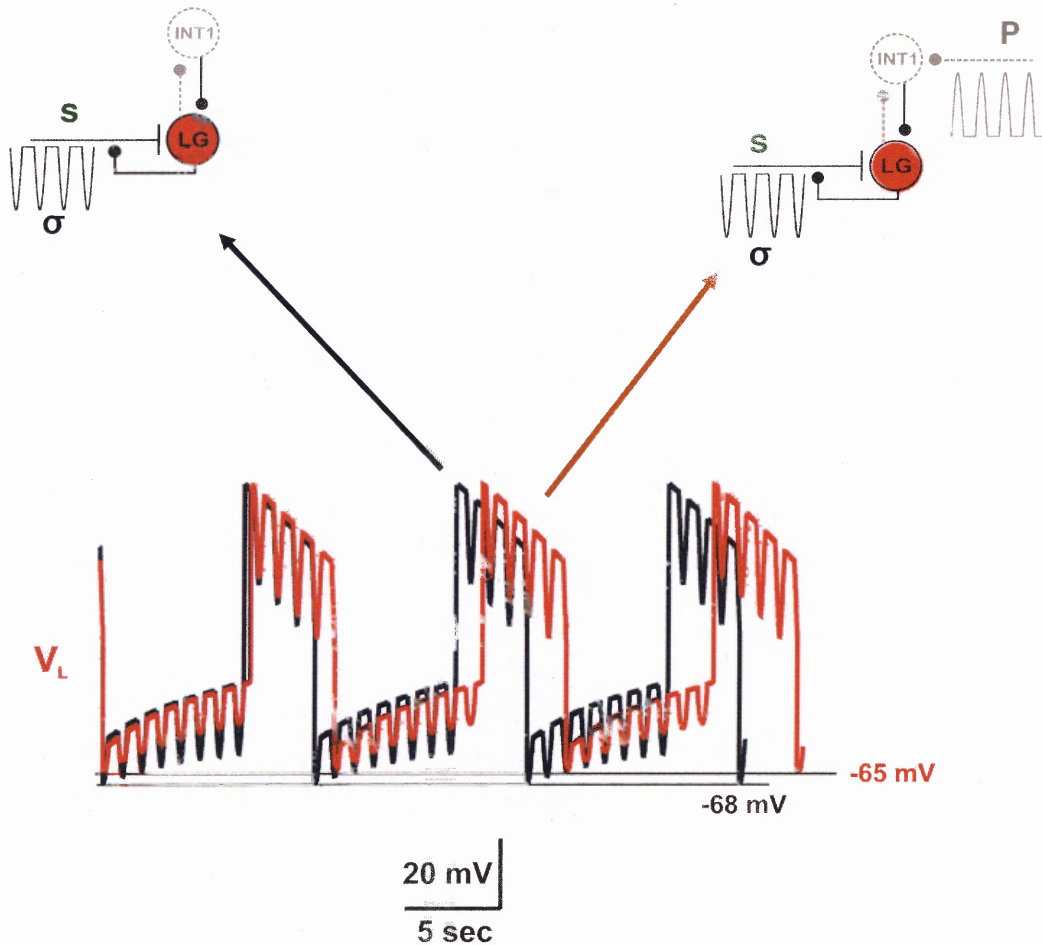


Figure 4.7 The Local AB to INT1 Inhibition Prolongs the Duration of the LG Burst Phase and Slows the Frequency of Network Oscillations in this MCN1-Elicited Gastric Mill Rhythm. The jump back to the left branch of the V_L -nullcline only occurs after a greater decay in s when the AB to INT1 inhibition is present (see Figure 4.6.B.1). As a result, this prolongs the duration of the LG burst phase, where an additional pyloric-timed hyperpolarization occurs in the presence of the AB to INT1 inhibition. Moreover, the LG membrane potential exhibits smaller pyloric-timed hyperpolarizations when the AB to INT1 inhibition is present due to the effect of the forcing function P which interferes with the hyperpolarizing effect of σ .

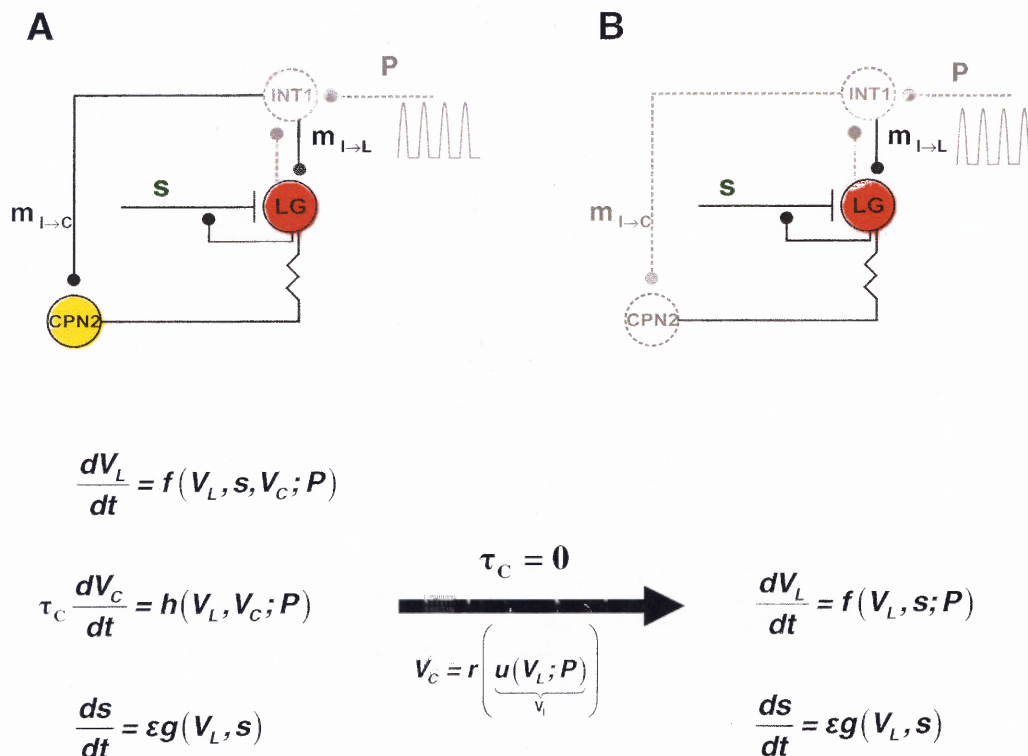


Figure 4.8 Building a 2-Dimensional Model of the MCN1/CPN2-Elicited Gastric Mill Rhythm. **A**, The addition of CPN2 to the existing model adds an extra dimension to the system. **B**, The 3-dimensional model is reduced to 2 dimensions by exploiting the difference in synaptic time scales, as was done in developing the 2-dimensional model of the MCN-elicited rhythm (see Figure 4.2). In particular, since CPN2 is only affected by the fast inhibitory feedback synapse from INT1, its membrane potential can be assumed to adjust instantaneously to its steady state for each value of the remaining state variables V_L and s . As a result, the dynamics of CPN2 are absorbed into the dynamics of the state variable V_L . Moreover, the effect of the inhibitory feedback synapse from INT1 to CPN2 is absorbed into the CPN2 to LG electrical synapse.

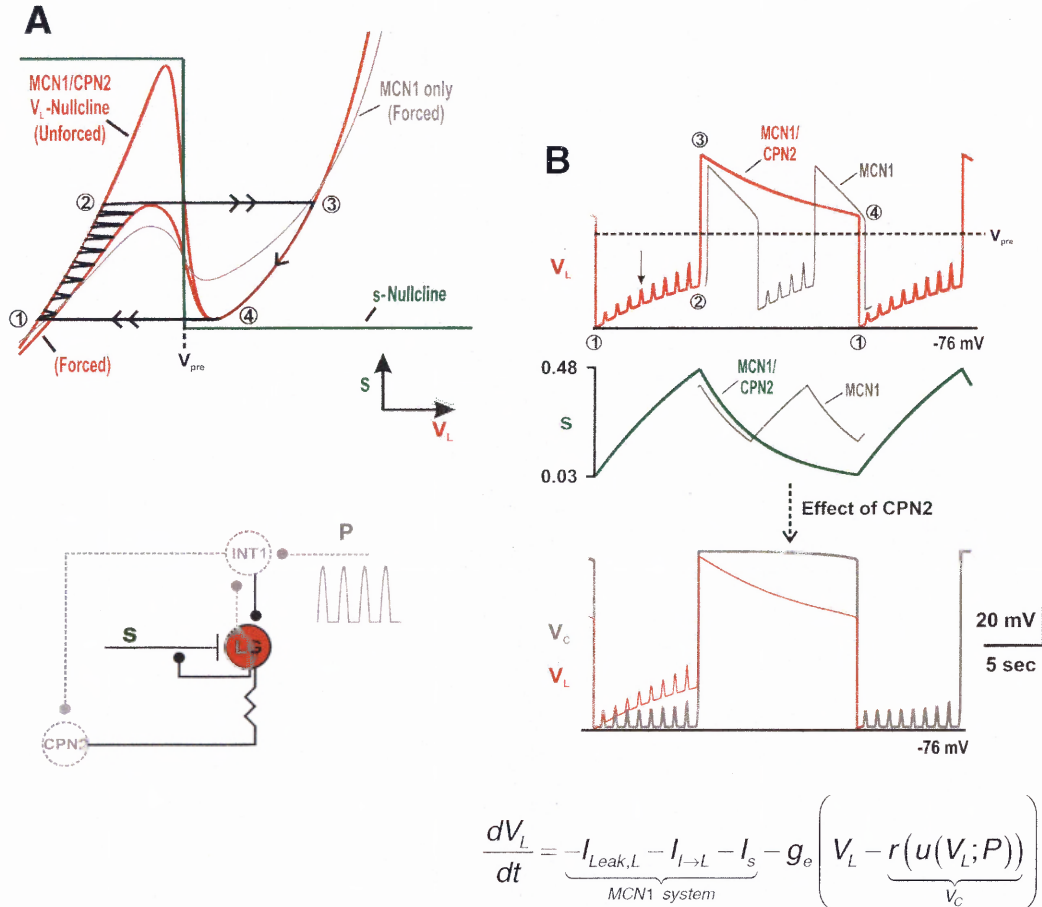


Figure 4.9 Investigating How CPN2 Affects the Network Dynamics of the Gastric Mill Rhythm. **A**, During the LG interburst phase, CPN2 is more hyperpolarized than the LG neuron due to the feedback inhibition from INT1. As a result, $V_L > V_C$, and CPN2 pulls down the LG membrane potential via the local electrical coupling with the LG neuron. This raises the left knee of the V_L -nullcline so that a greater buildup of MCN1 excitation (s) is required before the LG neuron can jump into its active state. Then, during the LG burst phase where the INT1 to CPN2 feedback inhibition is inactive, $V_L < V_C$ and CPN2 pulls up the LG membrane potential. This lowers the right knee of the V_L -nullcline so that a greater decay of s is required before the LG neuron can fall back down into its inactive state. **B**, The addition of CPN2 to the system slows the frequency of network oscillations compared to that of the MCN1-elicited rhythm. The pyloric-timed depolarizations in CPN2 are due to the effect of the AB to INT1 inhibition which releases CPN2 from INT1 inhibition. Also, the effect of the AB to INT1 inhibition on the LG neuron is indicated by the arrow in the voltage trace of LG.

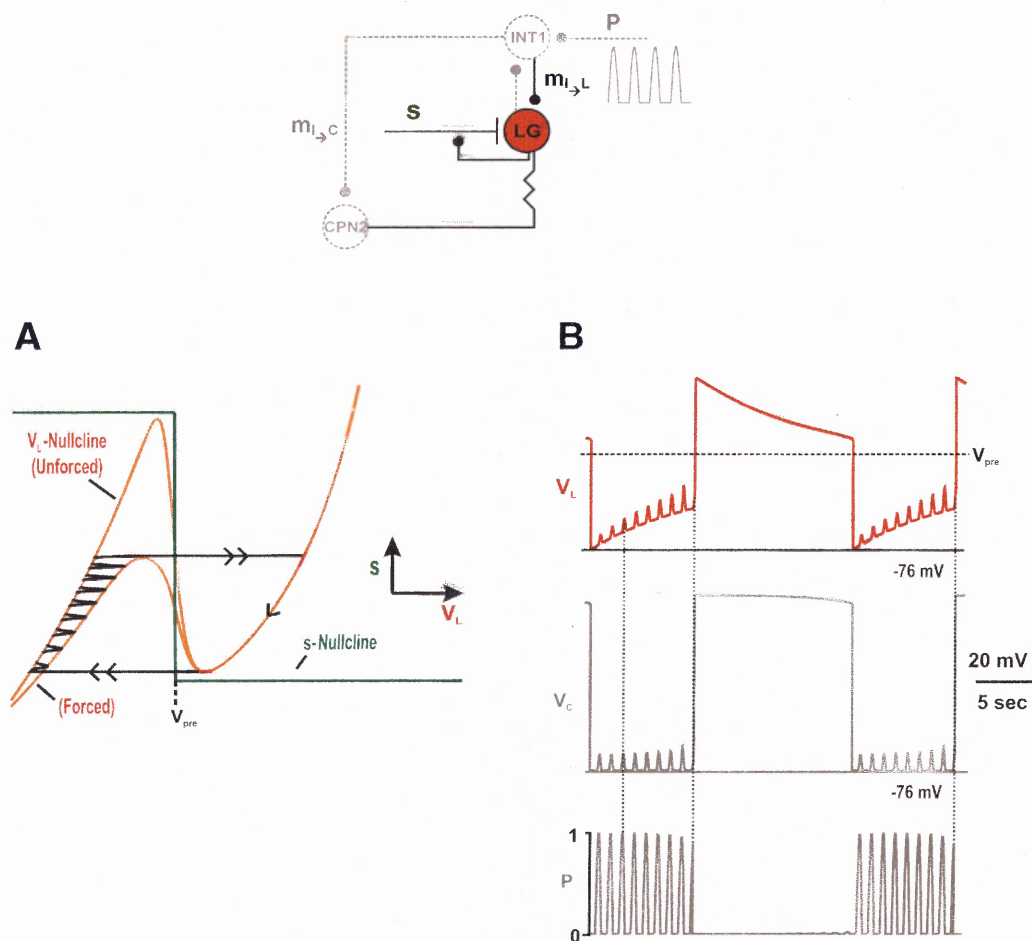


Figure 4.10 The Local AB to INT1 Inhibition Triggers the Onset of the LG Burst Phase During the MCN1/CPN2-Elicited Gastric Mill Rhythm (When MCN1 is Tonically Active). **A**, The jump to the right branch of the V_L -nullcline is triggered by a forcing peak of P as it shifts the left knee of the cubic below the phase point, where $dV_L/dt > 0$ above the V_L -nullcline. **B**, The effect of the AB to INT1 inhibition is transmitted to the LG neuron via both the INT1 to LG synapse ($m_{I \rightarrow L}$) and the INT1 to CPN2 feedback synapse ($m_{I \rightarrow C}$). The latter pathway facilitates the pyloric-timed depolarizations in CPN2.

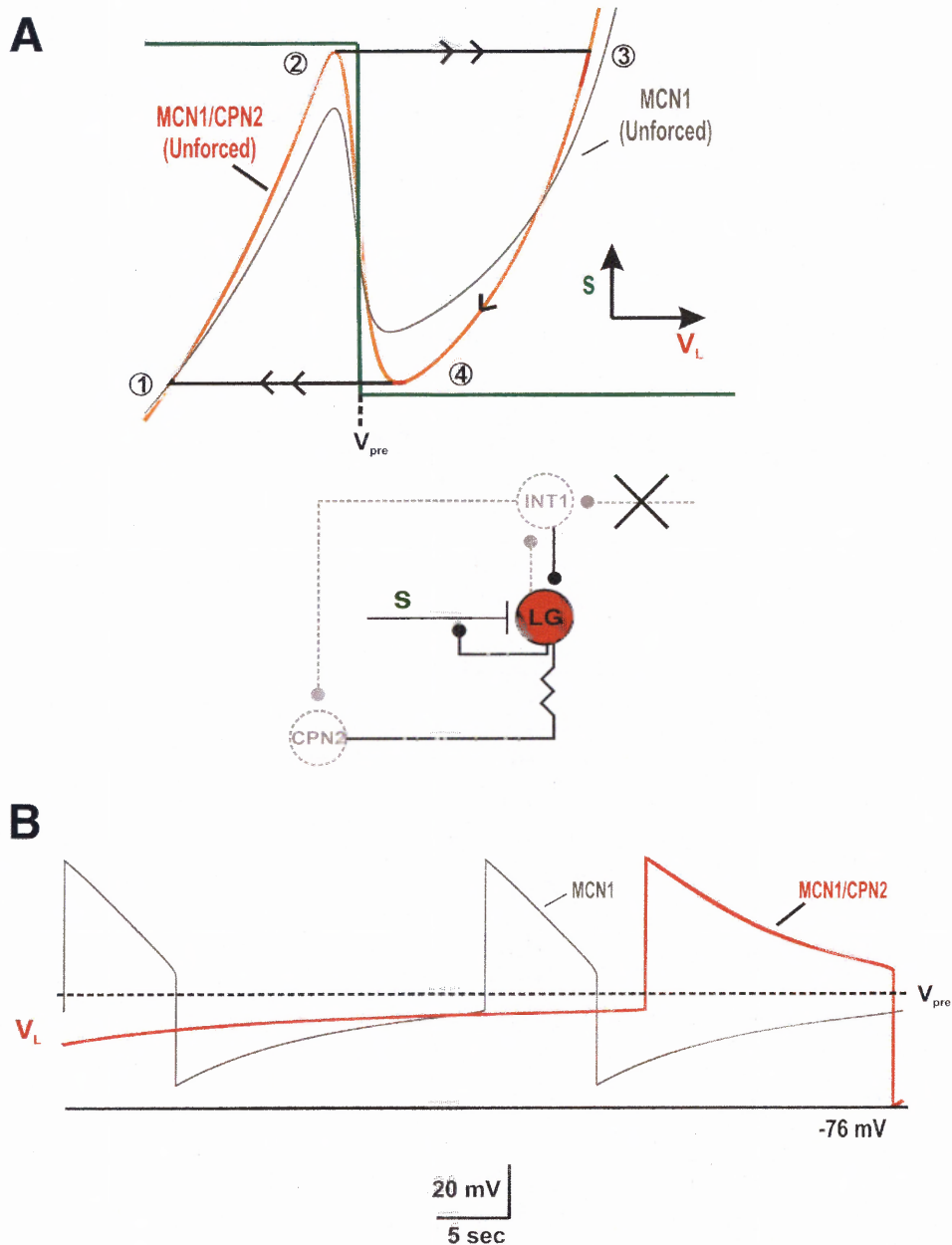


Figure 4.11 The Frequency of Network Oscillations is Slower When the AB to INT1 Inhibition is Removed. **A**, When the forcing effect of P is removed from the system, the jump to right branch of the V_L -nullcline only occurs at the higher (unforced) left knee so that the frequency of network oscillations decreases. Moreover, the frequency of network oscillations in the unforced MCN1/CPN2-elicited gastric mill rhythm is slower than that of the unforced MCN1-elicited rhythm, since a phase point must climb up to a higher left knee and fall down to a lower right knee in the presence of CPN2. **B**, The frequency of network oscillations becomes slower in the absence of the AB to INT1 inhibition.

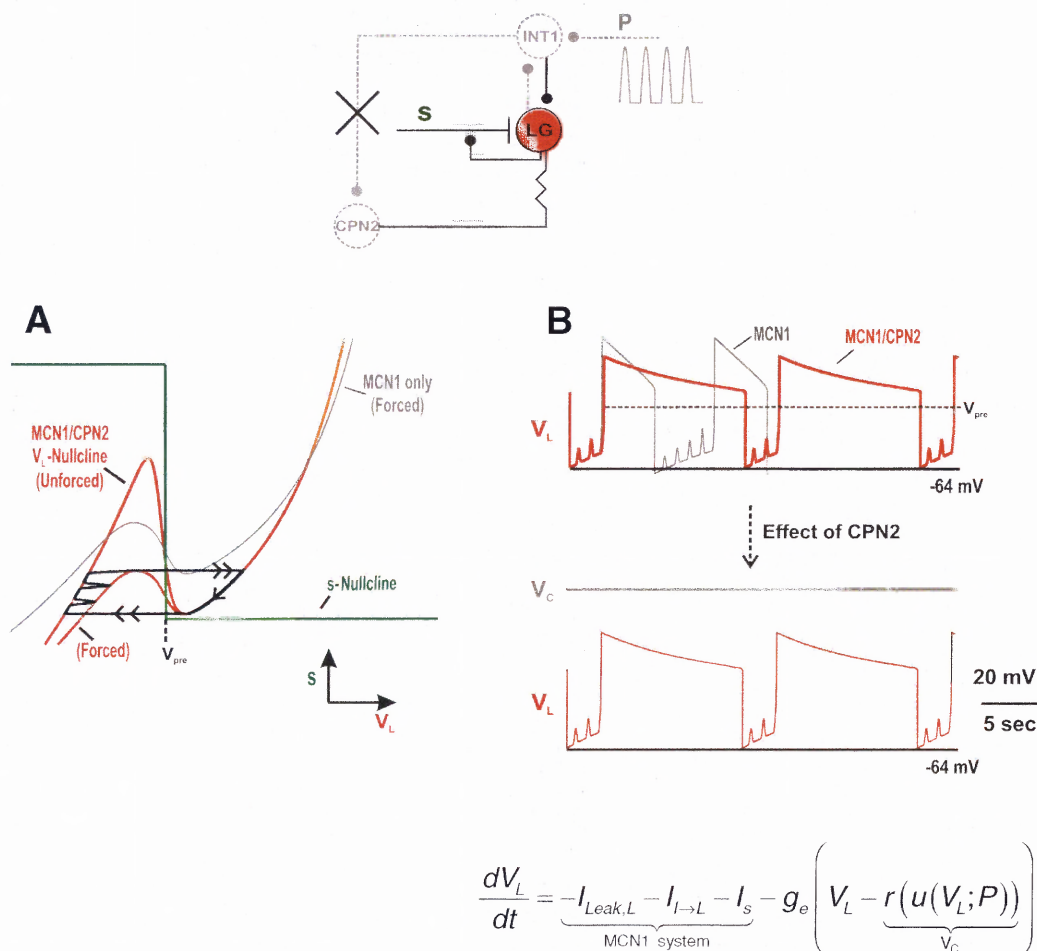


Figure 4.12 The Duration of the LG Interburst Phase is Shorter Without the INT1 to CPN2 Feedback Inhibition. **A**, When the INT1 to CPN2 feedback inhibition is removed, CPN2 is uninhibited, so its membrane potential remains more depolarized than the LG membrane potential, where $V_L < V_C$ in **B**. As a result, CPN2 always pulls up V_L via its local electrical coupling with the LG neuron. This lowers the left knee of the V_L -nullcline compared to that of the MCN1-elicited rhythm so that less buildup of MCN1 excitation (s) is required for the LG neuron to jump into its active state. However, during the LG burst phase, the INT1 to CPN2 feedback inhibition is inactive, so its removal does not significantly affect the duration of the LG burst phase. **B**, Removal of the INT1 to CPN2 feedback inhibition shortens the duration of the LG interburst phase during the MCN1/CPN2-elicited gastric mill rhythm.

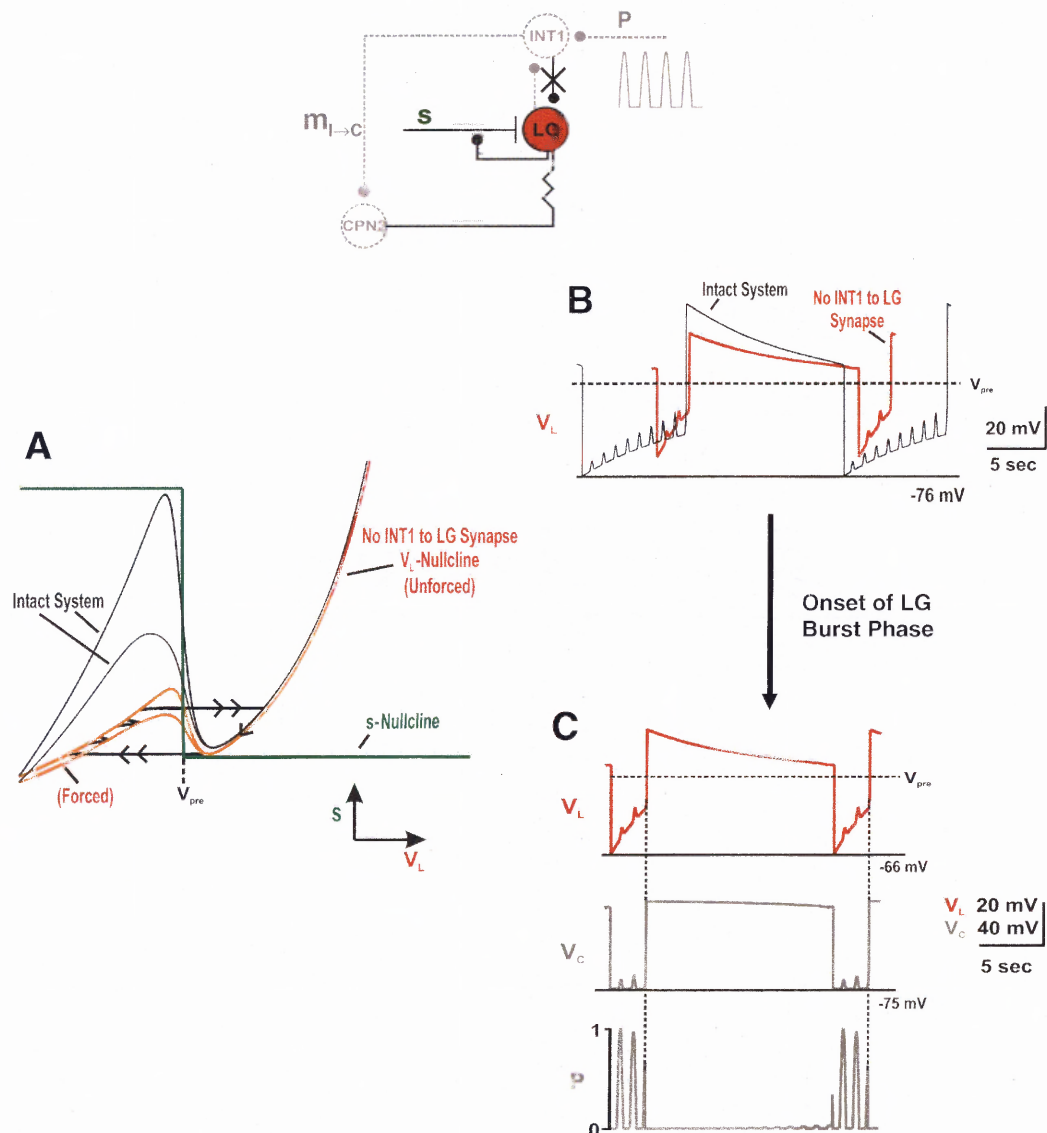


Figure 4.13 Network Oscillations Persist After the INT1 to LG Inhibitory Synapse is Removed. **A**, In the absence of the INT1 to LG inhibitory synapse, INT1 still inhibits the LG neuron via the INT1 to CPN2 feedback pathway ($m_{I \rightarrow C}$). However, the LG neuron is inhibited more weakly when INT1 to LG synapse is removed, so less buildup of MCN1 excitation (s) is required before the jump to the right branch. As a result, the duration of the LG interburst phase is shorter in the absence of the INT1 to LG synapse. **B-C**, In the presence of CPN2, reciprocal inhibition between INT1 and the LG neuron is not required to produce a gastric mill rhythm. Moreover, the AB to INT1 inhibition, via its effect that is transmitted through the INT1 to CPN2 feedback pathway ($m_{I \rightarrow C}$), triggers the onset of the LG burst phase during this gastric mill rhythm.

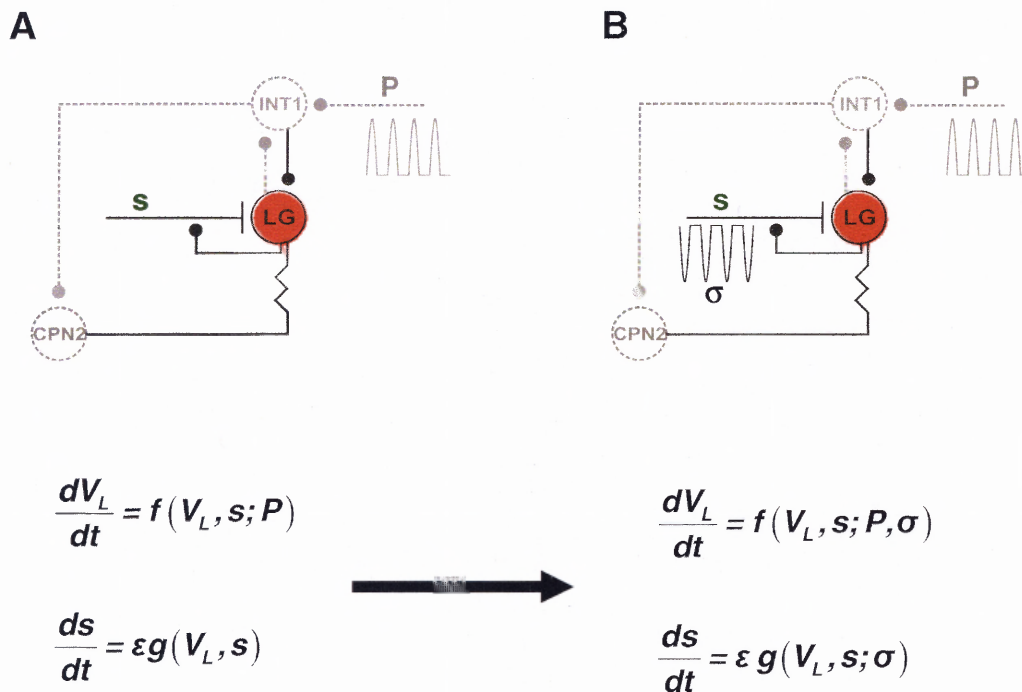


Figure 4.14 The Effect of the AB to MCN1 Feedback Inhibition is Added to the 2-Dimensional Model of the MCN1/CPN2-Elicited Gastric Mill Rhythm. **A**, The 2-dimensional model of the MCN1/CPN2-elicited rhythm where MCN1 is tonically active (see Figure 4.8). **B**, The forcing function σ is added to the model. As in the MCN1-elicited rhythm (see Figure 4.4), the effect of σ interrupts the feed-forward excitatory synapse from MCN1 to LG neuron. Moreover, the forcing functions σ and P oscillate in phase in order to simplify the network dynamics in the model.

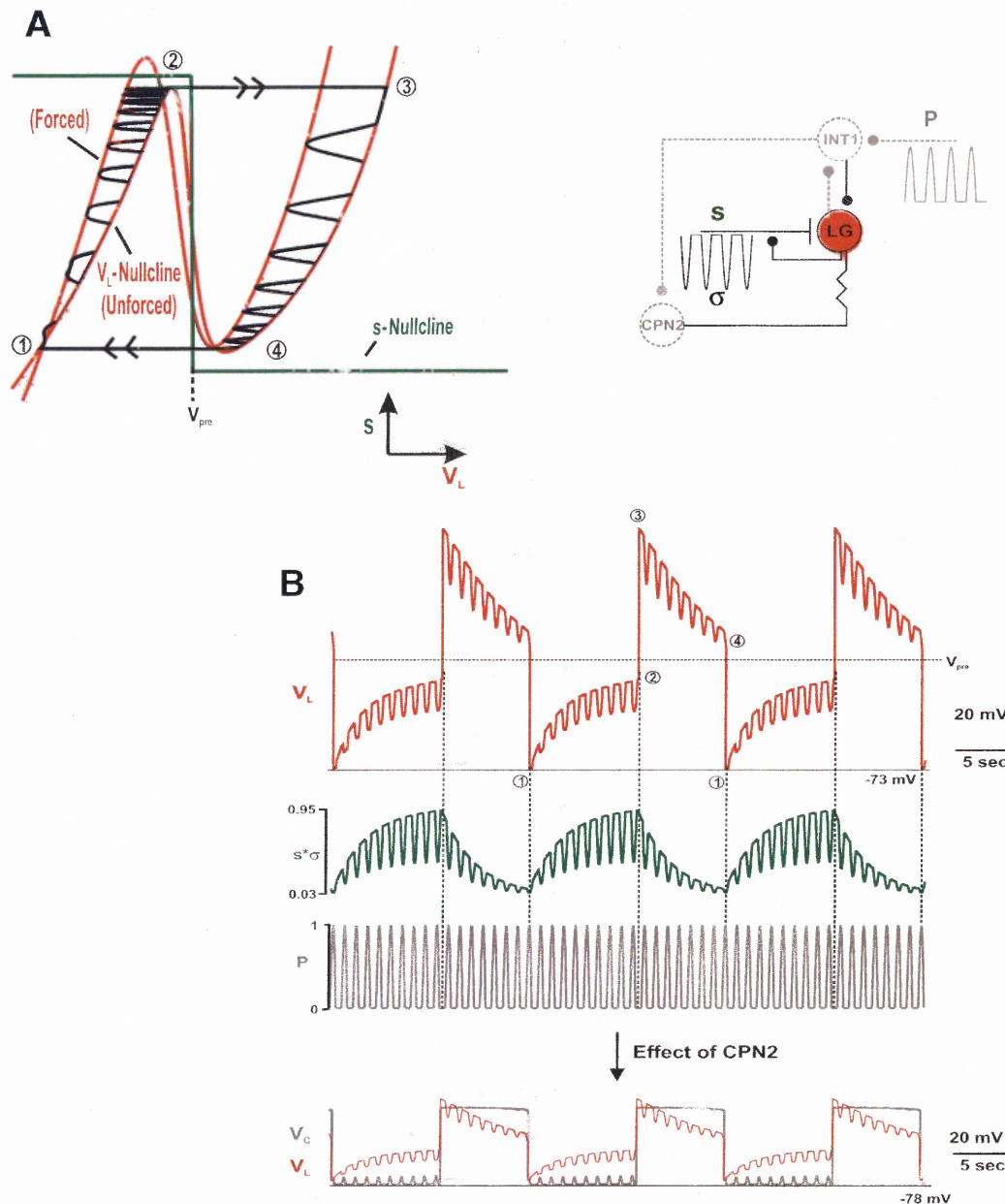


Figure 4.15 Investigating How the AB to MCN1 Feedback Inhibition Affects the MCN1/CPN2-Elicited Gastric Mill Rhythm. *A*, In the presence of both the σ and P forcing functions, the lower (higher) cubic corresponds to the unforced (maximally forced) system. However, CPN2 slows the frequency of network oscillations compared to the MCN1-elicited rhythm (Figure 4.6). *B*, The LG membrane potential exhibits pyloric-timed hyperpolarizations when the AB to MCN1 feedback inhibition is present. The onset of the LG burst phase is initiated during an episode of the MCN1 to LG excitation that is uninterrupted by the AB to MCN1 feedback inhibition. The termination of the LG burst phase is triggered by the AB to MCN1 feedback inhibition. Thus, the conditions for the onset and termination of the LG burst phase are the same as that for the MCN1-elicited rhythm (Figure 4.6). However, CPN2 slows the frequency of network oscillations in this system.

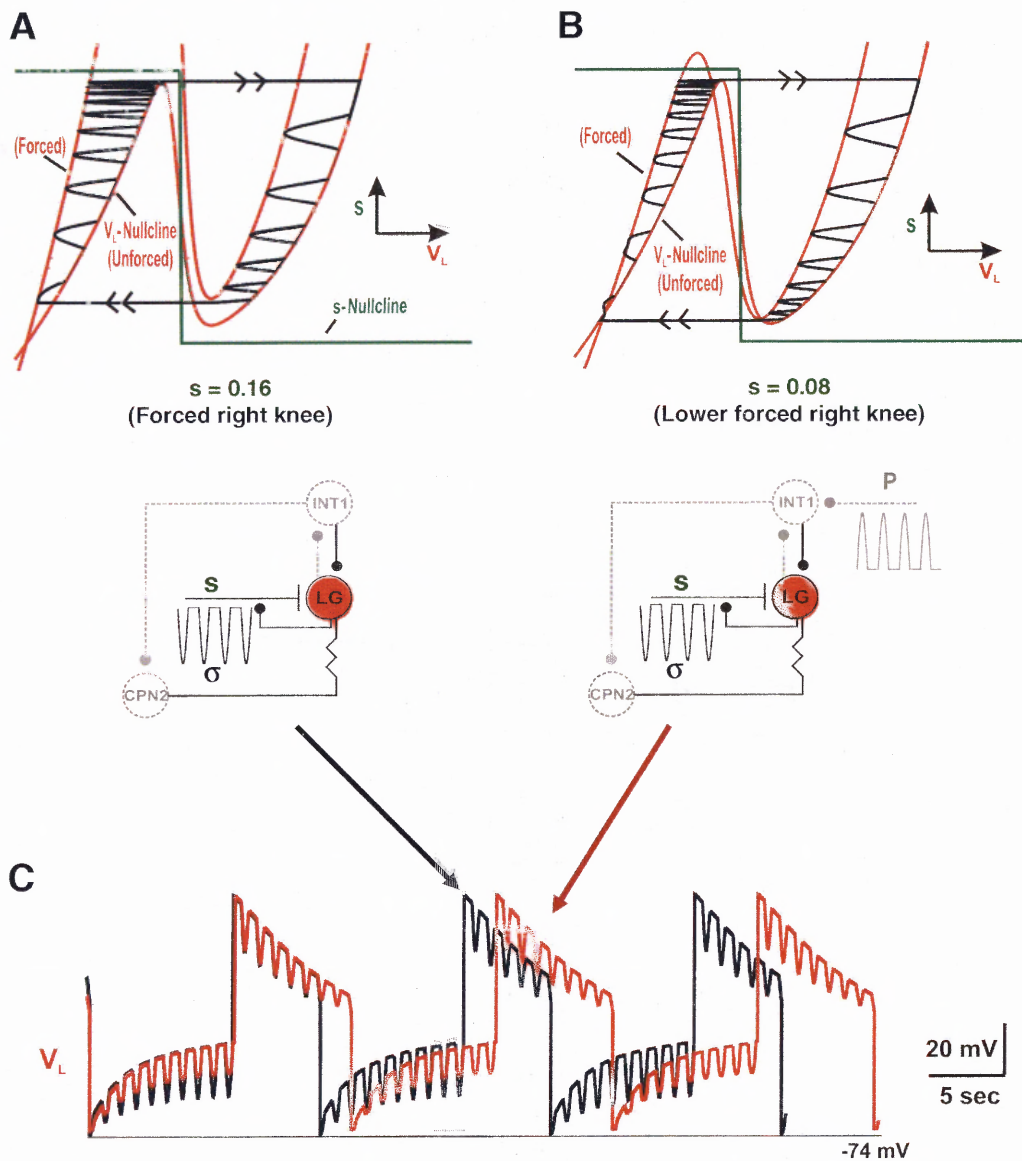
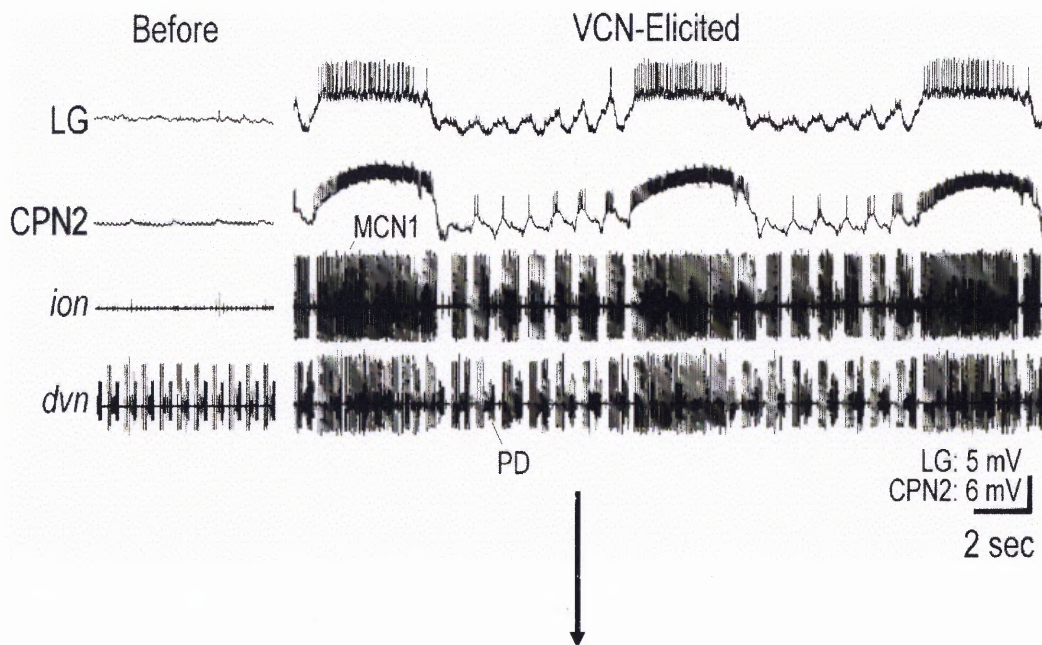


Figure 4.16 The Local AB to INT1 Inhibition Prolongs the Duration of the LG Burst Phase and Slows the Frequency of Network Oscillations in this MCN1/CPN2-Elicited Gastric Mill Rhythm. **A**, Phase plane diagram when the AB to INT1 inhibition is removed. **B**, Phase plane diagram when the AB to INT1 inhibition is present (same as in Figure 4.15). The jump back to the left branch of the V_L -nullcline occurs after a greater decay of s when the AB to INT1 inhibition is present. **C**, Similar to that which occurs in the MCN1-elicited rhythm (see Figure 4.7), the forcing function P (which models the AB to INT1 inhibition) interferes with the hyperpolarizing effect of σ (which models the AB to MCN1 feedback inhibition) and prolongs the duration of the LG burst phase, as shown by the additional pyloric-timed hyperpolarizations in the LG membrane potential. Moreover, the prolonged LG burst phase slows the frequency of network oscillations.



Use 2-D Model to Investigate Network Dynamics

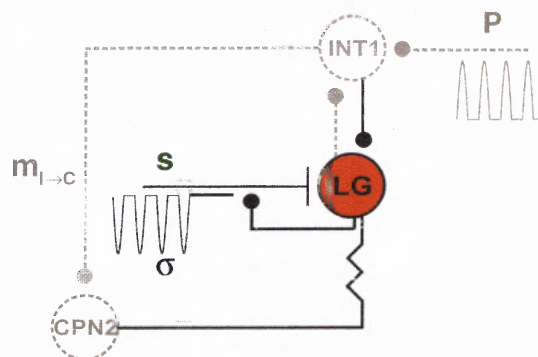


Figure 4.17 The Ventral Cardiac Neurons (VCN) Elicit a Gastric Mill Rhythm in the Biological System via Co-activation of MCN1 and CPN2 (Adapted by permission from the Society for Neuroscience: *Journal of Neuroscience* (Beenhakker and Nusbaum, 24:6741-50, 2004), copyright (2004)). MCN1 (activity in the *ion*) is rhythmically active during the LG interburst phase but tonically active during the LG burst phase of the VCN-elicited rhythm. When MCN1 is rhythmically active, the interruptions in its activity pattern are correlated with PD/AB neuron bursts. This MCN1 activity pattern is produced in the 2-dimensional model by having the forcing function σ interrupt the MCN1 to LG synapse only during the LG interburst phase. CPN2 exhibits a similar activity pattern to that in the previous gastric mill rhythms.

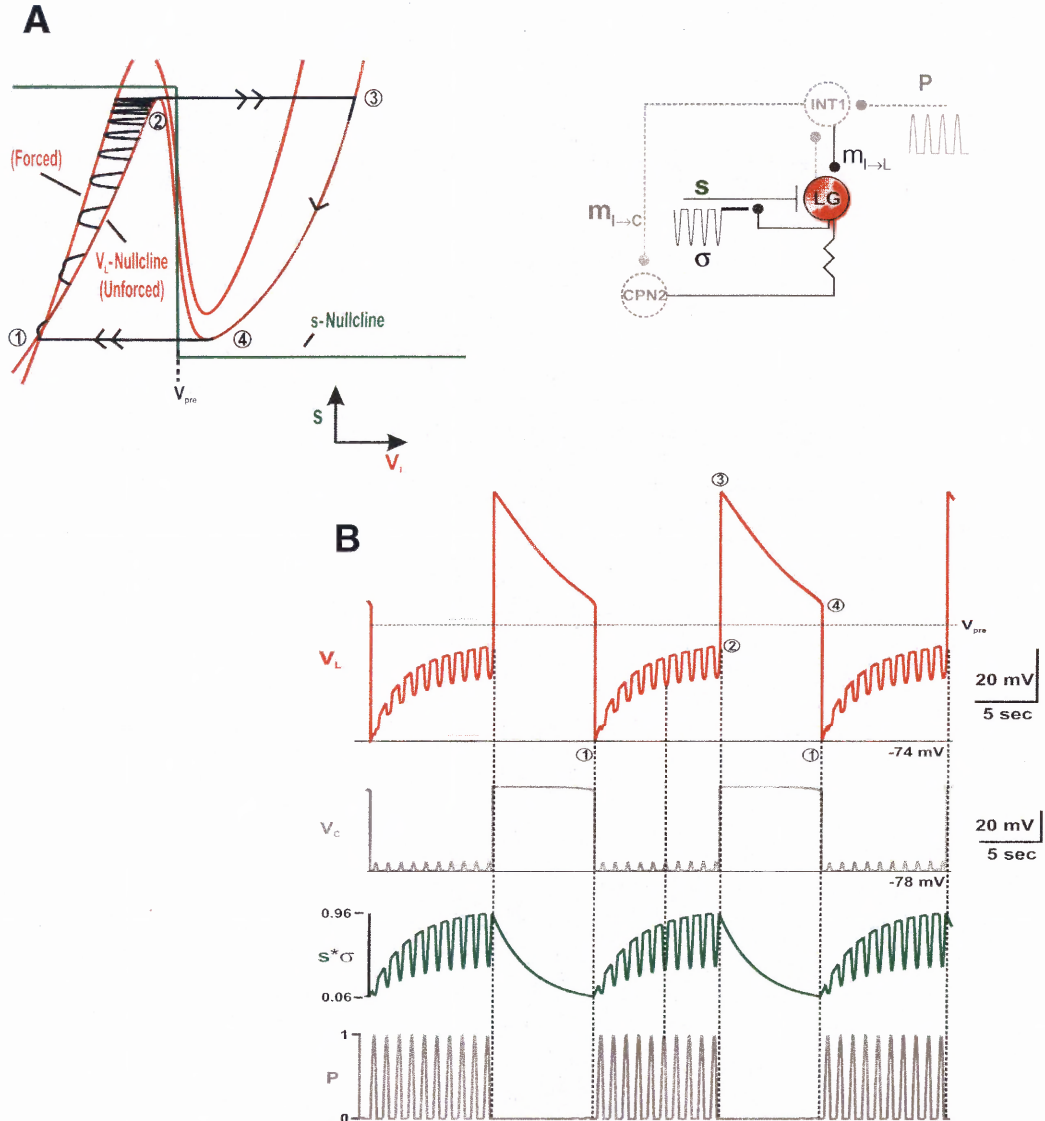


Figure 4.18 The Gastric Mill Rhythm Elicited by MCN1 and CPN2 in Their VCN-Influenced Activity Patterns. **A**, The model is only forced during the LG interburst phase, so a phase point is only shifted between the left branches of the V_L -nullcline, which corresponds to the pyloric-timed hyperpolarizations in the LG membrane potential. **B**, The onset of the LG burst phase is initiated by an episode of the MCN1 to LG excitation that is uninterrupted by the AB to MCN1 feedback inhibition (jump to the right branch in A occurs when the system is unforced). The termination of the LG burst phase is mediated by the graded inhibition from INT1 (jump back to the left branch in A occurs when the phase point reaches the lower, unforced right knee). Note that the pyloric-timed activity in CPN2 (V_C) occurs in phase with the pyloric-timed hyperpolarizations in the LG neuron since the forcing effect of the AB to INT1 inhibition (P) is transmitted simultaneously through the INT1 to LG synapse ($m_{I \rightarrow L}$) and the INT1 the CPN2 feedback pathway ($m_{I \rightarrow C}$).

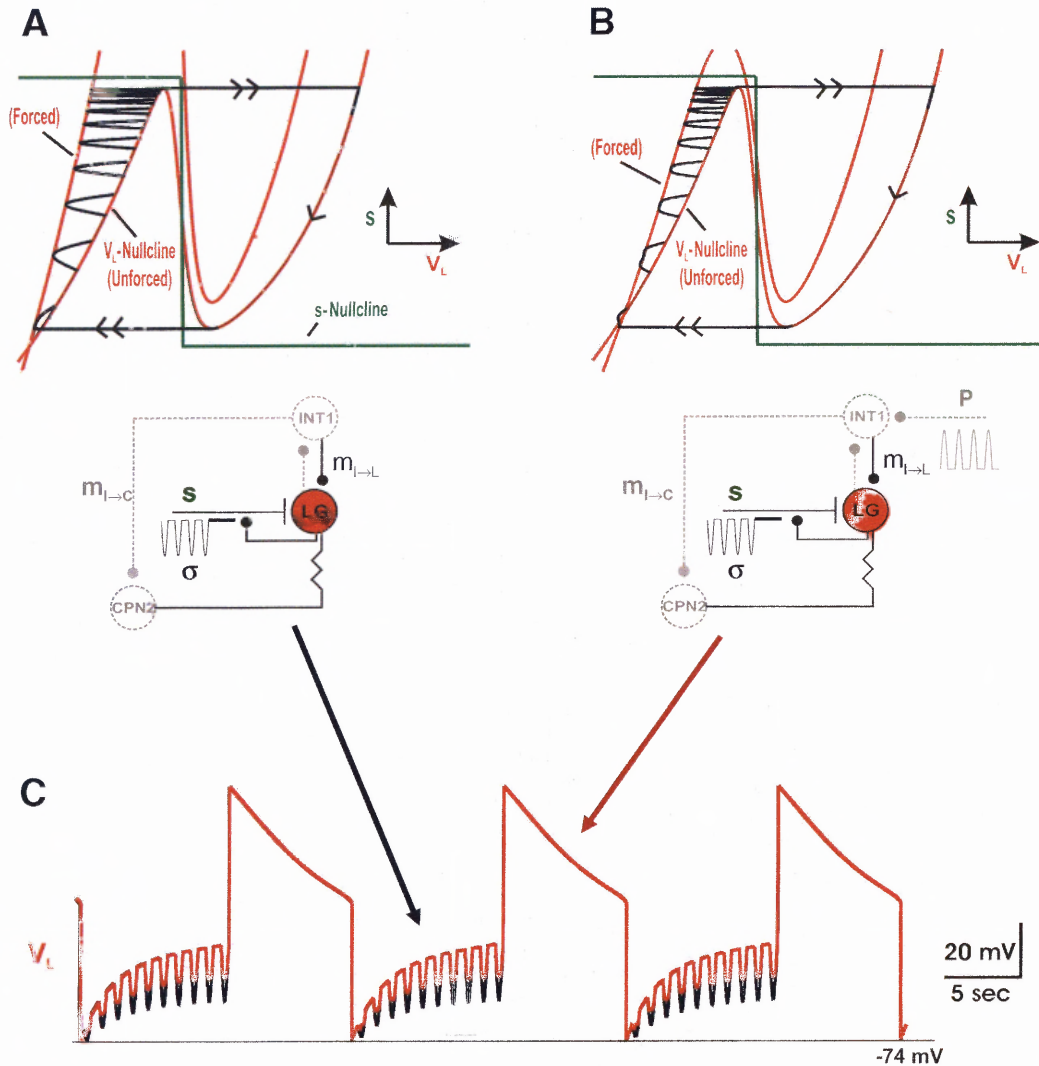


Figure 4.19 The AB to INT1 Inhibition (P) Has No Influence on the Frequency of Network Oscillations When its Effect is Transmitted Simultaneously Through the INT1 to LG Synapse ($m_{I \rightarrow L}$) and the INT1 to CPN2 Feedback Pathway ($m_{I \rightarrow C}$).

A, Phase-plane diagram when the AB to INT1 inhibition is removed. **B**, Phase-plane diagram when the AB to INT1 inhibition is present. **C**, Removal of the AB to INT1 inhibition from the system has no effect on the frequency of network oscillations. The system only exhibits smaller pyloric-timed hyperpolarizations during the LG interburst phase when the AB to INT1 inhibition is present.

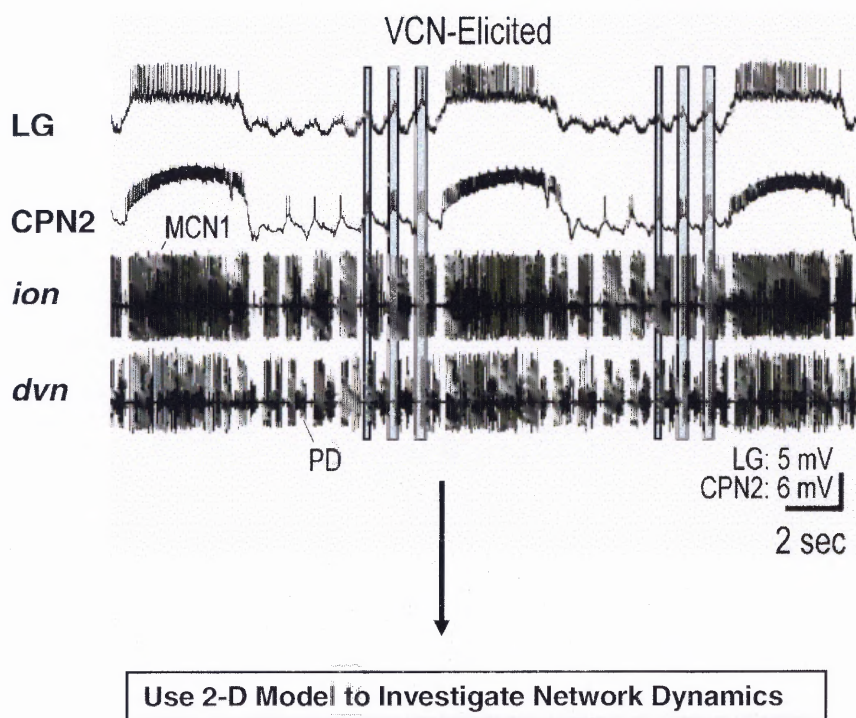


Figure 4.20 In the Biological System, the Pyloric-Timed Activity in CPN2 During the LG Interburst Phase Occurs Approximately in Anti-Phase With the Pyloric-Timed Interruptions in MCN1 and Hyperpolarizations in the LG Neuron (Adapted by permission from the Society for Neuroscience: *Journal of Neuroscience* (Beenhakker and Nusbaum, 24:6741-50, 2004), copyright (2004)). However, in the 2-dimensional model, all three pyloric-timed events occur in phase (see Figure 4.18). To model the timing of CPN2 activity as in the biological system, the forcing effect of the AB to INT1 inhibition, (P), is transmitted through the INT1 to CPN2 feedback pathway ($m_{I \rightarrow C}$) with a delay of $\frac{1}{2}$ of a pyloric period (P_{μ}). This will allow the pyloric-timed depolarizations in CPN2 to occur in anti-phase with the pyloric-timed hyperpolarizations in the LG neuron and interruptions of the MCN1 to LG synapse in the model.

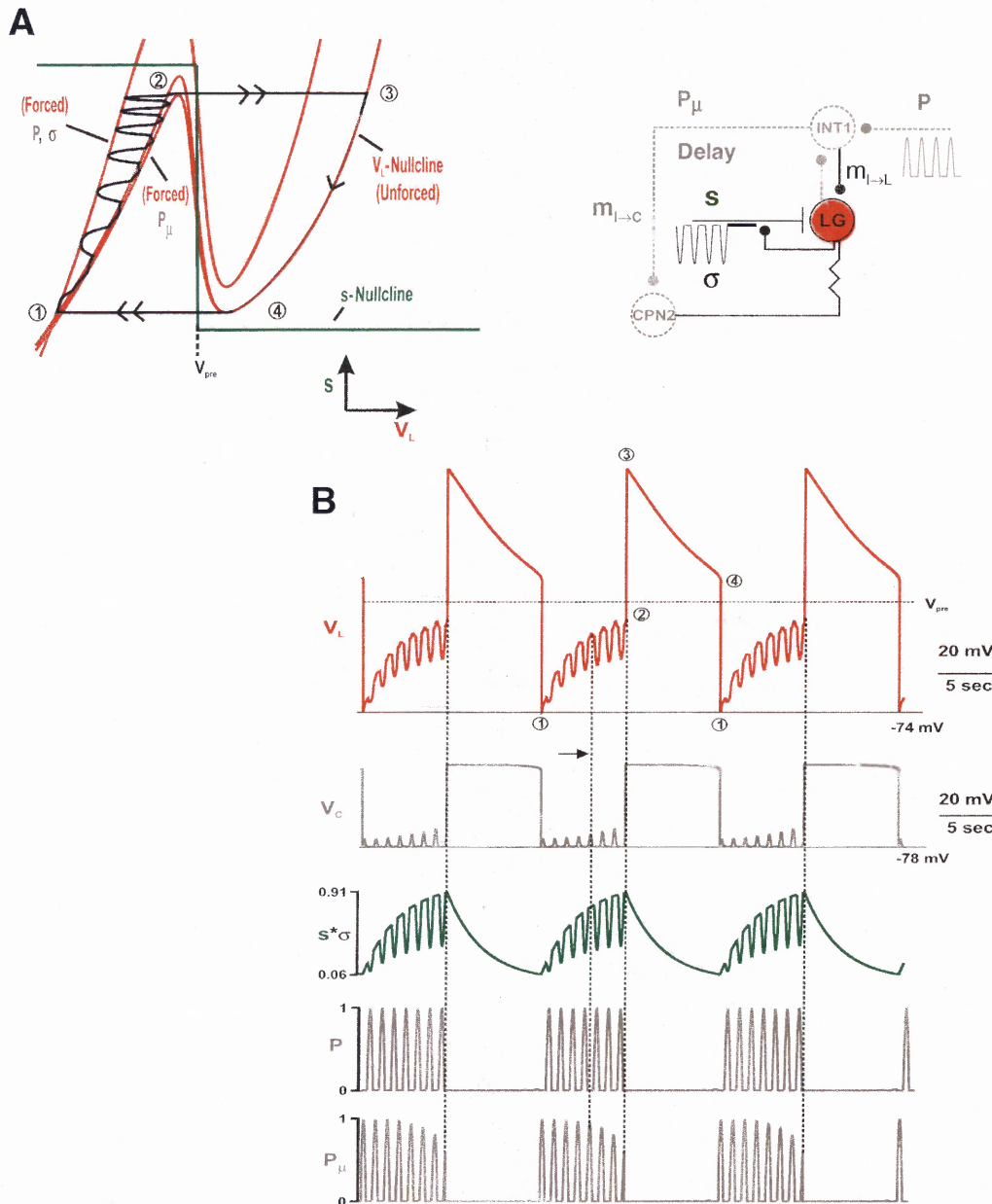


Figure 4.21 Pyloric-Timed Activity Through the INT1 to CPN2 Feedback Pathway ($m_{I \rightarrow C}$) Influences the Network Dynamics of This Gastric Mill Rhythm. *A*, The forcing effect of the AB to INT1 inhibition is transmitted through $m_{I \rightarrow C}$ with a delay of $\frac{1}{2}$ of a pyloric period. The highest cubic in the phase plane occurs when the system is maximally forced by the AB to MCN1 feedback inhibition (σ) and the AB to INT1 inhibition (P) that is locally transmitted through the INT1 to LG synapse ($m_{I \rightarrow L}$). The lowest cubic occurs when the system is maximally forced by the AB to INT1 inhibition (P_μ) that is transmitted through $m_{I \rightarrow C}$. The middle cubic corresponds to the unforced system. *B*, As in the biological system (Figure 4.20), the pyloric-timed depolarizations in CPN2 depolarize the LG membrane potential (arrow) since the forcing peak of P_μ occurs in anti-phase with the peaks of P and σ . The onset of the LG burst phase is triggered by a peak of P_μ .

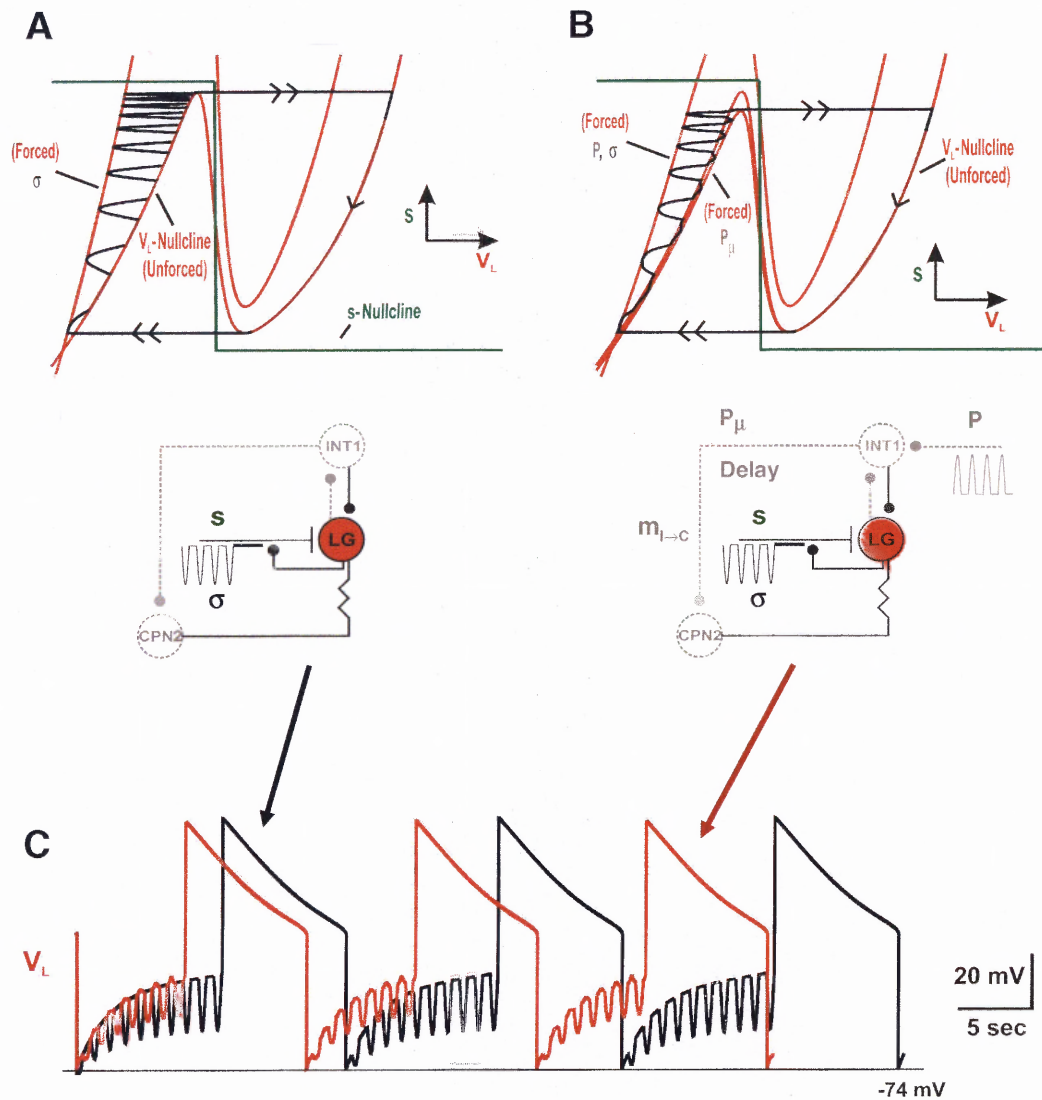


Figure 4.22 The AB to INT1 Inhibition Increases the Frequency of Network Oscillations When its Forcing Effect is Delayed Through the INT1 to CPN2 Feedback Pathway. *A*, Phase-plane diagram when the AB to INT1 inhibition is removed. *B*, Phase-plane diagram when the AB to INT1 inhibition is present. *C*, Network oscillations occur with increased frequency when the AB to INT1 inhibition is present. In particular, the jump to the right branch of the V_L -nullcline in *B* is initiated below the unforced left knee by a forcing peak of P_μ . This increases the frequency of network oscillations since the jump to the right branch occurs below the unforced left knee in *B*.

CHAPTER 5

INVESTIGATING HOW COACTIVE PROJECTION NEURONS SHAPE ACTIVITY IN A RHYTHMIC NETWORK USING A BIOPHYSICALLY- REALISTIC MODEL

5.1 Introduction

In this chapter, the network properties of the MCN1-elicited and MCN1/CPN2-elicited gastric mill rhythms are compared in the context of a more biophysically-realistic model. In particular, the biophysically-realistic model, which was first introduced in Chapter 3, is now used to compare the MCN1-elicited and MCN1/CPN2-elicited gastric mill rhythms for the case in which MCN1 is tonically active. This case corresponds to Figures 4.3 and 4.8 – 4.13 in the previous chapter. Therefore, the predictions of the 2-dimensional model (previous chapter) in the case where MCN1 is tonically active are now assessed in the context of the biophysically-realistic model.

First, CPN2 is added to the biophysically-realistic model. Physiologically, the axon of CPN2 descends into the STG where its terminals excite the LG neuron (Norris et al., 1994). This excitation is believed to occur via a local electrical coupling in the STG (M.P. Nusbaum, personal communication). In addition, the cell body of CPN2 (in the CoG) is strongly inhibited by a feedback synapse from INT1 (see Figure 5.1). As a result, co-stimulation of MCN1 and CPN2 in the biological system elicits a distinct gastric mill rhythm from that elicited by MCN1 stimulation alone (Norris et al., 1994; Blitz and Nusbaum, 1997; Beenhakker and Nusbaum, 2004). In particular, the MCN1/CPN2-elicited gastric mill rhythm exhibits a prolonged LG burst duration and slower cycle frequency compared to that of the MCN1-elicited rhythm (Blitz and Nusbaum, 1997). Moreover, although the reciprocal inhibition between INT1 and the LG

neuron is necessary for the MCN1-elicited rhythm to occur (Bartos et al., 1999), recent experiments showed that the MCN1/CPN2-elicited gastric mill rhythm still persists without this reciprocal inhibition. In particular, the MCN1/CPN2-elicited rhythm persists when the INT1 to LG synapse is pharmacologically removed in the biological system (Akay et al., 2004). Thus, this chapter uses the biophysically-realistic model to investigate the network properties of the MCN1/CPN2-elicited gastric mill rhythm that were reported in the biological system.

Using the 2-dimensional model of the MCN1-elicited rhythm (previous chapter), the addition of CPN2 to the system was shown to slow the frequency of network oscillations (see Figure 4.9). Moreover, the MCN1/CPN2-elicited rhythm was shown to persist when the INT1 to LG inhibitory synapse was removed in the 2-dimensional model (see Figure 4.13). In particular, the INT1 feedback inhibition to CPN2 was shown to facilitate network oscillations in the absence of the INT1 to LG synapse. However, several details of the biological system were not included in the reduced 2-dimensional model of the previous chapter. For example, INT1 and LG were treated as passive neurons so that action potential generation in them was ignored. Now, this chapter develops a biophysically-realistic model of the MCN1/CPN2-elicited gastric mill rhythm that includes more details of the biological system. As a result, the network properties of the MCN1-elicited and MCN1/CPN2-elicited gastric mill rhythms are compared in the context of the biophysically-realistic model.

5.2 Methods

The biophysically-realistic model was first introduced in Chapter 3. In this model, MCN1, AB, INT1, and LG are treated as Hodgkin-and-Huxley type neurons. Moreover, each neuron in this model is described by a multi-compartment structure in order to separate the neuronal sites of synaptic input from that of action potential generation, and adjacent compartments of a neuron are connected via an axial resistance (see Chapter 3). However, in the present chapter, the DG neuron is not included in the biophysically-realistic model. In particular, in the biological system, DG is only a follower neuron during the MCN1-elicited and MCN1/CPN2-elicited gastric mill rhythms due to its lack of functional synaptic connections within the STG (Norris et al., 1994; Coleman et al., 1995). Therefore, since the DG neuron does not play an active role in shaping the MCN1-elicited or MCN1/CPN2-elicited gastric mill rhythms, it is not included in this chapter for the purpose of simplicity.

The biophysically-realistic model was described in detail in Chapter 3. Therefore, a shorter overview of the model is given here. The projection neuron CPN2 is included in the model for this chapter in order to build a biophysically-realistic model of the MCN1/CPN2-elicited gastric mill rhythm (see Figure 5.2). Each neuron is described with a multi-compartment structure in this model, so the membrane potential of a given neural compartment is obtained by numerical integration a first-order differential equation of the form

$$C \frac{dV}{dt} = I_{Ext} - (I_{Leak} + \sum I_{axial} + \sum I_{ion} + \sum I_{syn}), \quad (5.1)$$

where V designates the membrane potential of the given compartment while the parameter C designates its membrane capacitance. In addition, I_{Ext} represents external current that can be injected into the compartment, and I_{Leak} designates the leak current of the compartment, which is modeled by

$$I_{Leak} = g_{Leak} (V - E_{Leak}). \quad (5.2)$$

The parameters g_{Leak} and E_{Leak} represent the conductance and reversal potential of the leak current, respectively, which is described in more detail in Chapter 3. Next, each I_{axial} represents an axial current that is induced in the given compartment due to a voltage difference with its adjacent compartments. In particular, the sum of axial currents that affect a given compartment in Equation (5.1) is modeled by

$$\sum I_{axial} = g^{i+1} (V - V^{i+1}) + g^{i-1} (V - V^{i-1}), \quad (5.3)$$

where V represents the membrane potential of the i^{th} compartment. In addition, V^{i+1} represents the membrane potential of the adjacent compartment to the right, while V^{i-1} represents the membrane potential of the adjacent compartment to the left. Moreover, g^{i+1} represents the axial conductance for the voltage difference $(V - V^{i+1})$, while g^{i-1} represent the axial conductance for the voltage difference $(V - V^{i-1})$. More details about I_{axial} are given in Chapter 3.

Next, each voltage-gated ionic current in Equation (5.1) is modeled by an equation of the form

$$I_{ion} = \bar{g}_{ion} m^p h^q (V - E_{ion}), \quad (5.4)$$

where \bar{g}_{ion} and E_{ion} designate its maximal conductance and reversal potential, respectively. Moreover, m and h represent activation and inactivation of the ionic conductance, respectively, where p and q are non-negative integers with $q = 0$ for a non-inactivating conductance. Furthermore, activation (or inactivation) of the ionic conductance is modeled by equations of the form

$$\tau_x(V) \frac{dx}{dt} = x_\infty(V) - x \quad x = m, h \quad (5.5)$$

$$x_\infty(V) = \frac{1}{1 + \exp(k(V - v_k))} \quad (5.6)$$

$$\tau_x(V) = \tau_1 + \frac{\tau_2}{1 + \exp(l(V - v_l))}. \quad (5.7)$$

In particular, the steady-state behavior of activation (or inactivation) for the ionic conductance is modeled by the sigmoidal function in Equation (5.6), where the parameters v_k and k represent the inflection point voltage and steepness of the sigmoid respectively. Moreover, $k < 0$ for activation while $k > 0$ for inactivation. Furthermore, the corresponding time constant for activation (or inactivation) is modeled by the sigmoid in Equation (5.7). For more details about the voltage-gated ionic current, see Chapter 3.

Then, each synaptic conductance in Equation (5.1) is modeled by an equation of the form

$$I_{syn} = \bar{g}_{syn} S(V - E_{syn}), \quad (5.8)$$

where \bar{g}_{syn} and E_{syn} designate its maximal conductance and reversal potential, respectively. Moreover, the synaptic gating function S , which is dependent upon the membrane potential of the presynaptic compartment (V_{pre}), is modeled by equations of the form

$$\tau_S(V_{pre}) \frac{dS}{dt} = S_\infty(V_{pre}) - S \quad (5.9)$$

$$S_\infty(V_{pre}) = \frac{1}{1 + \exp(\alpha(V_{pre} - v_\alpha))} \quad (5.10)$$

$$\tau_S(V_{pre}) = \tau_3 + \frac{\tau_4}{1 + \exp(\beta(V_{pre} - v_\beta))}. \quad (5.11)$$

The steady-state behavior of the synapse is modeled by the sigmoidal function in Equation (5.10), whose inflection point voltage and steepness are designated by the parameters v_α and α , respectively. Moreover, the synaptic time constant is modeled by the sigmoid in Equation (5.11). For more details about the synaptic conductance, see Chapter 3.

Electrical synapses in the network are modeled by an equation of the form

$$I_{elec} = g_{elec} (V - V_{couple}), \quad (5.12)$$

where V designates the membrane potential of a given compartment while V_{couple} designates the membrane potential of the compartment it is electrically coupled to. In the biological system, the MCN1 axon terminals (Coleman et al., 1995) and the CPN2 axon terminals (M.P. Nusbaum, personal communication) are electrically coupled to the LG neuron locally within the STG, and this electrical coupling is included in the biophysically-realistic model (see Figure 5.2). Finally, all parameter values for the biophysically-realistic model of the MCN1/CPN2-elicited gastric mill rhythm are given in Appendix C.

5.3 Results

Now, the biophysically-realistic model is used to examine the network properties of the MCN1/CPN2-elicited gastric mill rhythm. In particular, for the case in which MCN1 is tonically active, the biophysically-realistic model is used to investigate how the network properties of the MCN1-elicited rhythm are changed when a second projection neuron (CPN2) is co-activated in the system.

5.3.1 Network Dynamics of the MCN1-Elicited Gastric Mill Rhythm

First, the network dynamics of the MCN1-elicited rhythm are described. During the inactive state of the LG neuron where it is inhibited by INT1, MCN1 excitation (s) slowly builds up in LG (Figure 5.3.A). The small-amplitude depolarizations in the LG membrane potential are due to the effect of the AB to INT1 inhibition. In particular, as described in Chapter 3, AB inhibition of INT1 in turn disrupts INT1 inhibition of the LG neuron (inset of Figure 5.3.A), which effectively disinhibits the LG neuron from INT1. After a sufficient buildup of MCN1 excitation (s), the LG neuron escapes from INT1 inhibition and begins to burst (Figure 5.3.A). As a result, the LG neuron inhibits INT1 and presynaptically inhibits MCN1. This presynaptic inhibition blocks all chemical synaptic input from MCN1 axon terminals in the STG. However, since s decays slowly in the LG neuron (Figure 5.3.A), the LG burst phase continues during the presynaptic inhibition of MCN1. In addition, the electrical coupling between MCN1 axon terminals and the LG neuron, which is not affected by the presynaptic inhibition, is believed to prolong the LG burst phase (Coleman et al., 1995). However, the role of this electrical coupling during the MCN1-elicited rhythm is not clearly understood. Also, it is noted that the AB to INT1 inhibition does not affect the LG burst phase, as reported in the biological system (Bartos et al., 1999). In particular, during the LG burst phase where LG inhibits INT1, the reverse INT1 to LG synapse (inset of Figure 5.3.A) becomes inactive; therefore, the effect of the AB to INT1 inhibition is not effectively transmitted to the LG neuron through the inactive synapse. Subsequently, the LG burst phase terminates after a sufficient decay of s excitation in LG (Figure 5.3.A), and MCN1 is released from the presynaptic inhibition as the LG neuron falls back down into its

inactive state where it is inhibited by INT1. Then, the cycle begins again as s builds up in the LG neuron.

In the biological system, CPN2 remains inactive during the MCN1-elicited gastric mill rhythm. However, CPN2 is still inhibited by the feedback synapse from INT1 (inset of Figure 5.3.A) during the LG interburst phase of the MCN1-elicited rhythm (M.P. Nusbaum, personal communication). Therefore, the membrane potential of CPN2 remains more hyperpolarized than the LG membrane potential during the MCN1-elicited rhythm (see legend of Figure 5.3.A). As a result, since the CPN2 axon terminals are electrically coupled to the LG neuron, the biophysically-realistic model includes the fact that CPN2 axon terminals still pull down the LG membrane potential during the MCN1-elicited rhythm (see Figure 5.3.A). It is noted that this biological fact was not included in the reduced 2-dimensional model of the MCN1-elicited rhythm (Figure 4.3 of previous chapter).

5.3.2 Network Dynamics of the MCN1/CPN2-Elicited Gastric Mill Rhythm in the Biophysically-Realistic Model

When MCN1 and CPN2 are co-active, the MCN1/CPN2-elicited gastric mill rhythm exhibits a slower frequency than that of the MCN1-elicited rhythm (Figure 5.3.B). In particular, a prolonged LG burst phase facilitates the slower frequency of the MCN1/CPN2-elicited gastric mill rhythm.

5.3.2.1 Network Dynamics During the LG Burst Phase. First, the network dynamics of the LG burst phase are discussed. During this phase, the LG-mediated presynaptic

inhibition of MCN1 causes s to slowly decay in the LG neuron (Figure 5.3.B). However, the LG neuron also inhibits INT1, which in turn removes the INT1 to CPN2 feedback inhibition (inset of Figure 5.3.B). As a result, CPN2 is no longer inhibited by INT1 during the LG burst phase, so the membrane potential of CPN2 becomes more depolarized than the LG membrane potential (see legend of Figure 5.3.B). Therefore, since the CPN2 axon terminals are electrically coupled to the LG neuron, the CPN2 terminals pull up the LG membrane potential during the LG burst phase of the MCN1/CPN2-elicited gastric mill rhythm. As a result, a greater decay of MCN1 excitation (s) is required in the LG neuron before it can fall back down into its inactive state (Figure 5.3.B). Therefore, the LG burst phase of the MCN1/CPN2-elicited gastric mill rhythm is prolonged compared to that of the MCN1-elicited rhythm (Figure 5.3.B).

5.3.2.2 Network Dynamics During the LG Interburst Phase. Next, the network dynamics of the LG interburst phase are discussed. During this phase, MCN1 is released from the presynaptic inhibition so that s slowly builds up in the LG neuron (Figure 5.3.B). Moreover, the LG neuron is inhibited by INT1, and CPN2 is inhibited by the feedback synapse from INT1 (inset of Figure 5.3.B). As a result, the membrane potential of CPN2 becomes more hyperpolarized than the LG membrane potential (see legend of Figure 5.3.B). Therefore, since the CPN2 axon terminals are electrically coupled to the LG neuron, the CPN2 terminals pull down the LG membrane potential during the LG interburst phase. However, the prolonged LG interburst phase of the MCN1/CPN2-elicited gastric mill rhythm is not due to the electrical coupling between the CPN2 axon terminals and the LG neuron, which already occurs during the MCN1-elicited rhythm

(Figure 5.3.A). Instead, the prolonged LG interburst phase is due to the fact that MCN1 excitation (s) decays to a lower minimum value during the MCN1/CPN2-elicited gastric mill rhythm compared to that of the MCN1-elicited rhythm (Figure 5.3.B). Therefore, s begins to rise from a lower minimum value, which prolongs the LG interburst phase of the MCN1/CPN2-elicited gastric mill rhythm. It is noted that s rises to the same maximum value during both the MCN1-elicited and MCN1/CPN2-elicited gastric mill rhythms (Figure 5.3.B), since the electrical coupling between CPN2 axon terminals and the LG neuron is included in both gastric mill rhythms.

Thus, the biophysically-realistic model includes the biological fact that CPN2 axon terminals are electrically coupled to the LG neuron during both the MCN1-elicited and MCN1/CPN2-elicited gastric mill rhythms. Therefore, this electrical coupling is only responsible for prolonging the LG burst phase of the MCN1/CPN2-elicited rhythm, where CPN2 is uninhibited by the feedback synapse from INT1 (Figure 5.3.B). On the other hand, the prolonged LG interburst phase of the MCN1/CPN2-elicited gastric mill rhythm is due to the fact that s begins to rise from a lower minimum value when MCN1 and CPN2 are co-active (Figure 5.3.B).

5.3.3 Effect of the Local AB to INT1 Inhibition

In the biological system, the AB to INT1 inhibition both (1) triggers the onset of the LG burst phase and (2) increases the frequency of network oscillations during the MCN1-elicited rhythm (Bartos et al., 1999). These effects are reproduced in the biophysically-realistic model. In particular, the AB to INT1 inhibition triggers the onset of the LG burst phase in the model MCN1-elicited rhythm (Figure 5.4.A.1). Moreover, the

frequency of the MCN1-elicited rhythm decreases when the AB to INT1 inhibition is removed in the model (Figure 5.4.A.2).

Next, the AB to INT1 inhibition produces similar effects in the biophysically-realistic model of the MCN1/CPN2-elicited gastric mill rhythm. In particular, the onset of the LG burst phase during the MCN1/CPN2-elicited rhythm is triggered by the AB to INT1 inhibition (Figure 5.4.B.1). Moreover, the MCN1/CPN2-elicited gastric mill rhythm exhibits a slower frequency when the AB to INT1 inhibition is removed (Figure 5.4.B.2).

In both cases (with or without the AB to INT1 inhibition), the MCN1/CPN2-elicited gastric mill rhythm exhibits a prolonged LG burst phase compared to that of the MCN1-elicited rhythm (Figure 5.4.B). In particular, since CPN2 is not inhibited by the feedback synapse from INT1 during the LG burst phase, the CPN2 axon terminals, via their electrical coupling with the LG neuron, pull up the LG membrane potential during the LG burst phase. As a result, a greater decay of MCN1 excitation (s) is required in the LG neuron before it can fall back down into its inactive state. Therefore, the prolonged LG burst phase slows the frequency of the MCN1/CPN2-elicited gastric mill rhythm compared to that of the MCN1-elicited rhythm (Figure 5.4.B).

5.3.4 Effect of the INT1 to CPN2 Feedback Inhibition

When the INT1 to CPN2 feedback inhibition is removed from the model, CPN2 is no longer inhibited by INT1 during the LG interburst phase of the MCN1/CPN2-elicited gastric mill rhythm (Figure 5.5). As a result, CPN2 becomes more depolarized than the LG membrane potential throughout the MCN1/CPN2-elicited rhythm (Figure 5.5.B).

Therefore, the CPN2 axon terminals, via their electrical coupling with the LG neuron, pull up the LG membrane potential during the LG interburst phase, and, as a result, less MCN1 excitation (s) is required for the LG neuron to transition into its burst phase (Figure 5.5.B). Thus, removal of the INT1 to CPN2 feedback inhibition shortens the duration of the LG interburst phase during the MCN1/CPN2-elicited gastric mill rhythm (compare Figures 5.5.A and 5.5.B).

During the LG burst phase, the INT1 to CPN2 feedback inhibition is inactive, so its removal does not significantly affect the duration of the LG burst. In particular, the CPN2 axon terminals, via their local electrical coupling with the LG neuron, still pull up the LG membrane potential, as in the intact system; therefore, a greater decay of s is required for the LG neuron to fall back down into its inactive state compared to that of the MCN1-elicited rhythm (Figure 5.5.B). Thus, when the INT1 to CPN2 feedback inhibition is removed, the MCN1/CPN2-elicited gastric mill rhythm still exhibits a prolonged LG burst phase and slower frequency compared to that of the MCN1-elicited rhythm (Figure 5.5.B).

5.3.5 Effect of the Local INT1 to LG Inhibition

In the biological system, the reciprocal inhibition between INT1 and the LG neuron is required for the MCN1-elicited rhythm to occur (Bartos et al., 1999). This behavior is also reproduced in the biophysically-realistic model. In particular, the MCN1-elicited rhythm is disrupted when the local INT1 to LG inhibitory synapse is removed in the model (Figure 5.6.A).

On the other hand, during the MCN1/CPN2-elicited gastric mill rhythm, INT1 inhibits the LG neuron both directly (via the local INT1 to LG inhibitory synapse) and indirectly (via the INT1 to CPN2 feedback pathway). In the biological system, the MCN1/CPN2-elicited gastric mill rhythm persists when the direct INT1 to LG inhibitory synapse is removed (Akay et al., 2004). Similarly, in the biophysically-realistic model, the MCN1/CPN2-elicited gastric mill rhythm still persists when the direct INT1 to LG inhibitory synapse is removed (Figure 5.6.B). In particular, INT1 still inhibits the LG neuron indirectly via the INT1 to CPN2 feedback pathway (inset of Figure 5.6.B). However, during the LG interburst phase, the excitatory synaptic input from MCN1 to the LG neuron is only weakly balanced by the indirect INT1 to CPN2 feedback pathway (Figure 5.6.B). Therefore, when the INT1 to LG inhibitory synapse is removed, the LG interburst phase becomes more depolarized compared to that of the MCN1/CPN2-elicited rhythm for the intact system (Figure 5.6.B). Thus, although the INT1 to LG inhibitory synapse is not necessary for producing a gastric mill rhythm when MCN1 and CPN2 are co-active, the model suggests that it is necessary for producing the MCN1/CPN2-elicited gastric mill rhythm that is observed in the intact system. Moreover, the model suggests that the INT1 to CPN2 feedback pathway changes the locus of coordination in the gastric mill rhythm, since reciprocal inhibition between INT1 and the LG neuron is not necessary for generating a gastric mill rhythm when MCN1 and CPN2 are co-active.

5.3.6 Summary of Results

In this chapter, a biophysically-realistic model of the MCN1/CPN2-elicited gastric mill rhythm was developed to check the predictions of the 2-dimensional model (of the last

chapter) for the case in which MCN1 is tonically active (not affected by feedback). It was shown that the predictions of the 2-dimensional model are reproduced with the more biophysically-realistic model. In particular,

- The MCN1/CPN2-elicited gastric mill rhythm exhibits a slower frequency than the MCN1-elicited rhythm.
- The locus of pattern generation is different for both gastric mill rhythms in that the MCN1/CPN2-elicited rhythm persists without reciprocal inhibition.
- The $AB \rightarrow INT1$ inhibition (1) increases the frequency of network oscillations (2) determines the onset of the LG burst phase for both gastric mill rhythms.
- The $INT1 \rightarrow CPN2$ feedback inhibition prolongs the duration of the LG interburst phase for the MCN1/CPN2-elicited rhythm.

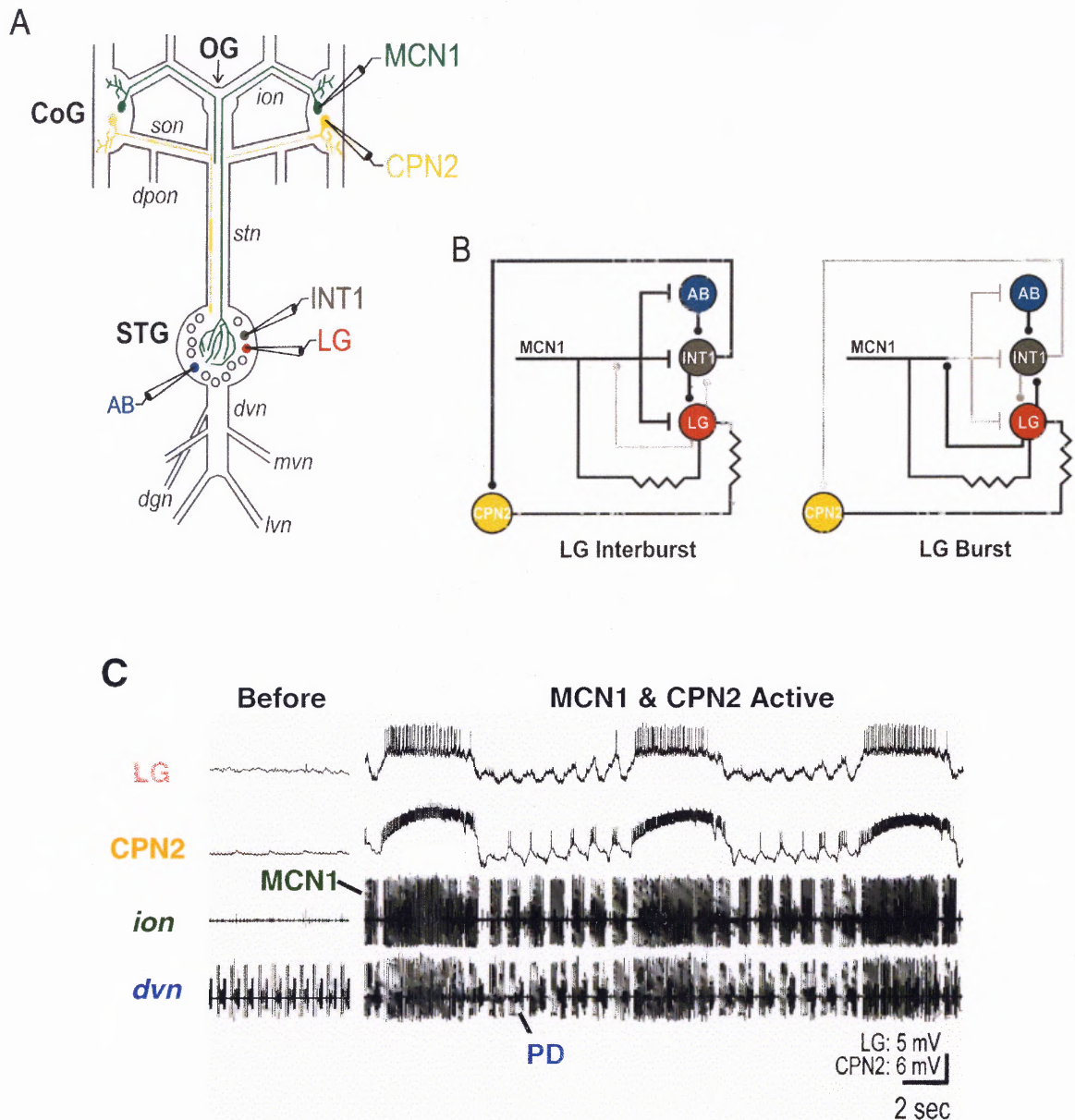


Figure 5.1 The MCN1/CPN2-Elicited Gastric Mill Rhythm. *A*, MCN1 descends into the STG via the *ion* and *stn* nerves, while CPN2 descends through the *son* and *stn* nerves (see Figure 1.2). *B*, Circuitry diagram for the MCN1/CPN2-elicited gastric mill rhythm, which consists of two phases due to the reciprocal inhibition between INT1 and the LG neuron. During the LG interburst phase, MCN1 axon terminals excite the AB, INT1 and LG neurons. During the LG burst phase, the LG neuron presynaptically inhibits MCN1, which blocks all chemical synaptic input from MCN1 within the STG. The LG neuron is also electrically coupled to the MCN1 and CPN2 axon terminals in the STG, while the cell body of CPN2 is inhibited by an inhibitory feedback synapse from INT1. *C*, In the biological system, co-stimulation of MCN1 and CPN2 elicits a gastric mill rhythm. Most hyperpolarized membrane potentials: LG -57 mV; CPN2 -66 mV (Adapted by permission from the Society for Neuroscience: Journal of Neuroscience (Beenhakker and Nusbaum, 24:6741-50, 2004), copyright (2004)). The AB and PD neurons are strongly electrically coupled and burst simultaneously.

MCN1/CPN2-Elicited Gastric Mill Rhythm

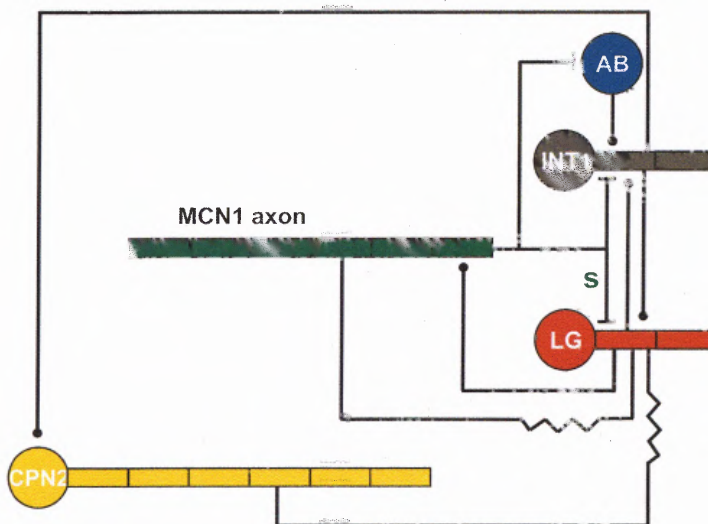
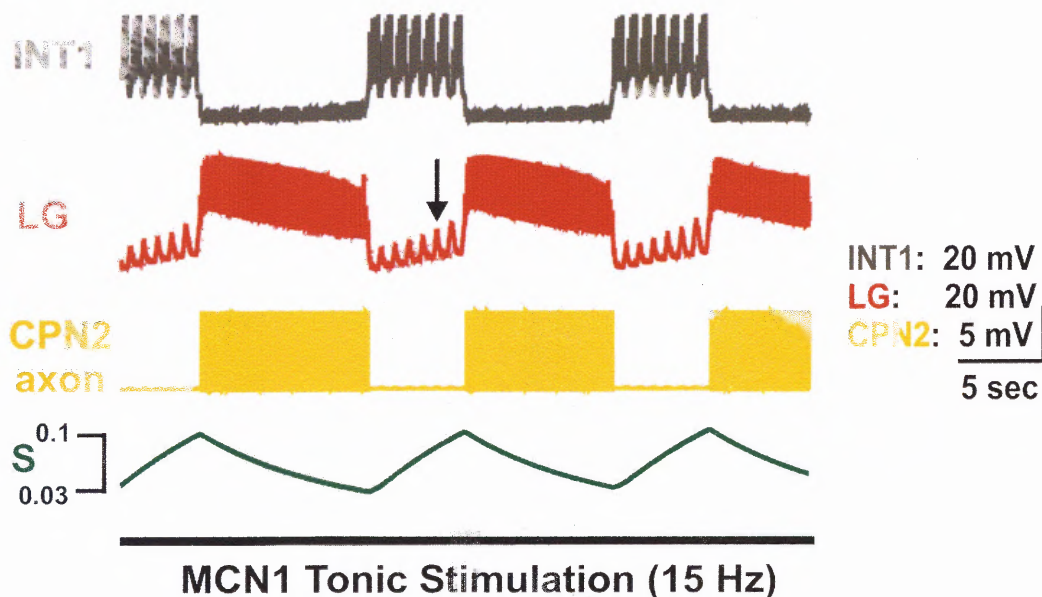


Figure 5.2 The Biophysically-Realistic Model of the MCN1/CPN2-Elicited Gastric Mill Rhythm. INT1 and the LG neuron reciprocally inhibit each other and burst in anti-phase during the gastric mill rhythm. The subthreshold depolarizations (arrow) in the LG membrane potential are due to the effect of the AB to INT1 inhibition. CPN2 is active except when inhibited by the feedback synapse from INT1. The voltage trace of CPN2 is for its axon compartment that is electrically coupled to the LG neuron. MCN1 is tonically active in the model. The slow excitation from MCN1 to the LG neuron (*s*) is also shown. In particular, *s* builds up in the LG neuron during its interburst phase but decays during the LG burst phase due to the presynaptic inhibition of MCN1. Also shown is the circuit diagram of the full biophysically-realistic model.

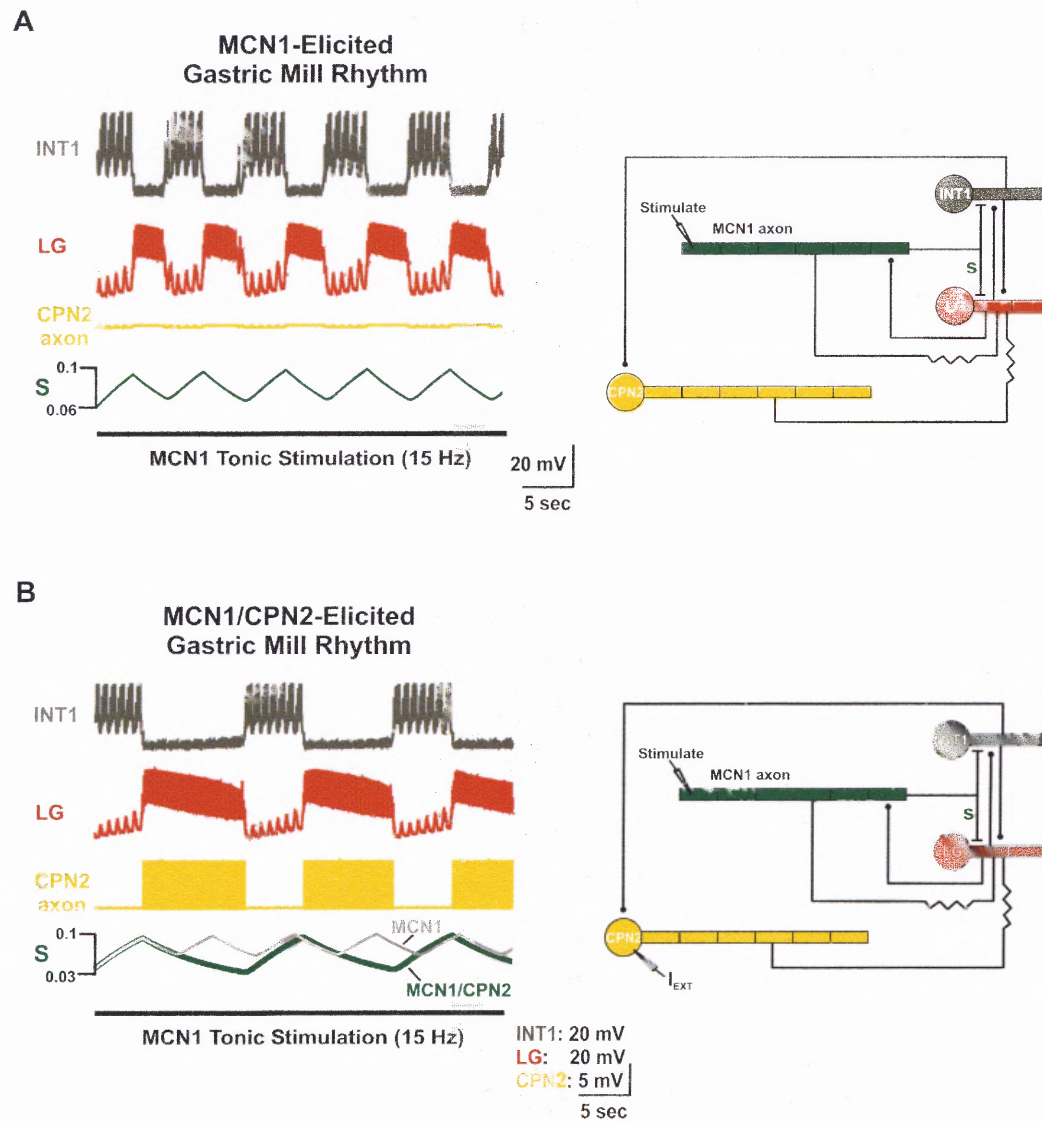


Figure 5.3 Comparing the MCN1-Elicited and MCN1/CPN2-Elicited Gastric Mill Rhythms. **A**, During the MCN1-elicited rhythm, MCN1 is tonically stimulated while CPN2 remains inactive. However, the CPN2 axon is still electrically coupled to the LG neuron and, since it is more hyperpolarized, the CPN2 axon pulls down the LG membrane potential. The slow build up and decay of MCN1 excitation (s) in the LG neuron drives the MCN1-elicited rhythm. Most hyperpolarized membrane potentials: INT1 -62 mV; LG -54 mV; CPN2 -77 mV. **B**, During the MCN1/CPN2-elicited rhythm, MCN1 and CPN2 are coactive (MCN1: tonic stimulation, CPN2: current injection). During the LG interburst phase where INT1 inhibits CPN2, the CPN2 axon still pulls down the LG membrane potential. However, during the LG burst phase where CPN2 is no longer inhibited by INT1, the CPN2 axon (max: 38 mV) pulls up the LG membrane potential (max: -15 mV) via electrical coupling. This prolongs the LG burst phase (greater decay of s) and slows the frequency of the MCN1/CPN2-elicited gastric mill rhythm compared to that of the MCN1-elicited rhythm. Most hyperpolarized membrane potentials: INT1 -62 mV; LG -57 mV; CPN2 -78 mV.

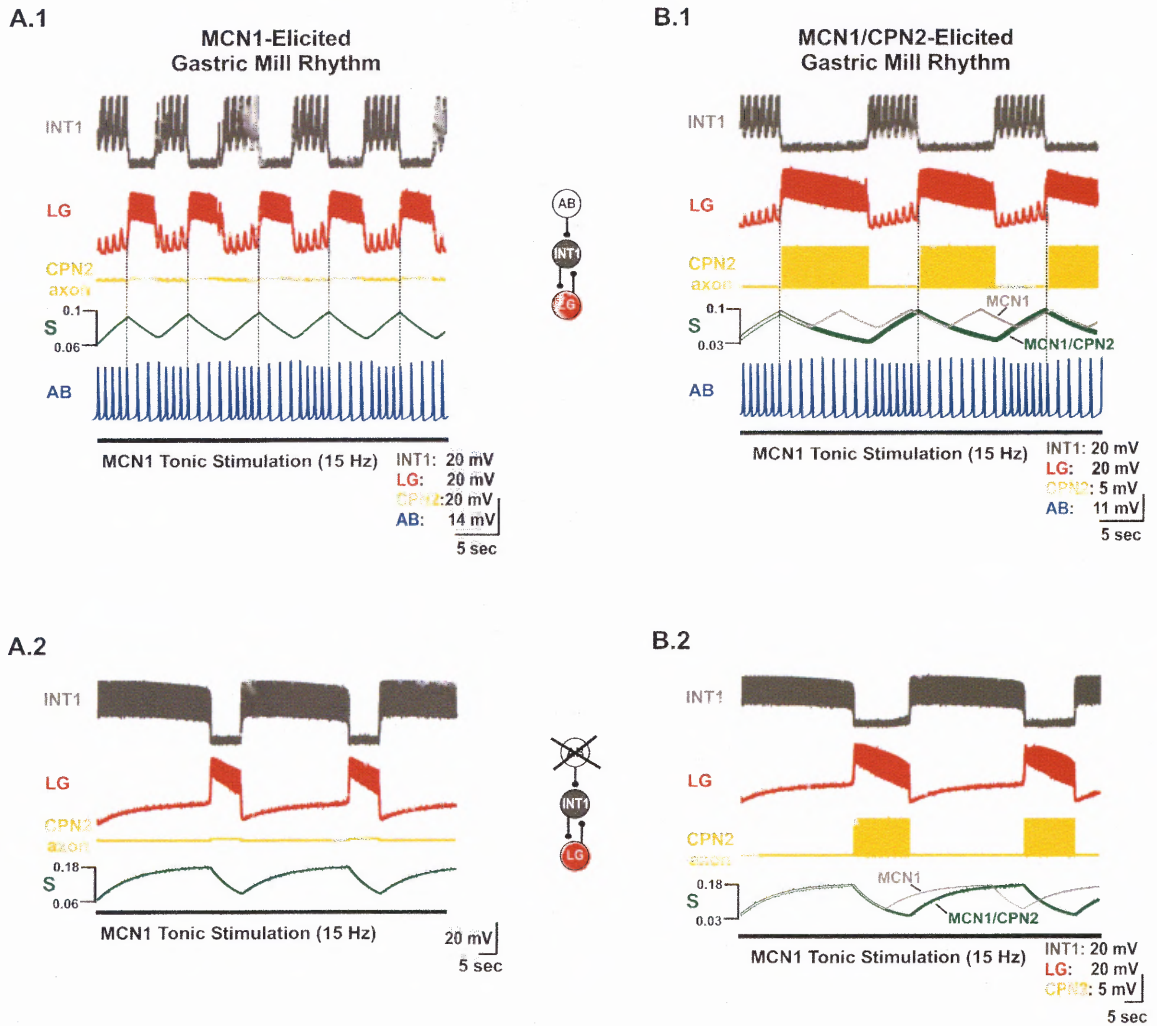


Figure 5.4 Effect of the Local AB to INT1 Inhibition. *A1*, The AB to INT1 inhibition triggers the onset of the LG burst phase during the MCN1-elicited rhythm. *A2*, The MCN1-elicited rhythm exhibits a slower frequency when the AB to INT1 inhibition is removed. *B1*, The AB to INT1 inhibition triggers the onset of the LG burst phase during the MCN1/CPN2-elicited gastric mill rhythm. *B2*, The MCN1/CPN2-elicited gastric mill rhythm exhibits a slower frequency when the AB to INT1 inhibition is removed. In both cases, the prolonged LG burst phase of the MCN1/CPN2-elicited gastric mill rhythm slows its frequency compared to that of the MCN1-elicited rhythm. Most hyperpolarized membrane potentials – same as in Figure 5.3.

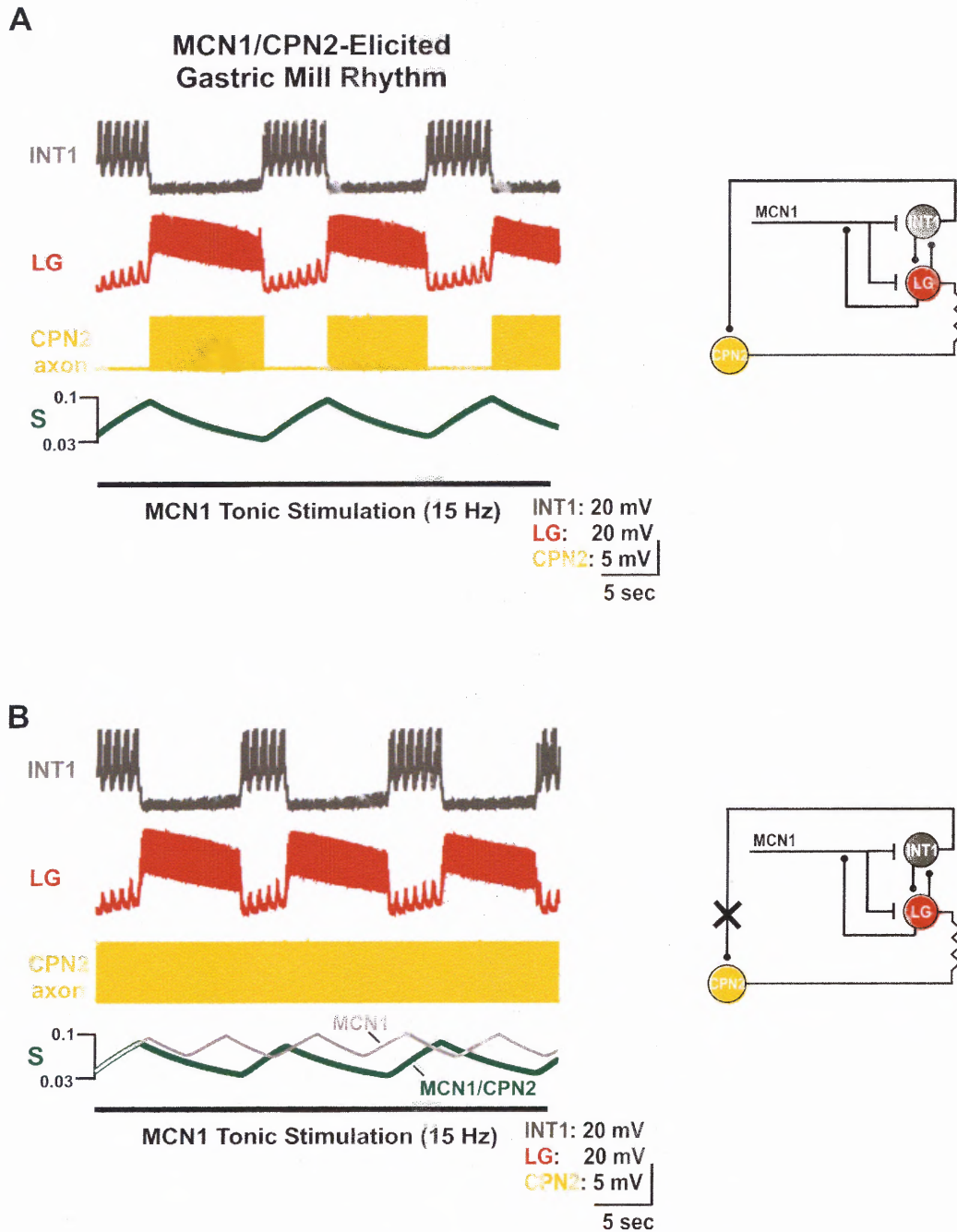


Figure 5.5 Effect of the INT1 to CPN2 Feedback Inhibition. *A*, The MCN1/CPN2-elicited gastric mill rhythm for the intact system. *B*, Removal of the INT1 to CPN2 feedback inhibition shortens the duration of the LG interburst phase compared to that of the intact system in *A*. In particular, CPN2 remains uninhibited by INT1, so the CPN2 axon pulls up the LG membrane potential (via electrical coupling) throughout the gastric mill rhythm. However, since the INT1 to CPN2 feedback inhibition is inactive during the LG burst phase, its removal does not significantly affect the duration of the LG burst. Therefore, the MCN1/CPN2-elicited gastric mill rhythm still exhibits a slower frequency than the MCN1-elicited rhythm when the INT1 to CPN2 feedback inhibition is removed. Most hyperpolarized membrane potentials – same as in Figure 5.3.

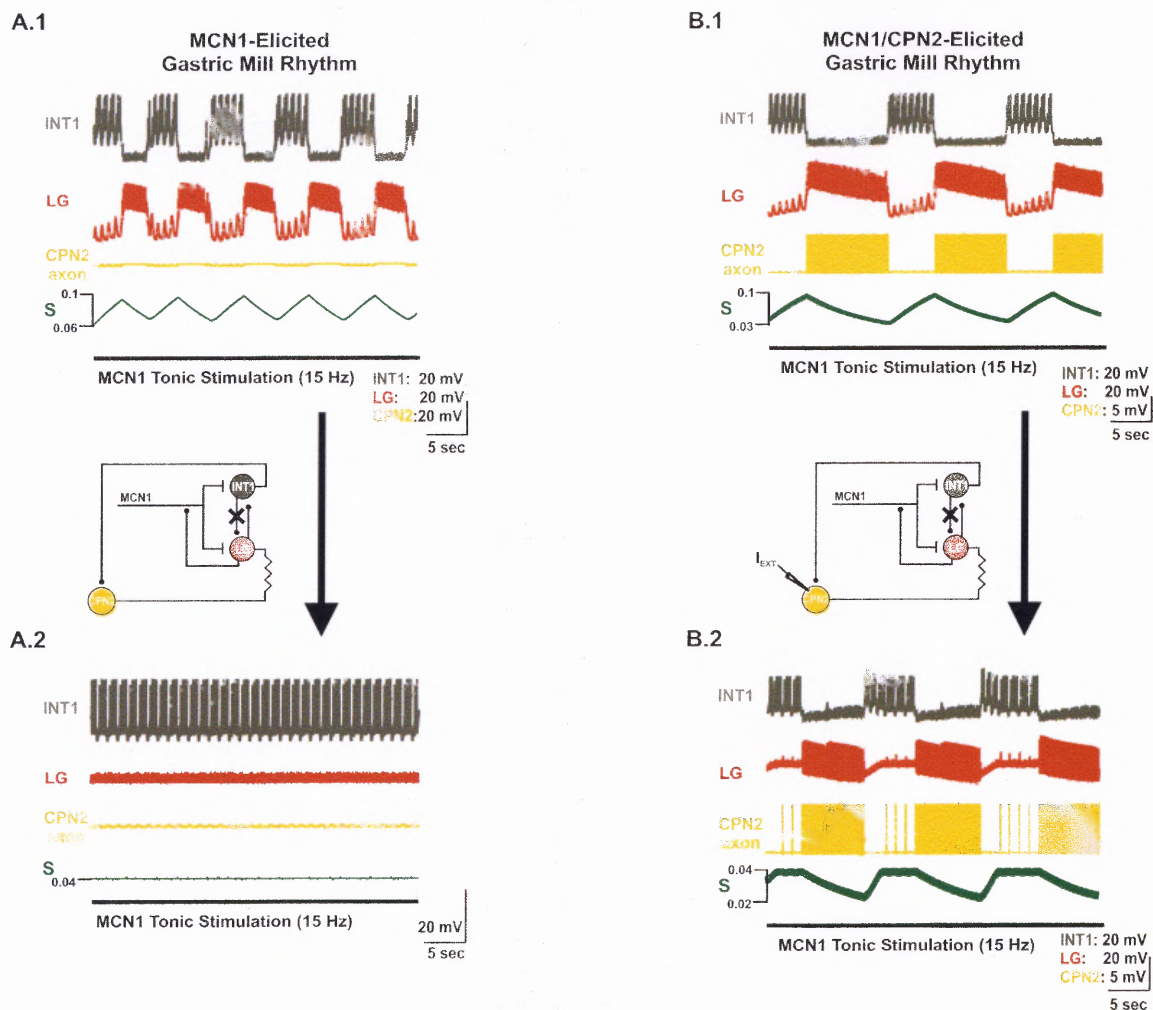


Figure 5.6 Effect of the Local INT1 to LG Inhibitory Synapse. *A.1*, The MCN1-elicited rhythm for the intact system. *A.2*, The MCN1-elicited rhythm is disrupted when the INT1 to LG inhibitory synapse is removed. Most hyperpolarized membrane potentials (*A.1* – same as in Figure 5.3), *A.2*: INT1 -59 mV; LG -39 mV; CPN2 -77 mV. *B.1*, The MCN1/CPN2-elicited gastric mill rhythm for the intact system. *B.2*, The MCN1/CPN2-elicited rhythm persists when the INT1 to LG inhibitory synapse is removed. In particular, INT1 still inhibits the LG neuron via the INT1 to CPN2 feedback pathway. However, when the INT1 to LG synapse is removed, (1) the LG interburst becomes more depolarized than in the intact system and (2) the LG neuron transitions into its burst phase after less buildup of MCN1 excitation (*s*). Most hyperpolarized membrane potentials (*B.1* – same as Figure 5.3), *B.2*: INT1 -62 mV; LG -48 mV; CPN2 -79 mV.

CHAPTER 6

CONCLUSION

6.1 Summary of Results and Discussion

The focus of this dissertation was to investigate how: (1) the neuromodulator PK can elicit a gastric mill rhythm that is similar to the MCN1-elicited rhythm (2) descending input from coactive projection neurons (MCN1 and CPN2) plus ascending feedback to these projection neurons shapes the gastric mill rhythm.

In the first case, a 2-dimensional model of the MCN1-elicited gastric mill rhythm was developed. Both state variables in this model were directly involved in generating network oscillations, which allowed for the network dynamics of this gastric mill rhythm to be fully described via a phase-plane analysis. Next, three different mechanisms were proposed by which PK could elicit a gastric mill rhythm that is similar to the MCN1-elicited rhythm. Then, all three PK mechanisms that were proposed in the 2-dimensional model were also shown to elicit a gastric mill rhythm that is similar to the MCN1-elicited rhythm in the context of a more biophysically-realistic model. Finally, the network-level properties of the MCN1-elicited and PK-elicited gastric mill rhythms were compared to investigate which circuit components coordinate activity in each gastric mill rhythm.

In the second case, a 2-dimensional model was developed to compare the network dynamics of the MCN1-elicited and MCN1/CPN2-elicited gastric mill rhythms via their geometrical properties in the phase plane. In particular, both gastric mill rhythms were studied for the cases in which (1) MCN1 is tonically active and (2) MCN1 is rhythmically active due to inhibitory feedback from the pyloric circuit. Then, the network dynamics of the MCN1/CPN2-elicited gastric mill rhythm were examined for a

third case in which MCN1 exhibits an alternating (rhythmic/tonic) activity pattern. In this third case, pyloric-timed activity in CPN2 was shown to play a crucial role for shaping the motor pattern of the gastric mill rhythm. Finally, the predictions of the 2-dimensional model were assessed with a more biophysically-realistic model for the case in which MCN1 is tonically active. In particular, the MCN1/CPN2-elicited gastric mill rhythm was shown to persist in the absence of reciprocal inhibition between INT1 and the LG neuron.

Now, the findings of this dissertation are outlined. First, the comparison of the MCN1-elicited and PK-elicited gastric mill rhythms (Chapters 2 and 3) is discussed. Then, the investigation into the network dynamics of the MCN1-elicited and MCN1/CPN2-elicited gastric mill rhythms (Chapters 4 and 5) is discussed.

6.1.1 Comparing the MCN1-Elicited and PK-Elicited Gastric Mill Rhythms

The purpose of this work was to investigate how the neuromodulator PK can elicit a gastric mill rhythm that is similar to the MCN1-elicited rhythm. In the biological system, the gastric mill rhythm is generally not spontaneously active, but tonic stimulation of the projection neuron MCN1 elicits a gastric mill rhythm *in vitro* (Coleman et al., 1995). Recent experiments showed that bath application of PK elicits a similar gastric mill rhythm in the absence of MCN1 participation (Hertzberg and Nusbaum, 2004, 2005). Moreover, PK is the first known neuromodulator that faithfully elicits a gastric mill rhythm when bath applied to the STG. However, the mechanism by which PK elicits a gastric mill rhythm is unknown.

This dissertation used mathematical modeling to propose three different mechanisms by which PK could elicit a gastric mill rhythm that is similar to the MCN1-elicited rhythm. First, a 2-dimensional model of the MCN1-elicited gastric mill rhythm was developed that was based upon the 3-dimensional model of (Manor et al., 1999). In particular, the geometrical properties of the 3-dimensional model were used to reduce it down to 2 dimensions. This allowed for the network dynamics of the MCN1-elicited rhythm to be fully described via a phase-plane analysis. Then, three different mechanisms were proposed by which PK could elicit a similar gastric mill rhythm in the absence of MCN1 participation. In the biological system, the reciprocally inhibitory gastric mill neurons INT1 and LG sit at high and low membrane potentials, respectively, in the absence of projection neuron input (Bartos et al., 1999). As a result, the gastric mill rhythm is generally not spontaneously active in the biological system. Therefore, the hypothesis of this dissertation was that PK elicits a gastric mill rhythm by inducing voltage-gated ionic currents in the LG neuron. This would allow for LG to overcome its inhibition by INT1, which would therefore activate the gastric mill rhythm in the absence of MCN1 participation.

First, PK-induction of a low-threshold, slowly-inactivating inward current (I_{Plat}) in the LG neuron was shown to elicit a gastric mill rhythm that is similar to the MCN1-elicited rhythm. I_{Plat} has both a fast activation and a slow inactivation. In particular, activation of I_{Plat} facilitates depolarization of the LG neuron, while inactivation of I_{Plat} repolarizes LG. Moreover, when PK induces I_{Plat} in the LG neuron, the PK-elicited gastric mill rhythm is controlled by the slow inactivation dynamics of I_{Plat} . Next, a second mechanism was proposed by which PK-induction of a slow, hyperpolarization-

activated inward current (I_h) in the LG neuron also elicits a similar gastric mill rhythm. However, I_h is a non-inactivating current, and the dynamics of I_h are mathematically equivalent to the mechanism by which MCN1 elicits a gastric mill rhythm. Thus, the second mechanism (I_h) was used to suggest that PK-induction of an inactivating current (such as I_{Plat}) is not necessary for eliciting a gastric mill rhythm. Then, a third mechanism was proposed that involved PK-induction of two non-inactivating currents in the LG neuron. In particular, a fast inward current (I_{Proc}) plus a slow outward current (I_K) was also shown to elicit a similar gastric mill rhythm when induced by PK in the LG neuron. Moreover, I_{Proc} facilitates depolarization of the LG neuron while I_K repolarizes LG during this PK-elicited gastric mill rhythm. In addition, the slow dynamics of I_K control the PK-elicited rhythm for the third proposed mechanism. Thus, all three PK mechanisms elicit a similar gastric mill rhythm in the 2-dimensional model.

In addition, all three PK mechanisms generate plateau properties in the LG neuron. In particular, each proposed mechanism involves the induction of a slow current in the LG neuron, which generates a plateau potential in LG after a brief depolarizing current pulse. Similarly, in the biological system, bath application of PK also generates plateau properties in the LG neuron (Hertzberg and Nusbaum, 2004). Thus, all three proposed PK mechanisms elicit a gastric mill rhythm that exhibits the properties of the PK-elicited rhythm in the biological system. Therefore, this dissertation predicts that PK-modulation of the LG neuron alone is sufficient for eliciting a gastric mill rhythm and that PK-modulation of INT1 is therefore not necessary.

Next, the individual MCN1-elicited and PK-elicited gastric mill rhythms were generalized into a single 2-dimensional model. This generalized model was used to

describe the properties of the gastric mill rhythm without worrying about the specifics of the individual MCN1-elicited or PK-elicited systems. Then, geometric singular perturbation theory (Mishchenko and Rozov, 1980) was used to track the phase-plane trajectory of the generalized model with a singular trajectory composed from lower dimensional sets of equations. The simplified properties of the singular trajectory were then used to compute bounds on the gastric mill period. These bounds were computed by estimating the minimum and maximum values of the slow variable on the cubic V_L -nullcline in the phase plane. Physiologically, these bounds model the cycle-to-cycle variability of the gastric mill period that is observed in the biological system (Bartos et al., 1999). In particular, the local AB to INT1 inhibition, which triggers the onset of the LG burst phase, also varies the period of the gastric mill rhythm in the biological system.

Next, the MCN1-elicited and PK-elicited gastric mill rhythms were compared with a more biophysically-realistic model. First, all three PK mechanisms that were proposed in the 2-dimensional model were also shown to elicit a gastric rhythm that is similar to the MCN1-elicited rhythm in the biophysically-realistic model as well. Then, each PK mechanism also produced plateau properties in the LG neuron of the biophysically-realistic model. Finally, each PK mechanism failed to elicit a gastric mill rhythm when the AB to INT1 inhibitory synapse was removed. Similarly, in the biological system, bath application of PK does not elicit a gastric mill rhythm when the AB to INT1 inhibition is removed (Hertzberg and Nusbaum, 2004). Thus, all three PK mechanisms are equivalent from the perspective of the biophysically-realistic model since they each elicit a gastric mill rhythm that exhibits the same properties.

The predictions of the model can be checked through the use of current blockers in the biological system. In particular, pharmacological agents that block the proposed PK-induced currents can be used to check if these currents are also involved in the PK-elicited gastric mill rhythm of the biological system. For example, to check the second proposed mechanism, bath application of cesium (Cs^+) can be used to block I_h in the biological system (Angstadt and Calabrese, 1989). Thus, if Cs^+ application during the PK-elicited gastric mill rhythm modifies or disrupts the activity of the LG neuron, then this would indicate that PK indeed induces I_h in the LG neuron to elicit a gastric mill rhythm. On the other hand, if Cs^+ application leaves the activity of the LG neuron unchanged, then this would indicate that I_h is not involved in the PK-elicited rhythm of the biological system. In the third mechanism, PK was proposed to induce $I_{Proc} + I_K$ in the LG neuron. However, this mechanism would be difficult to test in the biological system because there are no known pharmacological agents that effectively block proctolin receptors in the biological system (M.P. Nusbaum, personal communication). However, the biophysically-realistic model was used to check if I_{Proc} is necessary for eliciting a gastric mill rhythm (see Figure 3.3). In particular, I_{Proc} , which facilitates depolarization of the LG neuron, was removed from the model, and the LG neuron was instead depolarized by current injection (I_{Ext}). However, since a modified gastric mill rhythm was elicited in the absence of I_{Proc} , the model predicts that I_{Proc} is necessary for PK to elicit a gastric mill rhythm that is similar to the MCN1-elicited rhythm. Finally, in the first mechanism, PK was proposed to induce a low-threshold, slowly-inactivating inward current (I_{Plat}) in the LG neuron. This current describes a low-threshold calcium (Ca^{2+}) current in the biological system. However, there are no known pharmacological

agents that effectively block low-threshold Ca^{2+} currents in the STG, so the first mechanism can not be checked through the use of current blockers in the biological system.

Next, the functional circuits that control the MCN1-elicited and PK-elicited gastric mill rhythms were compared. In particular, since PK elicits a gastric mill rhythm in the absence of MCN1 participation, the PK-elicited rhythm does not involve presynaptic inhibition of projection neurons. Therefore, the role of this presynaptic inhibition during the gastric mill rhythm was investigated using the biophysically-realistic model. First, the DG neuron was added to the biophysically-realistic model. Then, presynaptic inhibition during the MCN1-elicited gastric mill rhythm was shown to be necessary for both (1) generating rhythmic bursting between INT1 and the LG neuron and (2) coordinating the timing of DG neuron activity. In contrast, during the PK-elicited rhythm, which does not involve presynaptic inhibition, rhythmic bursting between INT1 and the LG neuron was controlled by the PK-induced plateau properties in the LG neuron. Moreover, the timing of network activity during the PK-elicited gastric mill rhythm was shown to be coordinated by a PK-strengthened inhibitory synapse from the DG to LG neuron, but this synapse is not functional during the MCN1-elicited rhythm. Thus, although the MCN1-elicited and PK-elicited gastric mill rhythms appear similar, their locus of coordination is different. In particular, presynaptic inhibition of MCN1 is crucial for coordinating network activity in the MCN1-elicited gastric mill rhythm, while PK-induced plateau properties in the LG neuron plus a PK-strengthened DG to LG synapse coordinate network activity during the PK-elicited rhythm.

Finally, the behavioral significance of the MCN1-elicited and PK-elicited gastric mill rhythms was studied. In particular, the biophysically-realistic model was used to investigate what types of chewing modes can be activated by each gastric mill rhythm. *In vivo*, the LG neuron controls protraction of the lateral gastric teeth, while the DG neuron controls retraction of the medial gastric tooth. During the MCN1-elicited gastric mill rhythm, the LG neuron, via presynaptic inhibition of MCN1, (1) controls the timing of DG neuron activity and (2) can reset the MCN1-elicited rhythm. Therefore, the model suggests that MCN1 elicits a gastric mill rhythm that is controlled by the protraction phase of the lateral gastric teeth. In contrast, during the PK-elicited rhythm, which does not involve presynaptic inhibition, the LG neuron does not control the timing of DG neuron activity. Instead, the PK-strengthened DG to LG inhibitory synapse allows the DG neuron to (1) control the timing of LG neuron activity and (2) reset the PK-elicited gastric mill rhythm. Therefore, the model suggests that PK elicits a gastric mill rhythm that is controlled by the retraction phase of the medial gastric tooth.

6.1.2 Network Dynamics of the MCN1-Elicited and MCN1/CPN2-Elicited Gastric Mill Rhythms

The purpose of this work was to investigate the interaction between a rhythmic network and two co-active projection neurons. Generally, this interaction is studied assuming a feed-forward architecture, in which neural input from the projection neurons shapes the activity of the rhythmic network, as documented in both vertebrate (Swain et al., 1993; Bussieres et al., 1999; Burke, 2001; Yamaguchi, 2004) and invertebrate (Blitz et al., 2004; Jing and Weiss, 2005; Marder et al., 2005) systems. However, this dissertation

also includes the effect of rhythmic feedback from the target network to the projection neurons. Such rhythmic feedback can influence the pattern of projection neuron inputs (Weeks, 1981; Kasicki et al., 1989; Norris et al., 1994; Perrins and Weiss, 1996; Wood et al., 2004), but its role for shaping network activity is not well understood.

This dissertation addressed these issues using a reduced 2-dimensional model of the gastric mill rhythm. In the biological system, the gastric mill rhythm is elicited by stimulation of MCN1 (Bartos et al., 1999; Wood et al., 2004) or by co-stimulation of MCN1 and CPN2 (Blitz and Nusbaum, 1997; Beenhakker and Nusbaum, 2004). The 2-dimensional mathematical model in this work was used to investigate how (1) feed-forward synaptic input from MCN1 and CPN2 and how (2) rhythmic feedback to these projection neurons shapes the gastric mill rhythm. In particular, both state variables of the 2-dimensional model were directly involved in generating network oscillations, so the network dynamics of the MCN1-elicited and MCN1/CPN2-elicited gastric mill rhythms were readily described via a phase-plane analysis.

6.1.2.1 Effect of the Local AB to INT1 Inhibition on the MCN1-Elicited Gastric Mill Rhythm. First, the 2-dimensional model was used to investigate how the local AB to INT1 inhibition affects the network dynamics of the MCN1-elicited rhythm, for the case in which MCN1 is tonically active. In this case, the AB to INT1 inhibition (1) increases the frequency of network oscillations and (2) triggers the onset of the LG burst phase during the MCN1-elicited rhythm. Both of these effects were also documented in previous modeling (Nadim et al., 1998) and experimental (Bartos et al., 1999) studies. Thus, the 2-dimensional model reproduced the effects of the local AB to INT1 inhibition

on the MCN1-elicited rhythm. In particular, the AB to INT1 inhibition shortens the duration of the phase-plane trajectory on the left and right branches of the V_L -nullcline, which increases the frequency of network oscillations (Figure 4.3). Moreover, the AB to INT1 inhibition initiates the jump to the right branch of the V_L -nullcline, which triggers the onset of the LG burst phase during the MCN1-elicited rhythm.

6.1.2.2 *Effect of the AB to MCN1 Feedback Inhibition on the MCN1-Elicited Rhythm.*

Next, the effect of the AB to MCN1 feedback inhibition was included in the 2-dimensional system in order to investigate its effect on the network dynamics of the MCN1-elicited rhythm. In the biological system, MCN1 is rhythmically active in the presence of the AB to MCN1 feedback inhibition (Coleman and Nusbaum, 1994). Moreover, the frequency of the MCN1-elicited rhythm becomes insensitive to the effect of the local AB to INT1 inhibition (in the STG) when the AB to MCN1 feedback inhibition (in the CoG) remains intact (Wood et al., 2004). A previous mathematical model showed that the AB to INT1 inhibition (in the STG) must occur at nearly the same phase of the pyloric rhythm as the AB to MCN1 feedback inhibition (in the CoG) in order to elicit a gastric mill rhythm with the observed frequency in the biological system (Ambrosio et al., 2005; Ambrosio-Mouser et al., 2006). In the 2-dimensional model of this dissertation, the AB to INT1 inhibition and the AB to MCN1 feedback inhibition were assumed to occur at the same phase of the pyloric rhythm in order to simplify the network dynamics in the phase plane. Moreover, this assumption was a reasonable approximation of the biological system (Figure 4.5).

This dissertation showed that the onset of the LG burst phase is no longer triggered by the local AB to INT1 inhibition (in the STG) when MCN1 is rhythmically active. Instead, an episode of the feed-forward MCN1 to LG excitation, that is uninterrupted by the AB to MCN1 feedback inhibition (in the CoG), triggers the onset of the LG burst phase (Figure 4.6), as was also reported in the biological system (Wood et al., 2004). In particular, when MCN1 is rhythmically active, the onset of the LG burst phase is initiated during an episode of the feed-forward MCN1 to LG excitation in 93% of preparations in the biological system (Wood et al., 2004). In addition, the 2-dimensional model in this dissertation also showed that, when MCN1 is rhythmically active, a greater buildup of MCN1 excitation (s) is required to initiate the onset of the LG burst, since the jump to the right branch of the V_L -nullcline only occurs when a phase point reaches the unforced left knee (Figure 4.6). Therefore, a timing mismatch between the AB to INT1 inhibition (in the STG) and the AB to MCN1 feedback inhibition (in the CoG) would not only increase the frequency of network oscillations, as reported by (Ambrosio-Mouser et al., 2006), but would also allow for the AB to INT1 inhibition to initiate the jump to the right branch of the V_L -nullcline, and hence trigger the onset of the LG burst phase, which does not occur in the biological system.

It was also shown that the AB to MCN1 feedback inhibition (in the CoG) terminates the LG burst phase of this MCN1-elicited gastric mill rhythm. In particular, the AB to MCN1 feedback inhibition initiates the jump back to the left branch of the V_L -nullcline in the model (Figure 4.6). Thus, when MCN1 is rhythmically active, the pyloric circuit (via the AB to MCN1 feedback inhibition) terminates the LG burst phase of the MCN1-elicited gastric mill rhythm.

Furthermore, the local AB to INT1 inhibition (in the STG) was shown to prolong the duration of the LG burst phase when MCN1 is rhythmically active (Figure 4.7). A similar result was reported in the biological system, where the AB to INT1 inhibition increases the duty cycle of the LG neuron (Wood et al., 2004), which is the fraction of the gastric mill period for which the LG neuron is in its burst phase. However, contrary to the findings of (Wood et al., 2004), where it was reported that the local AB to INT1 inhibition does not affect the frequency of the MCN1-elicited rhythm when MCN1 is rhythmically active, this dissertation showed that the AB to INT1 inhibition slows the frequency of this gastric mill rhythm since it prolongs the duration of the LG burst phase (Figure 4.7). Yet, similar to that reported by (Wood et al., 2004) in the biological system, this dissertation showed that the AB to INT1 inhibition decreases the latency between the onset of the LG burst phase and the onset of the preceding episode of the MCN1 to LG excitation during this MCN1-elicited rhythm (Figure 4.6).

Hence, the network dynamics of the MCN1-elicited gastric mill rhythm are changed by the AB to MCN1 feedback inhibition. In particular, the AB to INT1 inhibition (in the STG) no longer increases the frequency of network oscillations nor triggers the onset of the LG burst phase when MCN1 is rhythmically active. Instead, this dissertation showed that the AB to INT1 inhibition slows the frequency of network oscillations by prolonging the duration of the LG burst phase. Moreover, when MCN1 is rhythmically active, the pyloric circuit terminates the LG burst phase via the AB to MCN1 feedback inhibition (in the CoG).

6.1.2.3 *CPN2 Changes the Network Dynamics of the MCN1-Elicited Rhythm.* Next, the projection neuron CPN2 was incorporated into the 2-dimensional model to investigate how its addition to the network changes the dynamics of the MCN1-elicited rhythm. In the biological system, the MCN1/CPN2-elicited gastric mill rhythm exhibits a slower frequency than the MCN1-elicited rhythm (Blitz and Nusbaum, 1997), which was also shown to occur in the 2-dimensional model of this dissertation. In particular, during the LG interburst phase, CPN2 is strongly inhibited by a feedback synapse from INT1. As a result, CPN2 pulls down the LG membrane potential via its local electrical coupling with the LG neuron in the STG. As a result, a greater buildup of MCN1 excitation (s) is required in the LG neuron before it can transition into its burst phase (Figure 4.9). Then, during the LG burst phase of the MCN1/CPN2-elicited rhythm, CPN2 is no longer inhibited by INT1. As a result, CPN2 pulls up the LG membrane potential, via its local electrical coupling with LG, so that a greater decay of MCN1 excitation (s) is required before the LG neuron can transition back down into its interburst phase (Figure 4.9).

Moreover, for the case in which MCN1 is tonically active, the local AB to INT1 inhibition (in the STG) was shown to both increase the frequency of network oscillations and initiate the onset of the LG burst phase for the MCN1/CPN2-elicited gastric mill rhythm. Hence, when MCN1 is tonically active, the AB to INT1 inhibition has similar effects on the MCN1-elicited and MCN1/CPN2-elicited gastric mill rhythms.

Then, the MCN1/CPN2-elicited gastric mill rhythm was shown to persist after removal of the INT1 to LG inhibitory synapse. In the biological system, reciprocal inhibition between INT1 and the LG neuron is required for the MCN1-elicited rhythm to occur (Bartos et al., 1999). However, the MCN1/CPN2-elicited gastric mill rhythm

persists when the INT1 to LG inhibitory synapse is pharmacologically removed in the biological system (Akay et al., 2004). Using the 2-dimensional model, this dissertation showed that the INT1 to CPN2 feedback inhibition provides a second, indirect pathway by which INT1 inhibits the LG neuron (Figure 4.12). As a result, INT1 continues to inhibit the LG neuron through this indirect pathway so that the MCN1/CPN2-elicited gastric mill rhythm persists when the direct INT1 to LG inhibitory synapse is removed. Hence, although reciprocal inhibition between INT1 and the LG neuron is required for the MCN1-elicited rhythm, the INT1 to CPN2 feedback pathway changes the locus of pattern generation in the gastric mill rhythm so that the MCN1/CPN2-elicited rhythm persists without this reciprocal inhibition.

6.1.2.4 Effect of the AB to MCN1 Feedback Inhibition on the MCN1/CPN2-Elicited Gastric Mill Rhythm. Next, the AB to MCN1 feedback inhibition was included in the 2-dimensional model of the MCN1/CPN2-elicited gastric mill rhythm. During the MCN1-elicited rhythm (Figures 4.6-4.7), this feedback synapse (in the CoG) was assumed to occur at the same phase of the pyloric rhythm as the local AB to INT1 inhibition (in the STG) in order to simplify the network dynamics in the phase plane. Using this same approximation, the AB to MCN1 feedback inhibition was shown to have similar effects on the network dynamics of the MCN1/CPN2-elicited gastric mill rhythm.

In particular, the onset of the LG burst phase is no longer triggered by the AB to INT1 inhibition (in the STG) when MCN1 is rhythmically active. Instead, an episode of the feed-forward MCN1 to LG excitation, that is uninterrupted by the AB to MCN1 feedback inhibition (in the CoG), triggers the onset of the LG burst phase. Moreover, the

AB to MCN1 feedback inhibition initiates the termination of the LG burst phase during this MCN1/CPN2-elicited rhythm. Furthermore, as occurs in the MCN1-elicited rhythm, the local AB to INT1 inhibition (in the STG) prolongs the duration of the LG burst phase, which in turn slows the frequency of the MCN1/CPN2-elicited gastric mill rhythm (Figure 4.16).

In the biological system, stimulation of the post-oesophageal commissure (POC) neurons activates an MCN1/CPN2-elicited gastric mill rhythm in which MCN1 is rhythmically active (R.S. White, D.M. Blitz, and M.P. Nusbaum, unpublished data). Therefore, the predictions of the 2-dimensional model in this dissertation could provide meaningful insights for understanding the network properties of the gastric mill rhythm that is facilitated by POC stimulation in the biological system.

6.1.2.5 VCN-Influenced Activity in MCN1 and CPN2 Changes the Network Dynamics of the Gastric Mill Rhythm. In the biological system, the VCN sensory neurons elicit a gastric mill rhythm via co-activation of projection neurons in the CoG (Beenhakker and Nusbaum, 2004). However, co-stimulation of MCN1 and CPN2 in their VCN-influenced activity patterns is sufficient for eliciting a gastric mill rhythm that closely resembles the VCN-elicited rhythm in the biological system (Beenhakker and Nusbaum, 2004). During this gastric mill rhythm, MCN1 is rhythmically active during the LG interburst phase but tonically active during the LG burst phase. Therefore, the AB to MCN1 feedback inhibition only affects the network dynamics of this gastric mill rhythm during the LG interburst phase. On the other hand, the activity of CPN2 is similar to that described in the previous MCN1/CPN2-elicited gastric mill rhythms.

Using the 2-dimensional model, the network dynamics of this MCN1/CPN2-elicited gastric mill rhythm were shown to be crucially dependent upon the local AB to INT1 inhibition (in the STG). In particular, the AB to INT1 inhibition affects this gastric mill rhythm via two pathways (Figure 4.17). First, the AB to INT1 inhibition disrupts the INT1 to LG inhibitory synapse, which depolarizes the LG membrane potential. Moreover, the AB to INT1 inhibition also disrupts the INT1 to CPN2 feedback synapse (Figure 4.17), which depolarizes the CPN2 membrane potential, and whose effect is manifested in the LG neuron via its electrical coupling with CPN2.

First, the forcing effect of the AB to INT1 inhibition was assumed to be transmitted simultaneously through both pathways. In this case, the onset of the LG burst phase was initiated by an episode of the feed-forward MCN1 to LG excitation that is uninterrupted by the AB to MCN1 feedback inhibition (Figure 4.18). Moreover, the local AB to INT1 inhibition has no effect on the frequency of the MCN1/CPN2-elicited gastric mill rhythm for this case (Figure 4.19).

However, the network dynamics of the MCN1/CPN2-elicited rhythm are changed if the forcing effect of the AB to INT1 inhibition is transmitted through the two pathways in anti-phase. In particular, the forcing effect of the AB to INT1 inhibition through the latter CPN2 pathway was delayed by $\frac{1}{2}$ of a pyloric period in order to approximate the behavior of the biological system (Figure 4.20). In this case, the onset of the LG burst phase is instead triggered by the AB to INT1 inhibition, via its delayed forcing effect through the CPN2 pathway (Figure 4.21). Moreover, the AB to INT1 inhibition increases the frequency of the MCN1/CPN2-elicited rhythm in this case (Figure 4.22). Hence, the local AB to INT1 inhibition (in the STG) plays an important role for shaping the network

dynamics of this MCN1/CPN2-elicited gastric mill rhythm. In the biological system, recent experiments showed that the AB to INT1 inhibition increases the frequency of the MCN1/CPN2-elicited gastric mill rhythm when MCN1 and CPN2 exhibit their VCN-influenced activity patterns (M. Kirby and M.P. Nusbaum, unpublished data). Therefore, this implies that the forcing effect of the AB to INT1 inhibition is not transmitted simultaneously through both pathways, as suggested by this dissertation.

6.1.2.6 *Biophysically-Realistic Model of the MCN1/CPN2-Elicited Gastric Mill Rhythm.*

Then, the biophysically-realistic model was used to compare the MCN1-elicited and MCN1/CPN2-elicited gastric mill rhythms for the case in which MCN1 is tonically active. However, unlike the reduced 2-dimensional model, the biophysically-realistic model included the fact that CPN2 axon terminals are electrically coupled to the LG neuron during both gastric mill rhythms in the biological system. Therefore, CPN2 axon terminals pull down the LG membrane potential during the LG interburst phase of both gastric mill rhythms in the biophysically-realistic model. In contrast, the electrical coupling between CPN2 axon terminals and the LG neuron prolongs the LG burst phase of the MCN1/CPN2-elicited gastric mill rhythm but not the MCN1-elicited rhythm. Therefore, the MCN1/CPN2-elicited gastric mill rhythm exhibits a slower frequency in the biophysically-realistic model due its prolonged LG burst phase.

Moreover, reciprocal inhibition between INT1 and the LG neuron is necessary for producing the MCN1-elicited rhythm in the model. In contrast, the MCN1/CPN2-elicited gastric mill rhythm persists when the INT1 to LG inhibitory synapse is removed, as was also shown in the 2-dimensional model. Thus, reciprocal inhibition between INT1 and

the LG neuron is not necessary for producing a gastric mill rhythm when MCN1 and CPN2 are co-active. However, since the network activity of the MCN1/CPN2-elicited rhythm is modified when the INT1 to LG inhibitory synapse is removed, the biophysically-realistic model suggests that the INT1 to LG inhibitory synapse is necessary for producing the MCN1/CPN2-elicited gastric mill rhythm that is observed in the biological system.

6.2 Applications to More Complex Systems

This dissertation used mathematical and biophysically-realistic modeling to investigate how oscillations are elicited in a rhythmic network by way of (1) neuromodulation and (2) projection neuron input. Neuromodulation, which is pervasive in the nervous systems of animals, alters the cellular and/or synaptic properties within a neural network, which allows for the same network to generate multiple activity patterns (Katz, 1995b; Stein, 1997; Marder and Bucher, 2001; Marder and Thirumalai, 2002; LeBeau et al., 2005). One advantage of extensive neuromodulation is that it provides the same network with the flexibility to generate multiple activity patterns that may potentially underlie distinct behaviors (Nusbaum et al., 2001; Marder et al., 2005). However, such extensive neuromodulation is undoubtedly balanced out in the nervous system by circuit architectures that prevent overmodulation or loss of function (Marder and Thirumalai, 2002; Prinz et al., 2004). To this end, the neuromodulator PK elicits a gastric mill rhythm that is similar to the MCN1-elicited rhythm by way of a different functional circuit. Moreover, this example in which distinct inputs elicit a similar gastric mill

rhythm by using different functional circuits could have important implications for understanding how neural networks are configured within the more complex nervous systems of vertebrates. Therefore, the findings of this dissertation could provide insights for understanding how neuromodulators both elicit network oscillations and configure functional circuits within the more complex central nervous systems of vertebrates.

Projection neurons also play an important role for shaping network activity. For example, in mammals, descending projection neuron pathways from the brain influence the rhythmic motor networks that generate locomotor activity in the spinal cord (Burke, 2001; Matsuyama et al., 2004; Yamaguchi, 2004; Rossignol et al., 2006). Similarly, in the lamprey, feed-forward projection neurons from the reticular nuclei influence the rhythmic motor networks that generate swimming activity in the spinal cord (Swain et al., 1993; Bussi eres et al., 1999). Although projection neurons are in turn influenced by rhythmic feedback from their target networks (Perreault et al., 1993; Zelenin, 2005), the role of this feedback is not well understood. This dissertation investigated the interaction between two co-active projection neurons and a rhythmic network. In particular, this dissertation showed how feedback to projection neurons shapes the gastric mill rhythm. In the case of the MCN1/CPN2-elicited gastric mill rhythm, the INT1 to CPN2 feedback synapse was shown to change locus of pattern generation in the gastric mill rhythm, in that the MCN1/CPN2-elicited rhythm persists without reciprocal inhibition between INT1 and the LG neuron. The findings of this dissertation could provide insights for understanding how feedback to projection neurons shapes activity in the more complex neural circuits of the vertebrate spinal cord, whose circuitry is at best crudely known.

APPENDIX A

PARAMETERS FOR THE BIOPHYSICALLY-REALISTIC MODELS OF THE MCN1-ELICITED AND PK-ELICITED GASTRIC MILL RHYTHMS

This appendix gives the parameter values for the ionic and synaptic currents in the biophysically-realistic models of the MCN1-elicited and PK-elicited gastric mill rhythms (Chapter 3). First, a simplified circuit diagram for the model MCN1-elicited rhythm that includes the DG neuron is shown below.

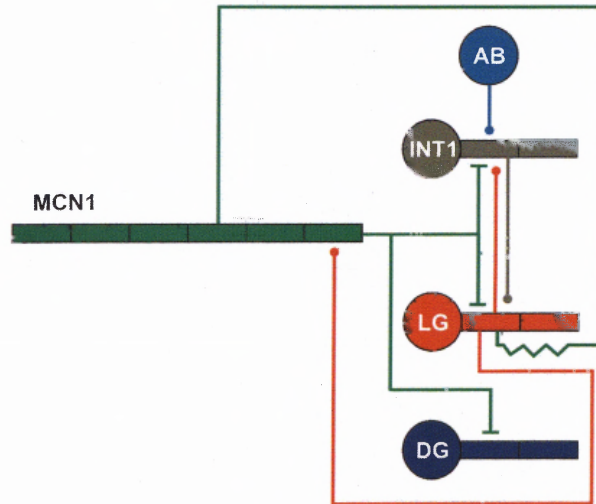


Figure A.1 Simplified Circuit Diagram of the Model MCN1-Elicited Gastric Mill Rhythm. The neurons are modeled as follows: **MCN1** the first four compartments (left to right) are axon compartments, while the last two are axon terminal compartments; **AB** soma; **INT1**, **LG**, and **DG** (left to right) are soma, neurite, and axon compartments.

The table below lists the parameters for the ionic currents in the biophysically-realistic model of the MCN1-elicited gastric mill rhythm.

Table A.1 Parameters for the Ionic Currents in the MCN1-Elicited Gastric Mill Rhythm

Cell	Current	Site	\bar{g}_{ion}	E_{ion}	State	k	v_K	l	v_l	τ_1	τ_2
MCN1	I_{Leak}	Axon	8.98	-80							
		Term.	3.59	-70							
	I_{Na}	Axon	565.47	45	m^3 h	-0.25 0.24	-62 -64	-0.24	-64	0 1	0 5
	I_K	Axon	565.47	-80	m^4	-0.24	-54	0.24	-54	8	20
INT1	I_{Leak}	Soma	0.31	-34							
		Neurite	0.08	-34							
		Axon	0.02	-34							
	I_h	Axon	0.63	-20	m	2	-65	2	-65	200	2500
	I_{Na}	Axon	11.00	45	m^3 h	-0.08 0.13	-26 -38	-0.12	-67	0 0	0 5
	I_K	Axon	18.85	-80	m^4	-0.045	-25	0.065	-30	4	150
LG	I_{Leak}	Soma	0.31	-40							
		Neurite	0.08	-40							
		Axon	0.02	-60							
	I_{Na}	Axon	18.00	45	m^3 h	-0.08 0.13	-21 -33	-0.12	-62	0 0	0 5
	I_K	Axon	12.57	-80	m^4	-0.045	-33	0.065	-5	4	100
DG	I_{Leak}	Soma	0.31	-40							
		Neurite	0.08	-50							
		Axon	0.02	-60							
	I_{Na}	Axon	18.00	45	m^3 h	-0.08 0.13	-21 -33	-0.12	-62	0 0	0 5
	I_K	Axon	12.57	-80	m^4	-0.045	-33	0.065	-5	4	100
		Neurite	0.6	-80	m	-1.5	-36	-1.5	-36	4000	6000
	I_h	Neurite	0.6	0	m	1	-65	-1	-65	3000	5000
	I_{Proc}	Neurite	*	0	m	-0.2	-35			50	0
AB	I_{Leak}	Soma	0.31	-63							
	I_{Ca}	Soma	1.26	120	m^3 h	-0.24 0.12	-61 -88	0.14	-84	0 40	0 **

(*) $\bar{g}_{proc} = 0.4 + 3 / (1 + \exp(-(V_{MCN1_{AxonTerm.}} + 50)))$, (**) $\tau_2 = 300 * \exp(0.03(V + 162))$

The units for the parameter values of the ionic currents are given as follows: \bar{g}_{ion} (nS); E_{ion}, v_k, v_l (mV); k, l (mV^{-1}); τ_1, τ_2 ($msec$).

The second table below lists the parameters for the synaptic currents in the biophysically-realistic model of the MCN1-elicited gastric mill rhythm.

Table A.2 Parameters for the Synaptic Currents in the MCN1-Elicited Rhythm

Synapse	Presyn. Site	Postsyn. Site	\bar{g}_{syn}	E_{syn}	α	v_α	β	v_β	τ_3	τ_4
MCN1→INT1	Term.	Neurite	0.002	45	-1	-50			30	0
MCN1→LG (chemical)	Term.	Neurite	2.14	45	-2	-68	-2	-68	8000	9000
MCN1→LG (electrical)	Axon	Axon	0.021							
MCN1→DG	Term.	Neurite	0 ^{***}	0	-1	-50			400	0
LG→MCN1	Neurite	Term.	150	-80	-2	-35	2	-35	5	270
INT1→LG	Soma	Neurite	1.40	-80	-0.5	-49			100	0
LG→INT1	Neurite	Soma	0.13	-80	-0.5	-45			50	0
	Axon	Neurite	1.30	-80	-1	-25	1	-25	3	97
	Axon	Axon	1.30	-80	-1	-25	1	-25	3	97
AB→INT1	Soma	Neurite	2.00	-70	-1	-55			80	0

(^{***}) $\bar{g}_{syn} = 0$; MCN1 instead activates I_{Proc} in the DG neuron, which follows the α and v_α parameters from this synapse (see * in Table A.1)

Units for the parameter values of the synaptic currents are given as follows: \bar{g}_{syn} (nS);

$E_{syn}, v_\alpha, v_\beta$ (mV); α, β (mV^{-1}); τ_3, τ_4 ($msec$).

Next, a simplified circuit diagram for the biophysically-realistic model of the PK-elicited gastric mill rhythm that includes the DG neuron is shown below.

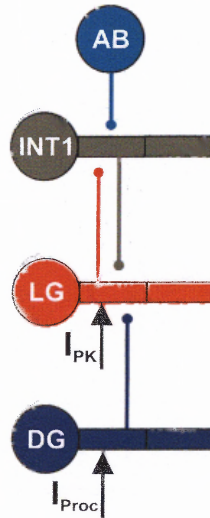


Figure A.2 Simplified Circuit Diagram of the Model PK-Elicited Gastric Mill Rhythm. The compartments of AB, INT1, LG, and DG are modeled in the same way as in Figure A.1. PK elicits a gastric mill rhythm by inducing voltage-gated ionic currents in the LG neuron (I_{PK}). The parameters for three different mechanisms by which PK can elicit a similar gastric mill rhythm are given in Table A.3. The DG neuron bursts in the model due to PK-induction of I_{Proc} .

The table below lists the parameter values for the ionic currents that are distinct to the biophysically-realistic model of the PK-elicited gastric mill rhythm.

Table A.3 Parameters for Ionic Currents that are Distinct to the PK-Elicited Gastric Mill Rhythm

Cell	Current	Site	\bar{g}_{ion}	E_{ion}	State	k	v_k	l	v_l	τ_l	τ_2
LG	Mechanism 1: I_{Plat}	Neurite	0.65	0	m h	-0.05 2	-65 -55	-2	-55	50 2000	0 6000
	Mechanism 2: I_h	Neurite	0.75	0	m	0.1	-45			8000	0
	Mechanism 3: I_{Proc} I_K	Neurite Neurite	0.9 0.3	0 -80	m m	-0.05 -1	-45 -45	-1	-45	50 4000	0 4000
DG	I_{Proc}	Neurite	1	0	m	-0.2	-35			50	0

The units for the parameter values of these ionic currents are the same as those given for Table A.1. Moreover, all other ionic currents in AB, INT1, LG, and DG are the same as those listed in Table A.1.

Finally, the table below lists the parameter values for the synaptic currents that are distinct to the biophysically-realistic model of the PK-elicited gastric mill rhythm.

Table A.4 Parameters for Synaptic Currents that are Distinct to the PK-Elicited Gastric Mill Rhythm

Synapse	Presyn. Site	Postsyn. Site	\bar{g}_{syn}	E_{syn}	α	v_{α}	β	v_{β}	τ_3	τ_4
DG→LG	Neurite	Neurite	0.035	-80	-1	-35			100	0

Units for the parameter values of this synaptic current are the same as those given for Table A.2. Moreover, all other synaptic currents that involve AB, INT1, and LG are the same as those listed in Table A.2.

APPENDIX B

PARAMETERS FOR THE 2-DIMENSIONAL MODELS OF THE MCN1-ELICITED AND MCN1/CPN2-ELICITED GASTRIC MILL RHYTHMS

This appendix gives the parameter values for the 2-dimensional models of the MCN1-elicited and MCN1/CPN2-elicited gastric mill rhythms (Chapter 4). First, the table below lists the parameter values for the MCN1-elicited rhythm in the case where MCN1 is tonically active.

Table B.1 Parameters for the 2-Dimensional Model of the MCN1-Elicited Gastric Mill Rhythm (Shown in Figure 4.3)

INT1	Pyloric	LG	MCN1
$g_{Leak,I} = 0.75$	$\bar{g}_p = 0.85$	$g_{Leak,L} = 1$	$\bar{g}_s = 3$
$E_{Leak,I} = 10$	$E_p = -60$	$E_{Leak,L} = -60$	$E_s = 50$
$\bar{g}_{L \rightarrow I} = 2$	$per = 1$	$\bar{g}_{I \rightarrow L} = 5$	$v_{pre} = -33$
$E_{L \rightarrow I} = -80$	$dur = 0.5$	$E_{I \rightarrow L} = -80$	$\tau_{LO} = 14$
$v_{L \rightarrow I} = -30$	$v_q = -35$	$v_{I \rightarrow L} = -30$	$\tau_{HI} = 5$
$k_{L \rightarrow I} = 5$	$k_q = 3$	$k_{I \rightarrow L} = 5$	

The parameter values in the above table are the same as those for the MCN1-elicited rhythm of Chapter 2 (see Table 2.1). Units for the parameters in the above table are given as follows: **INT1** $g_{Leak,I}$, $\bar{g}_{L \rightarrow I}$ (mS/cm^2), $E_{Leak,I}$, $E_{L \rightarrow I}$, $v_{L \rightarrow I}$, $k_{L \rightarrow I}$ (mV); **Pyloric**

\bar{g}_p (mS/cm^2), E_P , v_q , k_q (mV), per (sec); **LG** $g_{Leak,L}$, $\bar{g}_{I \rightarrow L}$ (mS/cm^2), $E_{Leak,L}$, $E_{I \rightarrow L}$, $v_{I \rightarrow L}$, $k_{I \rightarrow L}$ (mV); **MCN1** \bar{g}_s (mS/cm^2), E_s , v_{pre} (mV), τ_{LO} , τ_{HI} (sec).

The second table below lists the parameter values that are distinct for the 2-dimensional model of the MCN1/CPN2-elicited gastric mill rhythm in the case where MCN1 is tonically active.

Table B.2 Parameters that are Distinct for the 2-Dimensional Model of the MCN1/CPN2-Elicited Gastric Mill Rhythm (Shown in **Figures 4.8 – 4.13**)

CPN2	LG
$g_{Leak,C} = 1$	$g_e = 1$
$E_{Leak,C} = 10$	
$\bar{g}_{I \rightarrow C} = 5$	
$E_{I \rightarrow C} = -95$	
$v_{I \rightarrow C} = -30$	
$k_{I \rightarrow C} = 5$	

Units for the parameters in the above table are given by: **CPN2** $g_{Leak,C}$, $\bar{g}_{I \rightarrow C}$ (mS/cm^2), $E_{Leak,C}$, $E_{I \rightarrow C}$, $v_{I \rightarrow C}$, $k_{I \rightarrow C}$ (mV); **LG** g_e (mS/cm^2). All other parameters for this model are the same as in Table B.1.

The third table below lists the parameter values which are distinct for the MCN1-elicited and MCN1/CPN2-elicited gastric mill rhythms that include the effect of the AB to MCN1 feedback inhibition.

Table B.3. Parameters which are Distinct for the MCN1-Elicited and MCN1/CPN2-Elicited Gastric Mill Rhythms that Include the Effect of the AB to MCN1 Feedback Inhibition

MCN1 Rhythmic	MCN1/CPN2 Rhythmic	MCN1/CPN2 Alternating
(Figures 4.4 - 4.7)	(Figures 4.14 - 4.16)	(Figures 4.17 - 4.22)
$\bar{g}_\sigma = 0.6$	same	same
$\tau_{LO} = 6$	$\tau_{LO} = 3$	$\tau_{LO} = 3$
$\tau_{HI} = 5$	$\tau_{HI} = 3$	$\tau_{HI} = 3$
		$\mu = 0$ (Fig. 4.18, 4.19) $\mu = 0.5$ (Fig. 4.21, 4.22)

Units for the parameters in the above table are given by: \bar{g}_σ (mS/cm^2); τ_{LO} , τ_{HI} , μ (sec).

The left column of the above table gives the distinct parameter values for the MCN1-elicited rhythm in the case where MCN1 is rhythmically active (shown in Figures 4.4 – 4.7), and all other parameters for this model are the same as in Table B.1. The middle column gives the distinct parameter values for the MCN1/CPN2-elicited gastric mill rhythm when MCN1 is rhythmically active (shown in Figures 4.14 – 4.16), and all other parameters for this model are the same as in Tables B.1 and B.2. Finally, the right column gives the distinct parameter values for the MCN1/CPN2-elicited gastric mill rhythm when MCN1 exhibits its VCN-influenced activity pattern, and all other parameters for this model are the same as in Tables B.1 and B.2.

APPENDIX C

PARAMETERS FOR THE BIOPHYSICALLY-REALISTIC MODELS OF THE MCN1-ELICITED AND MCN1/CPN2-ELICITED GASTRIC MILL RHYTHMS

This appendix gives the parameter values for the ionic and synaptic currents in the biophysically-realistic models of the MCN1-elicited and MCN1/CPN2-elicited gastric mill rhythms (Chapter 5). First, a simplified circuit diagram is shown below.

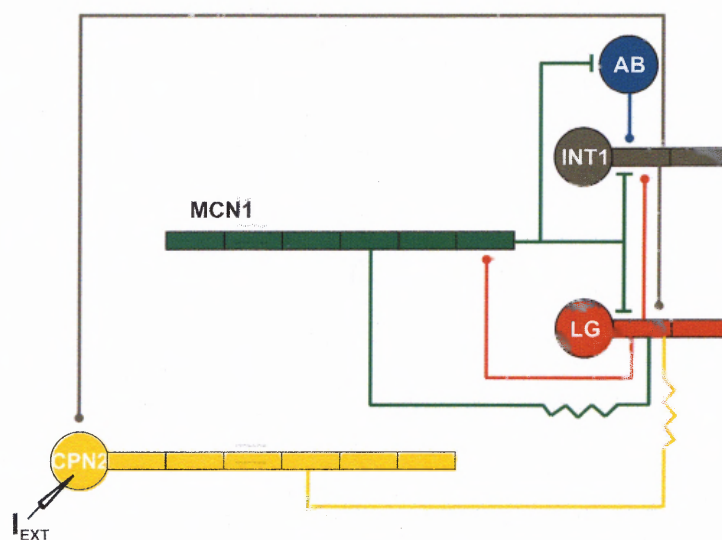


Figure C.1 Simplified Circuit Diagram of the Model MCN1/CPN2-Elicited Gastric Mill Rhythm. The compartments of CPN2 are modeled as follows (left to right): soma, axon (4 compartments), axon terminals (2 compartments). The compartments of MCN1 are modeled as: (left to right) axon (4 compartments), axon terminals (2 compartments). The compartments of INT1 and LG are modeled as (left to right): soma, neurite, axon. Finally, AB is modeled with a single soma compartment.

The MCN1-elicited rhythm is obtained by setting $I_{Ext} = 0$ in the model (which makes CPN2 inactive). Conversely, the MCN1/CPN2-elicited gastric mill rhythm is obtained by setting $I_{Ext} = 80 \text{ pA}$ in the model. Therefore, the value of I_{Ext} distinguishes between the MCN1-elicited and MCN1/CPN2-elicited gastric mill rhythms. The table below lists the parameters for the ionic currents in this model.

Table C.1 Parameters for the Ionic Currents in the Biophysically-Realistic Model

Cell	Current	Site	\bar{g}_{ion}	E_{ion}	State	k	v_K	l	v_l	τ_1	τ_2
MCN1	I_{Leak}	Axon	8.98	-80							
		Term.	3.59	-70							
	I_{Na}	Axon	565.47	45	m^3 h	-0.25 0.24	-62 -64	-0.24	-64	0 1	0 5
	I_K	Axon	565.47	-80	m^4	-0.24	-54	0.24	-54	8	20
CPN2	I_{Leak}	Soma	8.98	-60							
		Axon	8.98	-80							
		Term.	3.59	-70							
	I_{Plat}	Soma	0.5	0	m h	-0.05 1	-65 -61	-1	-61	50 1000	0 8000
	I_{Na}	Axon	565.47	45	m^3 h	-0.25 0.24	-62 -64	-0.24	-64	0 1	0 5
	I_K	Axon	565.47	-80	m^4	-0.24	-54	0.24	-54	8	20
INT1	I_{Leak}	Soma	0.31	-34							
		Neurite	0.08	-34							
		Axon	0.02	-34							
	I_h	Axon	0.63	-20	m	2	-65	2	-65	200	2500
	I_{Na}	Axon	11.00	45	m^3 h	-0.08 0.13	-26 -38	-0.12	-67	0 0	0 5
	I_K	Axon	18.85	-80	m^4	-0.045	-25	0.065	-30	4	150
LG	I_{Leak}	Soma	0.31	-40							
		Neurite	0.08	-40							
		Axon	0.02	-60							
	I_{Na}	Axon	11.00	45	m^3 h	-0.08 0.13	-21 -33	-0.12	-62	0 0	0 5
	I_K	Axon	12.57	-80	m^4	-0.045	-33	0.065	-5	4	100
AB	I_{Leak}	Soma	0.31	-63							
	I_{Ca}	Soma	1.26	120	m^3 h	-0.24 0.12	-61 -88	0.14	-84	0 40	0 **

(**) $\tau_2 = 300 * \exp(0.03(V+162))$

The units for the parameter values of the ionic currents are given as follows: \bar{g}_{ion} (nS); E_{ion}, v_k, v_l (mV); k, l (mV^{-1}); τ_1, τ_2 ($msec$).

The second table below lists the parameters for the synaptic currents in this biophysically-realistic model.

Table C.2 Parameters for the Synaptic Currents in the Biophysically-Realistic Model

Synapse	Presyn. Site	Postsyn. Site	\bar{g}_{syn}	E_{syn}	α	v_α	β	v_β	τ_3	τ_4
MCN1→INT1	Term.	Neurite	0.4	0	-1	-50			60	0
MCN1→LG (chemical)	Term.	Neurite	3	45	-2	-68	-2	-68	8000	9000
MCN1→LG (electrical)	Axon	Axon	0.06							
MCN1→AB	Term.	Soma	0.002	0	-1	-50	1	-50	2	500
LG→MCN1	Neurite	Term.	150	-80	-2	-33	2	-33	15	225
INT1→LG	Soma	Neurite	1.55	-80	-0.5	-49			100	0
LG→INT1	Neurite	Soma	0.19	-80	-0.5	-45			50	0
	Axon	Neurite	1.30	-80	-1	-25	1	-25	3	97
	Axon	Axon	1.30	-80	-1	-25	1	-25	3	97
AB→INT1	Soma	Neurite	3.00	-70	-1	-55			80	0
CPN2→LG (electrical)	Axon	Neurite	†							
INT1→CPN2	Neurite	Soma	18	-80	-2	-55			100	0

(†) $\bar{g}_{syn} = 0.1 + 0.3 / (1 + \exp(-2 * (V_{LGneurite} + 24)))$, this is a voltage-dependent electrical coupling

The units for the parameter values of the synaptic currents are given as follows: \bar{g}_{syn} (nS);

$E_{syn}, v_\alpha, v_\beta$ (mV); α, β (mV^{-1}); τ_3, τ_4 ($msec$).

REFERENCES

- Akay T, Wood D, Nusbaum MP (2004) Reciprocal Inhibition is not necessary for generation of all gastric mill rhythms. In: SfN 34th Annual Meeting. San Diego, CA.
- Ambrosio C, Bose A, Nadim F (2005) The effect of modulatory neuronal input on gastric mill frequency. *Neurocomputing* 65-66:623-631.
- Ambrosio CL (2005) The control of frequency of a conditional oscillator simultaneously subjected to multiple oscillatory inputs. In: *Mathematical Sciences*, p 149. Newark, NJ: New Jersey Institute of Technology.
- Ambrosio-Mouser C, Nadim F, Bose A (2006) The effects of varying the timing of inputs on a neuronal oscillator. *SIAM J Applied Dynamical Systems* 5:108-139.
- Angstadt JD, Calabrese RL (1989) A hyperpolarization-activated inward current in heart interneurons of the medicinal leech. *J Neurosci* 9:2846-2857.
- Angstadt JD, Calabrese RL (1991) Calcium currents and graded synaptic transmission between heart interneurons of the leech. *J Neurosci* 11:746-759.
- Bartos M, Manor Y, Nadim F, Marder E, Nusbaum MP (1999) Coordination of fast and slow rhythmic neuronal circuits. *J Neurosci* 19:6650-6660.
- Beenhakker MP, Nusbaum MP (2004) Mechanosensory activation of a motor circuit by coactivation of two projection neurons. *J Neurosci* 24:6741-6750.
- Beenhakker MP, Blitz DM, Nusbaum MP (2004) Long-lasting activation of rhythmic neuronal activity by a novel mechanosensory system in the crustacean stomatogastric nervous system. *J Neurophysiol* 91:78-91.
- Beenhakker MP, DeLong ND, Saideman SR, Nadim F, Nusbaum MP (2005) Proprioceptor regulation of motor circuit activity by presynaptic inhibition of a modulatory projection neuron. *J Neurosci* 25:8794-8806.
- Blitz DM, Nusbaum MP (1997) Motor pattern selection via inhibition of parallel pathways. *J Neurosci* 17:4965-4975.
- Blitz DM, Beenhakker MP, Nusbaum MP (2004) Different sensory systems share projection neurons but elicit distinct motor patterns. *J Neurosci* 24:11381-11390.

- Blitz DM, Christie AE, Coleman MJ, Norris BJ, Marder E, Nusbaum MP (1999) Different proctolin neurons elicit distinct motor patterns from a multifunctional neuronal network. *J Neurosci* 19:5449-5463.
- Brown TG (1914) On the nature of the fundamental activity of the nervous centres; together with an analysis of the conditioning of rhythmic activity in progression, and a theory of the evolution of function in the nervous system. *J Physiol* 48:18-46.
- Burke RE (2001) The central pattern generator for locomotion in mammals. *Adv Neurol* 87:11-24.
- Bussieres N, Pflieger JF, Dubuc R (1999) Anatomical study of vestibulospinal neurons in lampreys. *J Comp Neurol* 407:512-526.
- Calabrese RL (1995) Oscillation in motor pattern-generating networks. *Curr Opin Neurobiol* 5:816-823.
- Calabrese RL, Nadim F, Olsen OH (1995) Heartbeat control in the medicinal leech: a model system for understanding the origin, coordination, and modulation of rhythmic motor patterns. *J Neurobiol* 27:390-402.
- Christie AE, Lundquist CT, Nassel DR, Nusbaum MP (1997) Two novel tachykinin-related peptides from the nervous system of the crab *Cancer borealis*. *J Exp Biol* 200:2279-2294.
- Coleman MJ, Nusbaum MP (1994) Functional consequences of compartmentalization of synaptic input. *J Neurosci* 14:6544-6552.
- Coleman MJ, Meyrand P, Nusbaum MP (1995) A switch between two modes of synaptic transmission mediated by presynaptic inhibition. *Nature* 378:502-505.
- De Schutter E, Angstadt JD, Calabrese RL (1993) A model of graded synaptic transmission for use in dynamic network simulations. *J Neurophysiol* 69:1225-1235.
- Deliagina TG, Zelenin PV, Orlovsky GN (2002) Encoding and decoding of reticulospinal commands. *Brain Res Brain Res Rev* 40:166-177.
- Dudel J, Kuffler SW (1961) Presynaptic inhibition at the crayfish neuromuscular junction. *J Physiol* 155:543-562.
- Ermentrout GB (2002) *Simulating, Analyzing, and Animating Dynamical Systems: A Guide to Xppaut for Researchers and Students (Software, Environments, Tools)*. Philadelphia: SIAM.

- Friesen WO (1994) Reciprocal inhibition: a mechanism underlying oscillatory animal movements. *Neurosci Biobehav Rev* 18:547-553.
- Furshpan EJ, Potter DD (1959) Transmission at the giant motor synapses of the crayfish. *J Physiol* 145:289-325.
- Gerstner W, van Hemmen JL, Cowan JD (1996) What matters in neuronal locking? *Neural Comput* 8:1653-1676.
- Golowasch J, Marder E (1992) Proctolin activates an inward current whose voltage dependence is modified by extracellular Ca^{2+} . *J Neurosci* 12:810-817.
- Graubard K, Raper JA, Hartline DK (1980) Graded synaptic transmission between spiking neurons. *Proc Natl Acad Sci U S A* 77:3733-3735.
- Gray CM (1994) Synchronous oscillations in neuronal systems: mechanisms and functions. *J Comput Neurosci* 1:11-38.
- Grillner S, Deliagina T, Ekeberg O, el Manira A, Hill RH, Lansner A, Orlovsky GN, Wallen P (1995) Neural networks that co-ordinate locomotion and body orientation in lamprey. *Trends Neurosci* 18:270-279.
- Harris-Warrick RM, Marder E, Selverston AI, Moulins M (1992) *Dynamic biological networks. The stomatogastric nervous system.* Cambridge, MA: MIT.
- Heinzel HG, Weimann JM, Marder E (1993) The behavioral repertoire of the gastric mill in the crab, *Cancer pagurus*: an in situ endoscopic and electrophysiological examination. *J Neurosci* 13:1793-1803.
- Hertzberg SR, Nusbaum MP (2004) Pevpyrokinin elicits a MCN1-like gastric mill rhythm using different cellular mechanisms. In: *SfN 34th Annual Meeting.* San Diego, CA.
- Hertzberg SR, Nusbaum MP (2005) Different central pattern generators elicit similar gastric mill rhythms. In: *SfN 35th Annual Meeting.* Washington, DC.
- Hertzberg SR, Huybrechts J, Schoofs L, Nusbaum MP (2003) Distinct mechanisms underlie similar activity patterns from the same circuit. In: *SfN 33rd Annual Meeting.* New Orleans, LA.
- Hodgkin AL, Huxley AF (1952) A quantitative description of membrane current and its application to conduction and excitation in nerve. *J Physiol* 117:500-544.
- Jing J, Weiss KR (2005) Generation of variants of a motor act in a modular and hierarchical motor network. *Curr Biol* 15:1712-1721.

- Kasicki S, Grillner S (1986) Muller cells and other reticulospinal neurones are phasically active during fictive locomotion in the isolated nervous system of the lamprey. *Neurosci Lett* 69:239-243.
- Kasicki S, Grillner S, Ohta Y, Dubuc R, Brodin L (1989) Phasic modulation of reticulospinal neurones during fictive locomotion and other types of spinal motor activity in lamprey. *Brain Res* 484:203-216.
- Katz PS (1995a) Intrinsic and extrinsic neuromodulation of motor circuits. *Curr Opin Neurobiol* 5:799-808.
- Katz PS (1995b) Neuromodulation and motor pattern generation in crustacean stomatogastric nervous system. In: *Neural Control of Movements* (Ferrell WR, Proske U, eds), pp 277-283. New York: Plenum press.
- Katz PS, Harris-Warrick RM (1989) Serotonergic/cholinergic muscle receptor cells in the crab stomatogastric nervous system. II. Rapid nicotinic and prolonged modulatory effects on neurons in the stomatogastric ganglion. *J Neurophysiol* 62:571-581.
- Katz PS, Frost WN (1995a) Intrinsic neuromodulation in the Tritonia swim CPG: the serotonergic dorsal swim interneurons act presynaptically to enhance transmitter release from interneuron C2. *J Neurosci* 15:6035-6045.
- Katz PS, Frost WN (1995b) Intrinsic neuromodulation in the Tritonia swim CPG: serotonin mediates both neuromodulation and neurotransmission by the dorsal swim interneurons. *J Neurophysiol* 74:2281-2294.
- Katz PS, Frost WN (1996) Intrinsic neuromodulation: altering neuronal circuits from within. *Trends Neurosci* 19:54-61.
- Kiehn O, Harris-Warrick RM (1992a) 5-HT modulation of hyperpolarization-activated inward current and calcium-dependent outward current in a crustacean motor neuron. *J Neurophysiol* 68:496-508.
- Kiehn O, Harris-Warrick RM (1992b) Serotonergic stretch receptors induce plateau properties in a crustacean motor neuron by a dual-conductance mechanism. *J Neurophysiol* 68:485-495.
- Kilman VL, Marder E (1996) Ultrastructure of the stomatogastric ganglion neuropil of the crab, *Cancer borealis*. *J Comp Neurol* 374:362-375.
- LeBeau FE, El Manira A, Grillner S (2005) Tuning the network: modulation of neuronal microcircuits in the spinal cord and hippocampus. *Trends Neurosci* 28:552-561.
- Lisman JE (1997) Bursts as a unit of neural information: making unreliable synapses reliable. *Trends Neurosci* 20:38-43.

- Manor Y, Nadim F (1997) A program for simulating synaptic activity using LabWindows/CVI. In, pp 207-215. Houston: National Instruments.
- Manor Y, Nadim F, Epstein S, Ritt J, Marder E, Kopell N (1999) Network oscillations generated by balancing graded asymmetric reciprocal inhibition in passive neurons. *J Neurosci* 19:2765-2779.
- Marder E (1996) Neural modulation: following your own rhythm. *Curr Biol* 6:119-121.
- Marder E (2002) Non-mammalian models for studying neural development and function. *Nature* 417:318-321.
- Marder E, Calabrese RL (1996) Principles of rhythmic motor pattern generation. *Physiol Rev* 76:687-717.
- Marder E, Bucher D (2001) Central pattern generators and the control of rhythmic movements. *Curr Biol* 11:R986-996.
- Marder E, Thirumalai V (2002) Cellular, synaptic and network effects of neuromodulation. *Neural Netw* 15:479-493.
- Marder E, Rehm KJ (2005) Development of central pattern generating circuits. *Curr Opin Neurobiol* 15:86-93.
- Marder E, Bucher D, Schulz DJ, Taylor AL (2005) Invertebrate central pattern generation moves along. *Curr Biol* 15:R685-699.
- Matsuyama K, Mori F, Nakajima K, Drew T, Aoki M, Mori S (2004) Locomotor role of the corticoreticular-reticulospinal-spinal interneuronal system. *Prog Brain Res* 143:239-249.
- McCormick DA, Bal T (1994) Sensory gating mechanisms of the thalamus. *Curr Opin Neurobiol* 4:550-556.
- McCormick DA, Bal T (1997) Sleep and arousal: thalamocortical mechanisms. *Annu Rev Neurosci* 20:185-215.
- Mishchenko EF, Rozov NK (1980) *Differential Equations with Small Parameters and Relaxation Oscillators*. New York: Plenum Press.
- Nadim F, Olsen OH, De Schutter E, Calabrese RL (1995) Modeling the leech heartbeat elemental oscillator. I. Interactions of intrinsic and synaptic currents. *J Comput Neurosci* 2:215-235.

- Nadim F, Manor Y, Nusbaum MP, Marder E (1998) Frequency regulation of a slow rhythm by a fast periodic input. *J Neurosci* 18:5053-5067.
- Norris BJ, Coleman MJ, Nusbaum MP (1994) Recruitment of a projection neuron determines gastric mill motor pattern selection in the stomatogastric nervous system of the crab, *Cancer borealis*. *J Neurophysiol* 72:1451-1463.
- Norris BJ, Coleman MJ, Nusbaum MP (1996) Pyloric motor pattern modification by a newly identified projection neuron in the crab stomatogastric nervous system. *J Neurophysiol* 75:97-108.
- Nusbaum MP, Marder E (1989) A modulatory proctolin-containing neuron (MPN). II. State-dependent modulation of rhythmic motor activity. *J Neurosci* 9:1600-1607.
- Nusbaum MP, Beenhakker MP (2002) A small-systems approach to motor pattern generation. *Nature* 417:343-350.
- Nusbaum MP, Blitz DM, Swensen AM, Wood D, Marder E (2001) The roles of co-transmission in neural network modulation. *Trends Neurosci* 24:146-154.
- Olsen OH, Nadim F, Calabrese RL (1995) Modeling the leech heartbeat elemental oscillator. II. Exploring the parameter space. *J Comput Neurosci* 2:237-257.
- Pearson KG (1993) Common principles of motor control in vertebrates and invertebrates. *Annu Rev Neurosci* 16:265-297.
- Perkel DH, Mulloney B (1974) Motor pattern production in reciprocally inhibitory neurons exhibiting postinhibitory rebound. *Science* 185:181-183.
- Perreault MC, Drew T, Rossignol S (1993) Activity of medullary reticulospinal neurons during fictive locomotion. *J Neurophysiol* 69:2232-2247.
- Perrins R, Weiss KR (1996) A cerebral central pattern generator in *Aplysia* and its connections with buccal feeding circuitry. *J Neurosci* 16:7030-7045.
- Prinz AA, Bucher D, Marder E (2004) Similar network activity from disparate circuit parameters. *Nat Neurosci* 7:1345-1352.
- Ramirez JM, Pearson KG (1990) Chemical deafferentation of the locust flight system by phentolamine. *J Comp Physiol [A]* 167:485-494.
- Rinzel J, Ermentrout GB (1998) Analysis of neural excitability and oscillations. In: *Methods in Neuronal Modeling: From Ions to Networks* (Koch C, Segev I, eds), pp 251-291. Cambridge, MA: MIT Press.

- Rossignol S, Dubuc R, Gossard JP (2006) Dynamic sensorimotor interactions in locomotion. *Physiol Rev* 86:89-154.
- Sharp AA, Skinner FK, Marder E (1996) Mechanisms of oscillation in dynamic clamp constructed two-cell half-center circuits. *J Neurophysiol* 76:867-883.
- Sharp AA, O'Neil MB, Abbott LF, Marder E (1993a) The dynamic clamp: artificial conductances in biological neurons. *Trends Neurosci* 16:389-394.
- Sharp AA, O'Neil MB, Abbott LF, Marder E (1993b) Dynamic clamp: computer-generated conductances in real neurons. *J Neurophysiol* 69:992-995.
- Skinner FK, Turrigiano GG, Marder E (1993) Frequency and burst duration in oscillating neurons and two-cell networks. *Biol Cybern* 69:375-383.
- Skinner FK, Kopell N, Marder E (1994) Mechanisms for oscillation and frequency control in reciprocally inhibitory model neural networks. *J Comput Neurosci* 1:69-87.
- Sommer MA, Wurtz RH (2004a) What the brain stem tells the frontal cortex. I. Oculomotor signals sent from superior colliculus to frontal eye field via mediodorsal thalamus. *J Neurophysiol* 91:1381-1402.
- Sommer MA, Wurtz RH (2004b) What the brain stem tells the frontal cortex. II. Role of the SC-MD-FEF pathway in corollary discharge. *J Neurophysiol* 91:1403-1423.
- Stein P (1997) *Neurons, networks, and motor behavior*. Cambridge, MA: MIT Press.
- Steriade M, McCormick DA, Sejnowski TJ (1993) Thalamocortical oscillations in the sleeping and aroused brain. *Science* 262:679-685.
- Swain GP, Snedeker JA, Ayers J, Selzer ME (1993) Cytoarchitecture of spinal-projecting neurons in the brain of the larval sea lamprey. *J Comp Neurol* 336:194-210.
- Swensen AM, Marder E (2000) Multiple peptides converge to activate the same voltage-dependent current in a central pattern-generating circuit. *J Neurosci* 20:6752-6759.
- Swensen AM, Marder E (2001) Modulators with convergent cellular actions elicit distinct circuit outputs. *J Neurosci* 21:4050-4058.
- Van Vreeswijk C, Abbott LF, Ermentrout GB (1994) When inhibition not excitation synchronizes neural firing. *J Comput Neurosci* 1:313-321.
- Wang XJ, Rinzel J (1992) Alternating and synchronous rhythms in reciprocally inhibitory model neurons. *Neural Comp* 4:84-97.

Weeks JC (1981) Neuronal basis of leech swimming: separation of swim initiation, pattern generation, and intersegmental coordination by selective lesions. *J Neurophysiol* 45:698-723.

White JA, Chow CC, Ritt J, Soto-Trevino C, Kopell N (1998) Synchronization and oscillatory dynamics in heterogeneous, mutually inhibited neurons. *J Comput Neurosci* 5:5-16.

Wong RK, Traub RD, Miles R (1986) Cellular basis of neuronal synchrony in epilepsy. *Adv Neurol* 44:583-592.

Wood DE, Stein W, Nusbaum MP (2000) Projection neurons with shared cotransmitters elicit different motor patterns from the same neural circuit. *J Neurosci* 20:8943-8953.

Wood DE, Manor Y, Nadim F, Nusbaum MP (2004) Intercircuit control via rhythmic regulation of projection neuron activity. *J Neurosci* 24:7455-7463.

Yamaguchi T (2004) The central pattern generator for forelimb locomotion in the cat. *Prog Brain Res* 143:115-122.

Zelenin PV (2005) Activity of individual reticulospinal neurons during different forms of locomotion in the lamprey. *Eur J Neurosci* 22:2271-2282.